Alma Mater Studiorum – Università di Bologna

DOTTORATO DI RICERCA IN

SCIENZE GEOLOGICHE

Ciclo XXVI

Settore Concorsuale di afferenza: 04/A3

Settore Scientifico disciplinare: GEO/04

SPELEOGENESIS AND SECONDARY CAVE MINERALS IN QUARTZ-SANDSTONE AND QUARTZITE ENVIRONMENT

Presentata da: **Francesco Sauro**

Coordinatore Dottorato

Prof. Roberto Barbieri

Relatore

Prof. Jo De Waele

Correlatore

Prof. Leonardo Piccini

Esame finale anno 2014

... and the moon appeared as on a dead world of sole geology. You really had up there, the sense of the earth and rock as living bodies ... Seemed to be dreaming in terms of mineral.

... e apparve la luna come su un mondo morto di sola geologia. Si aveva veramente lassù, il senso della terra e della roccia come corpi viventi... Pareva di sognare in termini di minerale.

Alfonso Vinci, Auyan Tepui, 1949

SPELEOGENESIS AND SECONDARY CAVE MINERALS IN QUARTZ-SANDSTONE AND QUARTZITE ENVIRONMENT

ABSTRACT

The main objective of this research is to improve the comprehension of the processes controlling the formation of caves and karst-like morphologies in quartz-rich lithologies (more than 90% quartz), like quartz-sandstones and metamorphic quartzites. Quartz is considered one of the less soluble minerals of the Earth's crust, an thus hardly affected by chemical weathering. Despite this, since more than thirty years, it's clear that the formation of caves and peculiar superficial weathering morphologies in quartz-rich lithologies is common and very similar to the well-known "karstic" ones in carbonate rocks. In the scientific community the processes actually most retained to be responsible of these formations are explained in the "Arenisation Theory". This implies a slow but pervasive dissolution of the quartz grain/mineral boundaries increasing the general porosity until the rock becomes incohesive and can be easily eroded by running waters. The loose sands produced by the weathering processes are then evacuated to the surface through processes of piping due to the infiltration of waters from the fracture network or the bedding planes. Recently this theory was debated after the discovery of some giant maze systems in the Venezuelan "tepui" table mountains. In fact, some authors support a new hypothesis (the so-called "Non-lithification Theory") where less cohesive layers characterising the caves would be related to an inhomogeneous lithification of the quartz-sandstone strata, while the arenisation process would play only a secondary role.

In the frame of this debate, the first part of this thesis was dedicated to a detailed and quantitative analyses of the arenisation process, both from a chemical-physical point of view and from its expected morphologic expression. The aim was to verify the reliability of the arenisation theory and its effective role in the speleogenesis. Nonetheless, the study also examined the problems related to the compatibility between the geologic history of the tepui area (type of sedimentation, burial metamorphism, exhumation and superficial erosion rates) and the non-lithification theory.

To deal with these problems we adopted a multidisciplinary approach through the exploration and the study of several cave systems in different tepuis. The first step was to build a theoretical model of the arenisation process, considering the most recent knowledge about the dissolution kinetics of quartz, the intergranular/grain boundaries diffusion processes, the primary diffusion porosity, in the simplified conditions of an open fracture crossed by a continuous flow of undersatured water. The results of the model were then compared with the world's widest dataset (more than 150 analyses) of water geochemistry collected till now on the tepui, in superficial and cave settings. This research allowed observing the signature of the arenisation process in the water-rock interaction, verifying the output of the theoretical model. Several samples of quartz-sandstone from the caves were characterised by means of diffrattometric (XRD), fluorescence (XRF), EDAX, thin section, SEM, Raman and picnometer analyses. Clear evidences of the arenisation process were identified in the samples and correlated to petrographic characteristics, like the presence of phyllosilicates, the degree of cohesion and the primary porosity.

The study examined not only the speleogenetic processes in the epigenic conditions of the tepui, but also the possibility to have the formation of such voids also in hypogenic deep settings, like in the case of Corona 'e Sa Craba Cave in Sardinia. Hydrothermal conditions and the presence of inorganic salts in the solution can drastically enhance the solubility of quartz suggesting that this type of voids may also form in deep settings.

All these studies allowed verifying the importance and the effectiveness of the arenisation process that is confirmed to be the main process responsible of the primary formation of these caves and of the karst-like superficial morphologies. The numerical modelling and the field observations allowed

evaluating a possible age of the cave systems around 20-30 million of years. The main controls in the arenisation process, and thus in speleogenesis, are given by peculiar layers of iron-hydroxides or silt working as inception horizons in the first speleogenetic phases, but also the degree of fracturing of quartz-sandstone strata, the primary porosity and the recharge types of the systems (diffuse infiltration or floodwater injection).

The second part of the thesis was dedicated to the study of secondary cave mineral deposits, mostly sulphates, phosphate-sulphates, iron hydroxides and silica biospeleothems. One of these phosphate-sulphates, rossiantonite, is a new mineral for science, found in only one cave of the tepuis. The genesis of these deposits can help to understand the speleogenetic history of the caves and the active weathering processes. Thanks to the study of sulphur and oxygen isotopes, examining the potential sources of sulphates and sulphides in the cave host rock and at the surface, we deduced that most of these chemical deposits derive from an external atmospheric source, likely dymethylsulphide (DMS). Air flow, water percolation or sinking streams are the main means of transport of these elements into the systems, whose accumulation is also most probably biologically mediated. This process of sulphate accumulation seems possible in quartz-sandstone caves also because of the extremely long times of the senile phase, lasting probably for hundred thousands to even millions of years. An attempt to date a tufa-like biospeleothem with the U-Th method showed that post-depositional alteration limits the ability to date these highly porous samples.

RIASSUNTO

Questa ricerca ha avuto come principale obiettivo la comprensione dei processi morfogenetici e speleogenetici in rocce composte principalmente da quarzo (oltre il 90%), quali le quarzoareniti e le quarziti metamorfiche. Nonostante il quarzo sia considerato uno dei minerali meno solubili della crosta terrestre, e quindi meno affetto da degradazione, da ormai oltre trent'anni è sempre più evidente che in tali litologie si sono sviluppate forme superficiali e sistemi di grotte sotterranee del tutto simili, sia nelle dimensioni che nelle morfologie, ai più noti fenomeni di dissoluzione carsica nelle rocce carbonatiche. La teoria maggiormente accreditata prevede una lenta ma pervasiva dissoluzione dei contatti intergranulari o del cemento siliceo che porta ad un progressivo aumento della porosità fino a rendere la roccia incoerente e facilmente erodibile (teoria dell'arenizzazione). Le sabbie prodotte dall'arenizzazione verrebbero poi evacuate dai sistemi sotterranei attraverso meccanismi di *piping* e processi di trasporto per mezzo di acque di infiltrazione lungo fratture e interstrati. Recentemente tale teoria è stata rimessa in discussione in seguito alla scoperta di alcuni sistemi di grotte caratterizzati da ambienti labirintici di enormi dimensioni sui massicci quarzitici dei tepui venezuelani. Alcuni autori, infatti, sostengono che tali livelli facilmente erodibili hanno un'origine primaria non essendosi litificati a causa di peculiari processi diagenetici (teoria della non-litificazione), mentre l'arenizzazione avrebbe un ruolo del tutto secondario nella speleogenesi.

Nel contesto di tale dibattito, la prima parte della tesi ha cercato di analizzare in modo approfondito e quantitativo il processo di arenizzazione, sia da un punto di vista chimico-fisico, sia nella sua espressone morfologica, per verificarne l'attendibilità e l'effettiva importanza speleogenetica e morfogenetica. Sono state inoltre analizzate le problematiche legate alla compatibilità tra la teoria della non litificazione, e la lunga storia geologica dell'area, dal seppellimento all'esumazione e ai tassi di erosione superficiale. Per affrontare queste problematiche è stato utilizzato un approccio multidisciplinare, attraverso l'esplorazione e lo studio di numerosi sistemi sotterranei in diversi massicci tepuiani. Il primo passo è stato rappresentato dalla realizzazione di un modello numerico del processo di arenizzazione basato sulle più avanzate conoscenze riguardanti la chimica e la cinetica di dissoluzione del quarzo, i processi di diffusione intergranulare, la porosità di diffusione, nelle condizioni di intorno di una frattura aperta caratterizzata da un flusso continuo di acqua sottosatura di silice. I risultati di tale modello sono quindi stati confrontati con il più vasto set di dati di geochimica delle acque mai raccolto fin d'ora nei corsi d'acqua di superficie e nelle grotte dei tepui, verificando l'effettiva corrispondenza tra modellizzazione e osservazioni di terreno. Diverse tipologie di quarzoareiniti sono state caratterizzate attraverso analisi di diffrattometria, fluorescenza, EDAX, sezioni sottili, SEM e Raman. Evidenze del processo di arenizzazione sono state individuate e descritte, mettendole in relazione a caratteristiche petrografiche quali la porosità primaria e il contenuto di fillosilicati.

Oltre all'arenizzazione in condizioni epigeniche, come nel caso dei tepui, è stata presa in considerazione anche la possibilità dello sviluppo di cavità ipogeniche in tali litologie, come nel caso della grotta di Corona e' Sa Craba, in Sardegna. Condizioni di idrotermalismo e la presenza di sali inorganici in soluzione come il bario possono, infatti, aumentare drasticamente la velocità di dissoluzione del quarzo suggerendo che tali cavità possono ritrovarsi frequentemente in profondità.

Tale analisi multidisciplinare ha permesso di verificare l'effettiva importanza del processo di arenizzazione che viene confermato come il principale responsabile nella formazione di tali grotte e nella modellazione dei paesaggi in rocce quarzitiche. La modellizzazione e i dati raccolti sul terreno hanno permesso di valutare l'età dei sistemi epigenici dei tepui ad oltre 20-30 milioni di anni,

confermando i lunghi tempi necessari allo sviluppo di tali cavità. I principali controlli nella formazione di tali cavità sono dati da particolari strati di idrossidi di ferro o siltiti che fungono da orizzonti di *inception*, il grado di fratturazione, la porosità primaria della quarzoarenite e il tipo di ricarica idrologica del sistema (per percolazione diffusa o regimi irregolari con iniezione di grandi volumi d'acqua durante le piene).

Nella seconda parte della tesi è stato affrontato lo studio dei minerali di formazione secondaria nelle grotte dei tepui, in particolare dei solfati, fosfati-solfati, e dei biospeleotemi di silice e idrossidi di ferro. La formazione di minerali secondari può, infatti, fornire importanti informazioni riguardo i processi di alterazione e la speleogenesi. Tale ricerca ha permesso la scoperta di un nuovo minerale per la scienza, la rossiantonite. Attraverso lo studio degli isotopi dello zolfo e dell'ossigeno contenuto nello ione solfato, l'analisi delle potenziali fonti di solfato o solfuri nell'area, si è giunti alla conclusione che tali depositi derivano dall'accumulazione di elementi di origine atmosferica, molto probabilmente dimetilsulfide, convogliato nelle grotte attraverso le correnti d'aria, o trasportato dalle acque per lenta percolazione attraverso la massa rocciosa o per infiltrazione diretta di torrenti. Il processo di accumulazione è certamente influenzato anche da fattori biologici.

Tali minerali hanno avuto la possibilità di accumularsi nelle cavità, anche grazie ai lunghissimi tempi (probabilmente milioni di anni) di inattività idrica di alcuni settori delle grotte in seguito alla loro formazione, confermando in generale l'antichità di tali sistemi. È stato inoltre effettuato un tentativo di datazione col metodo U-Th di un biospeleotemi di silice che ha mostrato la complessità di tali metodologie applicate a tali materiali altamente porosi.

1 - INTRODUCTION

1.1 Quartzite caves: beyond the quartz insolubility paradox

Metamorphic quartzites and quartz-sandstones are usually considered to be among the most insoluble rocks on Earth, with some authors asserting that quartz is practically immune to chemical weathering (Tricart, 1972). Although the rate of dissolution of quartz in the acidic to neutral solutions commonly found in natural settings is among the slowest ones, the wide subterranean conduits and some peculiar surface landforms formed in these rocks are clear evidences of intensive weathering (Wray, 1997a, and references therein). The resulting landscape has many features resembling karst and many authors (White et al., 1966; Martini, 1979, 1985, 2004; Piccini, 1995; Wray, 1997b; Doerr, 1999) have used such a term referring to this kind of geomorphic process although solution plays only a minor role, at least from a quantitative point of view.

Karst-like features and caves in quartz-sandstones are known to exist in all continents, but most commonly in tectonically stable cratonic areas (for instance the Guyana Shield of Venezuela and Brazil, the Kaapvaal craton of South Africa, or the Westralian craton and Sydney Basin in Australia), and more developed in humid tropical settings (like in the Minas Gerais state of Brazil, and in the quartz-sandstone outcrops in Thailand, Mozambique, and in the Hunan province of China). However caves in quartz-sandstones were documented also in actually hyperarid settings, like in Chad and Australia.

In the last twenty years several authors have discussed many hypotheses on the genesis of caves and karst-like features in quartzite and quartz-sandstones. All the theories so far presented require a process of rock softening with the final formation of loose sands along some preferential bedding planes or fractures, followed by the removal or winnowing out (piping) of these loose grains by flowing waters (Sczerban and Urbani, 1974; Galán and Lagarde, 1988).

The role in triggering speleogenesis by generating the “loose sands” has been assigned to rock dissolution by meteoric (Jennings, 1983; Martini, 2000; Wray, 2003; Piccini and Mecchia, 2009) or hydrothermal waters (Zawidzki et al., 1976) through a weathering dissolution process called “arenisation”. Other authors assign importance to microbially-driven alkaline dissolution (Marker, 1976; Barton et al., 2009), or refer to the existence of loose sands in unlithified beds, also produced by dissolution and weathering of aluminosilicates (Aubrecht et al., 2011; 2012). Some authors called in general these processes “phantomisation” (Quinif, 1999; Häuselmann and Tognini, 2005), because weathering predisposes the rock mass for the formation of caves that are afterward opened through piping and mechanical erosion. Nonetheless, all these theories are still under discussion and there is

not yet a clear understanding of the main speleogenetic and morphogenetic factors involved (Sauro et al., 2013a).

The main aim of this thesis is to demonstrate the reliability and the relative importance of each of these weathering processes in the formation of caves in quartzite and quartz-sandstones. In addition, understanding the mechanisms of formation of these underground systems can also give fundamental information on the landscape evolution of the areas where these peculiar forms developed.

1.2 The mechanisms of quartz and silica weathering

1.2.1 Forms of quartz and silica

Different types of crystalline and non-crystalline silica (SiO_2) are known, all potential sources of dissolved silica in water. In the conditions of low T and P present at the Earth surface the α-quartz is the most common and stable form of silica, constituting the most abundant mineral also in sedimentary rocks like sandstones. The other forms of crystalline silica (β-quartz, tridymite, cristobalite, coesite, etc.), are typical of high metamorphic and magmatic rocks and represent only a small fraction of the total silica found in surface conditions. On the other hand, non-crystalline forms of silica, normally referred to as "amorphous silica", are common on the Earth surface. Besides silica glasses (mainly of volcanic origin) and chemically precipitated amorphous silica cements, the most common non-crystalline forms are hydrated mineraloids like opal (in the form of opal-A, opal-C and opal-CT) (Siever, 1957). These forms of silica are normally made up of microorganism skeletons, like diatomea, radiolaria, or microbial tubular casts constituting silica biothems.

However, in the study of quartz weathering, the only silica species of real interest are ordinary α-quartz, amorphous silica and opal.

1.2.2 Characteristics of the silica-water system

Dissolved compounds of silica are present in all natural waters, but most often they are released not from direct solution of quartz but by the weathering of the numerous silicate minerals which are commonly more soluble than pure silica (Henderson, 1982). Nevertheless, also quartz and amorphous silica can be dissolved in form of monomolecular orthosilicic acid H_4SiO_4 and in smaller amounts in polycyclic acids, most of them colloidal (Krauskopf, 1956). The reaction with water is the following:

(I) $$SiO_{2(s)} + 2H_2O_{(l)} \rightarrow H_4SiO_{4(aq)}$$

The orthosilicic acid H_4SiO_4 is almost undissociated and the effects of complexion, hydrolysis and polymerisation are negligible at neutral pH. The ionisation of the orthosilicic acid only starts at basic pH (Harman, 1927; Govett, 1960), and at increasing alkaline conditions, with pH>8-9, it undergoes up to four consecutive dissociations, significantly increasing the amount of quartz which can be dissolved (Harman, 1927; Krauskopf, 1956; Govett, 1960; Ford and Williams, 2007), releasing H^+ ions according to the following reactions:

(II)

$$H_4SiO_{4(aq)} \rightarrow H_3SiO_4^- + H^+$$
$$H_3SiO_{4\,(aq)}^- \rightarrow H_2SiO_4^{2-} + H^+$$
$$H_2SiO_4^{2-}{}_{(aq)} \rightarrow HSiO_4^{3-} + H^+$$
$$HSiO_4^{3-}{}_{(aq)} \rightarrow SiO_4^{4-} + H^+$$

Rimstidt (1997) experimentally studied the dissolution constant of quartz in the range of temperatures 0-300° C in pure water, surface pressure and neutral pH. His constant of dissolution of quartz is the following:

(III) $$\log K = -0.0254 - (1107.12 / T_{kelvin})$$

The solubility of quartz increase with temperature, on the contrary to what happens for calcite and dolomite (Fig. 1A). However experiments of silica dissolution in low temperature waters (below 25°) are very few because of the extremely long times needed to reach the equilibrium (Tab. 1). Conversely, amorphous silica shows a solubility one order of magnitude higher than quartz and the same increasing T dependence (Rimstidt and Barnes, 1980). Using the Rimstidt (1997) constant the saturation at nearly neutral pH is 8.7 mg L^{-1} for quartz in pure water at 17 °C (the average temperature of water in tepui caves), and around 100 mg L^{-1} for amorphous silica.

Author	year	mg L^{-1} SiO_2
Van Lier et al.	1960	10.8
Siever	1962	10.8
Morey et al.	1962	6.0
Rimstidt and Barnes	1980	6.6
Fournier and Potter	1982	7.0
Johnson et al.	1992	6.1
Manning	1994	6.0
Rimstidt	1997	11.0
Verma	2000	8.6

Tab. 1 Quartz solubility in pure water at 25° calculated with experimental tests.

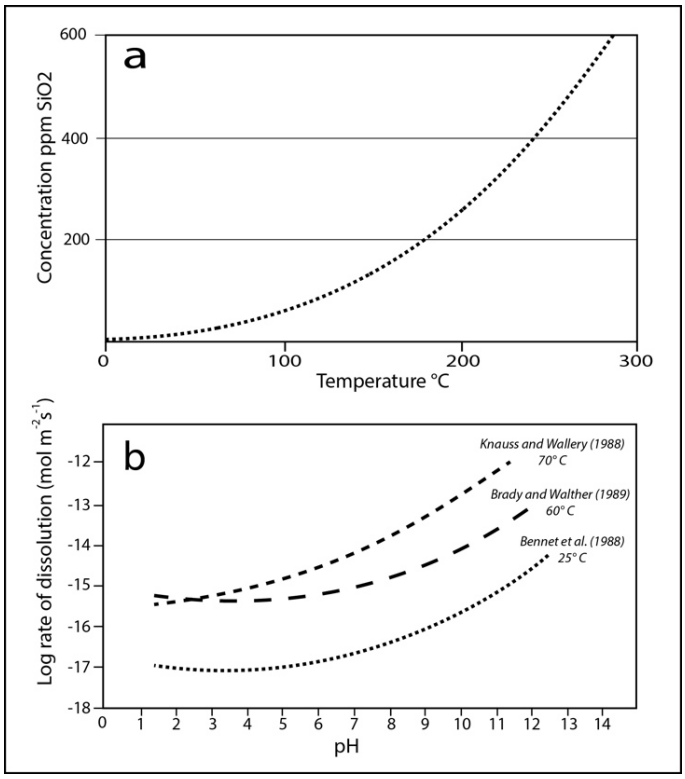

Fig. 1. a) Dependence of quartz solubility from temperature (Rimstidt, 1997. b) Dependence of quartz dissolution rate on the pH at different temperatures (Bennet et al., 1988; Knauss and Wolery, 1988; Brady and Walther, 1989).

Manning (1994) studied the influence of pressure on quartz solubility in pure water showing that the effect of this parameter on dissolution is almost negligible in epigenic or close- surface conditions. On the other hand, the surficial energy can influence the solubility, with noticeable increases for particles less than 1 µm in diameter (Iler, 1958; Stumm and Morgan, 1981).

The rate of quartz dissolution (k+) can be extremely low and depends mainly on temperature and pH of the solution (Bennet et al., 1988; Rimstidt and Barnes, 1980). The k+ values for quartz were determined measuring dissolution far from equilibrium in laboratory, obtaining values included between $1 \cdot 10^{-12}$ and $1 \cdot 10^{-13}$ mol m^{-2} s^{-1} at 25 °C in the pH range close to neutrality (Bandstra et al., 2008). Amorphous silica dissolves at a rate approximately ten times faster than quartz under comparable conditions (Brantley, 2008). The dissolution rate both for quartz and amorphous silica increases abruptly (up to four orders of magnitude) for values of pH higher than 9, because of the dissociation reaction described in formula II (Fig. 1B).

1.2.3 Influence of inorganic and organic cations

By now, it is well demonstrated that the presence of inorganic cations in the solution has a significant influence on the dissolution kinetics of quartz. Dove and Elston (1992) and Dove and Rimstidt (1994, and references therein) showed that adding low concentrations of alkali cations (of both groups IA and IIA) may enhance the dissolution rates and solubility of quartz with cation-specific effects. This effect increases with the following sequence of inorganic salts: $MgCl_2$<$CaCl_2$=LiCl=NaCl=KCl<$BaCl_2$.

Dove and Nix (1997) demonstrated that Ba^{2+} has the greatest quartz dissolution rate-enhancing effect above all other cations: a 0.005 molal Ba^{2+} solution enhances the dissolution rates and solubility of quartz as much as forty times compared to deionized water in a range between 20° and 200°C in near neutral-pH solutions. This factor can be really important in natural systems, especially in hydrothermal waters.

1.2.4 Influence of organic compounds and microbial activity

The biological activity and the related organic products can have an important influence on quartz weathering, through chemical processes (with chelate effects or modifying the pH through production of acids or fixing nitrogen) or physical effects (binding together thin particles and therefore increasing the surficial energy or retaining the water in the soil increasing the time of rock-water interaction; Drever, 1994).

Silverman and Munoz (1970) showed evidences that quartz can be chemically attacked by citric acid produced by fungi, but also by other organic acids produced by lichens. However, there is still not a clear understanding on the real effects of these organic compounds in quartz solubility, because of the great difficulties to set up reproducable experiments due to the problems of filtration of organic acid rich waters. Siever (1962) didn't found any increase of quartz solubility in organic acids produced in peat bogs, while Beckwith and Reeve (1964) and Surdam and MacGowan (1987) demonstrated that at least an increase in the solution rate is evident.

Bennet et al. (1988) and Bennet (1991) performed several experiments in aqueous solutions at 25° C with organic acids, asserting that in these experiments the oxalic, citric and salicylic acids significantly increase the solubility and dissolution rate. This effect seems to be more effective at pH between 5 and 7 (with values of dissolution rate almost ten times higher than in pure water), while it is almost insignificant at pH 3. On the contrary Fein and Hestrein (1994) experimentally observed that the complexation of quartz with the ossalic acid is not strong enough to significantly increase the silica solubility. Drever (1994) suggested that the overall influence on silicate weathering by acids complexion is probably moderate, with the exception of the microenvironments close to fungi hyphae and roots.

The role of bacteria in the weathering processes is still not well known. Barton et al. (2009) suggested that the role of nitrogen fixing bacteria could have a primary role in increasing the pH in the microenvironment and therefore the solubility, but conditions of high pH in natural settings at the microscale are still to be demonstrated. Hiebert and Bennett (1992) showed that quartz grains colonized by bacterial communities are subject to higher weathering rates respect to theoretically obtained values.

1.3 Quartzite and quartz-sandstone weathering

1.3.1 Orthoquartzite and Metaquartzite

Before starting our dissertation it is necessary to distinguish between different types of quartz-rich, sedimentary to metamorphic, rocks whose representative end-members are quartz-sandstone and metamorphic quartzite (Pettijohn et al., 1997). Orthoquartzite (Fig. 2A) is a sedimentary rock, synonymous of quartz-sandstone or quartz-arenite, meaning that the rock, even if affected by diagenesis and low grade burial metamorphism, preserves the original sedimentary structures, like planar and cross beddings, ripple marks and so on. Quartz-sandstones are the most mature sedimentary rocks possible, and are often referred to as ultra- or super-mature. Most of the time, they represent multicycle sands reworked over and over, even being eroded out of a lithified rock and becoming a brand new sediment and rock. The grains can be cemented by amorphous silica or, more often, if subjected to a certain burial diagenesis, by interlocked syntaxial grain overgrows. The shape of the original grains is still recognizable only under reflected light microscopy. These sedimentary rocks normally contain around 80-90 % of quartz, with only minor amounts of other minerals: feldspars, phyllosilicates, iron hydroxides and traces of resistant minerals like zircons, rutile and magnetite.

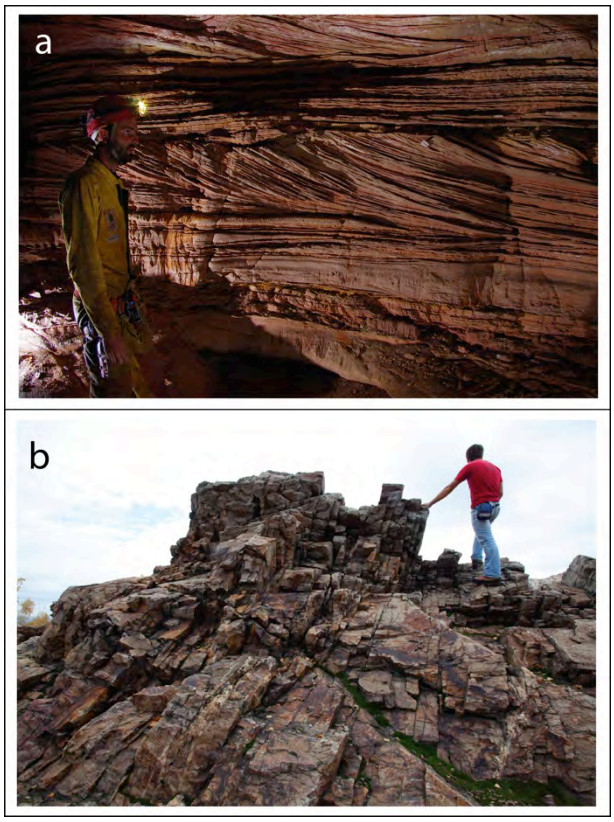

Fig. 2 a) Orthoquartzite from the Mataui Formation in the Venezuelan Tepuis: even if affected by low grade metamorphism, the sedimentary structures are well preserved (cross beddings, ripple marks, etc.) (photo V. Crobu). b) A ridge of massive metaquartzite in the Ural district of Sverdlosk (photo F. Sauro).

Conversely, the metamorphic quartzite (Fig. 2B), or metaquartzite, is an entirely recrystallized rock derived from an original quartz-sandstone. In this case the original sedimentary structures are completely cancelled, while metamorphic streaks and lenses can appear. The conditions of P-T could have been so high that all the other minerals migrate and leave an almost pure 99% quartz-composed rock with a glassy appearance.

Quartzites can be also formed directly by hydrothermal substitution-recrystallisation of other sedimentary rocks (like limestones and dolostones) by silica bearing fluids. The final petrographic textures in these rocks are very similar to those of high grade metaquartzites, with interlocked idiomorphic prisms of quartz, but without anisotropies or signatures of regional stress.

The traditional way to distinguish orthoquartzites from metaquartzites is that the quartz-sandstone breaks up between the grains, whereas metamorphic quartzite fractures across or through them. However the limit between these two typologies is sometimes difficult to address since they grade into one other.

In this thesis I will use the term "quartz-sandstone" for the orthoquartzites, and the former "quartzite" for the metaquartzites and hydrothermal quartzites.

1.3.2 Quartz weathering landscapes and caves of the World

Quartz-sandstone and quartzite karst-like features and caves are documented in all continents, with the only exception of Antartica (Fig. 3). The first documented and most famous areas are surely those of the Gran Sabana Tepuis (Wray, 2000) and the South Africa Eastern Transvaal and Kulk Bay-Table Mountain of Cape Town (Marker, 1976; Martini, 1979). However extended cave systems were documented also in other African states, like in the Chimanimani Park of Mozambique (Aucamp and

Fig. 3. World map showing the main sites where karst like features and cave systems in quartzite and quartz-sandstone were documented: 1) Colorado; 2) Alabama; 3) Gran Sabana's Tepuis; 4) Amazonas Tepuis; 5) Aracà Tepui; 6) Suriname and Guyana tepuis; 7) Mato Grosso; 8) Minas Gerais; 9) Furnas of Paranà; 10) Nigeria; 11) Kaulk Bay-Table Mountain; 12) Eastern Transvaal; 13) Chimanimani Mountains; 14) Ibity Massif; 15) Somalia; 16) Chad; 17) Niger; 18) Kent; 19) Galicia; 20) Iglesiente, Sardinia; 21) Czech Republic and Poland; 22) Central Ural; 23) Hunan, Zhangjiajie Geopark; 24) Thailandia; 25) Kimberley Region; 26) Arnhem Land; 27) Sturt Plateau; 28) Queensland; 29) Sydney Basin.

Swart, 1991), in the Republic of Chad (Mainguet, 1972) and Niger (Bushe and Sponholz, 1988, 1992), and in the inner quartzitic plateaus of Mount Ibity in Madagascar. Also in South America these phenomena are relatively widespread: in Brazil several horizontal and vertical caves are known, even some kilometres long in Minas Gerais, Mato Grosso, Roraima and Paranà states (Bret, 1962; Correa Neto et al. 1994; Dutra, 1996; Hardt et al., 2013). Vertical shafts and collapse dolines are known to exist also in Guyana and Suriname (Sergeart H., pers. commun., 2013). The Australian quartz-sandstone outcrops of the Sydney Basin and Kimberly regions show spectacular surficial karst-like features but only tens to hundred metres long caves (Jennings, 1983). Small caves are known also to exist in Hunan (China; Yang et al., 2012), Thailand (Wray, 1997), in the Urals (Russia; Tsurikin E., pers. commun., 2012), in the western European basins of Poland and the Czech Republic (Vitek, 1979; Zimerman, 1984), in hydrothermal quartzite bodies in Spain and Sardinia (Italy). In the United States few areas with karst-like features in quartz-sandstones were documented, mainly in Colorado and Alabama (Netoff et al., 1995).

Several deep seated voids carved in quartzite were intersected during mine excavations in the Urals chain (Russia; Ermakov, 1978), in Kirghizstan (Leven, 1961; Kornilov, 1978), Colorado (USA; Lovering et al., 1978) and in the Krivoy Rog iron ore basin of Ukraine (Tsykin, 1989).

As in classical limestone karst, caves in quartzites and quartz-sandstones can be divided in two main morphological groups: stratigraphically and tectonically controlled. The first class is characterised by extended horizontal drainage systems, in some case up to few kilometres long. The most important examples of this typology of systems were found in South Africa (Magnet Cave, 2.5 km long; Martini, 1990), Minas Gerais in Brazil (Bromelias Cave, 2.6 km long; Correa Neto et al., 1994), and in the Gran Sabana's Tepuis, where the longest caves of the world in this kind of lithologies were recently discovered (Muchimuk System, 17.5 km; Imawarì Yeuta 15.5 km; Roraima Sur System, 8.5 km). A peculiar case of a stratigraphically controlled system is the one discovered on Sarisariñama plateau, where giant sinkholes more than 250 metres deep and 300 metres of diameter are formed because of the collapse of wide deep horizontal galleries (Zawidzki et al., 1976). A horizontal cave needs to be mentioned also in the Autana Tepui in the Amazonas region. This cave represents a dissected relict of an ancient, probably paleo-phreatic, system now suspended 1300 metres above the surrounding low lands. For this reason some authors suggested that Autana could be some hundred of milions of years old, representing one of the most ancient caves of the world (Galán, 1982).

Conversely, tectonically controlled caves are mainly vertical shafts with a geometric network pattern, developed along fractures to significant depths of hundreds of metres. The most representative systems of this category are those of the Aonda platform in the Auyan Tepui (several shafts up to 380 metres deep, feeding narrow horizontal collectors; Piccini and Mecchia, 2009), but also the deep

shafts of the Aracà Tepui (with Abyss Guy Collet considered the deepest cave of the world in quartz-sandstone with –670 m of depth; Ayub, 2006), the Gruta do Centenario in the Pico do Inflacionado in Brazil (–360 m; Dutra, 1996), and the deep vertical system of Mawenge Mwena in Mozambique (–350; Aucamp and Swart, 1991).

The volumes of these caves are comparable to those of classical karstic caves, with a wide variety of morphologies at all scales: shafts, big chambers, phreatic galleries, vadose canyons and meanders, collapse rooms, maze patterns, sinkholes and resurgences, etc..

Also the superficial karst-like morphologies present great similarities with those of classical karst and in most of cases they can be classified with the same nomenclature, as proposed by Wray (1997).

In general, since over 30 years of speleological researches, it is now evident that the formation of caves in these lithologies is common, and probably many other caves are waiting to be discovered in the extensive quartz-sandstone outcrops of China (Yang et al., 2009) and in the inner tepui massifs of the Amazonas and Rio Negro regions.

Fig. 4. Examples of stratigraphically and tectonically controlled cave systems: A) A canyon controlled by a tectonic fracture in the Aonda Cave System (Auyan Tepui, Venezuela) (poto La Venta); B) A gallery developed along an interstrata in the Akopan Dal Cin System (Akopan Tepui, Venezuela) (photo V. Crobu); C) Gallery developed along an iron hydroxide layer in the Guacamaya Cave (Auyan Tepui, Venezuela) (photo F. Sauro).

1.3.3 The Gran Sabana: the World's finest quartzite karst-like landscape

The Gran Sabana at the humid tropical borders of Venezuela, Guyana, and Brazil is among the most extraordinary landscapes of the world. The most impressive features of the Gran Sabana are the spectacular quartz-sandstone mesas called "tepui", developed in the Precambrian sedimentary rocks overlying the igneous and metamorphic basement of the Guyana Shield. The speleological explorations in this area started in the seventies and in the last twenty years several new cave systems have been discovered in different tepuis, developed in the youngest, around 1,7 By old, member of the Roraima Supergroup (Mataui Formation; Santos et al., 2003). Although many authors

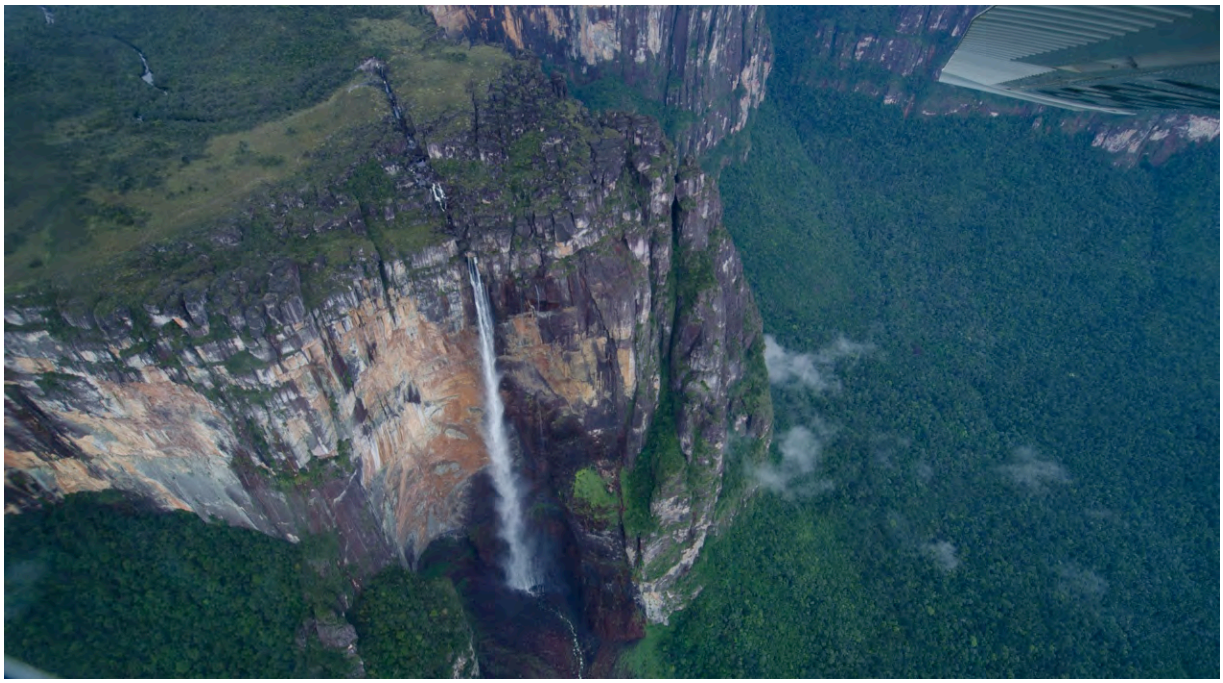

Fig. 5. The Angel fall, Kerepakupai Vená in Pemon indian language, situated on the border of Auyan Tepui, represents the highest waterfall in the world with a drop of 974 m (photo F. Sauro).

discussed the geomorphic modelling and speleogenesis in this area of South America as a combination of exceptional climatic, stable tectonic and geologic factors (see the review of Wray, 1997, but also Wray, 2000; Piccini and Mecchia, 2009; Young et al., 2009), recent explorations have shown that kilometres long karst systems are widespread in these quartz-sandstone massifs.

Actually, around 70 caves have been documented on the tepui massifs (a total of about 75 km of surveys), with the largest systems (Muchimuk System and Imawarì Yeuta) of more than 15 km of development, and volumes of some millions of cubic metres, well comparable to the largest cave systems known in classical limestone karst.

The most impressive morphologic features on the summit plateaus are the big shafts developed along the fractures, called *simas* or *grietas* in Spanish. *Simas* are up to 350 m deep (e.g. Aonda cave), and formed by the progressive collapse of underground voids that developed at the base of enlarged

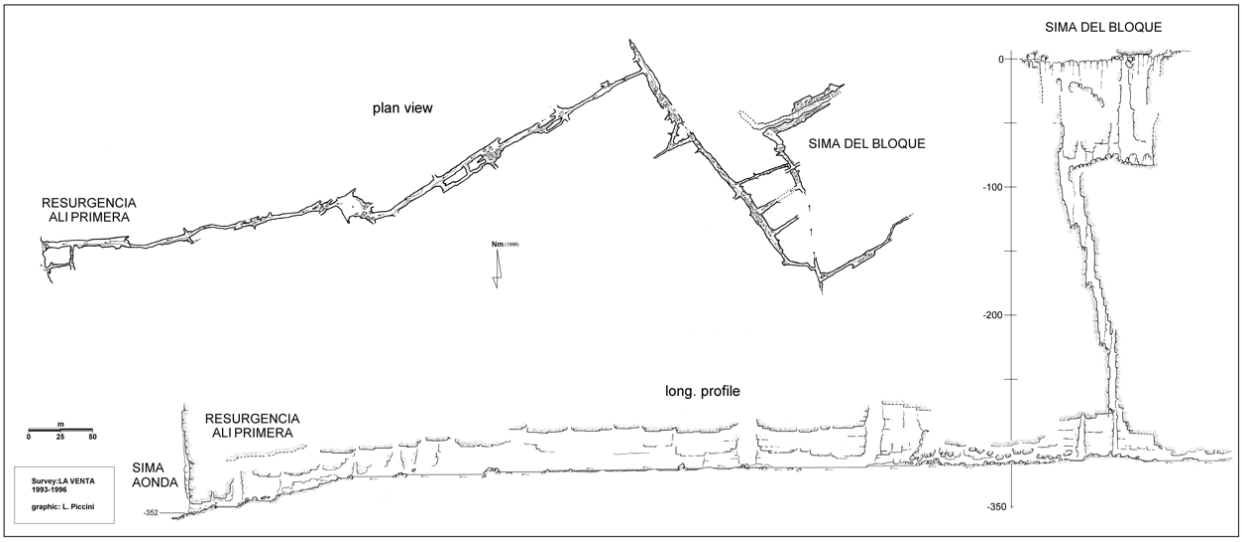

Fig. 6. A typical example of tectonically controlled cave system in the Aonda bench (Auyan Tepui), from the big shaft "grieta" of Sima del Bloque (about 330 meters deep) to the horizontal canyons of the Ali Primera Resurgence.

fractures, often where a coarse-grained quartz sandstone (arenite to rudite) lays on fine and more erodible sandstones and arkoses (Piccini, 1995).

In the inner sectors of the tepui plateaus wide areas of collapses are present, related to the presence of extended horizontal cave systems, only few tens of metres below the surface. The first extended horizontal system was discovered in 2003 on the Roraima Tepui (Brewer Carìas and Audy, 2011), showing a high complexity and the unexpected length of more than 8 km. In the years later two other horizontal, gigantic, caves were discovered, the Muchimuk System (a system of dissected cave more than 17.5 km long; Brewer Carìas and Audy, 2011) and recently the Imawarì Yeuta Cave in the Auyan Tepui (Sauro et al., 2013a). These last two caves reach impressive dimensions, huge galleries and single rooms with volumes of more than 10^6 m^3. These horizontal caves are clearly stratigraphically controlled and an interesting debate is on-going on which appear to be the main factors characterising the guiding layers (Sauro et al., 2013b, 2013b; Aubrecht et al., 2013).

In this thesis we focused our researches on five different cave systems, both stratigraphically and tectonically controlled, in three different tepui massifs (Auyan, Roraima and Chimantha). Some of them were explored by previous expeditions (Aonda Cave System, Roraima Sur; Bernabei, 1993; Brewer Carìas and Audy, 2011) while others were completely unknown before this research (Akopan-Dal Cin Cave System, Guacamaya Cave and Imawarì Yeuta; Mecchia et al., 2009; Sauro et al., 2013).

1.3.4 Corona 'e Sa Craba Cave: an example of hypogenic speleogenesis in quartzites

By the end of the twentieth century the term and concept of "hypogene" speleogenesis had been firmly established in the scientific community interested in carbonate karst. Hypogene speleogenesis

is defined as “the formation of solution-enlarged permeability structures by water that recharges the cavernous zone from below, independent of recharge from the overlying or immediately adjacent surface” (Ford, 2006; Klimchouk, 2007). This kind of speleogenesis involves hydrologic and physical conditions much different from caves carved by meteoric waters (epigenic), like those described for the Gran Sabana tepuis.

Up to now the existence of deep hypogenic voids in quartzites was believed to be common at depth, where the solubility of quartz could be even greater than that of calcite due to the higher temperatures and alkalinity of the solutions, as suggested by Zawidzki et al. (1976), Lovering et al. (1978), Andreychouk et al., (2009), and Klimchouk (2012). However clear and well studied examples

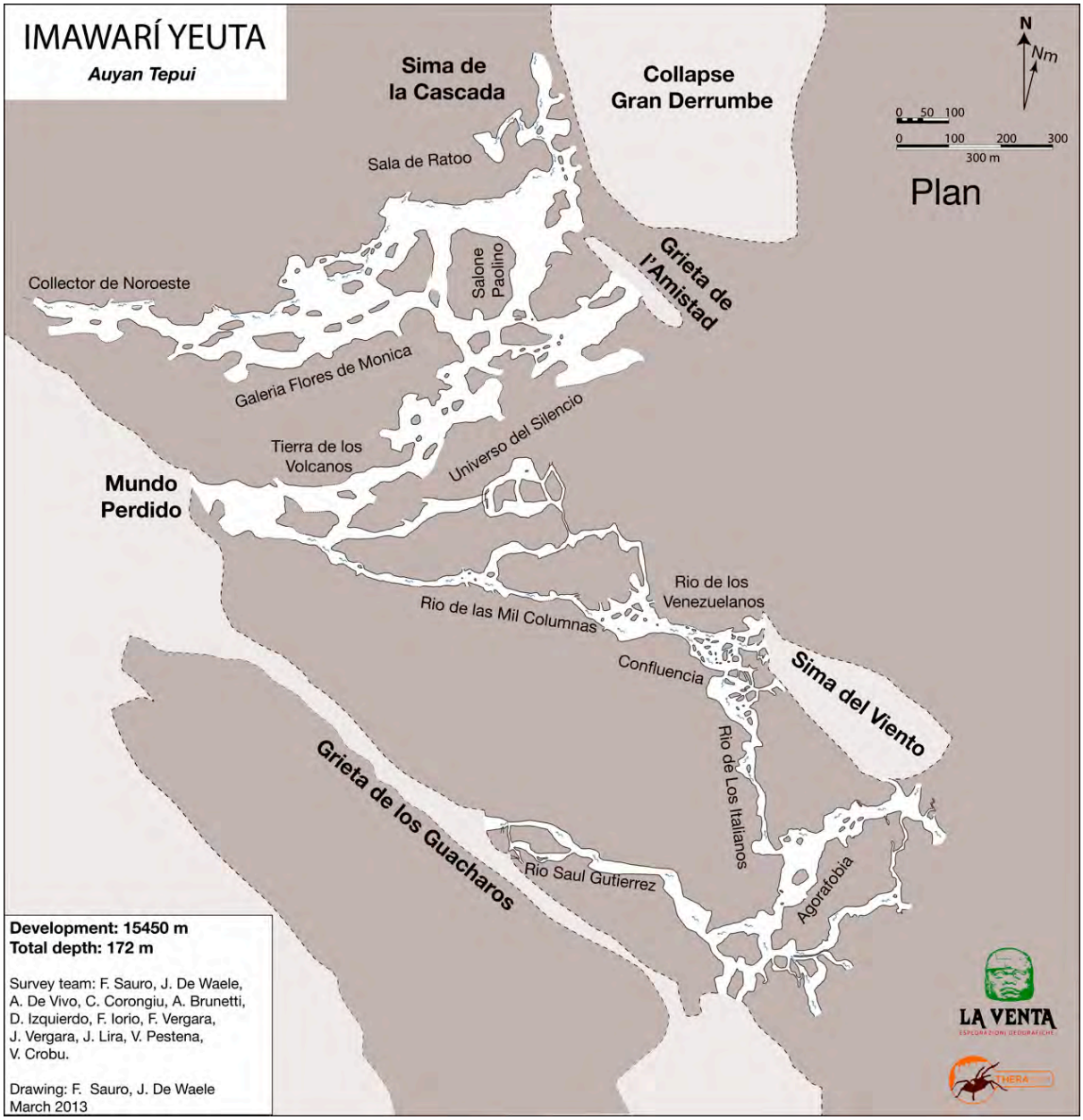

Fig. 7. The plan view of the Imawarì Yeuta Cave System, explored in the frame of this PhD project. With its 16 km of passages surveyed and much more still waiting to be explored this cave is candidate to become the longest quartz-sandstone system known in the World.

of hypogenic caves in quartzites, not the processes leading to the formation of these voids, were never described before.

During this thesis we searched for potential examples of hypogenic speleogenesis in quartzite and we found an exceptional case in the Corona e' Sa Craba Cave in the Mediterranean island of Sardinia. This cave is carved in a wide ridge of quartzite formed after hydrothermal silicification of Cambrian dolostones. The cave presents a large passage, around 150 metres long, up to 30 m wide, showing peculiar boxwork morphologies without signs of erosion by running waters.

The study of this cave and its secondary minerals with a variety of scientific methods (petrographic analyses with SEM, fluid incusion studies, sulphur isotopes, etc.) allowed us to describe for the first time the processes and main factors controlling the dissolution of quartz in thermal waters and to demonstrate that hypogenic speleogenesis in quartzite is a reality.

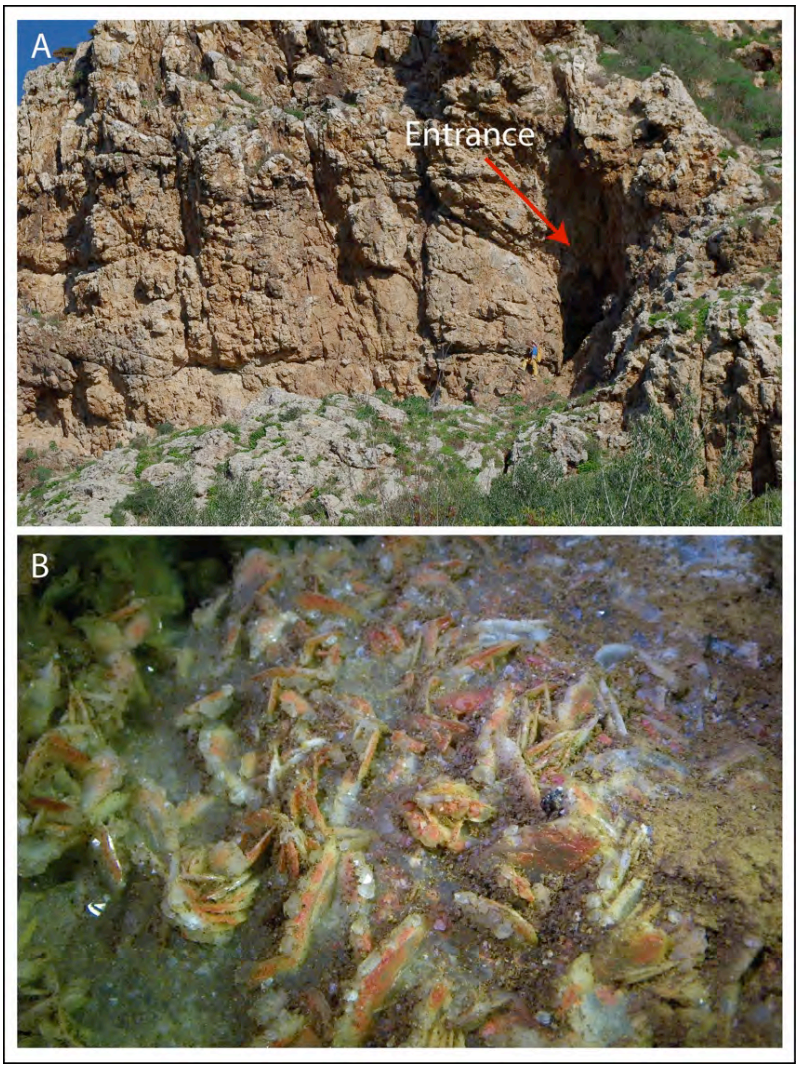

Fig. 8 A) The quartzite of the Corona Sa Craba ridge formed for silicification of Ordovician dolostone along the Barbusi Fault line. B) Barite crystals covered by cinnabar: the secondary minerals association and the sulphur isotopes were used as key-factors to understand the genesis of the cave.

1.4 Objectives and outline of the thesis

The main objectives of this thesis can be resumed as follows:

- Verify the reliability of the arenisation weathering process through modellisation of the main parameters controlling inter-granular dissolution processes in quartz-sandstone and quartzites.
- Quantify the effective silica dissolution in the epigenic cave systems explored in the tepui massifs of the Gran Sabana, in order to differentiate the potentially active weathering mechanisms and to evaluate the effective surface and underground erosion rates.
- Recognise the lithological controls and tectonic factors controlling the cave formation.
- Reconstruct the speleogenetic history of the caves and correlate it with the surrounding landscape evolution.
- Demonstrate that epigenic and hypogenic speleogenesis are both possible in these lithologies, as described for classical limestone caves.
- Identify the minerals found in these cave systems and relate their origin with speleogenesis or secondary processes, or external sources.

To achieve these goals I organised 4 expeditions to the Gran Sabana's tepuis, with the logistic support of La Venta Geographic Exploration Association. The first expedition in 2009 was focused on some caves of the Akopan and Churi Tepui, part of the Chimantha Massif. In 2010 a short expedition documented and explored the Cueva Guacamaya on the Auyan Tepui, while in 2012 we focused on the Roraima Tepui and on new sampling in the Akopan-Dal Cin Cave System. The last expedition in March 2013 discovered a new giant karst system in the North-Eastern Sector of the Auyan Tepui (Imawarì Yeuta, over 20 km of explored passages; Sauro et al., 2013). For the study of potential cases of hypogenic speleogenesis in quartzite I organised also a short expedition to the central Urals (Russia) and a field trip to the Corona e' Sa Craba Cave in Sardinia (Italy).

Fig. 9 A) The missions to the Venezuelan tepuis were charachterised by complex helicopter logistic and high expensive costs. B) Water sampling on the superficial streams of Churì tepui.

During the fieldwork I realised the following scientific researches:

- Sampling of different layers of fresh and weathered quartz-sandstone for petrographic and compositional studies.
- Sampling of secondary minerals for mineralogical and isotopic studies.
- Morphological observations and statistic measurements of peculiar features.
- (only in the Gran Sabana tepuis) Water sampling for geochemical studies on quartz dissolution and silicate weathering.
- (only in the Gran Sabana tepuis) Sampling of quartz- sandstones for fission track analyses and He-He of apatites in order to reconstruct the exhumation history of the area and correlate it to the cave system formation

After the field work, the following analyses were performed (partly directed by myself, others by laboratory technicians) in the laboratories of the University of Bologna, University of Modena, ETH of Zurich (Switzerland), Carleton University (Canada) and University of South Florida (USA):

- Major and minor element water chemical analyses
- X-ray diffraction (XRD) characterisation of rock and mineral samples
- WDS X-ray chemical analyses of rock and mineral samples.
- SEM imaging and EDAX chemical evaluation of the rock and mineral samples.
- Sulphur isotope analyses of sulphur bearing minerals
- U-Th isotopic series analyses for dating of opal speleothems
- Permeability measurements with picnometer
- Raman spectrums on rock thin sections for mineral recognition
- Heavy liquids separation of apatites and zircons

Unfortunately the set of quartz-sandstone samples from the Gran Sabana revealed to be scarce in apatites usable for fission track and He-He thermo-chronological studies. Therefore this research topic was abandoned.
All the other objectives were achieved and addressed in eight articles/manuscripts presented in two sections, the first concerning speleogenesis, while the second related mainly to secondary minerals.

FIRST SECTION: SPELEOGENESIS

Chapter 1

A model simulation of the "arenisation" weathering process in quartz-sandstones: a key factor for speleogenesis and geomorphic evolution in quartz-sandstone environment. Marco Mecchia, Francesco Sauro, Leonardo Piccini, Jo De Waele. *To be submitted to Geochimica et Cosmochimica Acta.*

In this chapter we propose a numerical model useful to understand the timing and the effective reliability of the arenisation process proposed by Martini (1979) to explain the formation of caves and karst-like features in quartz-sandstones. Similar models were widely used for understanding the first phases of speleogenesis in classic limestone caves. The model is based on the different SiO_2 concentration existing between waters in the external film at the surface of an open fracture (renewed and undersatured) and the intergranular porosity water (supposed to be at the saturation point). The chemical potential allows the removal of silica from the rock without significant movement of water. Dissolution causes an increase in porosity in the first layers of quartz grains in a water-filled fracture. When a critical value of porosity is reached in these layers, individual grains can disintegrate and be washed away by the flowing water, boosting the opening of the fracture.
The model addresses all the equations related to the chemical equilibrium of SiO_2, the chemical and physical characteristics of water, the flow rate in the fracture, the porosity of the quartz-sandstone, in two different scenarios (vertical fracture and low dipping layer).
The results are finally compared with field observations and geochemical data from the Gran Sabana region, Venezuela.

Chapter 2

Geochemistry of surface and subsurface waters in quartz-sandstones: significance for the geomorphic evolution of tepui table mountains (Gran Sabana, Venezuela). Marco Mecchia, Francesco Sauro, Leonardo Piccini, Jo De Waele, Laura Sanna, Nicola Tisato. Jesus Lira, Freddy Vergara. *Published in Journal of Hydrology, doi:1 0.1016/j.jhydrol.2014.01.029*

In this chapter we present the most complete set of water chemistry data currently available for the tepui table mountains and their cave systems carved in the quartz-sandstones of the Guyana Shield, in the Bolivar region of Venezuela. Repeated in situ measurements of discharge, pH, electric conductivity (EC), temperature, and SiO_2 in different hydrodynamic conditions (surface streams and

rivers, ponds, subterranean drainages, etc.), coupled with petrographic and chemical analyses of the hostrock, give fundamental information on the weathering processes active on these quartz-sandstone massifs. This research demonstrates that the dissolved silica load derives mainly from direct dissolution of quartz in the underground, while hydrolysis plays only a secondary role. The results are in agreement with previous studies on surface erosion rates from the tepui plateaus and surrounding lowlands and confirms that the arenisation weathering process, recently discredited by previous researches (Aubrecht et al. 2011, 2013), is really active with dissolution playing a primary role in the geomorphic evolution.

Chapter 3

Comment on "Sandstone caves on Venezuelan tepuis: Return to pseudokarst?" by R. Aubrecht, T. Lánczos, M. Gregor, J. Schlögl, B. Smída, P. Liscák, Ch. Brewer-Carías, L. Vlcek, Geomorphology 132 (2011), 351-365. Francesco Sauro, Leonardo Piccini, Marco Mecchia, Jo De Waele. *Published in Geomorphology, 197, 190-196.*

In the recent work of Aubrecht et al. (2011) the presence of "unlithified or poorly-lithified beds" of sands in the quartz-sandstone stratigraphic succession is proposed as a key factor for speleogenesis in the Venezuelan tepuis. In this chapter we observe that in the cited work the geologic history of the region, in terms of sedimentation environment, diagenesis and low grade burial metamorphism, has not been considered. Furthermore, the peculiar "pillar flow" columns that Aubrecht et al. describe as a proof of the unlithification are lacking in many other different cave systems in the same area.
Four critical points are discussed: the burial metamorphism of the Mataui Formation, the significance of the Schmidt Hammer measurements, the cave morphologies, and the role of SiO_2 dissolution. Finally we suggest that weathering, in terms of arenisation, is probably the triggering process in speleogenesis, and there is no need to invoke a differential diagenesis of the sandstone beds.

Chapter 4

The pattern of quartz-sandstone caves: evidences of the arenisation process. Francesco Sauro, Jo De Waele, Leonardo Piccini. *Manuscript to be submitted to Geomorphology*.

A detailed petrographic, structural and morphometric investigation of different types of caves carved in the quartz-sandstones of the "tepui" table mountains allowed to identify the main speleogenetic factors guiding the cave patterns development and the formation of peculiar features commonly found in these caves like funnel shape pillars, pendants and floor bumps. Samples of fresh and

weathered quartz-sandstone of the Mataui Formation (Roraima Supergroup) collected into the caves were characterised through WDS dispersive X-Ray chemical analyses, picnometer measurements, EDAX punctual analyses, SEM and thin sections microscopy observations. In all the caves an alternation of two compositionally different strata was identified: almost pure quartz-sandstones with content of silica over 95 % and high primary porosity (around 4 %), and phyllosilicate-rich quartz-sandstone with contents of aluminium over 10 % and low primary porosity (lower than 0.5 %). Phyllosilicates are mainly pyrophyllite and kaolinite. SEM images on weathered samples showed clear evidences of dissolution on quartz grains with characteristic features at different degree of development, depending on the frailty of the samples. Grain boundary dissolution increases the rock porosity and gradually releases the quartz grains showing that arenisation is a widespread weathering process in these caves. The primary porosity and the degree of fracturing of the quartz sandstone beds result as the main factors controlling intensity and distribution of the arenisation process. Arenisation along the inception horizons or strata-bounded fracture network predisposes the formation of caves in specific stratigraphic positions where the loose sands produced by weathering can be removed by piping, gradually anastomising the open fractures forming braided mazes, geometric networks, or main conduit patterns, depending on the local litological and structural guidances on the weathering process.

In this chapter we clearly demonstrates that all the peculiar morphologies documented in the caves can be easily explained as results of arenisation, which is guided by layers with peculiar petrographic charachteristics (primary porosity, content of phyllosilicates), different grade of fracturation (strata bounded fractures or continuous dilational joints), togever with the hydrologic recharge conditions of the systems (floodwater injection or diffuse infiltration).

Chapter 5

Hypogenic speleogenesis in quartzite: the case of Corona 'e Sa Craba cave (SW Sardinia, Italy). Francesco Sauro, Jo De Waele, Bogdan P. Onac, Ermanno Galli, Yuri Dublyansky, Eleonora Baldoni, Laura Sanna. *Published in Geomorphology*, doi: *10.1016/j.geomorph.2013.12.031*

In this chapter we deal with a case of hypogenic speleogenesis in Corona 'e Sa Craba, a quartzite cave in SW Sardinia. Here the mechanisms of dissolutions and related arenisation are completely different from those described for the Venezuelan quartz-sandstone caves in epigenic settings. The detailed morphologic and petrographic investigation of this cave revealed clear evidence of quartz dissolution morphologies, without signs of mechanical erosion by running waters. On the cave walls, extremely well-developed boxworks of quartz veinlets that project out of the quartzite bedrock argue for active

differential solution processes, probably also in subaerial conditions. Thin section microscopy and scanning electron microscope (SEM) images show pervasive dissolution morphologies, namely pits and notches on quartz crystals causing the deep arenisation of the cave walls.

The study of secondary cave minerals and the sulphur isotopic composition of sulphates and sulphides, coupled with data on fluid inclusion temperatures, allowed reconstructing the peculiar speleogenetic history of this hypogenic hydrothermal quartzite cave.

Corona 'e Sa Craba represents the world's first hypogenic cave in quartzites where the speleogenetic mechanisms have been studied and reconstructed in detail using a variety of modern methods. This study confirms that dissolution of quartz by hot and alkaline fluids at depth can also give rise to large dissolutional porosity in the apparently poorly soluble quartzite rocks.

SECOND SECTION: SECONDARY MINERALS IN THE QUARTZITE CAVE ENVIRONMENT

Chapter 1

Rossiantonite, $Al_3(PO_4)(SO_4)_2(OH)_2(H_2O)_{10} \cdot 4H_2O$, a new hydrated aluminium phosphate-sulfate mineral from Chimanta massif, Venezuela: description and crystal structure. Ermanno Galli, Maria Franca Brigatti, Daniele Malferrari, Francesco Sauro, Jo De Waele. *In American Mineralogist, 98, 1906-1913*.

In this chapter we present the mineralogical, chemical and crystallographic characteristics of a new mineral discovered in the Akopan-Dal Cin Cave System in the Chimantha Tepui. Rossiantonite, ideally $Al_3(PO_4)(SO_4)_2(OH)_2(H_2O)_{10} \cdot 4H_2O$, occurs as small (≤0.15 mm) and transparent crystals in a white to slightly pink fine-grained sand, filling spaces between boulders of weathered quartz sandstone. Associated phases are gypsum, sanjuanite, rare alunite, quartz and micro-spherules of amorphous silica.

Rossiantonite is colourless with a white streak and vitreous luster. The mineral is brittle with irregular to sub-conchoidal fracture and it shows a poorly developed cleavage. Rossiantonite is biaxial and not pleochroic, with mean refractive index of 1.504.

The calculated density is 1.958 g cm^{-3}. Electron microprobe analyses, with H_2O measured by thermogravimetric analysis, provided the following empirical formula based on 28 O apfu: $Al_{2.96}Fe_{0.03}P_{1.01}S_2H_{30.02}O_{28}$. The five strongest lines in the X-ray powder diffraction pattern, expressed as *d* (Å), *I*, (*hkl*) are: 4.647, 100, (210); 9.12, 56, (100); 4.006, 53, (220); 8.02, 40, (110); 7.12, 33, (011).

The crystal structure, refined using 3550 unique reflections to R = 0.0292, is built of PO_4 and AlO_6 polyhedral rings, creating complex chains parallel to **b** by sharing the OH-OH edge belonging to the Al(3) polyhedron. Three symmetrically independent Al sites can be identified, namely: Al(1), Al(2), and Al(3). Tetrahedral sites, occupied by P, share all their apexes with AlO_6 octahedra. Unshared octahedral apexes are occupied by water molecules. Four additional water molecules are placed in between the previously identified chains. Two oxygen tetrahedra, occupied by S atoms, are connected along the chains by means of weak hydrogen bonding. The rossiantonite structure shows similarities with minerals belonging to the sanjuanite-destinezite group.

Chapter 2

Source and genesis of sulphate and phosphate-sulphate minerals in a quartz-sandstone cave environment. Francesco Sauro, Nicola Tisato, Jo De Waele, Stefano M. Bernasconi, Tomaso R.R. Bontognali, Ermanno Galli. *In Sedimentology, doi: 10.1111/sed.12103*.

In this chapter we document the sulphur sources of sulphates and rare sulphate-phosphate deposits (sanjuanite and the newly described mineral rossiantonite) found in the quartz-sandstone tepui caves in south-east Venezuela.
In order to identify the potential sources of the sulphate minerals hosted in the caves we performed: i) chemical analyses on the minerals, host rock and silica biospeleothems present in the caves; ii) Scanning Electron Microscopy (SEM) and iii) stable isotope analyses of S and O of the sulphates.
Our study demonstrates that quartz-sandstone caves of the tepui mountains enclose a peculiar geochemical environment where sulphates come from a marine non sea salt sulphate mixed with terrestrial DMS and microbially reduced sulphur from the forests and peatbogs. The main means of transport of this aerosol is most probably air current accumulating these atmospheric sulphates in specific sites.

Chapter 3

Minerals and silica speleothems of the Guacamaya Cave, Auyan Tepui, Venezuela. Francesco Sauro, Joyce Lundberg, Jo De Waele, Nicola Tisato, Ermanno Galli. *Published in Bosak P. & Filippi M. (Eds.), Proceedings of the 16th International Congress of Speleology, Brno, Czech Republic, 21-28 July 2013, vol. 3, pp. 298-304*.

In this chapter we present a mineralogical and morphological characterisation of Guacamaya Cave, one of the longest horizontal caves explored on the Auyan Tepui table mountain. This cave presents

peculiar morphologies, developed along an obvious bed of iron hydroxides and amorphous silica (Banded Iron Formation, BIF) interposed between hard and massive quartzite banks. In the walls around this layer, a variety of opal speleothems, of unusual dimensions and shapes, together with gypsum flowers and crusts have been documented.

The speleogenetic control exerted by the BIF stratum is discussed, and put in relation with the collapse morphologies observed at the surface. An attempt to date the bio-speleothem with the U-Th system shows the difficulties of applying this method to these silica formations, because of post-depositional alteration in this porous material.

References

Andreychouk, V., Dublyansky, Y., Ezhov, Y., Lisenin, G., 2009. Karst in the Earth's Crust: its distribution and principal types. University of Silezia – Ukrainian Institute of Speleology and Karstology, Sosnovec-Simferopol, 72 p.

Aubrecht, R., Lánczos, T., Gregor, M., Schlögl, J., Smída, B., Brewer-Carías, Ch., Vlcek, L., 2011. Sandstone caves on Venezuelan tepuis: Return to pseudokarst? Geomorphology 132, 351-365.

Aubrecht, R., Barrio-Amorós, C.L., Breure, A.S.H., Brewer-Carías, C., Derka, T., Fuentes-Ramos, O.A., Gregor, M., Kodada, J., Kováčik, Ľ., Lánczos, T., Lee, N.M., Liščák, P., Schlögl, J., Šmída, B., Vlček L., 2012. Venezuelan tepuis: their caves and biota. Acta Geologica Slovaca Monograph, Comenius University, Bratislava, 168 p.

Aubrecht, R., Lánczos, T., Gregor, M., Schlögl, J., Šmída, B., Liščák, P., Brewer-Carías, Ch. & Vlček, L., 2013. Reply to the Comment on "Sandstone caves on Venezuelan tepuis: Return to pseudokarst?". Geomorphology 197, 197-202.

Aucamp, J.P. and Swart, D.P.R., 1991. The underground movement in Zimbabwe. Bulletin of the South African Speleological Association 32, 79-91.

Ayub, S., 2006. Geology and geomorphology aspects of the deepest quartzite cave in the world. Proceedings of the 10th International Symposium on Pseudokarst, Gorizia, 94-100.

Bandstra, J.Z., Buss, H.L., Campen, R.K., Liermann, L.J., Moore, J., Hausrath, E.M., Navarre-Sitchler, A.K., Jang, J.-H., Brantley, S.L., 2008. Compilation of Mineral Dissolution Rates. In: Brantley, S.L., Kubicki J.D., White, A.F. (Ed.), Kinetics of Water-Rock Interaction, Springer Science, pp. 737-823.

Barton, H., Suarez, P., Muench, B., Giarrizzo, J., Broering, M., Banks, E., Venkateswaran, K., 2009. The alkali speleogenesis of Roraima Sur Cave, Venezuela. In: White, W.B. (Ed.), Proceedings of the 15th International Congress of Speleology, Kerrville, Texas, July 19-26 2009, pp. 802-807.

Bennett, P.C., 1991. Quartz dissolution in organic-rich aqueous systems. Geochimica et Cosmochimica Acta 55, 1781-1797.

Bennett, P.C., Melcer, M.E., Siegel, D.I., Hassett, J.P., 1988. The dissolution of quartz in dilute aqueous solutions of organic acids at 25°C. Geochimica et Cosmochimica Acta 52, 1521-1530.

Bernabei, T., Mecchia, M., Pezzolato, P., Piccini, L, Preziosi, E., 1993. "Tepuy '93: ancora Venezuela!". Speleologia, Rivista della Società Speleologica Italiana 29, 8-23.

Beckwith, R.S., Reeve, R., 1964. Studies on soluble silica in soils. I. The sorption of silicic acid from soils. Australian Journal of Soil Research 2, 33-45.

Bret, M.L., 1962. Les Fumas de Vila-Veilha (Brasil). Spelunca 2(3), 27-30.

Corrêa Neto, A.V., Anisio, L.C.C., Brandão, C.P., 1994. Um Endocarste Quartzitico na Serra do Ibitipoca, Sudeste de Minas Gerais. An. VII Simposio Geologico Minas Gerais, 12, 83-86.

Brewer-Carías, C., Audy, M., 2011. Entrañas del mundo perdido. Charles Brewer-Carías (Ed.), Caracas, 290 p.

Doerr, S. H., 1999. Karst-like landforms and hydrology in quartzites of the Venezuelan Guyana shield: Pseudokarst or "real" karst? Zeitschrift für Geomorphologie 43, 1-17.

Dove, P. M., 1999. The dissolution kinetics of quartz in aqueous mixed cation solutions. Geochimica et Cosmochimica Acta 63(22), 3715-3727.

Dove, P.M., Elston, S.F., 1992. Dissolution kinetics of quartz in sodium chloride solutions: analysis of existing data and a rate model for 25°C. Geochimica et Cosmochimica Acta 56, 4147-4156.

Dove, P.M., Nix, C.J., 1997. The influence of the alkaline earth cations, magnesium, calcium, and barium on the dissolution kinetics of quartz. Geochimica et Cosmochimica Acta 61(16), 3329-3340.

Drever, J.I., 1994. The effect of land plants on weathering rates of silicate minerals. Geochimica et Cosmochimica Acta 58, 2325-2332.

Dutra, G., 1996. Geologia Informal da Região do Pica do Inflicionado. O Carste 8(3), 56-57.

Ermakov, N.P., 1958. Genetic basis for classification of the deposits of crystal-optic raw materials. Memoirs of VNIIP, T.2, V.1, 5-12. (In Russian).

Fein, J.B., Hestrin, J.E., 1994. Experimental studies of oxalate complexation at 80°C: Gibbsite, amorphous silica, and quartz solubilities in oxalate-bearing fluid. Geochimica et Cosmochimica Acta 58, 4817-4829.

Ford, D.C., Williams, P., 2007. Karst Hydrogeology and Geomorphology. Willey & Sons, 562 p.

Fournier, R.O, Potter, R.W., 1982. An equation correlating the solubility of quartz in water from 25° to 900°C at pressures up to 10,000 bars. Geochimica et Cosmochimica Acta, 46, 1969-1973.

Galán, C., 1982. Notas sobre la morfologia de la Cueva Autana y algunos comentarios generales sobre las formas pseudocarsicas desarrolladas en cuarcitas del Grupo Roraima, Guyana, Venezuela. Boletin Sociedad Venezolana de Espeleologia 10 (19), 115-128.

Galán, C., Lagarde, J., 1988. Morphologie et evolution des cavernes et formes superficielles dans les quartzites du Roraima. Karstologia 11-12, 49-60.

Govett, G.J.S., 1960. Critical factors in the colorimetric determination of silica. Analytica Chimica Acta 25, 69-80.

Hardt, R., Rodet, J., Ferreira Pinto, S.A., 2013. Karst evolution in sandstone: the Chapada dos Guimarães site, Brazil. in Bosak P. & Filippi M. (Eds.), Proceedings of the 16th International Congress of Speleology, Brno, Czech Republic, 21-28 July 2013, vol. 3, pp. 264-267.

Häuselmann, P. & Tognini, P., 2005: Kaltbach Cave (Siebenhengste, Switzerland): Phantom of the Sandstone? Acta carsologica 34(2), 383–396.

Harman, R.W., 1927. Aqueous solutions of sodium silicates. Journal of Physical Chemistry 31, 616.

Hiebert, F.K., Bennett, P.C., 1992. Microbial control of silicate weathering in organic-rich ground water. Science 258, 278-281.

Iler, R.K., 1955. The colloid chemistry of silica and silicates. Cornell University Press, Ithaca, New York.

Jennings, J.N., 1983. Sandstone pseudokarst or karst? In: Young, R.W., Nanson, G.C. (Eds.), Aspects of Australian Sandstone Landscape. Australia and New Zealand Geomorphology Group Special Publication, Wollongong, pp. 21-30.

Johnson, J.W., Oelkers, E.H., Helgeson, H.C., 1992. SUPCRT92: A software package for calculating the standard molal thermodynamic properties of minerals, gases, aqueous species, and reactions from 1 to 5000 bar and 0°to 1000°C. Comp. Geosci., 18, 899-947.

Klimchouk, A. B., 2007. Hypogene speleogenesis: Hydrogeological and morphogenetic perspective. Carlsbad, NM: National Cave and Karst Research Institute, 106 p.

Klimchouk, A., 2012. Speleogenesis, Hypogenic. In: White, W.B., Culver, D.C., 2012. Encyclopedia of caves. Academic Press. New York: 748-765.

Kornilov, V.F., 1978. The temperature regime of formation of the mercury-antimony mineralization (Southern Kirghizia). In: Ermakov, N.P. (Ed.), Thermobarogeochemsitry of the Earth's Crust. Moscow, Nauka: 155-161. (In Russian)

Krauskopf, K.B., 1956. Dissolution and precipitation of silica at low temperatures. Geochimica et Cosmochimica Acta 10, 1-26.

Leven, J.A., 1961. Problems of origin of optical-quality fluorite from deposits of the Zeravshan-Gissar Mountains. Transactions of The Samarkand University 16, 35-51. (In Russian)

Lovering, T.S., Tweto, O., Loweing, T.G., 1978. Ore deposits of the Gilman District, Eagle Country, Colorado. U.S. Geological Survey Professional Paper 1017, 90 p.

Mainguet, M., 1972. Le Modelé des Grès. Institut Géographique National Paris, 657 pp.

Manning, C.E., 1994. The solubility of quartz in H2O in the lower crust and upper mantle. Geochimica et Cosmochimica Acta 58, 4831-4839.

Marker, M.E., 1976. Note on some South African pseudokarst. Boletin Sociedad Venezolana Espeleologia 7(13), 5-12.

Martini, J.E.J., 1979. Karst in Black Reef quartzite near Kaapsehoop, Eastern transval. Annals of South African Geological Survey 13, 115-128.

Martini, J.E.J., 1985. Les phénomènes karstiques de quartzites d'Afrique du Sud. Karstologia 9, 45-52.

Martini, J.E.J., 1990. Magnet: a large quartzite cave system in the Eastern Transvaal. Bulletin of the South African Speleological Association 31.

Martini, J.E.J., 2000. Dissolution of quartz and silicate minerals. In: Klimchouk, A.B., Ford, D.C., Palmer, A.N., Dreybrodt, W. (Eds.), Speleogenesis. Evolution of karst aquifers. National Speleological Society, Huntsville: 452-457.

Martini, J.E.J., 2004. Silicate Karst. In: Gunn, J. (Ed.), Encyclopedia of Caves and Karst Science. Fitzroy Dearborn, London: 1385-1393.

Mecchia, M., Sauro, F., Corongiu, C., Crobu, V., 2009. Speleological explorations in the Chimanta massif quartzites (Gran Sabana, Venezuela). Supplement to Kur magazine 12, 16 p.

Morey, G.W., Fournier, R.O., Rowe, J.J., 1962. The solubility of quartz in water in the temperature interval from 25° to 300°C. Geochimica et C osmochimica Acta, 26,1029-1043.

Netoff, D.I. and Shroba, R.S., 1993. Giant weathering pits in the Entrada Sandstone, Southeastern Utah: preliminary findings. Geological Society of America Abstracts, 255: 98.

Pettijohn, J., Potter, P.E., Siever, R., 1987. Sand and Sandstone. Springer, Berlin, 553 p.

Piccini, L., 1995. Karst in siliceous rock: karst landforms and caves in the Auyán-tepui massif (Est. Bolívar, Venezuela). International Journal of Speleology 24, 41-54.

Piccini, L., Mecchia, M., 2009. Solution weathering rate and origin of karst landforms and caves in the quartzite of Auyan-tepui (Gran Sabana, Venezuela). Geomorphology 106, 15-25.

Quinif, Y., 1999. Phantômisation, cryptoaltération et altération sur roche nue, le triptyque de la karsti- fication. Etudes de géographie physique 28, 159-164.

Rimstidt, J.D., 1997. Quartz solubility at low temperatures. Geochimica et Cosmochimica Acta 61, 2553-2558.

Rimstidt, J.D., Barnes, H.L., 1980. The kinetics of silica-water reactions. Geochimica et Cosmochimica Acta, 44, 1683-1699.

Santos, J.O.S., Potter, P.E., Reis, N.J., Hartmann, L.A., Fletcher, I.R., McNaughton, N.J., 2003. Age, source, and regional stratigraphy of the Roraima Supergroup and Roraima-like outliers in northern South America based on U-Pb geochronology. Geological Society of America Bulletin 115, 331-348.

Sauro, F., Piccini, L., Mecchia, M., De Waele, J., 2013a. Comment on "Sandstone caves on Venezuelan tepuis: Return to pseudokarst?" by R. Aubrecht, T. Lánczos, M. Gregor, J. Schlögl, B. Smída, P. Liscák, Ch. Brewer-Carías, L. Vlcek, Geomorphology 132, 351-365. Geomorphology 197, 190-196.

Sauro, F., De Vivo, A., Vergara, F., De Waele, J., 2013b. Imawarì Yeuta: a new giant cave system in the quartz sandstones of the Auyan Tepui, Bolivar state, Venezuela. In Bosak P. & Filippi M. (Eds.), Proceedings of the 16th International Congress of Speleology, Brno, Czech Republic, 21-28 July 2013, vol. 2, pp.pp. 142-146 .

Sauro, F., Lundberg, J., De Waele, J., Tisato, N., Galli, E., 2013c. Speleogenesis and speleothems of the Guacamaya Cave, Auyan Tepui, Venezuela. In Bosak P. & Filippi M. (Eds.), Proceedings of the 16th International Congress of Speleology, Brno, Czech Republic, 21-28 July 2013, vol. 3, pp.298-304.

Sczerban, E., Urbani, F., 1974. Formas carsicas en areniscas Precambricas del Territorio Federal Amazonas y Estado Bolivar. Boletin Sociedad Venezolana Espeleologia 5 (1), 25-54.

Siever, R., 1957. The silica budget in the sedimentary cycle. The American Mineralogist 42, 821-841.

Siever, R., 1962. Silica solubility, 0°-200°C, and the diagenesis of siliceous sediments. The Journal of Geology, 70 (2), 127-150.

Silverman M.P., Munoz E.F., 1970. Fungal attak on rock: solubilization and altered infrared spectra. Science 169, 985-987.

Stumm, W., Morgan, J.J., 1981. Aquatic chemistry. Wiley and Sons, 2nd ed., pp. 780.

Surdam, R.C., MacGowan, D.B., 1987. Oilfield waters and sandstones diagenesis. Applied Geochemistry 2, 613-620.

Tricart, J., 1972. The Landforms of the Humid Tropics, Forests and Savannas. Longman. London, 306 p.

Tsykin, R.A., 1989. Paleokarst of the Union of Soviet Socialistic Republics. In: Bosák, P., Ford, D.C., Głazek, J., Horáček, I. (Eds.). Paleokarst: a systematic and regional review, Vidala Academia, Praha, pp. 253-295.

Van Lier, J.A., De Bruyn, P.L., Overbeek, J.Th.G., 1960. The solubility of quartz. Journal of Phys. Chem., 64, 1675-1682.

Vitek, J., 1979. Pseudokarst phenomena in block sandstones in north-east Bohemia. Rozpr. Cesk. Akad. Véd 89(4), l-57.

Verma, M.P., 2000. Revised quartz solubility temperature dependence equation along the water-vapor saturation curve". Proceedings World Geothermal Congress 2000, Kyushu – Tohoku, Japan, May 28 – June 10, 2000, 1927-1932.

White, W.B., Jefferson, J.L., Haman, J.F., 1966. Quartzite karst in Southeastern Venezuela. International Journal of Speleology 2, 309-314.

Wray, R.A.L., 1997a. A global review of solutional weathering forms on quartz sandstones. Earth Science Reviews 42, 137-160.

Wray, R.A.L., 1997b. Quartzite dissolution: karst or pseudokarst? Cave and Karst Science 24, 81-86.

Wray, R.A.L., 2000. The Gran Sabana: The World's Finest Quartzite Karst? In: Migon, P. (Ed.), Geomorphological Landscapes of the World. Springer, Dordrecht, pp. 79-88.

Yang, G., Tian, M., Zhang, X., Chen, Z., Wray, R.A.L., Ge, Z., Ping, Y., Ni, Z., Yang, Z., 2012. Quartz sandstone peak forest landforms of Zhangjiajie Geopark, northwest Hunan Province, China: pattern, constraints and comparison. Environmental Earth Sciences 65, 1877-1894.

Young, R.W., Wray, R.A.L., Young, A.R.M., 2009. Sandstone Landforms, Cambridge University Press, Cambridge, 314 p.

Zawidzki, P., Urbani, F., Koisar, B., 1976. Preliminary notes on the geology of the Sarisariñama plateau, Venezuela, and the origin of its caves. Boletin Sociedad Venezolana de Espeleologia 7, 29-37.

Zimerman, V., 1984. Pseudokrasove jeskyne u Hradska. Pamatky Prir., 9, 505-506.

FIRST SECTION

SPELEOGENESIS

CHAPTER 2.1

To be submitted to Geochimica et Cosmochimica Acta

A MODEL SIMULATION OF THE "ARENISATION" WEATHERING PROCESS IN QUARTZ-SANDSTONES

Marco Mecchia[1], Francesco Sauro[1,2,], Leonardo Piccini[1,3], Jo De Waele[1,2]*

1) La Venta Esplorazioni Geografiche Association, Via Priamo Tron 35/F, 31100, Treviso, (Italy)
2) Department of Biological, Geological and Environmental Sciences, Italian Institute of Speleology, Via Zamboni 67, 40126, Bologna, (Italy)
3) Dipartimento di Scienze della Terra, Università di Firenze, Via La Pira 4, 50121, Firenze, (Italy)

Corresponding author: Francesco Sauro

Abstract

In this article we propose a numerical model useful to understand the timing and the effective reliability of the arenisation weathering process, used by several authors to explain the formation of caves and karst-like features in quartz-sandstones. Similar models were widely used for understanding the first phases of speleogenesis in classic limestone caves. The model is based on the different SiO_2 concentration existing between continuously renewed and undersaturated waters in the external film at the surface of an open fracture and the intergranular porosity water supposed to be at the saturation point. The chemical potential allows the removal of silica from the rock without significant movement of water. Dissolution causes an increase in porosity in the first layers of quartz grains in a water-filled fracture. When a critical value of porosity is reached in these layers, individual grains can be released and washed away by the flowing water, boosting the opening of the fracture (breakthrough).

The model addresses all the equations related to the chemical equilibrium of SiO_2, the diffusion mechanism, the flow rate in the fracture, the chemical and physical characteristics of water and the porosity evolution in the quartz-sandstone. Two different base scenarios are tested, a vertical fracture with steep hydraulic gradient and a low dipping layer with a low hydraulic gradient. The outcomes of the model, tested with different parameter ranges, clearly show that the main factors controlling the breakthrough times are the primary aperture of the fracture and the initial diffusion porosity of the quartz-sandstone. The silica concentration along the fracture almost never reaches

saturation, even after hundred thousands of years, showing that the extremely slow rate of reaction of quartz is the key-factor in the formation of karst-like features in quartz-sandstone.

Finally, the results are in good agreement with the field data from the Gran Sabana (Venezuela) quartz-sandstone caves, confirming that arenisation is a reliable mechanism well explaining the geomorphologic features and geochemical data found in these and similar geological and climatic settings.

2.1.1 Introduction

"Arenisation" is considered the most important weathering process driving the formation of superficial karst-like features and underground cave systems in quartzite and quartz-sandstone environment (Wray, 1997). In general, the term arenisation describes a process of dissolution acting along the grain boundaries of an arenite-type rock, that progressively increases the porosity until the volume of voids is such that the rock becomes mechanically weak and the grains can be easily washed away by flowing waters.

Even if arenisation is sometimes related to dissolution of carbonate cement (Adamovič et al., 2013), this process is widely active also in Precambrian quartz-sandstone cemented by silica or characterised by interlocked syntaxial quartz overgrowth structure (White et al, 1966; Chalcraft and Pye, 1984; Pouylleau and Seurin, 1985; Doerr, 1999, Piccini and Mecchia, 2009). In this case dissolution involves directly the quartz grains/crystal boundaries. The evidences of dissolution morphologies along grain boundaries in highly quartzose sandstones have been reported by several authors, from the Venezuelan tepui table mountians (Chalcraft and Pye, 1984; Ghosh, 1991), the Sydney and Kimberly regions of Australia (Young, 1988; Wray, 1995), the Black Reef quartzite of South Africa (Martini, 1979), South Wales (Wilson, 1979), and other quartz-sandstone outcrops of the world (Wray, 1997 and references therein). However similar processes are supposed to be active also in deeply buried sandstones having a great importance in the development of secondary porosity in hydrocarbon reservoirs (Hurst and Bjorkum, 1986).

Martini (1979) suggested that dissolution along quartz grain boundaries is due to water undersaturated in silica circulating very slowly through the rock mass (advection). The water would remain undersaturated in silica over a long distance, and therefore remain chemically aggressive, because of the extremely slow dissolution kinetics of quartz (Rimstidt and Barnes, 1980; Wray, 1997). However, fluid advection does not seem to be an effective mechanism of mass transport, given the small size of intergranular pores in the unaltered quartz-sandstone (Pettijohn et al., 1987). As Derjaguin and Churaev (1986) inferred, on the basis of a capillary model, the solute transport from pores smaller than 1000 nm in diameter must be controlled by diffusion. In fact, aqueous diffusion is

generally the dominant transport mechanism within fluid bearing rocks, where diffusion occurs along each mineral grain boundary interconnected with continuous paths (Garrels et al., 1949).

A numerical model for the widening of an individual fracture by arenisation driven mainly by molecular diffusion is here proposed. This model explains the development of karst-like forms (open crevices, corridors, grikes and rock cities) and subterranean conduits (caves) in quartz-sandstones. In this model, we assume that the arenisation process occurs in pure quartz-sandstones, composed of a mosaic of interlocked overgrown grains, along a single fracture in the vadose zone of the aquifer fed by a continuous water flow. We consider the dissolution kinetics of quartz, the diffusion of silica molecules, the rock porosity, and the water flow conditions in the fracture as the main parameters influencing the process. The conceptual model can help us to depict: 1) the propagation of the arenisation process into the fracture walls; 2) the silica concentration all along a flowpath and at the outflow; 3) the fissure enlargement; 4) the time of the arenisation breakthrough; 5) the changes in hydraulic conditions.

Similar models have been widely used to understand the evolution of primary fissures enlarged by pure dissolution in classical carbonate karst (Dreybrodt, 1990; Dreybrodt et al., 1999, 2005; Palmer, 2000; Gabrovšek and Dreybrodt, 2001).

The final aim of this research is to evaluate if the arenisation weathering process can really explain the formation and the development of karst-like features and cave systems that have been found in this lithotype (Wray, 1997) and to understand the timing in which this process could work. The model is applied to estimate the relationship between breakthrough times, initial fissure aperture, fissure length-hydraulic gradient, and the petrographic characteristics of the quartz-sandstone (grain size, initial diffusion porosity). The scenarios tested in the modelling are based on previous researches regarding water geochemistry and geomorphology on karst-like features and caves in the tepui table mountains of the Guyana Shield, considered the world's finest quartzite karst (Wray, 2000).

2.1.2 Model structure

The conceptual model for the enlargement of a fissure, considered as a closed system, through the arenisation mechanism, identifies five stages of development (Fig. 1):

1. *Pre-inception phase:* the quartz-sandstone formation is composed of interlocked quartz grains/crystals having homogeneous texture; the rock pores, equally distributed in the whole rock mass, are filled by still water saturated in silica because of the extremely long time of contact with the quartz grains (Fig. 1A).
2. *Inception stage – plug flow*: a fracture opens in the vadose zone due to tectonic or gravitational stress. Water strongly silica-undersaturated infiltrates from the surface, completely filling the fracture down to an outflow point, under plug flow conditions. Passing through the fissure, the

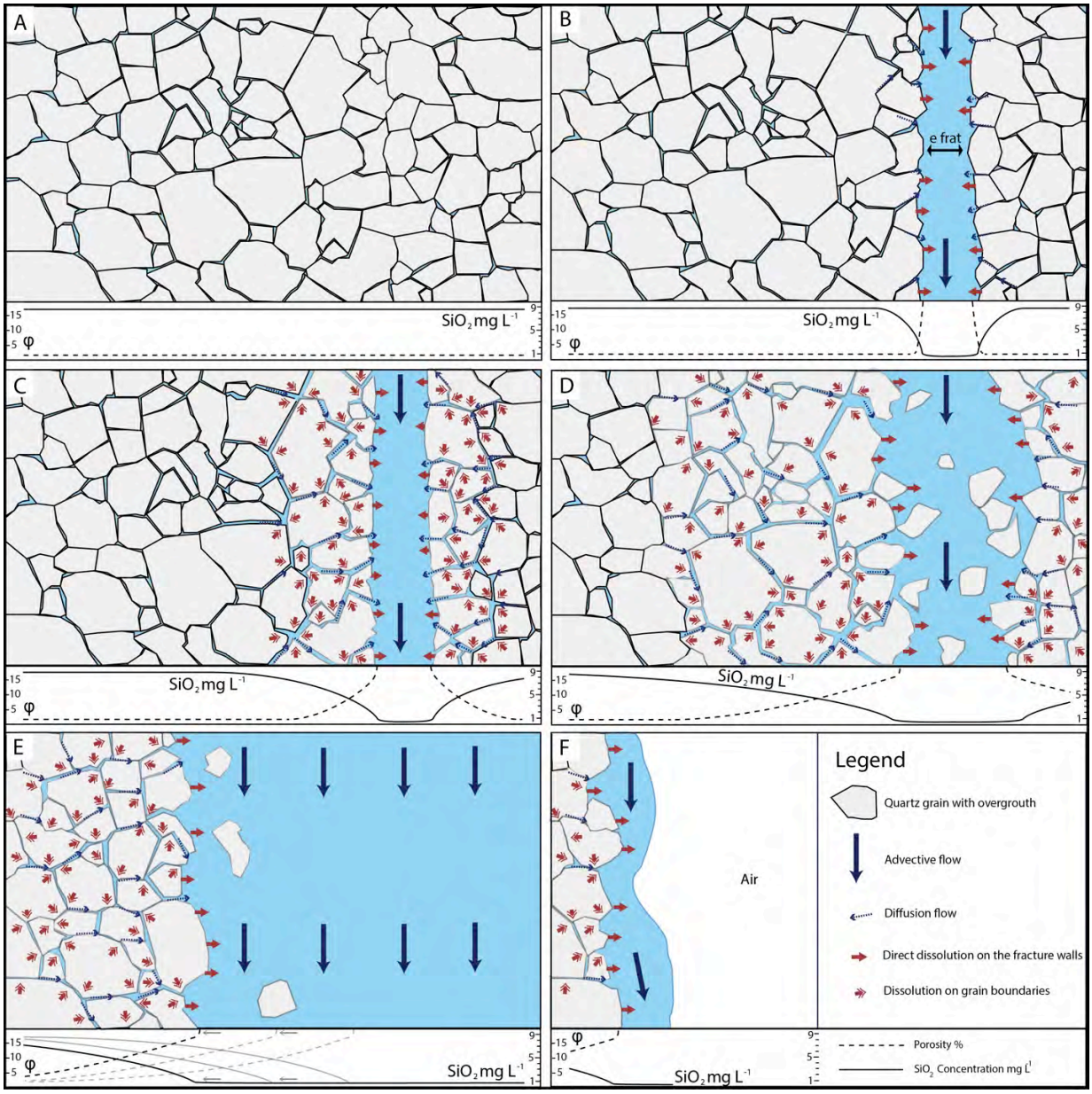

Fig.1. The main phases characterising the model (see the text for a full explanation). A) the initial quartz-sandstone settings, where the intergranular water is satured in silica and the diffusion porosity is around 0.1-1 % in the whole rock mass; B) As soon as the fracture opens, a flow of water undersaturated in silica starts, causing dissolution on the fracture walls and diffusion of silica molecules from the rock pores; C) Because of diffusion, the silica concentration of the intergranular water decreases below the saturation level leading to the start of dissolution between the quartz grains (arenisation), the porosity slowly increase inside the wall; D) When a critical value of porosity is achieved, the grains of the first layer (on the fracture wall surface) are released and washed away by the water flow; E) The porosity profile is maintained and the enlargement becomes stationary; F) the infiltration discharge becomes insufficient to saturate the enlarging fissure and a film of water flows down on the walls of the partially air-filled fracture, changing the hydraulic conditions.

3. solution dissolves quartz so that silica concentration increases between the inflow and the outflow points. Initially, the fissure enlarges only through extremely slow dissolution of the wall surfaces (Fig. 1B). At the same time, the concentration gradient between the still pore water in the rock and water flowing in the fissure activates the diffusion of silica molecules toward the fracture, therefore triggering dissolution (arenisation) on the surfaces of quartz grains inside the rock. The depth of the band of rock involved in the process progressively increases, and a porosity profile develops (Fig. 1C). After a long span of time, the porosity reaches a value at which the loosen grains of the first layer on the fracture walls are released and washed away by the water flow (breakthrough, Fig. 1D).
4. *Stationary enlargement stage – plug flow*: the removal of the grains dislodged from the walls boosts the enlargement of the fracture, strongly increasing the water flow and reducing the concentration of silica in the fissure. The model adopts the assumption that, starting from the breakthrough time, the diffusion/dissolution process propagates in the inner arenised rock at the same rate of the fracture enlargement, establishing a steady-state porosity profile, that is maintained from this time on (stationary enlargement, Fig. 1E).
5. *Stationary enlargement stage - free-surface film flow*: when the infiltration discharge becomes insufficient to saturate the enlarging fissure, air penetrates in the fracture and the infiltration water flows down the fracture walls forming a free-surface film. Nonetheless, the arenisation process continues to propagate inside the rock in a stationary mode, as in the previous phase, even if the hydraulic conditions of flow in the fracture have changed (Fig. 1F).
6. *Deactivation of the fracture*: when, for any reasons, the infiltration water comes to an end, the fracture dries and the arenisation stops. The fracture walls can be affected by evaporation (causing precipitation of silica on the surfaces) but condensation can also occur, and in this case the arenisation process could still go on, but another model is needed to describe these complex conditions.

The single fracture is modelled as a closed system along a pathway distance z, continuous from the water inflow point to the outflow point, such as a spring or an underground cave passage (Fig. 2).
The difference between the inflow and the outflow elevations, H, represents the hydraulic head when the fracture is water saturated. The hydraulic gradient, J, is then calculated as the ratio H/z. Different scenarios with different hydraulic gradients and pathway distances can be tested, with steep and low dipping geometries, as shown in Figure 2. The fracture evolution is studied by using a finite-difference model in which the pathway distance z is divided in small segments i of length Δz, and the iteration of calculation progresses at time increments Δt small enough compared to the velocity of the processes, with temporal frames up to several millions of years.

The fracture has an initial aperture e_0 and length l, where $e_0 \ll l$. In the model, the initial aperture must be wider than the diameter of the quartz grains, otherwise the particles could not be washed out of the fracture. Values of e_0 between 70 µm and 1 mm were used to study the influence of the initial aperture. Fractures with initial aperture as low as 50 µm have often been found (Zimmerman and Bodvarsson, 1996) and 50-1000 µm of e_0 are typically used also in models related to fracture karstification in carbonate rocks (Dreybrodt, 1990; Palmer, 2000).

If the fracture system is continuous from inflow to outflow, the water in the vadose zone flows under the influence of gravity (plug flow). The model calculates the water's mean velocity, v_p, according to the laws proposed by Louis (1974), where the flow shifts from the laminar to the turbulent type depending on the Reynolds number and the fracture roughness, ω [adimensional]. The roughness is defined as the ratio between the height of its asperities and twice the opening of the fracture e (Louis, 1974). In our model, the height of the asperities was hypothesized equal to the grain size, δ, so that $\omega = \delta/(2 \cdot e)$ (Fig. 2).

2.1.3 Theory and equations

The model resolves contemporarily the equations controlling the following processes: 1) the direct dissolution of the rock walls (dissolution flux); 2) the diffusion/dissolution from the rock pores (diffusion flux); 3) The evolution of porosity in the rock mass during the arenisation; 4) the enlargement of the fracture in the inception stage and in the stationary enlargement stage; 5) the change in hydraulic conditions during the fracture evolution (plug flow and free-surface film flow).

2.1.3.1 Dissolution flux and diffusion flux

The model uses the simplified reaction for quartz dissolution $SiO_2 + 2H_2O \rightleftarrows H_4SiO_4$ proposed by Rimstidt and Barnes (1980) for dilute, neutral to slightly acidic solutions in water. Based on transition state theory, the equilibrium constant for the reaction is $K_{eq} = k_{dis}/k_{prec}$, that assumes that the forward and backward rates occur as elementary reactions described by rate constants k_{dis} and k_{prec} (mol m^{-2} s^{-1}), for dissolution and precipitation respectively. The equilibrium constant is calculated according with the data revised by Rimstidt (1997) for the temperature range 0-300°C (Tab. 1). The equilibrium composition can also be expressed as $K_{eq} = m_{sat}$ where m_{sat} is the molal solubility. Therefore, the concentration of silica at saturation in mg L^{-1}, is $c_{sat} = \rho_w \cdot W_{Qtz} \cdot m_{sat}$, where ρ_w (kg L^{-1}) is the density of water, and W_{Qtz} (mg mol^{-1}) is the molar weight of quartz. The value for the dissolution constant k_{dis} for the kinetics of the quartz-water reaction, recalculated by using the Rimstidt (1997) equilibrium constant, depends on the water temperature (Tab. 1) and is, for example, k_{dis} =2.57 10^{-14} mol m^{-2} s^{-1} at 15°C.

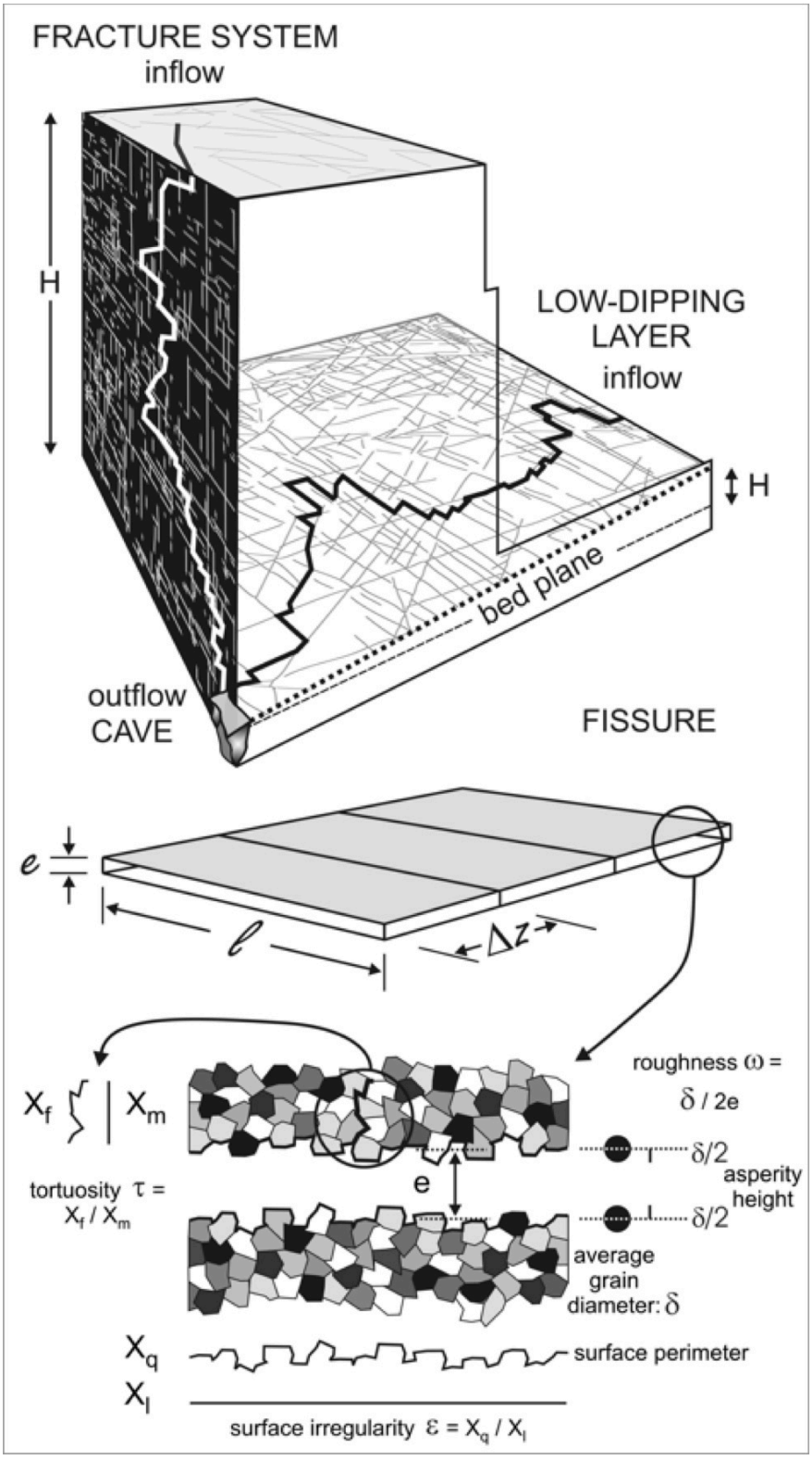

Fig. 2. Geometry of the fracture system. The high angle fracture and the low dipping layer scenarios are shown in the upper picture. The pathway distance from inflow to outflow points, z, is given by the sum of all the segments. Three segments of the fracture are represented in the middle part of the figure. The lowest picture shows a section across the fracture, where the rock is represented by a mosaic of equidimensional grains. Roughness ω, tortuosity τ, and surface irregularity ε are represented.

At every iteration of the model computation, the increment of silica concentration, Δc_i, in the water flow entering into the next segment, $i+1$, of the fracture depends on the contribution of two processes occurring in the segment i: direct dissolution along the fracture walls ($F_{dis,i}$) and dissolution-diffusion in the arenised rock ($F_{dif,i}$).

The rate of quartz dissolution directly on the fracture walls, $F_{dis,i}$ (mol m^{-2} s^{-1}), in a segment i of the fracture, is given by (Rimstidt and Barnes, 1980):

$$F_{dis,i} = k_{dis} \cdot \left(1 - \frac{c_i}{c_{sat}}\right) \qquad (1)$$

where c_i (mg L^{-1}) is the concentration of dissolved silica in the segment i.

The increase of silica concentration due to direct dissolution of the fracture walls, $\Delta c_{dis,i}$ (mg L^{-1}), in the time $T = \Delta z / v_p$ necessary to flow through the segment i, is:

$$\Delta c_{dis,i} = F_{dis,i} \cdot (A_{wall} \cdot \varepsilon) \cdot \frac{W_{Qtz}}{Q_i} \qquad (2)$$

where $Q_i = M_i/(T \cdot \rho_w)$ is the water discharge in the segment i, $M_i = e_i \cdot l \cdot \Delta z \cdot \rho_w$ is the mass of water in the segment i, $A_{wall} = 2\Delta z \cdot l$ is the surface area of the two walls of the fracture, and ε is a dimensionless coefficient that takes into account that the fracture wall surfaces are not flat, but rough and irregular (Fig. 2).

Conversely, the diffusion flux $F_{dif,i}$ depends on the concentration disequilibrium between the water flowing in the fissure, undersaturated in silica, and the water in the intergranular pores of the rock, supposed to be saturated in silica with respect to quartz (8.2 mg L^{-1} at 15°C; Rimstidt, 1997). A slow flow of silicic acid molecules from the rock pores toward the fracture should then start by diffusion.

Several mathematical models have been proposed to describe the diffusion of dissolved molecules through porous media (Anikouchine, 1967; Tzur, 1971; Hurd, 1973; Lichtner, 1988; House et al., 2000). These models assume a quasi-stationary state approximation to coupled mass transport and fluid-rock interaction. In our model, the concentration of dissolved silica in a pore (i.e., in a segment) always decreases in time during the arenisation process, because of the positive difference between the flux of SiO_2 molecules leaving the pore toward the fracture by diffusion and that incoming by diffusion from the opposite side, plus the flux of molecules dissolved on the quartz grain surfaces enclosing the pore. In addition the empty space created as the pore steadily enlarges is filled with water absorbed from the fracture flow. This process should cause a decrease of concentration in the pore, enhancing dissolution and diffusion. In the model the quasi-stationary conditions are also applied to the inception stage, even if this assumption is not strictly valid because a steady-state behaviour has not been reached yet.

The Fick law describes the ideal mass flux of molecular diffusion, F_{dif}, driven by local gradient in concentration:

$$F_{dif} = \frac{\partial m}{\partial t} = -k_{dif} \cdot S \cdot \frac{\partial c}{\partial x} \qquad (3)$$

where $\partial \mathrm{m}$ is the solute mass diffusing in the time unit, ∂t, through a surface of area S, depending on the concentration gradient $\partial \mathrm{c}/\,\partial \mathrm{x}$ in the direction x orthogonal to the surface, and $\mathrm{k_{dif}}$ is the diffusion coefficient. The negative sign indicates that the flux is toward the direction of decreasing concentration. The diffusion coefficient of dissolved silica (uncharged silicic acid H_4SiO_4) has been determined by Applin (1987) as $\mathrm{k_{dif}}$=2.2 10^{-9} m^2 s^{-1} in mildly acidic solutions at 25.5°C; this value is assumed in our model.

However, since the average length of the fluid path through the intergranular pores is longer than a straight line path, the tortuosity, τ, of the diffusing path of molecules through the intergranular pores has to be included in the equation, and the effective diffusion coefficient $\mathrm{K'_{dif}} = \mathrm{k_{dif}}/\tau^2$ replaces the diffusion coefficient $\mathrm{k_{dif}}$ in equation (3). The model adopts the equation proposed by Weissberg (1963), where the tortuosity τ increases with decreasing porosity φ_T,: $\tau = 1 - y \cdot ln(\varphi_T)$. The adimensional parameter y was obtained experimentally by Weissberg as y =0.5. To test the validity of the Weissberg equation, we used the experimental data of porosity and tortuosity given by Oelkers et al. (1996) and found them in good agreement with the equation.

Therefore, the flux of the dissolved molecules of silica through diffusion, $F_{dif,i}$ (mol m^{-2} s^{-1}), in a segment i of the fracture, is given by:

$$F_{dif,i} = \overline{\varphi}_{dif,i} \cdot K'_{dif} \cdot (c_{sat} - c_i) \cdot \sqrt{\frac{K'_{dis}}{K'_{dif}}} \qquad (4)$$

where $\overline{\varphi}_{dif,i}$ is the average diffusion porosity in the rock thickness involved in the arenisation process in the segment i, c_i and c_{sat} are the concentrations of silica in the fracture and at saturation, and

$$K'_{dis} = \frac{\rho_{Qtz} \cdot A_S \cdot k_{dis} \cdot \left(1 - \overline{\varphi}_{dif,i}\right)}{c_{sat}} \qquad (5)$$

It should be noted that K'_{dis} is expressed in s^{-1}, while the effective diffusion coefficient K'_{dif} is expressed in m^2 s^{-1}. Equation (5) draws attention to the importance of knowing the reactive surface area $\mathrm{A_s}$. In fact, the estimation of this parameter is considered the cause of the greatest cumulative error in many kinetic models for natural systems (White and Plummer, 1990). Large differences between field and laboratory weathering rates have often been observed, where laboratory measurement are in general higher than those inferred from field studies (Schnoor, 1990; White and Brantley, 2003). In our model, we use the equation derived by Parks (1990) for the quartz data: $\log(\mathrm{A_s}) = -5.33 - \log(\delta)$, that correlates the size of grains (grain diameter δ expressed in m) with the reactive surface area $\mathrm{A_s}$ (m^2 g^{-1}), obtained by argon and nitrogen BET measurements in

laboratory experiments (the coefficient of the equation was recalculated according to the units of measurement used in our model).

The increase of silica concentration due to diffusion-dissolution from the arenised rock, $\Delta c_{i,dif}$ (mg L^{-1}), in a segment i of the fracture, in the time $T = \Delta z / v_p$ necessary for the water flow to cross the segment, is:

$$\Delta c_{dif,i} = F_{dif,i} \cdot A_{wall} \cdot \frac{W_{Qtz}}{Q_i} \qquad (6)$$

Finally, the concentration of silica c_{i+1} entering into the next segment $i+1$ depends on the contributions of both diffusion and direct dissolution on the walls:

$$c_{i+1} = c_i + \Delta c_{dis,i} + \Delta c_{dif,i} \qquad (7)$$

2.1.3.2 Porosity profile evolution

Because of the diffusion/dissolution arenisation process, the porosity increases with time progressing into the rock mass. The porosity profile that develops through the arenised rock (Fig. 3) plays an important role in the calculation of the diffusion-dissolution flux rate defined above, determining the average diffusion porosity, $\overline{\varphi}_{dif,i}$, in the segment i.

Unfortunately, there are no measured data or cores available to directly observe the supposed porosity profile in quartz-sandstones. Several reports (Sociedad Venezolana de Espeleologia, 1984; Gori et al., 1993; Bernabei et al., 1993; AA.VV., 1994; Rigamonti, 1995) describe the occurrence of a centimetres thick layer of “friable” rock on the walls of the deep shafts of the tepui quartz-sandstone caves. Direct observation of the authors of weathered walls in these shafts showed a minimum softened thickness around 10-15 cm.

In the analogue diffusion/dissolution process of seawater and freshwater sediments, the curve depth vs. porosity/silica concentration obtained from sediment core samples showed a typical shape, in which a 90% decrease in porosity/silica concentration occurred at depths in the sediments of 14 cm (Siever et al., 1965), 13 cm (Anikouchin, 1967), 13-27 cm (Hurd, 1973), 6-32 cm (Robbins and Edgington, 1975).

Taking into account all these data, we propose the following equation for the relation between depth and diffusion porosity (arenisation profile):

$$\varphi_{dif,x} = \varphi_{dif,0} + \left[\left(\varphi_{dif,ext} - \varphi_{dif,0}\right) \cdot exp(m \cdot x)\right] \qquad (8)$$

where $\varphi_{dif,x}$ is the diffusion porosity at depth x from the fracture wall, $\varphi_{dif,0}$ is the diffusion porosity in the unaltered quartz-sandstone, $\varphi_{ext,ext}$ is the diffusion porosity in the most external

sheet of quartz grains, and m is a dimensionless parameter that provides the shape of the curve (Fig. 3). From a qualitative point of view the evolution of the curve calculated with equation (8) well approximate the porosity evolution profiles calculated by Lagneau and van der Lee (2009) for porous media with the reactive transport code HYTEC (Van der Lee et al., 2003)

Regarding porosity, Norton and Knapp (1977) assert that molecular diffusion is strictly controlled also by anisotropies and grain size and is effective only through a small fraction of the total pores. In fact, their laboratory experiments on an unaltered quartzite sample gave a total porosity $\varphi_{\mathrm{tot},0} \approx 4\%$ and a "diffusion porosity", meaning the porosity that is suitable for molecular flux, $\varphi_{dif,0} \approx 0.1\%$. Therefore, the initial diffusion porosity, $\varphi_{dif,0}$, represents only a minor part of the initial total porosity, $\varphi_{tot,0}$. In our model, the difference $\varphi_{tot,0} - \varphi_{dif,0}$ is maintained all over the arenisation process and does not contribute to diffusion-dissolution (Fig. 4).

Martini (1979; 2000) suggested that a loss of 20% of the grain mass is enough to cause the grain

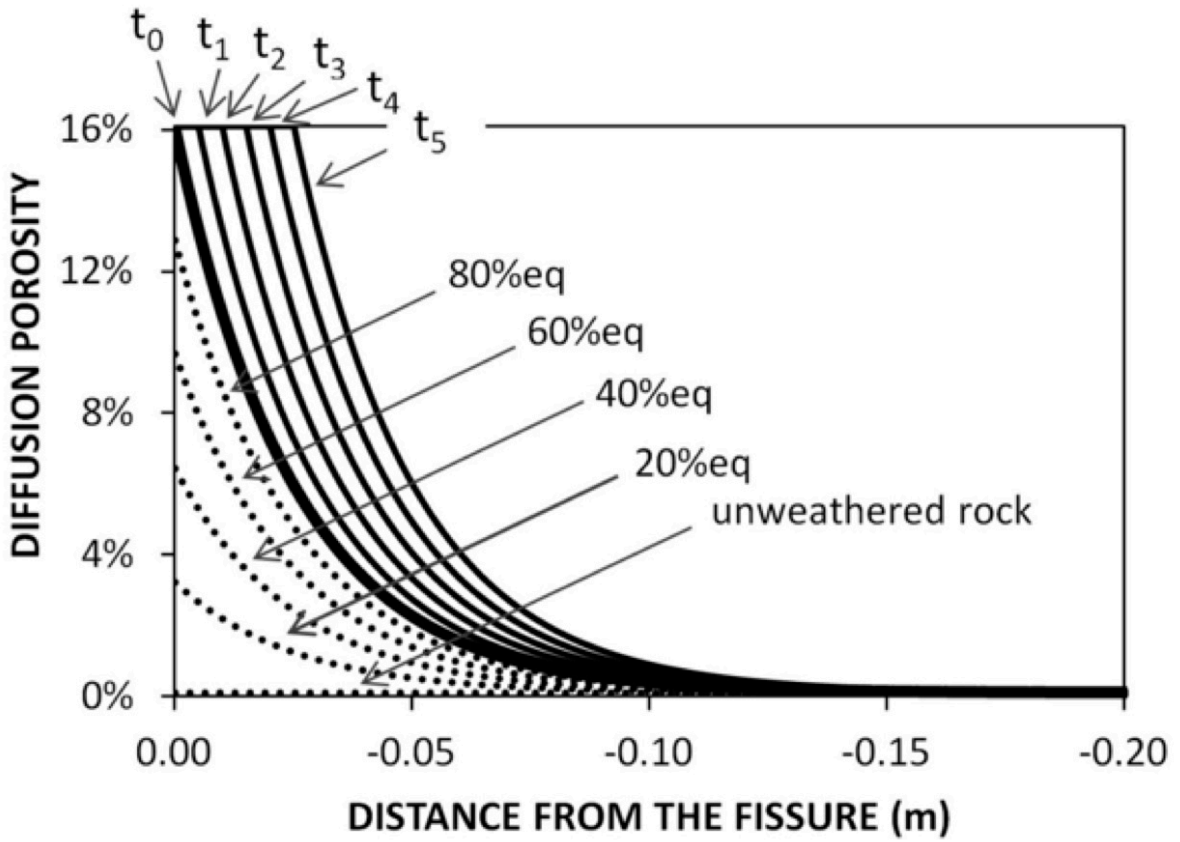

Figure 3. Diffusion porosity evolution according to the model (high angle fracture base scenario). The unweathered quartz sandstone diffusion porosity is $\varphi_{dif,0}$=0.1%. When the arenisation process starts, a porosity profile develops and gradually approaches the steady state condition. Dotted lines represent profiles at 20%, 40%, 60% and 80% of steady state porosity, according with equation (8). When the diffusion porosity in the more external sheet of rock reaches the value $\varphi_{dif,ext,eq}$ (16.1% in this example; thick solid line), the grains get loose, fall by gravity into the fissure and are supposed to be transported away by the water flow. Thin solid lines represent porosity profiles at subsequent steps of simulation, and show the retreat of the fracture wall while the same arenisation profile is maintained (steady state condition). All the curves are calculated according to the same equation (8).

dislodgement from the rock matrix ($\varphi_{tot,ext,eq}$ =20%); this value is assumed in our model. Thus, recalling the value chosen for initial diffusion and total porosities found by Norton and Knupp (1977), the value $\varphi_{dif,ext,eq} = \varphi_{tot,ext,eq} - (\varphi_{tot,0} - \varphi_{dif,0})$ =16.1% is calculated. However, this is only a exemplificative value, because a variation of ±5% in the defined $\varphi_{dif,ext,eq}$ is expected to change around $\pm 10\%$ the breakthrough time, therefore not affecting significantly the final geologic interpretations, given the many simplifying assumptions of the model. As regards the parameter m, a value of 40 has been chosen, so that a 90% decrease in diffusion porosity occurs at a depth of approximately 10 cm in the rock matrix. This value well fits the porosity profile shapes for seawater and freshwater sediments reported in the papers mentioned above.

2.1.3.3 Fracture enlargement

During the inception stage, the enlargement of the fracture, $\Delta e_{dis,i}$, is due only to the direct dissolution on the fracture walls. After every iteration, the volume of rock, $\Delta V_{dis,i}$, dissolved from the fracture walls in the segment i, is calculated as:

$$\Delta V_{dis,i} = \frac{\Delta c_{dis,i} \cdot \Delta z \cdot e_i \cdot l \cdot \Delta t}{T \cdot \rho_{Qtz}} \qquad (9)$$

where ρ_{Qtz} (mg m^{-3}) is the density of quartz.

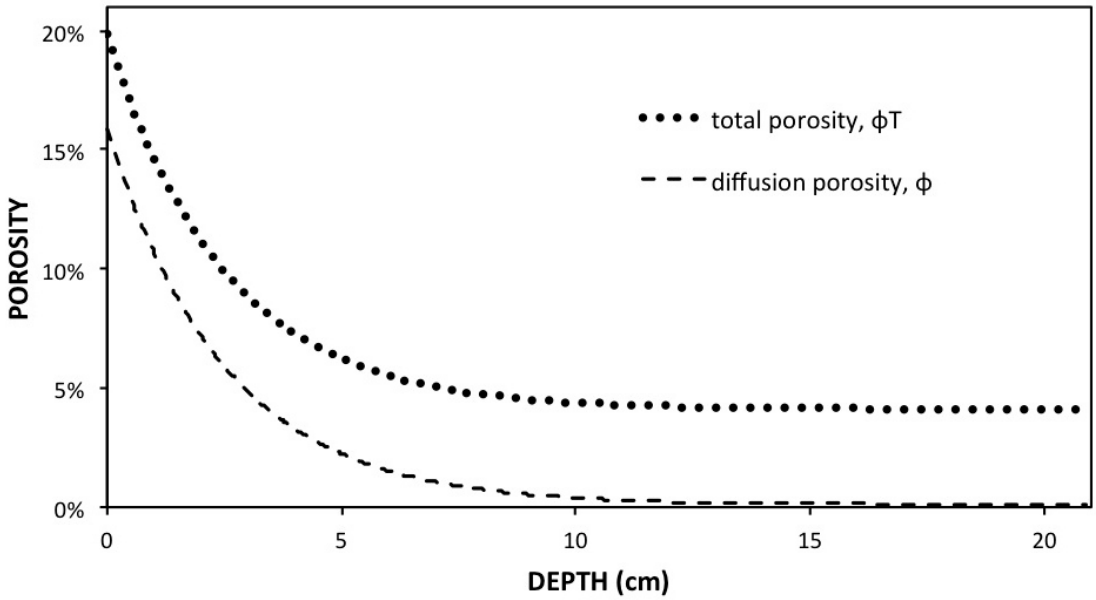

Fig. 4. The porosity steady state profiles hypothesized in the modelling for diffusion and total porosities, based on previous studies in analogue environments. The difference between total porosity and diffusion porosity is maintained in the model during the whole process.

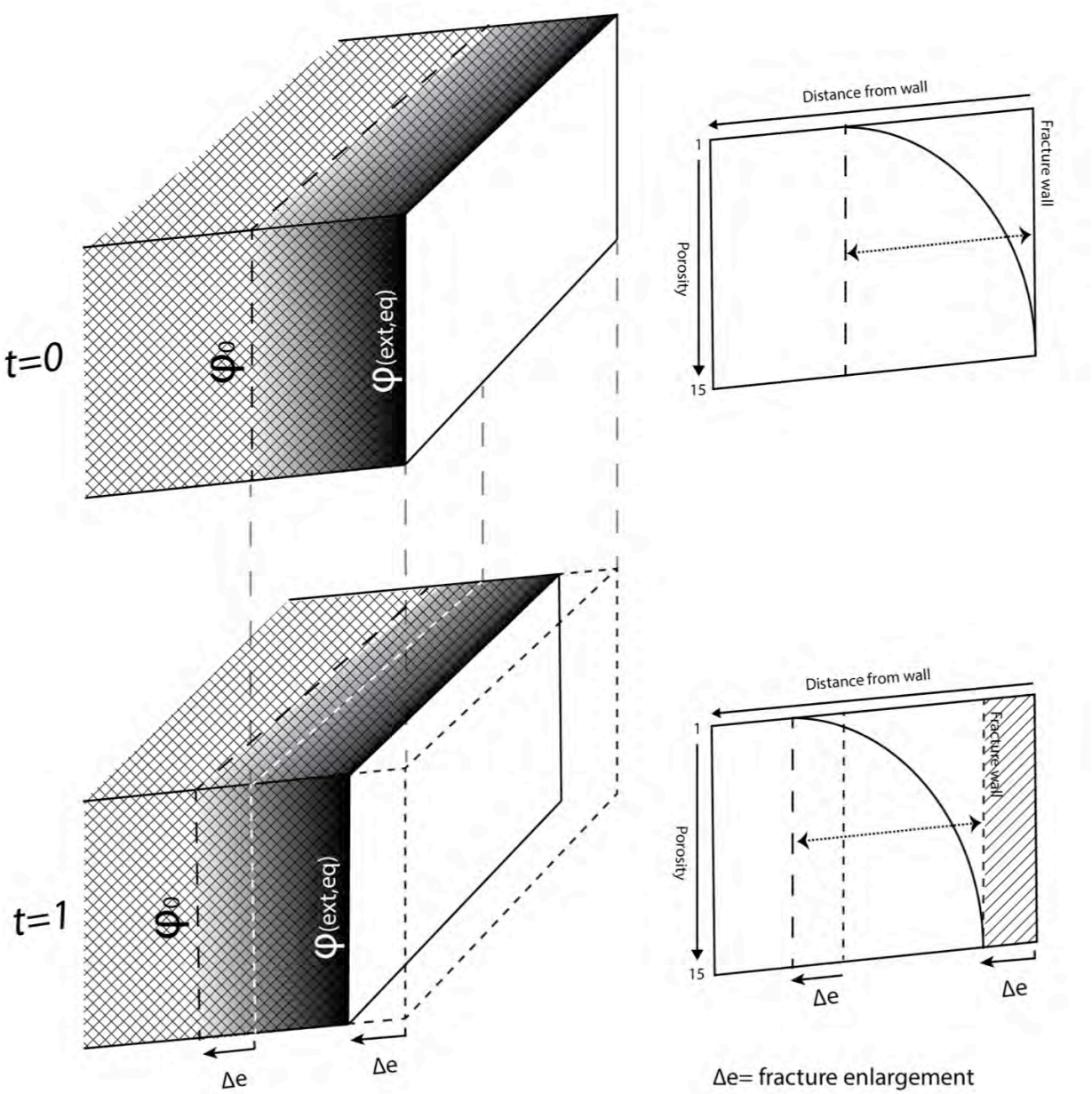

Fig. 5. The enlargement during the stationary phase, when the arenisation profile is maintained constant after every iteration of the calculation.

Thus, the enlargement of the fracture, $\Delta e_{dis,i}$, in the same segment i, is given by:

$$\Delta e_{dis,i} = \frac{\Delta V_{dis,i}}{\Delta z \cdot l \cdot (1 - \varphi_{tot,ext,t})} \qquad (10)$$

where $\varphi_{tot,ext,t}$ is the total porosity, at the time t of the simulation, in the sheet of grains that directly face the fissure. At the fracture opening time: $\varphi_{tot,ext,0} = \varphi_{tot,0}$, where $\varphi_{tot,0}$ is the total porosity in the unweathered quartz-sandstone.

The enlargement mechanism of the fracture in the segment i switches from the type described by equation (9) to that for the arenisation steady state, $\Delta e_{\mathrm{dif,i}}$, when the critical value $\varphi_{\mathrm{dif,ext,eq}}$ is

reached ($\varphi_{\mathrm{dif,ext,eq}}$=16.1% using the assumptions described above, value corresponding to the release of the first layer of grains). This event is defined as the breakthrough, since it boosts the enlargement of the fissure and the velocity of water flow, resulting in a cascade of consequences.
The volume of rock dissolved inside the rock matrix, $\Delta V_{dif,i}$, in the segment i is:

$$\Delta V_{dif,i} = \frac{\Delta c_{dif,i} \cdot \Delta z \cdot e_i \cdot l \cdot \Delta t}{T \cdot \rho_{Qtz}} \qquad (11)$$

In the stationary enlargement stage, $\Delta V_{dif,i}$ is supposed to correspond exactly to the volume of the first grain layer released, and:

$$\Delta e_{dif,i} = \frac{\Delta V_{dif,i}}{\Delta z \cdot l \cdot \varphi_{dif,ext,eq}} \qquad (12)$$

In this equation $\varphi_{dif,ext,eq}$ takes the place of $\left(1 - \varphi_{tot,ext,t}\right)$ in equation (10). The term $\varphi_{dif,ext,eq}$, in fact, represents the rock that is necessary to remove to reach a porosity sufficient to free the grains in the more external sheet of rock.
Our model assumes that, after the breakthrough, the porosity profile is maintained in a quasi-stationary state. When the walls retreat after losing the external grain layers, a temporary disequilibrium appears in the profile and the diffusion/dissolution process gain speed until a new steady state is attained. At this point again the first layer of grains reaches the critical value of $\varphi_{tot,ext,eq}$ and is released from the rock, and the cycle restarts (Fig. 5).
From the breakthrough point onward, the fracture enlargement rate becomes much faster than that of the inception stage, even by several orders of magnitude.
Moreover, the model does not consider the effect in the arenisation process of the advective flow that could start when a certain value of porosity is exceeded. According to Derjaguin and Churaev (1986), pores smaller than 1000 nm in width are controlled by diffusion. To predict the influence of advection, we can consider the unaltered quartz sandstone formed by an idealized array of equidimensional cubic grains, where each grain is delimited by an interconnected pore space system amounting to a certain porosity. Using the base value for our modeling, the equivalent diameter of grains is 140 µm and diffusion porosity is 0.1%. The calculation according to the described geometrical arrangement gives a width of 20 nm for the pores, so that diffusion results as the only possible mechanism for transportation of molecules dissolve in unaltered quartz sandstones. During the arenisation process, the pore size increases while the grain slowly dissolves, and a pore width of 1000 nm is reached when porosity gets to approximately 5%. The porosity profile at stationary condition (Fig. 3) presents values of porosity >5% only in the outer 3 cm thickness of rock. In conclusion, given the high porosity reached in the more external layer of grains, it is probable that in

the steady-state stage, advection can significantly enhance arenisation, speeding up the enlargement process.

Also, the assumption that the difference $\varphi_{tot,0} - \varphi_{dif,0}$ remains constant all over the arenisation process is not very plausible. Probably, as the arenisation process advances most of the pores initially not connected, join the diffusion pore path, and, approaching the end, diffusion porosity comes close to total porosity, further speeding up the process.

Therefore the outcome of this model for the breakthrough time can probably be considered as a maximum time.

After the breakthrough, the quartz grains released from the rock matrix are supposed to be washed away by the water flowing in the fracture. The flow velocity in the fracture is expected to be the main process controlling the particle transport, and the first release of grains in the fracture is quickly followed by a considerable enhancement of water velocity, due to the enlargement of the fissure. However, a reliable prediction of suspended particles transport in a fracture is subject to a considerable degree of uncertainty for several reasons. Therefore this process is not considered here, and the additional effect of mechanical erosion by fast running turbulent water in the fracture is also not considered in the model.

2.1.3.4 Hydraulic conditions in the free film stage

Generally, very soon after the breakthrough the infiltration discharge becomes insufficient to fill the widened fissure (unless a very high discharge is available for infiltration at the inflow point), a water film flows down on one (in the case of a low-dipping surface) or both walls of the fracture, and air fills the space between the film and the opposite fracture wall.

Experimental measurements show that along a descending flow path the water film becomes thinner proceeding downward. All vertical films are naturally wavy, carried downstream by ever-increasing roll waves composed of liquid lumps flowing over a thin substrate (Miller and Keyhani, 2001). However, for the scope of our modelling, very simplified assumptions can be made without significantly invalidating the results of our simulations.

In our model, the downward film flow implies a complete wetting of the fracture surface by a sheet of water. Laminar flow conditions are applied, even if at very high flow rates these assumptions are not always suitable because such films are susceptible to instabilities. It should also be noted that the hydrodynamic film considered in the model is generally much thicker and significantly different from adsorbed films, that are in the orders of a few to several molecular layers (Ghezzehei, 2004). According to Nusselt's theory for smooth laminar flow, the uniform film thickness, h, can be predicted as:

$$h = \sqrt[3]{\frac{3Q_f \cdot \mu}{l \cdot g \cdot cos(\alpha)}} \qquad (13)$$

where α is the fracture inclination angle measured from the vertical, obtained by the same data used for the calculation of the hydraulic gradient J, and Q_f is the water discharge flowing in the film, corresponding to the maximum infiltration discharge Q_{max}, kept constant in our model. A simplified calculation of the mean velocity, v_f, across the thickness of the film, sufficient for the objective of our model, is given by:

$$v_f = \frac{Q_f}{h \cdot l} \qquad (14)$$

This film flows much faster than an equivalent volume of water descending according to the plug flow mode. A free-surface film can occur in small-aperture as well as large aperture fractures, depending on the available water discharge, but the aperture does not directly controls the flow rate (Dragila and Wheatcraft, 2001).

During the free-surface film flow stage, the arenisation still continues with a steady-state profile, and the flux of the dissolved molecules of silica, $F_{dif,i}$, is calculated by the same equation (4) given for the plug flow although the concentration of silica, c_i, is expected to diminish because the flow is faster. The increase of silica concentration due to diffusion-dissolution from the arenised rock, $\Delta c_{dif,i}$, over the time $T = \Delta z / v_f$ necessary for the water to cross the segment is calculated with equation (6), and the volume of quartz dissolved inside the rock, $\Delta V_{dif,i}$, by means of equation (11) substituting e_i with h, and using the new value for $\Delta c_{dif,i}$. The fracture enlargement, $\Delta e_{dif,i}$, is finally calculated by applying equation (12) inserting the new value for $\Delta V_{dif,i}$.

2.1.4 Base scenarios

Many parameter ranges used to depict the studied base scenarios were obtained directly on the field, in the natural settings where karst-like features and caves in quartz-sandstone were found. In our case, the model is based on the boundary conditions of cave development described by several authors for the tepui table mountains (Guyana Shield, between Venezuela and Brazil; Doerr, 1999; Piccini and Mecchia, 2009; Aubrecht et al., 2012). The described characteristics of the ideal quartz-sandstone fit well the petrographic features of the Precambrian Mataui Formation (Reid, 1974), in which the majority of tepui caves and karst-like features develop. Actually, these sandstones are commonly made of more than 90% quartz, showing the interlocked overgrowth grain structure supposed by the model (Fig. 6), with grain sizes ranging between 50-200 µm in diameter.

Porosity analyses on five dried quartz-sandstone samples from the Mataui Formation were performed with an helium picnometer (MicroMeritics-AccuPyc-1330), which measures the porosity by means of gas displacement and the sample volume/gas pressure relationship (Hartikainen et al., 1996). The values obtained for total porosity varied from 1.5 to 6.9 % (mean 4.9 %), showing to be strictly controlled by the presence of anisotropies like cross-bedding or ripple marks. Therefore, accordingly to the observations of Norton and Knapp (1977), in the base scenario of this model the

initial diffusion porosities for quartz-sandstones unaffected by arenisation are tested in a range between 0.1-1%, while $\varphi_{tot,0}$ is considered 4%.

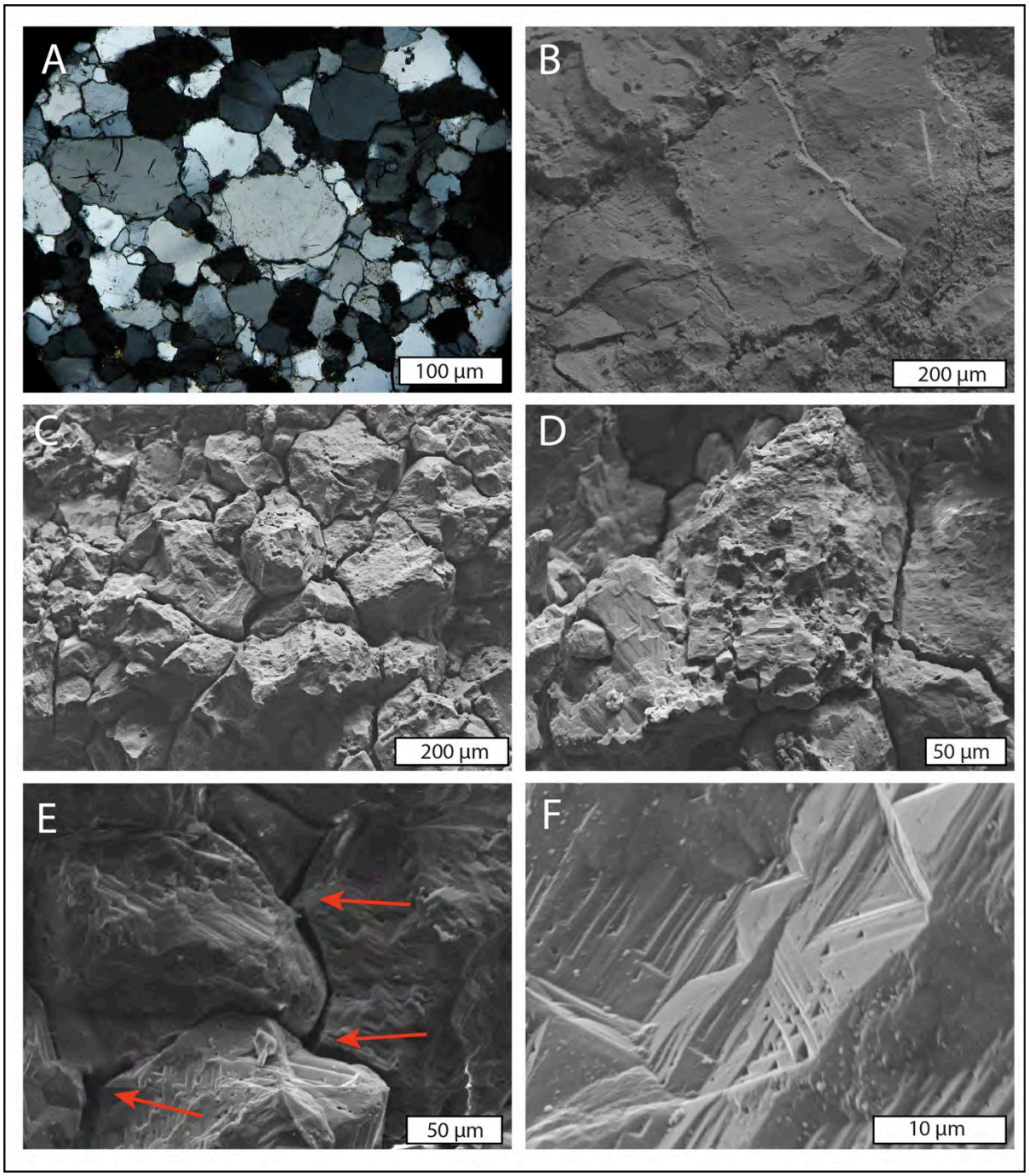

Fig. 6. Examples of quartz-sandstones from the Mataui Formation (Roraima Group, Reid, 1976): A) Thin section of a typical unweathered quartz-sandstone composed almost totally of quartz monocrystalline grains with interlocked overgrowth structures due to burial pressure solution (X Nicols). B) SEM image of an unweathered quartz-sandstone with interlocked quartz grains. C-D) Arenised quartz-sandstone showing the gradual increasing porosity between the grains; E) the dissolution process is more active in high energy sites like triple points and edges (arrows). F) Typical V-shaped pitch and notch features typical of slow dissolution kinetics.

In addition, the average physical and chemical characteristics of water found in the caves of tepuis (Mecchia and Piccini, 1999) are used in the base scenarios: slightly acidic solutions (pH=4-5), extremely low mineralization (electrical conductivity of 15 µS cm^{-2}), a temperature range between 10-20°C, concentration of SiO_2 at the inflow c_0=0.20 mg L^{-1} (mean concentration of stream water measured on the tepui plateaus) (Mecchia and Piccini, 1999).

From the hydraulic point of view, two different base scenarios have been set, referred to a high-angle fracture (with steep hydraulic gradient) and to a low-dipping layer. The Aonda cave system explored in the Auyan Tepui (Mecchia & Piccini, 1999) inspired the high angle fracture base scenario, in which a depth H=300 m was set and a percolating pathway z=1000 m long was supposed to connect many single fissures from inflow to outflow. The percolating pathway in considered at least three times higher than H in the vertical fracture system because in real settings the water is supposed to fallow a non-linear and complex path along the fracture walls, at least in the first phases of the process (see Fig. 2). For the low-dipping layer base scenario, inspired by the near-horizontal cave systems explored in the Churi Tepui (Aubrecht et al., 2012), and in the Auyan Tepui (Sauro et al., 2013b), the same pathway length z=1000 m was used in combination with a depth H=30 m, so that the water flows on a surface with 1.5° of apparent inclination.

At the surface the fracture is imagined, in the base scenario, to cross and partially drain a stream with a mean discharge of 15 L s^{-1}, that represents an arbitrary maximum infiltration discharge rate, Q_{max}. Since at the beginning the fracture will be too narrow to drain all the available discharge, the fissure will be water filled all along its pathway, and the excess of discharge will flow away on the surface. In a later stage of the evolution, the entire discharge is bound to sink into the enlarging fissure, and when the drainage potential of the fracture will exceed the Q_{max} the free-surface film flow phase will start.

2.1.5 Results

The outcomes of the numerical calculations for the base scenarios representing the evolution of a fissure in the vadose zone of a quartz-sandstone aquifer are presented in Figures 7-10.

As expected, the fracture enlargement rate achievable only by dissolution of the fracture walls is extremely low, of the order of less than 0.1 mm in 1 million years. Formation of man-sized conduits in quartz-sandstones by only dissolution mechanism would thus not be possible, even over very long geological time frames. Therefore, the time of arenisation breakthrough, where the enlargement is not only given by direct dissolution but mainly by weakening and loosening of grain layers, is the most important step in the formation of caves and karst-like features in quartz-sandstones.

Similarly to the classical karst fissure modelling (Palmer, 1984; Dreybrodt et al., 1999), the time needed to reach the stationary enlargement phase (breakthrough) depends on the initial fracture

aperture, but with times from one to two orders of magnitude longer than those described for classical carbonate karst (Palmer, 2007). In the steep hydraulic gradient base scenario (1000 m percolating patway, hydraulic head of 300 m), a breakthrough minimum time of 590 ka is required for an initial aperture of 1 mm and around 1 Ma for initial apertures less than 0.1 mm (Fig. 7, continuous line). However, the initial aperture of the fracture becomes less important at higher values. No significant changes in breakthrough times are observed from e_0=0.5-0.7 mm onward, with values around 550-600 ka.

Another factor strictly controlling the arenisation process, and therefore the breakthrough time, is the primary diffusion porosity (φ_0), which depends on the quartz-sandstone anisotropies and petrographic features. An initial diffusion porosity change from 0.1% to 1% produces a sharp increase in the quartz-sandstone arenisation (Fig. 7, segmented line), with breakthrough times at 200 ka for an initial aperture of 1 mm, and 700 ka for an initial aperture of 0.1 mm.

In the base scenario representing the low-dipping layer, the evolution of the fissure is slowed down, but only when the fissure aperture is very narrow, while fissure apertures in the order of a millimetre revealed almost no difference compared to the subvertical fracture system base scenario (Fig. 7, dot line).

Before the breakthrough, the direct dissolution along the fissure walls has almost no effect on the fracture enlargement. Once the breakthrough has occurred, the fissure enlargement proceeds with a linear trend (Fig. 8A).

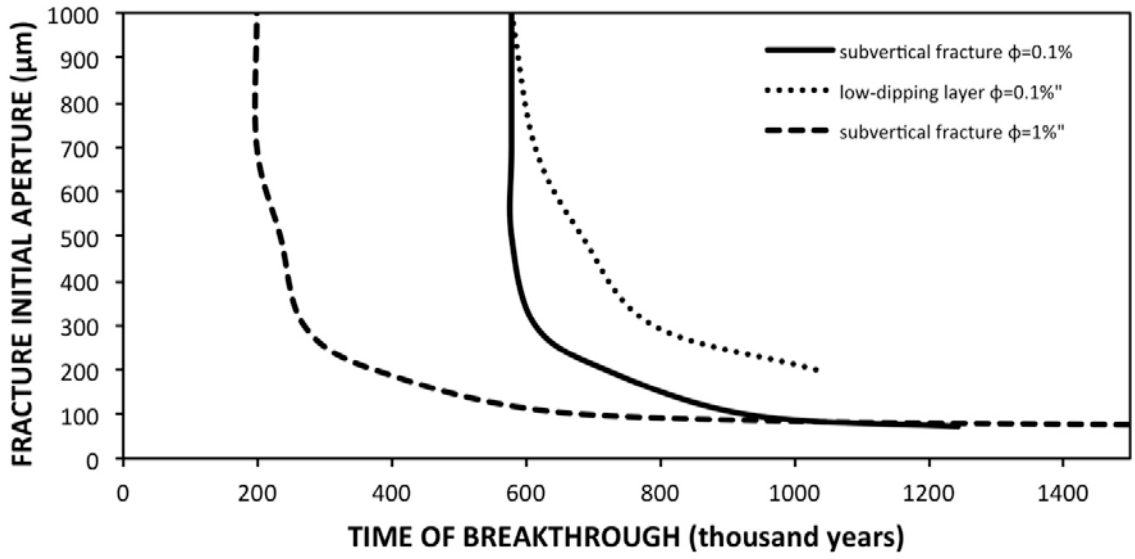

Fig. 7. Times of breakthrough versus initial fracture aperture e^0 for an high angle fracture system with initial diffusion porosity 0.1 (continuous line); an increase of the initial diffusion porosity from 0.1 to 1 causes an anticipation of the breakthrough times of around 400 ka (segmented line); differences in the breakthrough time between the high angle fracture system and the low dipping system (dot line).

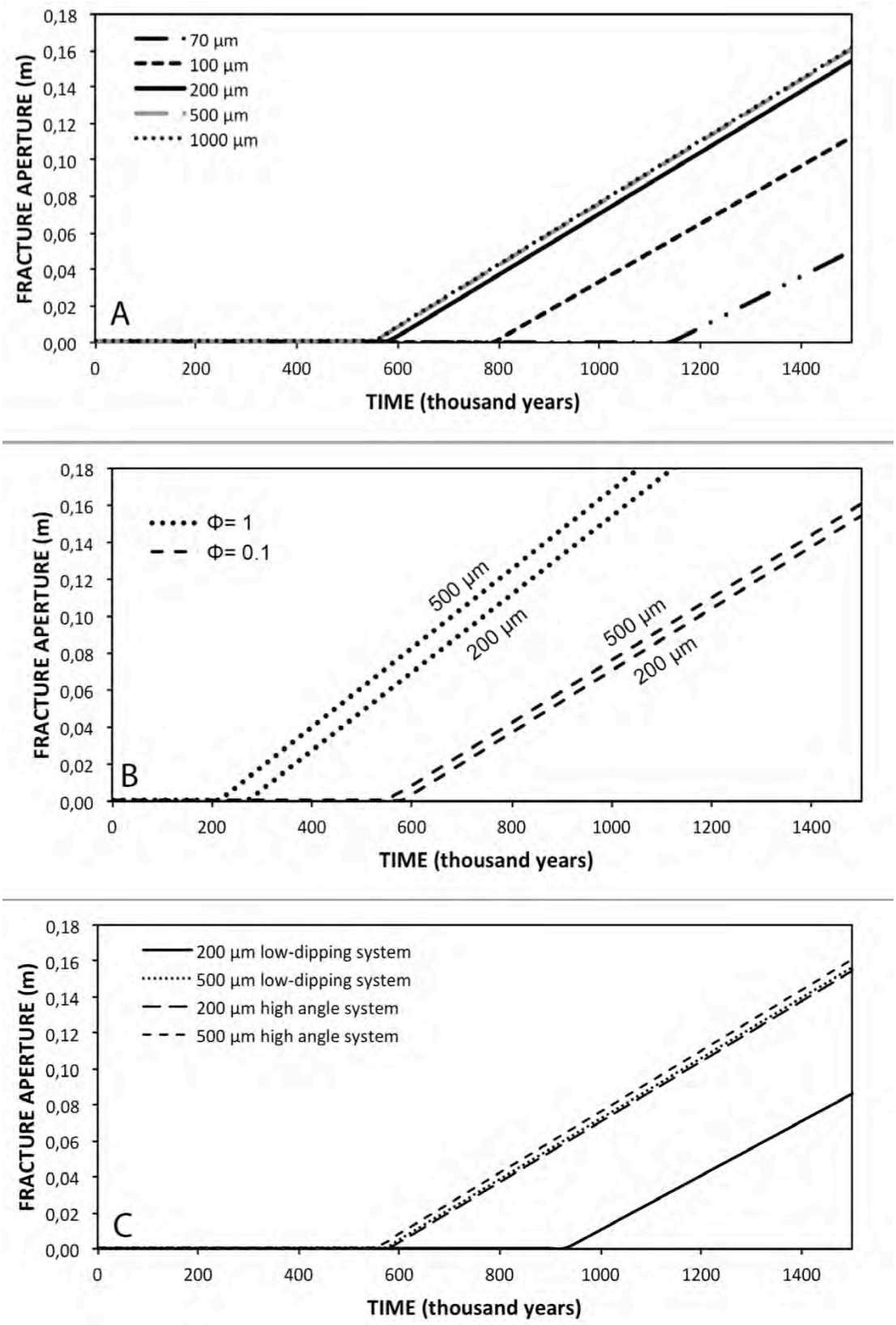

Fig. 8. Enlargement rates before and after breakthrough: A) fracture enlargement rate in dependence of the initial fracture aperture for the high angle fracture system; B) differences in the enlargement rate between initial diffusion porosity=0.1% (0.14-0.17 mm ka^{-1}) and initial diffusion porosity of 1% (0.21 mm ka^{-1}) in the high angle fracture system with fracture aperture $e_{0=}$ 200 and 500 µm; C) differences of breakthrough and enlargement rates with different initial apertures ($e_{0=}$ 200 and 500 µm) for the high angle and low dipping system.

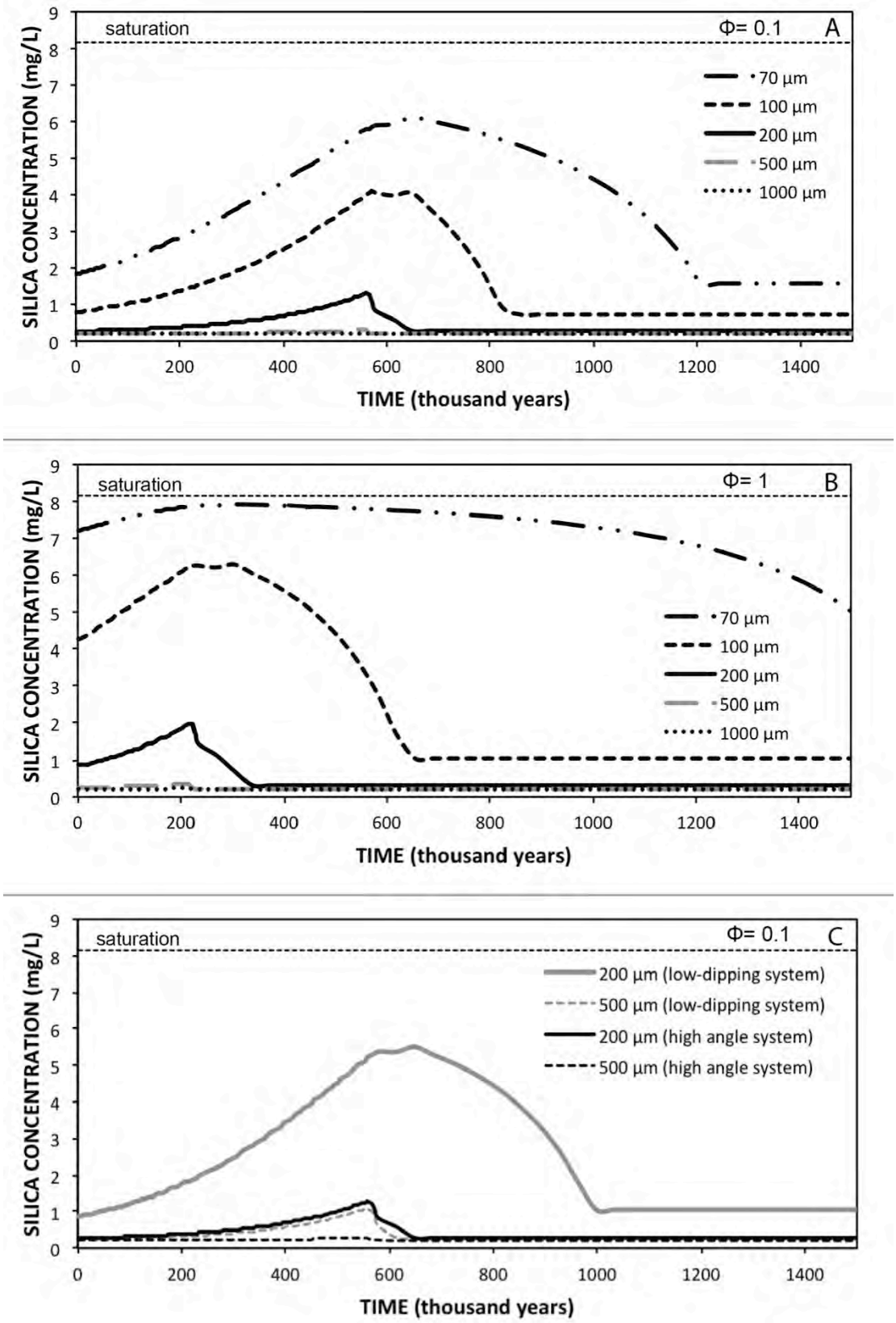

Fig. 9. Silica concentration versus time at the outflow of the fracture: A) Silica concentration at the outflow of the high angle fracture system depending on the initial fracture aperture e_0 with initial diffusion porosity 0.1 %; B) Silica concentration at the outflow of the high angle fracture system depending on the initial fracture aperture e_0 with initial diffusion porosity 1 %; C) Differences of the silica concentration at the outflow in the high angle fracture system and in the low dipping system with an initial diffusion porosity 0.1 %.

The fissure enlargement rate is between 0.14-0.17 mm ka^{-1} for both the fracture system and the low-dipping layer base scenarios (Fig. 8B), and increases up to 0.21 mm ka^{-1} in a fracture system with diffusion porosity of 1% (Fig. 8C).

The process is also temperature-dependent, because of the dissolution kinetics of quartz. A temperature increase from 15 to 20°C anticipates by around 30% the breakthrough time in the base scenario. Conversely, quartz grain size does not seem to have significant control on the breakthrough time. In fact, a grain size of 70 µm anticipates breakthrough by only 3% compared to a grain size of 200 µm.

The concentration of dissolved silica at the fracture outflow, for example a dripping in a cave gallery, can also give us information on the reliability of the model. In the fracture system base scenario (Fig. 9A) the concentration never reaches the saturation limit for dissolved silica with respect to quartz at 15°C (approximately 8 mg L^{-1}). However, it approaches the saturation when the initial aperture is less than 100 µm (6 mg L^{-1} for e_0=70 µm) (Fig. 9A) and is almost saturated in the thinner fractures if an initial diffusion porosity of 1% is assumed (Fig. 9B).

The passage from plug flow to free-surface film flow does not change the arenisation rate, assumed that the fracture is continuously fed. The evolution of flow velocity and mechanism is depicted in Figure 10, that shows that a laminar flow is effective also in narrow fissures (Louis law No. 4, equation 1) before breakthrough is reached, while turbulent flow rules when the aperture is large

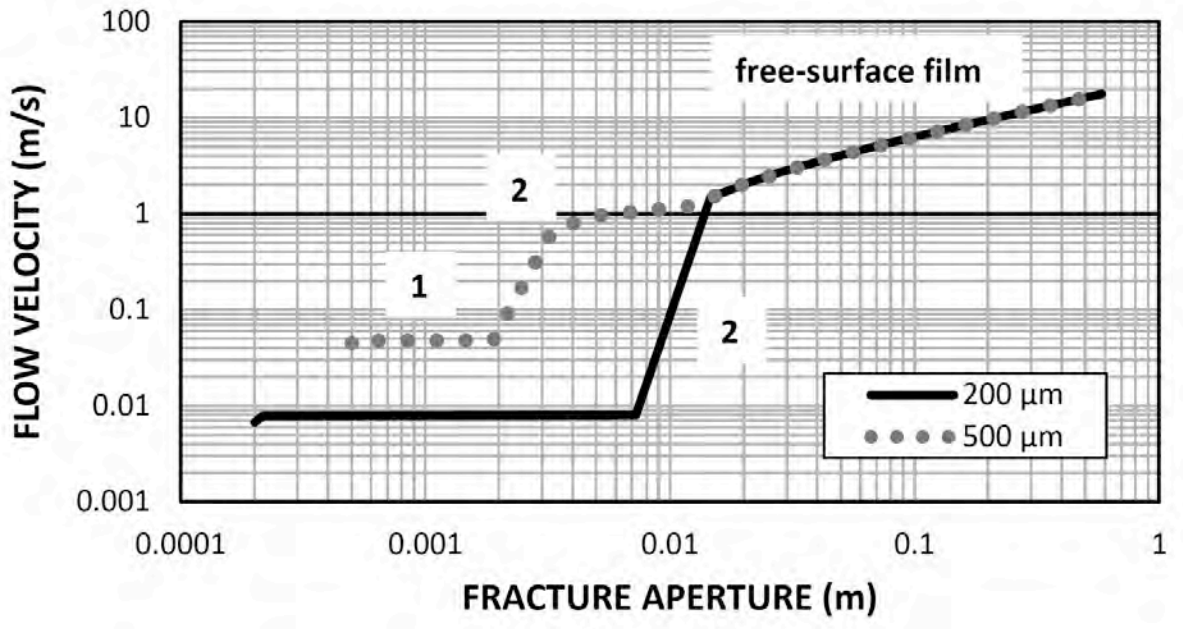

(Louis laws No. 1 and 2). After breakthrough, the velocity increases, the flow becomes turbulent, and

Fig. 11. Flow velocity evolution calculated by the model for the high angle fracture system with initial apertures of 200 and 500 µm respectively. The numbers refer to the Louis law (4: laminar flow, 1-2: turbulent flow) effective in the fracture, while the last segment represents the free-surface film flow condition.

2.1.6 Discussion and conclusions

The modelling results are in good agreement with previous studies on weathering-speleogenesis and water geochemistry of silica in the quartz-sandstone environment (Piccini and Mecchia, 2009; Mecchia et al., 2013; Sauro et al., 2013).

The modelling demonstrates that the process can be active along extensive fissure paths (more than 1 km), where saturation in dissolved silica is hardly reached. This result confirms the general theory of Martini (1979), even though we consider diffusion to be the driving mechanism instead of advection. The model clearly demonstrates that the extremely slow reaction rate is the most important factor in the formation of karst-like features in quartz-sandstones. The high silica concentrations close to saturation reported by several authors (Piccini and Mecchia, 2009, Aubrecht et al., 2011, 2012; Mecchia et al., 2013) for drippings falling from thin fissures on cave walls seems to confirm the model outputs (Fig. 10), ideally representing the outflows of those paths which have not yet reached the arenisation breakthrough.

The initial fissure aperture and the primary diffusion porosity of the unweathered rock constitute the main controls in the arenisation process. This latter factor could explain why the arenisation process appears more effective in some beds rather than in others and why caves and karst-like features are not present everywhere in quartz-sandstones around the world and even less in high metamorphic quartzites. Therefore the petrographic control (anisotropies, grade of burial metamorphism, pressure release due to exhumation, presence of clay minerals, etc.) seems to be confirmed as one of the most sensitive factors in the arenisation process.

The time needed for the arenisation breakthrough (inception phase) in quartz-sandstones is much longer than in limestone, 600-1000 ka for the base scenarios, and the following fracture enlargement (stationary enlargement phase) occurs at a rate of approximately 0.17 mm ka^{-1}. This outcome suggests that the time of cave development in these lithologies, with the boundary conditions described for the tepui table mountains, is at least one order of magnitude higher than the inception phase, i.e. around 6-10 My, or even more, as suggested by Piccini and Mecchia (2009). In conclusion, the numerical calculation confirms that arenisation driven by molecular diffusion is a reliable weathering mechanism that well explains the geomorphologic features and geochemical data found in real settings.

Acknowledgements

We would like to thank Nicola Tisato for the analyses of porosity with the picnometer at the ETH of Zurich, and La Venta Association for the logistics and economic support to this research project.

References

AA.VV, 1994. Tepui 1993. Progressione 30, 120 p.

Adamovič, J., Mikuláš, R., Navrátil, T., Mertlík, J., 2013. Cave formation initiated by dissolution of carbonate cement in quartzose sandstones. In: Filippi, M., Bosak, P. (Eds.), Proceedings of the 16th International Congress of Speleology, Brno 19-27 July 2013, Volume 3, pp. 217-220.

Anikouchine, W.A., 1967. Dissolved Chemical Substances in Compacting Marine Sediments. Journal of Geophysical Research 72(2), 505-509.

Applin, K.R., 1987. The diffusion of dissolved silica in dilute aqueous solution. Geochimica et Cosmochimica Acta 51, 2147-2151.

Aubrecht, R., Lánczos, T., Gregor, M., Schlögl, J., Smída, B., Brewer-Carías, Ch., Vlcek, L., 2011. Sandstone caves on Venezuelan tepuis: Return to pseudokarst? Geomorphology 132, 351-365.

Aubrecht, R., Barrio-Amorós, C.L., Breure, A.S.H., Brewer-Carías, C., Derka, T., Fuentes-Ramos, O.A., Gregor, M., Kodada, J., Kováčik, Ľ., Lánczos, T., Lee, N.M., Liščák, P., Schlögl, J., Šmída, B., Vlček L., 2012. Venezuelan tepuis: their caves and biota. Acta Geologica Slovaca Monograph, Comenius University, Bratislava, pp. 168.

Bernabei, T., Mecchia, M., Pezzolato, P., Piccini, L, Preziosi, E., 1993. Tepuy '93: ancora Venezuela! Speleologia, Rivista della Società Speleologica Italiana 29, 8-23.

Chalcraft, D., Pye, K., 1984. Humid tropical weathering of quartzite in southeastern Venezuela. Zeilschrift fur Geomorphologie 28, 321-332.

Doerr, S. H., 1999. Karst-like landforms and hydrology in quartzites of the Venezuelan Guyana shield: Pseudokarst or "real" karst? Zeitschrift fur Geomorphologie 43, 1-17.

Derjaguin, B.V. and Churaev, N.V. (1986) Properties of water layers adjacent to interfaces. In C.A. Croxton, Ed., Fluid Interfacial Phenomena, p. 748. Wiley, New York.

Dragila, M. I., Wheatcraft, S. W., 2001. FreeSurface Films, Ch. 7, in Conceptual Models of Flow and Transport in the Fractured Vadose Zone, National Academy of Sciences, National Academy of Sciences, National Academy Press, Washington DC. 2001: 217-242.

Dreybrodt, W., 1990. The role of dissolution kinetics in the development of karst aquifers in limestone: A model simulation of karst evolution. The Journal of Geology 98(5): 639-655.

Dreybrodt, W., Gabrovšek, F., Romanov, D., 2005. Processes of a Speleogenesis: A Modeling Approach, Carsologica, 4. Založba ZRC, 376 p.

Dreybrodt, W., Gabrovšek, F., Siemers, J., 1999. Dynamics of the early evolution of karst. Karst Water Institute, Special Publication 5, Karst Modeling, pp. 106-119.

Frondel, C., 1962. Dana's system of mineralogy. Quartz (density), 3, 114-116.

Garrels, R.M., Dreyer, R.M., Howland, A.L., 1949. Diffusion of ions through intergranular spaces in water-saturated rocks. Bulletin of the Geological Society of America 60, 1809-1828.

Gabrovšek, F., Dreybrodt, W., 2001. A model of the early evolution of karst aquifers in limestone in the dimensions of length and depth. Journal of Hydrology 240(3), 206-224.

Ghezzehei, T.A., 2004. Constraints for flow regimes on smooth fracture surfaces. Water Resources Research 40, W11503, doi:10.1029/2004WR003164.

Ghosh, S.K., 1985. Geology of the Roraima Group and its implication. Boletin Geologico Venezolano, Publicacion Especial 10, 33-50.

Ghosh, S.K., 1991. Dissolution of silica in nature and its implications. Bull. Can. Pet. Geol., 39, 212.

Gori, S., Inglese, M., Tognini, P., Trezzi, G., Rigamonti, I., 1993. Auyan-tepui, speleologia tropicale nelle quarziti. Speleologia, Rivista della Società Speleologica Italiana 28, 23-33.

Hartikainen, K., Hautojärvi, A., Kuoppamäki, K., Timonen, J., 1996. Helium gas methods for rock characteristics and matrix diffusion. POSIVA OY, 96-22, Helsinki.

House, W.A., Denison, F.H., Warwick, M.S., Zhmud, B.V., 2000. Dissolution of silica and the development of concentration profiles in freshwater sediments. Applied Geochemistry 15, 425-438.

Hurd, D.C., 1973. Interaction of biogenic opal, sediment and seawater in the Central Equatorial Pacific. Geochimica et Cosmochimica Acta 37, 2257-2282.

Hurst, A., Bjorkum, P.A., 1986. Discussion, thin section and SEM textural criteria for the recognition of cement-dissolution porosity in sandstones. Sedimentology 33, 605-614.

Lagneau, V., van der Lee, J., 2010. Operator splitting-based reactive transport models in strong feedback of porosity change: the contribution of analytical solutions for accuracy validation and estimator improvement. Journal of Contaminant Hydrology 112, (1-4) 118-129.

Lichtner, P.C., 1988. The quasi-stationary state approximation to coupled mass transport and fluid–rock interaction in a porous medium. Geochimica et Cosmochimica Acta 52, 143-165.

Louis, C., 1974. Introduction à l'hydraulique des roches. Bulletin B.R.G.M. III(4), 283-356.

Martini, J. E. J., 1979. Karst in Black Reef Quartzite near Kaapsehoop, Eastern Transvaal. Annals of the South African Geological Survey 13, 115-128.

Martini, J.E.J., 2000. Dissolution of quartz and silicate minerals. In: Klimchouk, A.B., Ford, D.C., Palmer, A.N., Dreybrodt, W. (Eds.), Speleogenesis. Evolution of karst aquifers. National Speleological Society, Huntsville, pp. 452-457.

Mecchia, M., Piccini, L., 1999. Hydrogeology and SiO_2 geochemistry of the Aonda Cave system (Auyantepui, Bolivar, Venezuela). Boletin Sociedad Venezolana de Espeleologia 33, 1-11.

Mecchia, M., Piccini, L., Sauro, F., De Waele, J., Sanna, L., Tisato, N., Lira, J., Vergara, F., 2013. Geochemistry of surface and subsurface waters in quartz-sandstones: significance for the geomorphic evolution of tepui table mountains (Gran Sabana, Venezuela). Submitted to Journal of Hydrology.

Miller, W.A., Keyhani, M., 2001. The effect of roll waves on the hydrodynamics of falling films observed in vertical column absorbers. Paper presented at ASME Heat Pump Technical Session, New York City, Nov. 2001.

Norton, D., Knapp, R., 1977. Transport phenomena in hydrothermal systems: the nature of porosity. American Journal of Science 277, 913-936.

Oelkers, E.H., Bjorkum, P.A., Murphy, W.M., 1996. A petrographic and computational investigation of quartz cementation and porosity reduction in North Sea sandstones. American Journal of Science 296, 420-452.

Palmer, A.N., 1984. Geomorphic interpretation of karst features. In: La Fleur, R.G. (Ed.), Groundwater as a geomorphic agent. Boston Massachusetts, Allen and Unwin, 173-209.

Palmer, A.N., 2000. Digital modeling of individual solution conduits. In: Klimchouk, A.B., Ford, D.C., Palmer, A.N., Dreybrodt, W. (Eds.), Speleogenesis. Evolution of karst aquifers. National Speleological Society, Huntsville, pp. 194-200.

Parks, G.A. (1990) Surface energy and adsorption at mineral-water interfaces: An introduction. In Mineralogical Society of America Reviews in Mineralogy. Vol. 23, 133–175.

Pettijohn, J., Potter, P.E., Siever, R., 1987. Sand and Sandstone. Springer, Berlin, 553 p.

Piccini, L., Mecchia, M., 2009. Solution weathering rate and origin of karst landforms and caves in the quartzite of Auyan-tepui (Gran Sabana, Venezuela). Geomorphology 106, 15-25.

Pouylleau, M., Seurin, M., 1985. Pseudo-karst dans des roches gréso-quartzitiques de la formation Roraima. Karstologia 5, 45-52.

Reid, A. R., 1974. Stratigraphy of the type area of the Roraima Group, Venezuela. Bolletin de Geologia, Venezuela, Pub. Especial 6, 343-353.

Rigamonti, I., 1995. La roccia. In “Spedizione speleologica italiana all’Auyantepui”, Il Grottesco (Gruppo Grotte Milano CAI-SEM), pp. 32-40.

Rimstidt, J.D., 1997. Quartz solubility at low temperatures. Geochimica et Cosmochimica Acta 61, 2553-2558.

Rimstidt, J.D., Barnes, H.L., 1980. The kinetics of silica-water reactions. Geochimica et Cosmochimica Acta 44, 1683-1699.

Robbins, J.A., Edgington, D.N., 1975. Determination of recent sedimentation rates in Lake Michigan using Pb-210 and Cs-137. Geochimica et Cosmochimica Acta 39, 285-304.

Sauro, F., Piccini, L., Mecchia, M., De Waele, J., 2013. Comment on “Sandstone caves on Venezuelan tepuis: Return to pseudokarst?” by R. Aubrecht, T. Lánczos, M. Gregor, J. Schlögl, B. Smída, P. Liscák, Ch. Brewer-Carías, L. Vlcek, Geomorphology 132, 351-365. Geomorphology 197, 190-196.

Schnoor J.L, 1990. Kinetics of chemical waethering: A comparison of laboratory and field weathering rates. In *Aquatic Chemical Kinetics*, W. Stumm, Ed., Wiley-Interscience, New York.

Siever, R., Beck, K., Berneh, R., 1965. Composition of interstitial waters of modern sediments. Journal of Geology, 73: 39-73.

Sociedad Venezolana de Espeleologia, 1984. Catastro Espeleologico National. Boletin Sociedad Venezolana de Espeleologia 22, 65-75.

Tzur, Y., 1971. Interstitial diffusion and advection of solutes in accumulating sediments. Journal of Geophysical Research 76, 4208-4211.

van der Lee, J., De Windt, L., Lagneau, V., Goblet P., 2003. Module- oriented modeling of reactive transport with HYTEC. Computers & Geo- sciences, 29, 265-275.

Weissberg, H. L. 1963. Effective Diffusion Coefficient in Porous Media. Journal of Applied Physics 34, 2636-2640.

White A.F., S.L. Brantley, 2003. The effect of time on the weathering of silicate minerals: why do weathering rates differ in the laboratory and field? Chemical Geology 202 (2003) 479–506.

White, A.F. and Peterson, M.L. (1990) Role of reactive-surface-area characterization in geochemical kinetic models. In Chemical Modeling of Aqueous Systems II, American Chemical Society Symposium Series 416, 461–475.

White, W.B., Jefferson, J.L., Haman, J.F., 1966. Quartzite karst in Southeastern Venezuela. International Journal of Speleology 2, 309-314.

Wilson, P., 1979. Experimental investigation of etch pit formation on quartz sand grains. Geological Magazine 116, 477-482.

Wray, R.A.L., 1995. Solutional landforms in quartz sandstones of the Sydney Basin. Unpublished PhD thesis. University of Wollongong, 381 p.

Wray, R.A.L., 1997. A Global review of solutional weathering forms on quartz sandstones. Earth Science Reviews 42 (3), 137-160.

Wray, R.A.L., 2000. The Gran Sabana: the world's finest quartzite karst? In: Migon, P. (Ed.), Geomorphological Landscapes of the World. Springer, Dordrecht, 79-88.

Young, R W., 1988. Quartz etching and sandstone karst: examples from the East Kimberleys, Northwestern Australia. Zeitschrift fur Geomorphologie 32, 409-423.

Zimmerman, R. W., Bodvarsson, G. S., 1996. Hydraulic conductivity of rock fractures. Transport in porous media 23(1), 1-30.

Chapter 2.2

Published in Journal of Hydrology, doi:1 0.1016/j.jhydrol.2014.01.029

GEOCHEMISTRY OF SURFACE AND SUBSURFACE WATERS IN QUARTZ-SANDSTONES: SIGNIFICANCE FOR THE GEOMORPHIC EVOLUTION OF TEPUI TABLE MOUNTAINS (GRAN SABANA, VENEZUELA)

Marco Mecchia[1], Francesco Sauro[1,2], Leonardo Piccini[1,3], Jo De Waele[1,3], Laura Sanna[4], Nicola Tisato[5], Jesus Lira[6], Freddy Vergara[1,7]

1) La Venta Geographic Explorations Association, Via Priamo Tron 35/F, 31100, Treviso (Italy)

2) Department of Biological, Geological and Environmental Sciences, Italian Institute of Speleology, Bologna University, Via Zamboni 67, 40126, Bologna (Italy)

3) Department of Earth Sciences, Florence University, Via La Pira 4, 50121, Florence (Italy)

4) Institute of Biometeorology, National Research Council of Italy, Traversa La Crucca 3, 07100 Sassari (Italy)

5) ETH Zurich, Geological Institute, Soneggstrasse 5, 8092 Zurich (Switzerland)

6) Istituto Nacional de Parques, Caracas (Venezuela)

7) Teraphosa Exploring Team, Puerto Ordaz (Venezuela)

Corresponding Author: Francesco Sauro

Abstract

In situ measurements of discharge, pH, electric conductivity (EC), temperature, and SiO_2 content have been carried out during five expeditions in the last 20 years on the summit plateaus, inside caves and along the rivers of the surrounding lowlands of three tepui massifs in Venezuela (Auyan, Roraima, and Chimanta). Additionally, detailed chemical analyses were performed on waters sampled in a newly discovered extensive quartz-sandstone cave system on the Auyan Tepui. Rock samples of the quartz-sandstone bedrock from different locations have been analysed to obtain their chemical composition with a wavelength dispersive X-ray fluorescence spectrometer. These data show that the majority of silica present in surface and subsurface water comes from dissolution of quartz and only in minor amount from hydrolysis of other silicate minerals. Probably the presence of a hardened crust of iron hydroxides limits the dissolution of silica on the top surface of tepuis. Dissolution in the subsurface, instead, is more significant and causes, in the long term, the

"arenisation" of the quartz-sandstone and its subsequent removal by mechanical erosion. On the other hand, waters flowing on the arkosic rock outcropping on the lowland below the tepuis obtain their high dissolved silica content mainly from hydrolysis of silicates.

The morphological evolution of these table mountains appears thus to be controlled mainly by the underground weathering of the quartz-sandstone, with the opening of deep fractures (*grietas*) and the collapse of large underground horizontal cave systems. Scarp retreat, instead, seems to be related to the higher weathering rate of the more arkosic formations underlying the quartz-sandstones.

Keywords: SiO_2 geochemistry, quartz-sandstone caves, landscape evolution, dissolution, weathering

2.2.1 Introduction

Extensive cave systems are found in quartz-sandstones of Precambrian age outcropping in few areas around the world. These peculiar features are commonly developed in tectonically stable cratonic areas (for instance the Guyana Shield of Venezuela and Brazil, the Kaapvaal craton of South Africa, or the Westralian craton and Sydney Basin in Australia), being more prominent in humid tropical settings (like in the Minas Gerais state of Brazil, and in the quartz-sandstone outcrops in Thailand, Mozambique and in the Hunan province of China). However caves in quartz-sandstones were documented also in actually hyperarid settings, like in Chad and Australia (for a complete list see Wray, 1997a, and references therein).

Although the rate of dissolution of quartz in the acidic solutions commonly found on quartz-sandstones is among the slowest ones, the wide subterranean conduits and some peculiar surface landforms formed in these rocks are clear evidences of intensive weathering (Wray, 2013). The resulting landscape has many features resembling karst and many authors (White et al., 1966; Martini, 1979, 1985, 2004; Piccini, 1995; Wray, 1997b; Doerr, 1999) have used such a term referring to this kind of geomorphic process although solution plays only a minor role, at least from a quantitative point of view.

This work is focused on the quartz-sandstones of the tepui table mountains in the Gran Sabana (Venezuela), considered the world finest quartz-sandstone karst (Wray, 2000).

Many hypotheses on the genesis of caves and karst-like features in quartz-sandstones have been discussed by previous authors. All the theories so far presented require the formation of loose sands along some preferential bedding planes, followed by their winnowing out (piping) from the quartzitic rocks by underground flowing waters (Sczerban and Urbani, 1974; Galán and Lagarde, 1988).

The role in triggering speleogenesis by generating the "loose sands" has been assigned to rock dissolution by meteoric (Jennings, 1983; Martini, 2000; Wray, 2003; Piccini and Mecchia, 2009) or

hydrothermal waters (Zawidzki et al., 1976) through a weathering dissolution process called “arenisation”. Other authors assign importance to microbially-driven alkaline dissolution (Marker, 1976; Barton et al., 2009), or refer to the existence of loose sands in unlithified beds, also produced by dissolution and weathering of aluminosilicates (Aubrecht et al., 2011; 2012). All these theories are still under discussion and there is not yet a clear understanding of the main speleogenetic and morphogenetic factors involved (Sauro et al., 2013a).

Sauro et al. (2013a) pointed out some problems related to the “unlithified beds” speleogenetic model proposed by Aubrecht et al. (2011), suggesting that the mineralogical composition and the petrographical features (grain size, sorting, depositional structures), and not the diagenetic degree of the bedrock probably control the intensity of the weathering processes along different beds.

Chemical field analyses of waters represent a useful tool to understand the mechanisms and roles of SiO_2 dissolution with respect to other weathering processes and to give information on how dissolution works in a real scenario. These data can then be compared with laboratory experiments of quartz dissolution (Krauskopf, 1956; Rimstidt, 1997 and references therein).

In this paper we focused on the geochemistry and SiO_2 content of surface and subsurface waters in the tepui table mountains. The most complete set of chemical data currently available is presented here: 159 field analyses on waters (dissolved H_4SiO_4 expressed in SiO_2 equivalent, pH, EC, temperature) carried out in three massifs (Auyan, Roraima and Chimanta) and six cave systems, in different hydrodynamic settings. In fact, previous studies (Briceño et al., 1990; Ipiña, 1994; Mecchia and Piccini, 1999, Piccini and Mecchia, 2009; Aubrecht et al., 2011) discussed data from single tepuis, or peculiar cave systems. In addition, the concentration of major elements, chlorides, sulphates, and nitrates in a very extensive cave system recently discovered on Auyan Tepui were measured. Finally, we coupled this dataset on water chemistry with wavelength dispersive X-ray fluorescence analysis (WD-XRF) performed on different tepuis quartz-sandstones in order to verify the potential signatures of mineral weathering.

2.2.2 Study Area

2.2.2.1 Geographical, geological, and climatic settings

The Gran Sabana is a vast geographical region located in northern South America, crossed by several tributaries of Caroní River, which flows into the Orinoco River. The main topographic elevations have the shape of large tablelands named "tepuis", meaning “mountains” in the local Pemon Indian language. In fact, quartz-sandstones (quartz-arenites cemented by quartz deposited in optical continuity with detrital quartz) (Pettijohn et al., 1987) often cap high hills, being among the most erosion-resistant rocks on Earth. The tepuis are bordered by vertical to overhanging walls, usually from 400 to more than 1000 m in height.

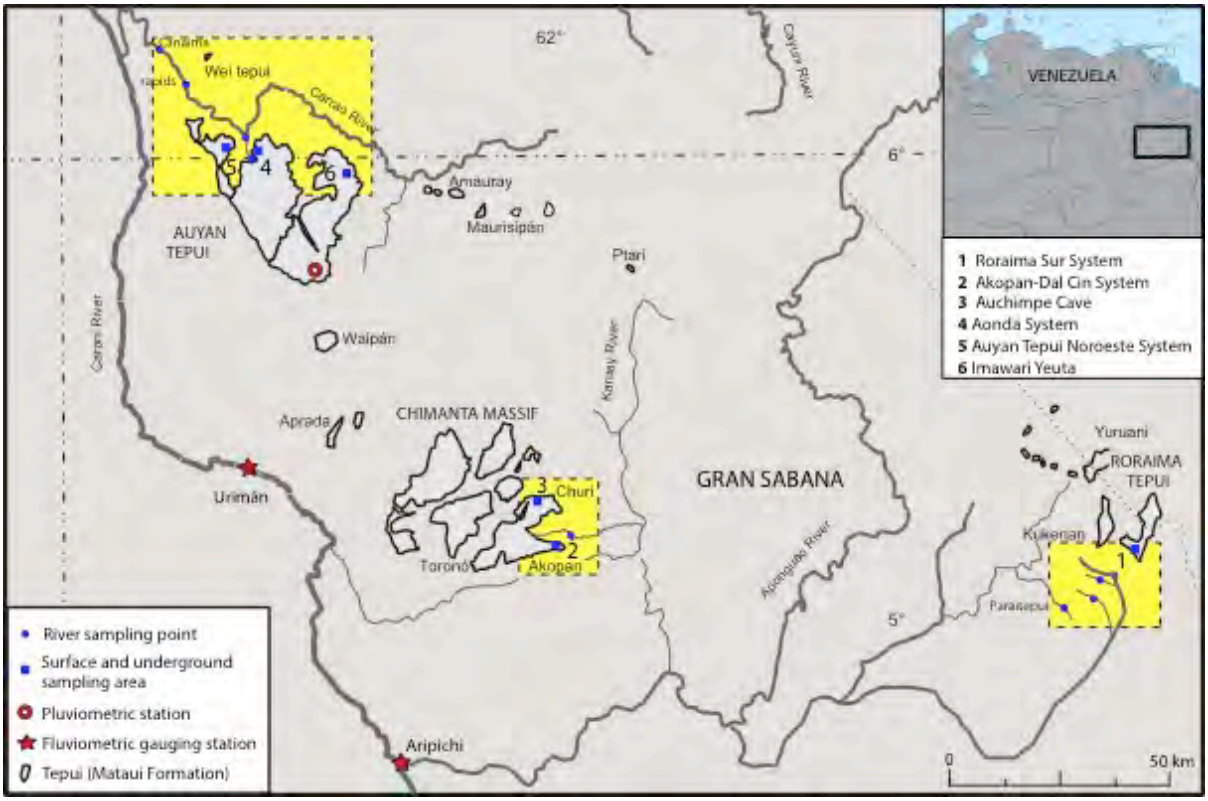

Fig. 1. Geographic settings of Gran Sabana and sampling areas (highlighted in yellow).

The Gran Sabana is part of the craton called the Guyana Shield. The igneous and ultra-metamorphic rocks in the northern side of the shield have an age reaching 3.5 Ga (Imataca-Bolivar Province, after Gonzáles de Juana et al., 1980; Gibbs and Barron, 1993). The overlying siliciclastic rocks (Roraima Group) belong to the continental to pericontinental environment of the Roraima-Canaima Province (Reid, 1974). The age of this arenaceous group was inferred thanks to the absolute dating of the granitic basement (2.3-1.8 Ga) and of the intrusions of basaltic dikes and the sills that cross the upper part of the Roraima Group (1.4-1.8 Ga) (Santos et al., 2003).

The quartzitic Mataui Formation, a cross bedded massive sandstone unit of unknown thickness, which encloses all the major cave systems so far explored, represents the youngest deposit of the Roraima Group, now situated in the highest topographical position and forming prominent plateaus with vertical cliffs. Quartz normally represents far over 80% of the rock, with well-sorted grains, commonly between 30 and 100 µm in diameter, cemented with microcrystalline quartz. Minor phyllosilicates (authigenic kaolinite and/or pyrophyllite) are included in the rock (Martini, 2000, 2004; Aubrecht et al., 2011). It is assumed that the Mataui arenites were covered by other sediments and therefore underwent metamorphic transformations (Urbani et al., 1977). Associations of minerals typical of a low grade metamorphic environment were found, including pyrophyllite and muscovite, which indicate the Mataui sandstones to have suffered a burial pressure of ~50 MPa. Such a pressure was exerted by 2000-3000 metres of bedrock (Briceño et al., 1990).

The slopes underlying the cliffs surrounding the tepuis are made of proto-quartzites, arkoses and graywackes, with beds of cherts, lutites and siltites (Uaimapué Formation; Reid, 1974). In the lowlands the main outcropping lithology is the Kukenán Formation, prevalently composed of siltstones and shales.

The entire area was probably raised to its current altitude as early as ~110 million years ago, at the end of the Aptian Age, as a consequence of the opening of the South Atlantic which broke up the Pangean supercontinent and separated South America from Africa (Long, 2002). A very low erosion rate, around 1 mm ky^{-1}, was calculated for the present top tepuis surface (Brown et al., 1992).

The regional climate is semi-humid/tropical with a relatively dry season lasting 3 to 4 months during winter (*Awi* in Köppen's classification system), with the driest months occurring between December and March, and the rainiest months between May and September (Nimer, 1989). This precipitation regimen is controlled by the seasonal migration from 5° to 15° of latitude North of the Inter Tropical Convergence Zone (ITCZ) (Snow, 1975).

There are no continuous rainfall gauges operating on the tepui summits. However, a pluviometric station has been recording precipitation data on the Auyan Tepui summit between 1980 and 1983 (although there are some gaps in the record), showing mean annual rainfalls of about 3000 mm.

In the same span of time, streamflow has been measured in Caroni river at the gauging stations of Urimàn and Aripichi, located SW and NW of Chimanta massif, about fifty and one hundred km respectively to the SW of Auyan Tepui (Galán, 1992).

Considering the differences of average discharges in the two gauging stations (522 $m^3 s^{-1}$) and of the extensions of the two catchment areas (6812 km^2) (Galán, 1992), the effective rainfall (difference between total rainfall and evapotranspiration) can be estimated in approximately 2400 mm. For the months of February and March, to which all our data are referred to, the average effective monthly rainfall are 62 and 67 mm, respectively. These values seem to be in good agreement with rainfalls measured at the Auyan Tepui temporary pluviometric station, and will later be used for a rough calculation of rainwater infiltration in tepui caves.

2.2.2.2 Investigated tepuis and cave systems

This study focuses on three of the most extended tepui massifs: Roraima (31 km^2), Chimanta (1470 km^2) and Auyan (700 km^2) (Fig. 1). Structural and climatic conditions of these sites are very similar. The tepui massifs rise from the lowlands of the Gran Sabana situated at an average altitude of about 1000 m a.s.l. (Wonken planation surface) (Briceño and Schubert, 1990). The upper plateaus have an average altitude >2000 m a.s.l. (Fig. 2). The principal structures of the Roraima Group are kilometric-sized radius anticlines and synclines, giving rise to cuestas and large areas of almost horizontal strata.

Some sets of fractures, mainly vertical, cut the plateaus forming a regular network of quadrangular prisms.

Peculiar landforms due to selective weathering are evident and widespread on the quartz-sandstone plateau surfaces (Wray, 2000). The most impressive morphologic features on the summit plateaus are the big shafts developed along the fractures, called *simas* or *grietas* in Spanish. *Simas* are up to 350 m deep (e.g. Aonda cave), and formed by the progressive collapse of underground voids that developed at the base of enlarged fractures, often where a coarse-grained quartz sandstone (arenite to rudite) lays on fine and more erodible sandstones and arkoses (Piccini, 1995).

When these fractures are not enlarged down to the base of the quartz-sandstone formation, they cause the progressive retreat of scarps on the summit plateau of the tepuis, and the modelling, along preferential nearly horizontal bedding planes, of peripheral surfaces at altitude lower than the summit plateau (Piccini and Mecchia, 2009). *Simas* and *grietas* are more abundant on the plateau rims, probably because of increasing decompressional opening of the joints near the external cliffs. Retreat of peripheral scarps of tepuis seems also to be related to the higher weathering rate of the underlying more arkosic formations.

Horizontal cave systems are found in correspondence of specific favourable horizons (beds) within

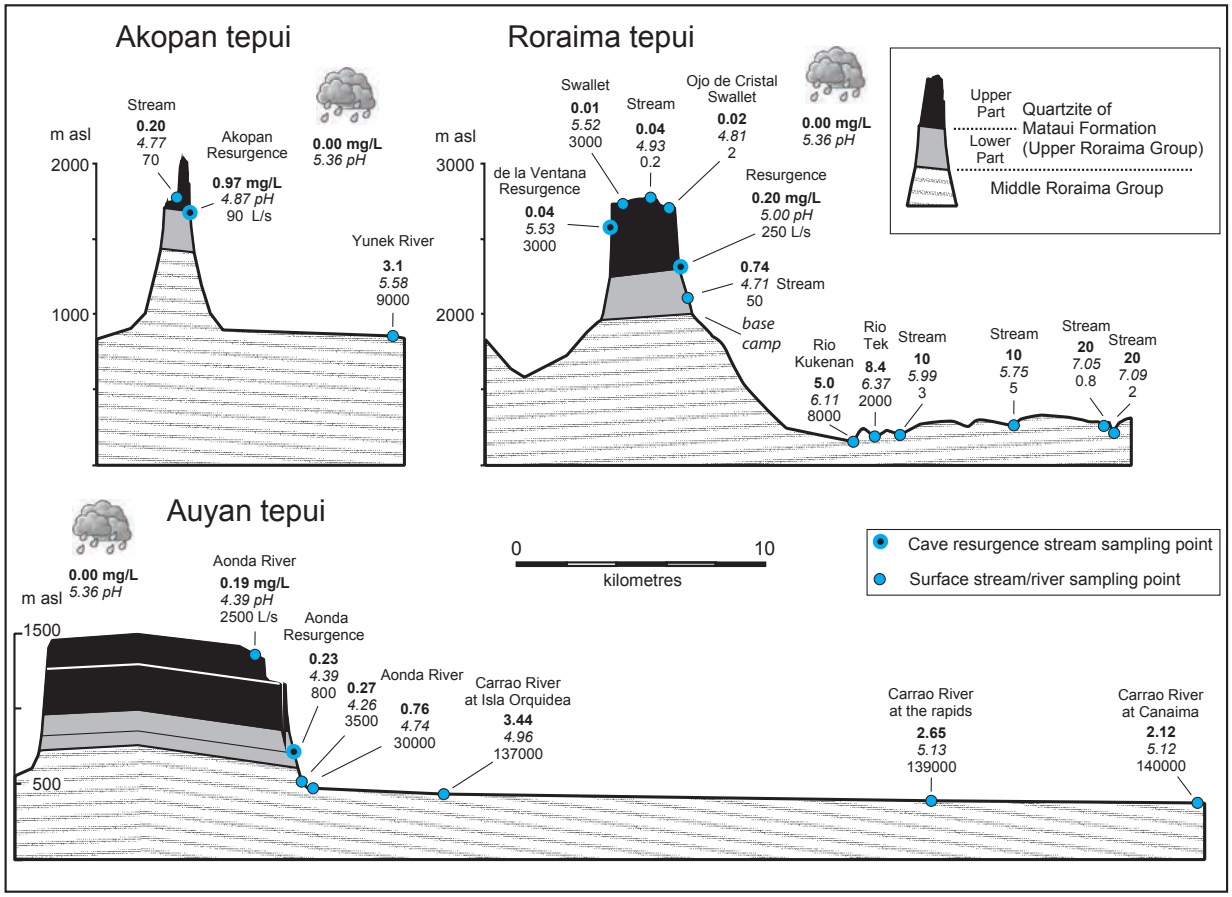

Fig. 2. Schematic hydrological sampling profiles of Akopan, Roraima and Auyan tepuis. The numbers in bold refer to silica content, the pH values are indicated in italics, while discharge is reported in litres per second. Rainfall values are below cloud symbols.

the Mataui Formation. Where these horizons are intersected by vertical fractures, a laminar flow developed and a system of interstratal protoconduits formed along the low dipping beds. Protoconduit enlargement was generated by piping of loose sands, derived from arenised rock (Sczerban and Urbani, 1974) or unlithified beds (Aubrecht et al., 2011), creating a horizontal drainage network of conduits. Since most of the explored cave systems consist of mainly parallel galleries developed along the gently dipping strata, a vadose flow fed by meteoric groundwater is supposed to represent the major pre-conduit flow pattern, as observed in limestone caves (Palmer, 1999).

In some cases, passages developed along these laterally widened stratigraphic horizons form huge environments (e.g. ~270x160x30 m in Imawarì Yeuta) where the ceiling is supported only by random pillars. When these voids develop at shallow depth, their collapse can create wide areas of boulders at the surface and might also be responsible for the formation of the giant collapse sinkholes clearly recognizable on the tepui's flat surface.

In this study we investigated six of the most important cave systems explored in the area: four with predominant stratigraphically controlled horizontal development (Roraima Sur, Akopan-Dal Cin, Auchimpe, Imawarì Yeuta cave systems), and two of mixed stratigraphically/structurally controlled vertical development (Aonda and Auyan Tepui Noroeste).

Roraima Sur represents the longest cave explored in Roraima Tepui (10.8 km in length) where different draining collectors created a horizontal maze network of passages (Fig. 3). The cave mostly developed along thin layers of shales and arkoses between the quartz-sandstone beds (Galán et al., 2004b; Aubrecht et al., 2012).

In the Chimanta massif our research focused on the Akopan-Dal Cin cave system (Akopan Tepui) 2.7 km long (Fig. 4). The highest cave entrance is a big collapse sinkhole very close to the bordering cliff, drained by a horizontal stream that intersects a main collector, stratigraphically controlled by a quartz-sandstone bed (Mecchia et al., 2009); thin layers of iron-hydroxides were observed along the conduits. Some chemical analyses were also performed in the Auchimpe cave (1.7 km), part of the Arañas cave system, in the Churì tepui (the south-eastern part of Chimanta massif hosts ~17 km of cave conduits explored by Czech and Slovak caver expeditions) (Mecchia et al., 2009; Aubrecht et al., 2012). In the northwestern sector of Auyan Tepui most of the analyses on waters were performed during two different expeditions in the Aonda cave system. This cave is composed of hundred metres deep vertical *simas* feeding horizontal collectors (Fig. 5). In this area, almost 5 km of conduits were explored and surveyed providing a good view on the subterranean hydrological network, from the sinkholes to the resurgence (Piccini and Mecchia, 2009). A few other analyses were also performed on the waters of Auyan Tepui Noroeste cave system, a cave with many entrances reaching 370 m of depth and totalling more than 3 km of conduits.

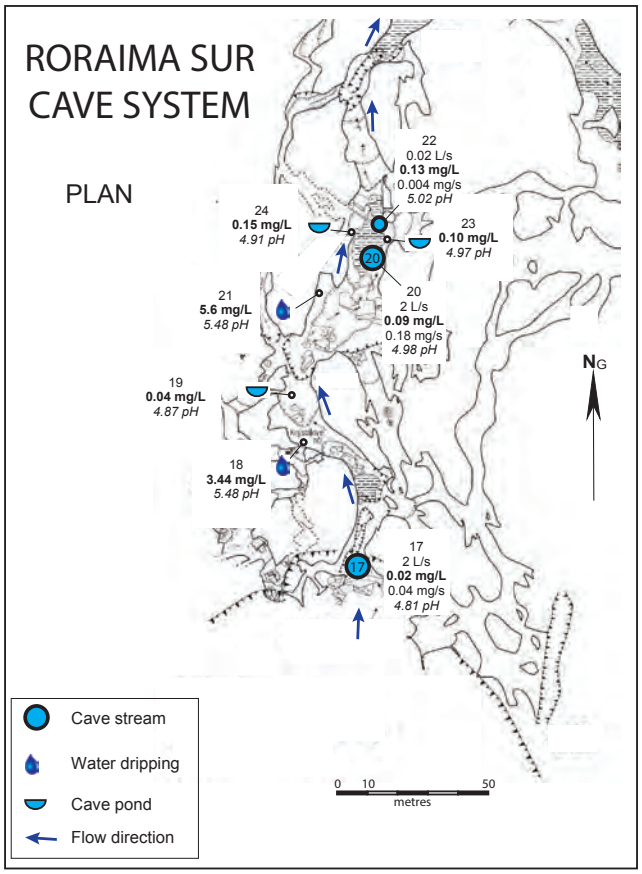

Fig. 3. Plan view of the Roraima Sur cave system (Ojo de Cristal Cave section only) with sampling points and analytic results. The numbers in bold refer to silica content in mg L^{-1} of SiO_2, while dissolved load is expressed in mg s^{-1}; the pH values are indicated in italics; discharge is reported in litres per second (Survey from Brewer-Carias and Audy, 2011).

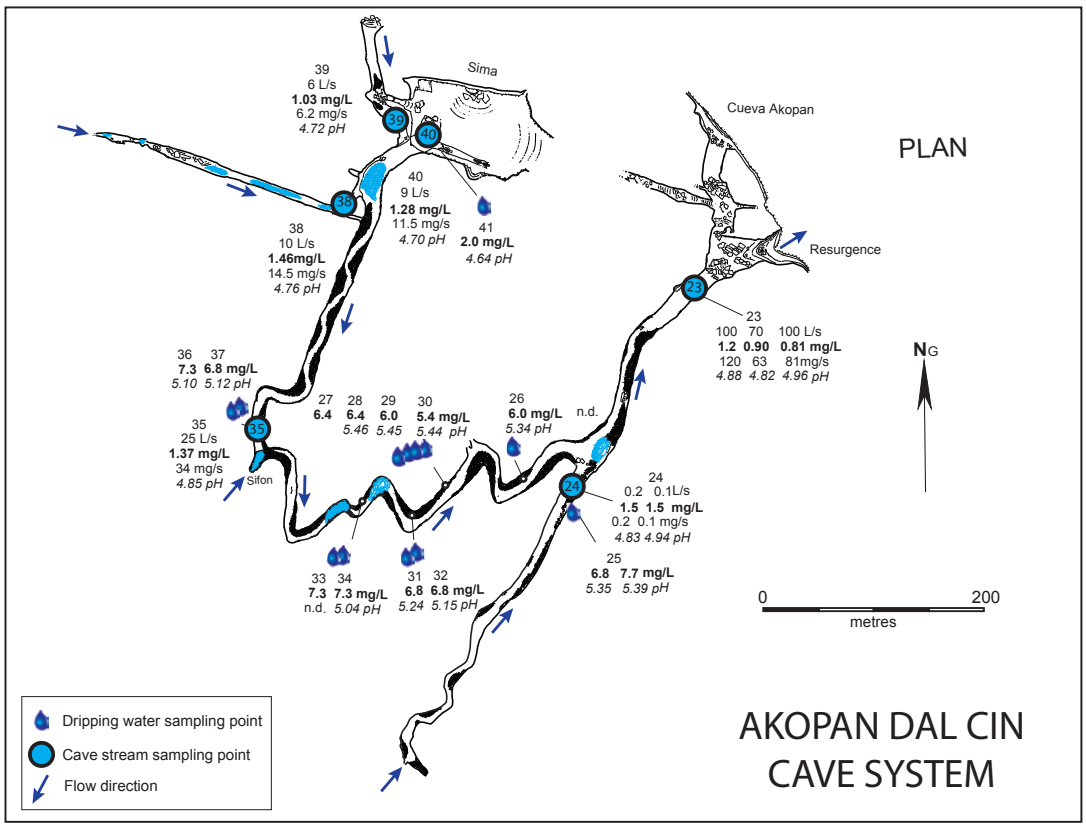

Fig. 4. Plan view of the Akopan-Dal Cin cave system with sampling points and analytic results. The numbers in bold refer to silica content in mg L^{-1} of SiO_2, while dissolved load is expressed in mg s^{-1}; the pH values are indicated in italics; discharge is reported in litres per second (Survey from La Venta Geographic Exploration).

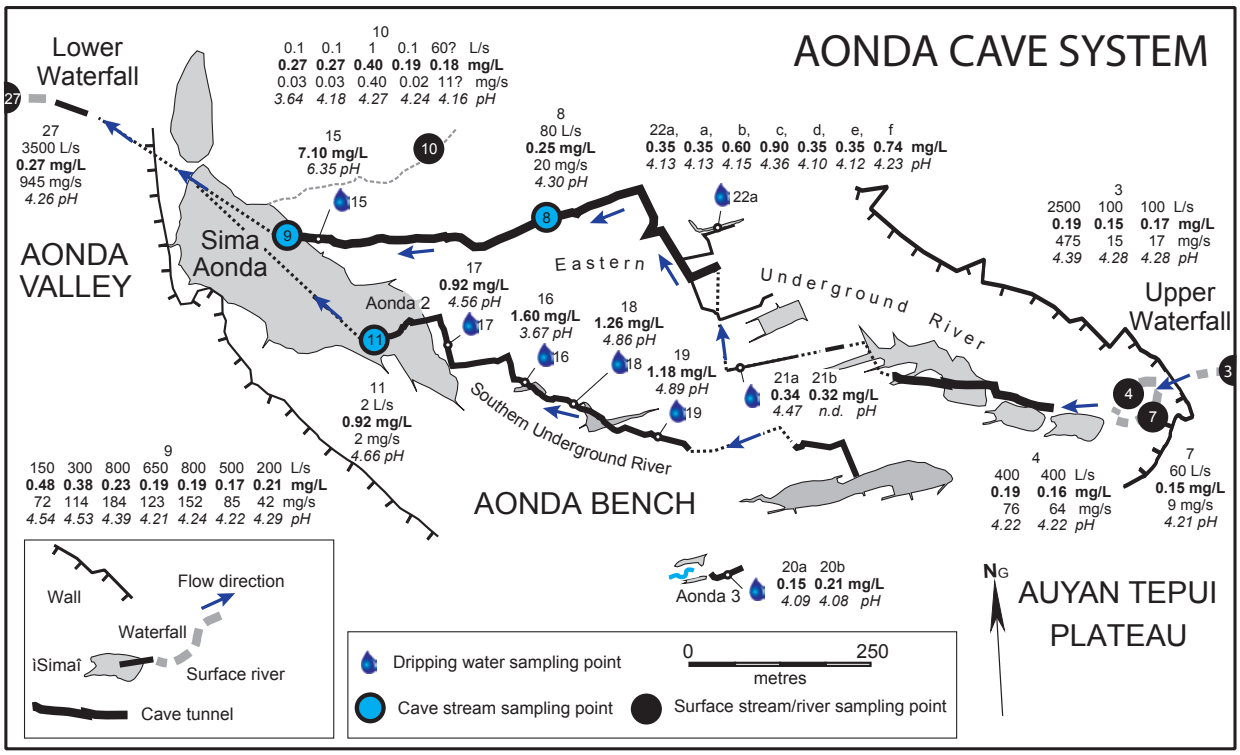

Fig. 5. Plan view and hydrological scheme of the Aonda cave system showing the main rivers, sinkholes and resurgences. Sampling points and analytic results at different conditions of discharge are reported. The numbers in bold refer to silica content in mg L^{-1} of SiO_2, while dissolved load is expressed in mg s^{-1}; the pH values are indicated in italics; discharge is reported in litres per second (Survey from La Venta Geographic Exploration).

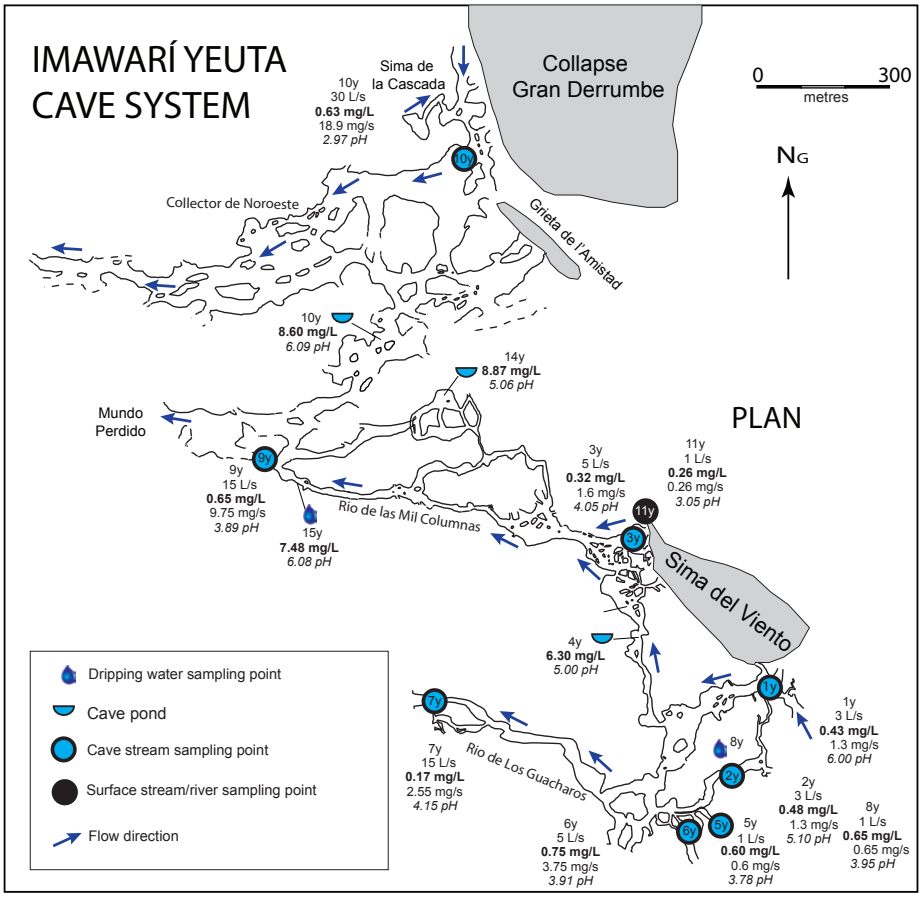

Fig. 6. Plan view of Imawarì Yeuta cave system with sampling points and analytic results. The numbers in bold refer to silica content in mg L^{-1} of SiO_2, while dissolved load is expressed in mg s^{-1}; the pH values are indicated in italics; discharge is reported in litres per second (Survey from La Venta Geographic Exploration).

Another set of analyses was carried out on the waters of Imawarì Yeuta cave, located in the NE sector of Auyan Tepui (Fig. 6). This cave probably represents the longest quartz-sandstone cave known in the world, with about 20 km of explored passages (15.5 km already surveyed) (Sauro et al., 2013b). With the exception of three underground collectors draining two sinkholes, most of these galleries are no longer hydrologically active, but host wide standing pools fed by drip and seepage waters.

2.2.3 Methods

2.2.3.1 Sampling and analysis of water

Water sampling and in situ analyses in different hydrodynamic conditions (rain, occasional ponds, peat deposits, surface and subterranean streams, and cave drips; fig. 7) were performed in March 1993, February 1996, March 2009, February 2012, and March 2013. The same instrumentation was used over this long period of time. Logistic problems make access to the tepuis during the rainy season extremely challenging if not impossible; therefore all the measurements here reported refer to the dry season.

Temperature (T), acidity (pH) and electrical conductivity (EC) were measured by handheld field instruments (Hanna Instruments) after calibration on site. Accuracy was 0.1 ºC, 0.01, and 1 $\mu S\ cm^{-1}$ respectively. Dissolved silica concentration (DSi) was measured by using a field colorimetric test kit (Aquaquant 14410 Silicon - Merck), that allows the determination of silica in the concentration range 0.01-0.25 mg L^{-1} with an error less than 20%. Samples with concentration higher than 0.25 mg L^{-1} were diluted with distilled water and then analysed. Results were expressed following the convention of representing dissolved silica as the oxide SiO_2. A number of sampling points were chosen for repeated measurements in the period of expedition, obtaining information on the variability of SiO_2 in different flow rate conditions.

In order to determine dissolved elements through ICP-MS analyses in the laboratory, double water samples were collected in 10 sampling points at Imawarì Yeuta in March 2013: a 250 mL bottle of untreated and unfiltered water, and a 100 mL bottle of 0.45 micron-filtered and 1 mL 65% HNO_3 acid-preserved water.

Inductively coupled plasma-mass spectrometry (ICP-MS) (method EPA 6020A) was applied for determination of multi-elemental sub $\mu g\ L^{-1}$ concentrations (Al, Sb, As, Ba, Cd, Ca, Fe, Mg, Pb, K, Na, Zn) where the recovery of the Laboratory Control Sample (LCS) resulted between 85 and 115%, as expected by the method lines. Anion Chromatography (method EPA 9056A) was used to determine chloride, fluoride, nitrate, and sulphate in the solution. NH_4 concentration was measured on the untreated sample with the method APAT CNR IRSA 4030 A2 MAN 29 2003 (IRSA-CNR, 2003).

2.2.3.2 Discharge measurements in subterranean streams

Stream discharges in caves were estimated close to each sampling point by measuring repetitively the flow speed of floating objects and estimating the cross section of the stream. Cross sections characterised by a regular shape and a sufficiently slow and not too turbulent flow of water were preferably chosen. Since the objects were floating in the centre of the channels, the mean velocity was estimated as 80% of the measured surface velocity. For these reasons, discharges are considered

Fig. 7. Different hydrodynamic conditions characterising the set of samples: A) Peat bogs and ponds on the tepui surface (photo La Venta). B) Stream on the tepui plateaus surface (Akopan Tepui) (photo Corrado Conca). C) The characteristic amber colour of cave streams in Imawarì Yeuta cave system (photo Vittorio Crobu). D) Crystal-clear water in standing pools feed by drippings in the fossil branches of Imawarì Yeuta (photo Vittorio Crobu). E) Waterfalls falling from the external cliffs of Chimanta Tepui (photo Vittorio Crobu). F) The Kukenán river at the base of Roraima Tepui (photo Vittorio Crobu).

affected by an uncertainty of at least 30% and therefore can only be considered as indicative. Dripping rates from cave walls were measured as number of drops falling in the unit time.

2.2.3.3 Chemical analysis of rock samples

Ten quartz-sandstone samples were ground to ultrafine powders and kept 24 hours at 110 °C for wavelength dispersive X-ray fluorescence (WD-XRF) chemical analysis. Ten grams of sample were mixed with 2.5-5 mL of Elvacite polymer resin, dissolved in acetone. The mixture was stirred to allow acetone evaporation and Elvacite distribution. The resultant powder was placed in a penny-shaped mold and compressed with a vertical pressure of 40 MPa for one minute.

A WD-XRF spectrometer Axios - Panalytical (Institute for Mineralogy and Petrology - IMP of ETH – Zurich) equipped with five diffraction crystals was used. The SuperQ software package provided by Panalytical was employed for calibration and data reduction. Calibration is based on 30 certified international standards. The precision of analysed elemental abundances is better than ±0.2% for SiO_2, and ±0.1% for the other major elements with the exception of MnO_2 and P_2O_5 that have concentration errors of approximately ±0.02%. For trace elements, relative errors are better than 10% for concentrations of 10-100 ppm, better than 5% for higher concentrations and can reach as much as 50% at levels below 10 ppm. Therefore, the detection limit is considered to be approximately 5-10 ppm.

2.2.4 Results

Samples, collecting sites and analytical results are reported in Table A1. The relationship among physical parameters (pH and EC) and dissolved silica (SiO_2) are reported in Figures 8, 9 and 10. The chemical results generally agree with previous literature (Briceño et al., 1990; Briceño & Paolini, 1992; Ipiña, 1994; Edmond et al., 1995; Aubrecht et al., 2011; 2012).

The mean values of physico-chemical parameters and ion concentrations from different tepui tablelands are similar. On the other hand, each hydrodynamic condition (rivers, streams, ponds, drippings, etc.) have common characteristics with similar SiO_2 concentrations, EC and pH from all the tepuis and both in structurally (vertical) and stratigraphically (horizontal) controlled cave systems (Fig. 8).

Ion concentrations of Imawarì Yeuta waters (Table A2) are very low as suggested by the low conductivity. Fe and Al have mean concentrations around 50 µg L^{-1}, K is present only in few samples with an average of 0.53 mg L^{-1}, while Ba is present in the stream and dripping waters with an average of 3.2 µg L^{-1}. In some cases also Cl, SO_4 and NH_4 occur with average concentrations respectively of 0.8, 0.6, and 0.4 mg L^{-1}. Other elements such as Sb, As, Ca, Mg, Pb, Na, Zn, if present, were below the instrument/method detection limits (i.e. <1 µg L^{-1}).

2.2.4.1 Rainwaters

Eleven rainwater samples were collected on Roraima, Akopan and Auyan tepuis. The pH ranged from 3.8 to 7.0, with an average value of 5.4: the EC was always low (1-24 μS cm^{-1}), and silica was always below the detection limit (Fig. 9A). The highest EC values (15-23 μS cm^{-1}) were measured after a long period without precipitation, whereas the lowest EC value (under the accuracy range of the instrument - 1 μS cm^{-1} - i.e. almost pure water) was detected in rainwater sampled during a heavy storm.

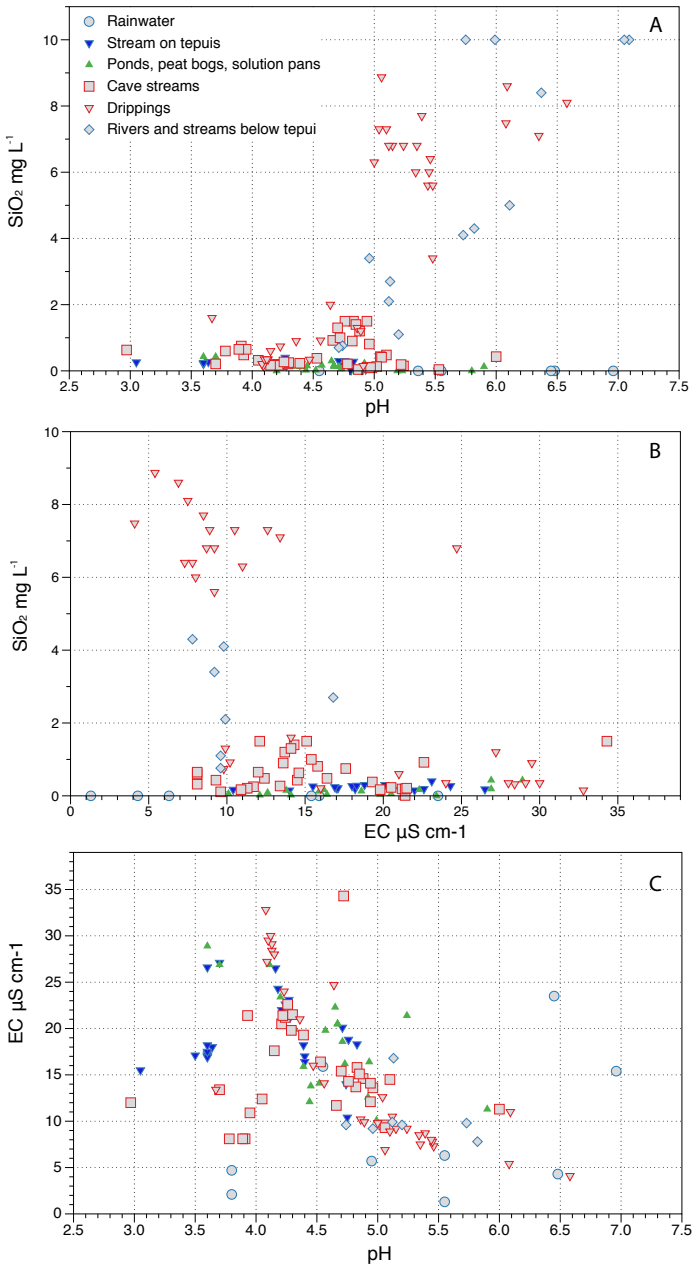

Fig. 8. Results for the whole set of samples analyses reported as correlations between SiO_2 concentration (mg L^{-1}), pH and EC (μS cm^{-1}). The different hydrological settings for each sample are reported in the legend. In A and B the extreme values of SiO_2 concentration up to 20 mg L^{-1} for the river below tepuis are not reported in order to have a better visualization of the dataset.

2.2.4.2 Stagnant surface water in peat, ponds and swamps

Twenty-seven samples were collected in ponds, swamps and peat deposits that cover wide areas on the summit tepuis plateaus (Fig. 7A). The pH ranged from 3.6 to 5.9 (average 4.7) (Fig. 9B), the EC between 10 and 29 µS cm^{-1} (average 19 µS cm^{-1}) (Fig. 9C). All samples were collected in daytime and water temperature was between 15 and 26 °C, depending on the altitude of the sample point, but also on the time of sunlight exposure in stagnant ponds. The dissolved silica concentration ranged from <0.01 to 0.43 mg L^{-1} (average 0.12 mg L^{-1}). A chemical analysis of water in a peat bog showed the presence of aluminium (68 µg L^{-1}), iron (34 µg L^{-1}), and also NH_4 (0.24 mg L^{-1}) probably related to decomposition of organic matter. In fact, all the

samples collected on the tepui plateaus present a characteristic amber colour, because of decomposing vegetation substance (Ertel et al., 1986).

2.2.4.3 Surface stream and river waters

Surface creeks and streams on the tepui plateaus

Thirty-one water samples were collected in creeks and streams flowing on the summit plateaus, where the outcropping lithologies are mostly quartz-sandstone and sometimes alkaline sills of diabase, and most of the area is covered by vegetation. All the flowing waters presented the typical amber colour (Fig. 7B). Creeks and streams with a variety of discharges (between 0.1 L s^{-1} and 3 m^3 s^{-1}) were sampled. Water temperature varied between 14 and 21 °C during sampling, corresponding mainly to an elevation gradient. Samples had pH ranging from 3.1 to 5.5 (average 4.2), EC from 10 to 27 µS cm^{-1} (average 19 µS cm^{-1}), and dissolved silica concentration comprised between 0.01 and 0.40 mg L^{-1} (average 0.20 mg L^{-1}) (Fig. 9 F-G-H). The chemical analysis of one sample showed it to contain low aluminium and iron concentrations, around 34 and 68 µg L^{-1}, respectively.

Surface streams and rivers in the lowlands on the pediments surrounding the tepuis

Fourteen water samples were collected in streams and rivers in the lowlands, on the pediments surrounding the tepuis (Fig. 7 F). All the flowing waters presented the typical amber colour and the water temperatures were similar to those measured in the streams on the tepui tablelands.

Seven streams with discharges ranging between 1 and approximately 8,000 L s^{-1} were sampled in the Kukenán drainage basin below the southern wall of the Roraima Tepui (Figs. 1 and 7 F). The highest pH, from 5.8 to 7.1 (average 6.4), as well as the highest dissolved SiO_2 concentrations were measured in these streams (from 5 to 21 mg L^{-1}, above the saturation for quartz and progressively increasing as the distance from the tepui increased, Fig. 2). All these values were higher than those obtained from all streams flowing on tepui summit plateaus. Unfortunately we did not have the possibility to measure the EC of these high silica samples because of failure of the EC instrument, but the higher (neutral) pH of these waters suggests that an alkalisation effect is active. Conversely, a sample collected in a creek on the slope near the so-called “Base Camp” along the normal ascending trail for

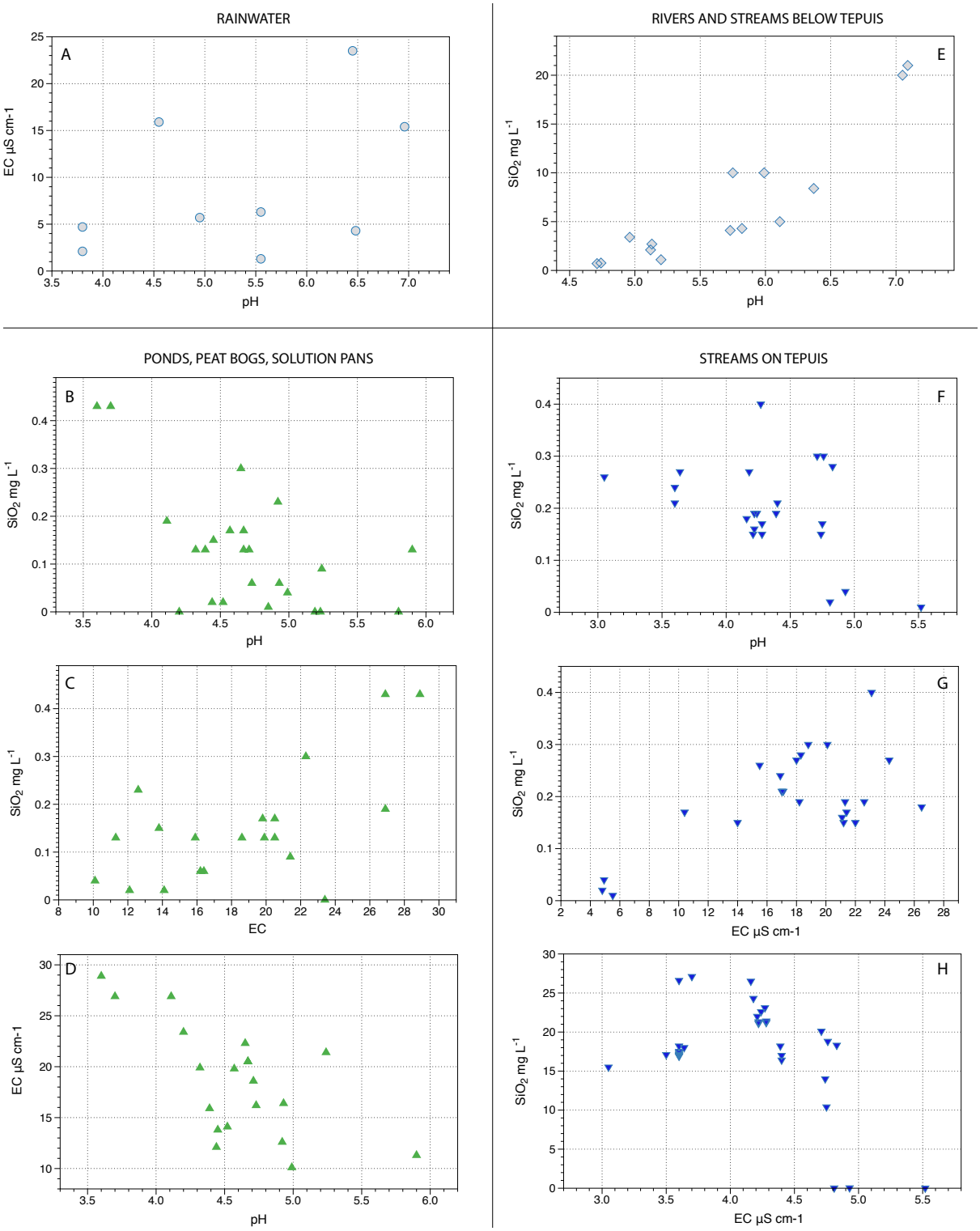

Fig. 9. Correlation of the main physical parameters for the surface water samples. A) Rainwaters reported as pH-EC relation graph (no graph is required for the SiO_2 concentration because always below the detection limit). B-C-D) Relationships between SiO_2 concentration, pH and EC in ponds, peat bogs and solution pans samples. E) Dissolved silica versus pH in samples from rivers and stream below tepuis. Unfortunately the dataset of EC for these samples is incomplete and therefore is not reported as a graph. F-G-H) Relationships between SiO_2 concentration, pH and EC in streams on the tepui plateaus.

Roraima showed the typical signature of tepui waters: low pH (4.7) and low dissolved silica concentration (0.7 mg L^{-1}).

Three measurements were performed in the Yunek river at the Yunek village, below the Eastern wall of Akopan Tepui. In low discharge conditions (approximately 6,000-9,000 L s^{-1}) pH values of 5.7 and 5.8 were measured, together with high levels of dissolved silica (4.1-4.3 mg L^{-1}). After a storm event, in a higher discharge condition (approximately 12,500 L s^{-1}), the pH dropped to 5.2 and the dissolved silica concentration to 1.1 mg L^{-1}, while the EC maintained a very low value (8-10 µS cm^{-1} in all three measurements).A set of three measurements was also taken in the large Carrao river, from Orquidea Island to Canaima waterfall, in the Gran Sabana to the north of the Auyan Tepui. The discharge reported in Figure 2, approximately 140,000 L s^{-1}, represents the mean discharge at Canaima measured in February between 1980 and 1983 (Galán, 1992). The pH increased along the course downstream from 5.0 to 5.1, while the dissolved silica concentration slightly decreased from 3.4 to 2.1 mg L^{-1} (Fig. 2 and 9E) perhaps because of dilution effects or biological intermediation along the river course. A sample collected in the Aonda valley river, tributary of Carrao river, provided a pH value of 4.7 and dissolved silica concentration of 0.76 mg L^{-1}, thus showing a trend similar to the one observed in the Kukenán catchment area. The EC (9-17 µS cm^{-1}) did not show a clear correlation with pH and SiO_2 concentration.

2.2.4.4 Underground waters

Cave streams and resurgences

Forty samples were collected in 6 cave streams and resurgences. All these waters present the typical amber colour (Fig. 7C). Water temperature measurements gave average values correlated with altitude: 13.8 °C in the upper part of Roraima Sur cave (2700 m asl), 14.6 °C in Imawarì Yeuta cave (1960 m asl), and 15.6 °C in Akopan-Dal Cin cave (1500 m asl). Very variable stream discharges characterise the different branches surveyed in this study, and also the same main stream in a cave in short periods of time. In the "Ali Primera" resurgence (inside Sima Aonda) several measurements were taken and discharge varied from 150 to 800 L s^{-1}. However, downstream the resurgence of the whole Aonda cave system, a discharge of 3,000 L s^{-1} was measured. In the 3 measurements performed at the Akopan-Dal Cin resurgence the discharges were estimated between 70 and 100 L s^{-1}. The resurgences of the Roraima cave system (two outlets at the base of the Southern Wall) showed a total discharge of approximately 500 L s^{-1}. In Imawarì Yeuta cave most of the conduits are no longer hydrologically active; a discharge of 30 L s^{-1} was measured in the main river of the cave during a dry period.

In all the cave streams the EC was quite similar, ranging between 8 and 34 µS cm^{-1} (average 16 µS cm^{-1}) (Fig. 10 B-C). An average pH of 4.6 resulted from measurements (Fig. 10 A-C), with both the

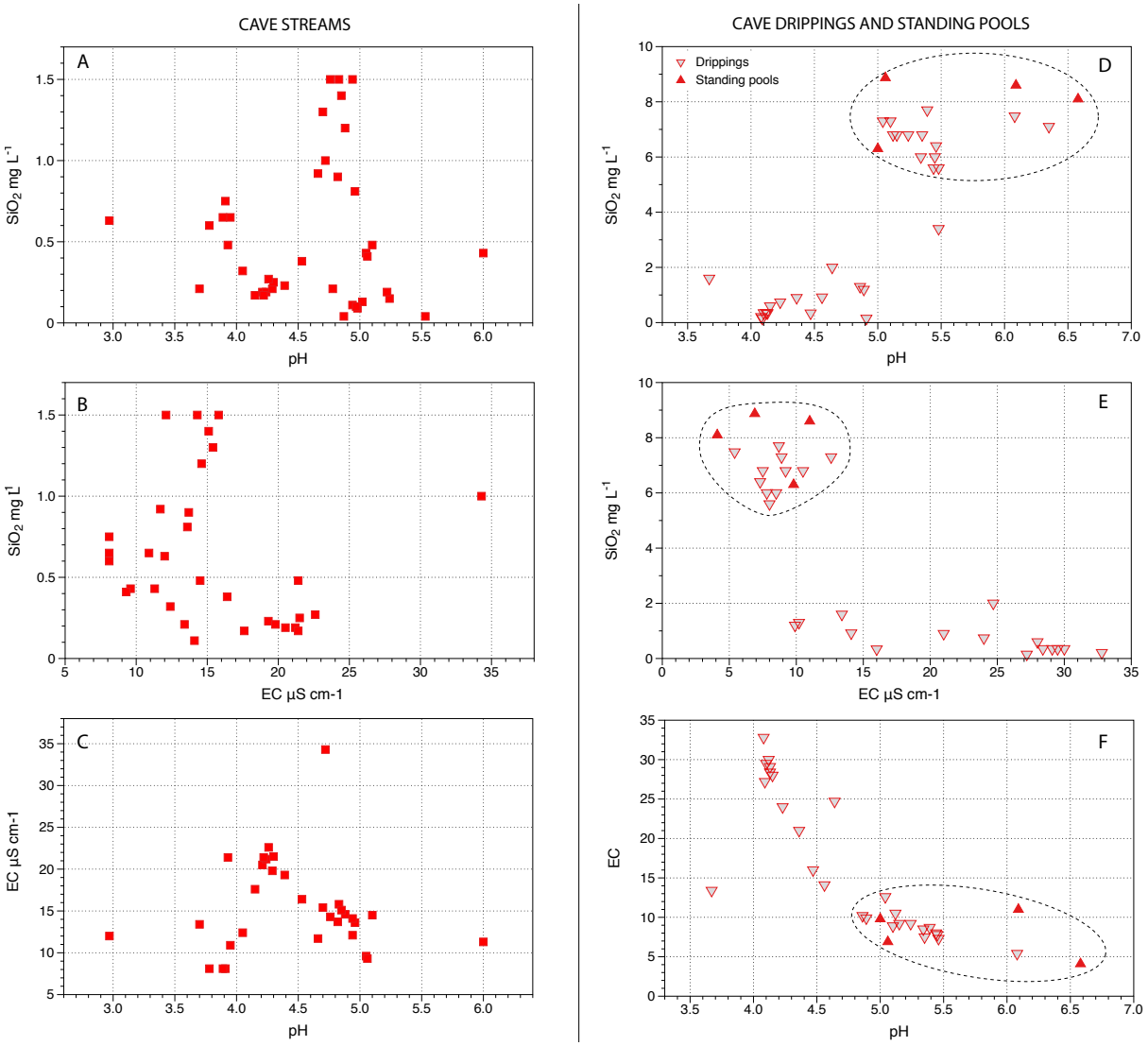

Fig. 10. Correlation of the main physical parameters for the cave waters samples. DSi (SiO_2 mg L^{-1}) versus pH and EC (mS cm^{-1}) in cave streams (A-B-C) and in cave drips and standing pools (D-E-F). The dashed line highlights the high silica drippings and standing pools.

extreme values encountered in the same cave (Imawarì Yeuta): 3.0 in the "Collector de Noroeste" and 6.0 at the beginning of the "Rio de Los Italianos".

Stream waters from Imawarì Yeuta cave were shown to contain only small amounts of aluminium and iron (averages of 53 and 56 µg L^{-1} respectively). Potassium was also present in some samples with values between 0.41 and 0.56 mg L^{-1}, together with small amounts of barium around 1.5 µg L^{-1}. The presence of NH_4 up to 0.7 mg L^{-1} confirmed that these waters take their origin from superficial sinking streams enriched in organic matter derived from decomposing vegetation in peat bogs.

The cave streams always show a relatively low concentration of dissolved SiO_2, from 0.17 up to 1.20 mg L^{-1} in the main streams. Dissolved silica content increases along their course downstream:

- from 0.19 on the summit plateau to 0.27 mg L^{-1} at the base of Auyan Tepui, passing through the Aonda cave system, less than 2 km long, in the same day of measurement (Fig. 2);
- from 0.32 to 0.65 mg L^{-1} in Imawarì Yeuta cave in only 1 km of stream course (samples 3y and 9y in Fig. 6);
- from 0.02 at the stream inflow to 0.20 mg L^{-1} at the resurgence in Roraima Sur System in around 1.5 km of supposed subterranean stream course (Galán et al., 2004a) (Fig. 2);
- from 0.20 mg L^{-1} measured in a surface creek before sinking underground to 0.80-1.20 mg L^{-1} at the resurgence in Akopan-Dal Cin cave system (around 2 km) (Fig. 2).

A relatively constant dissolved SiO_2 along the main subterranean stream of Akopan-Dal Cin cave

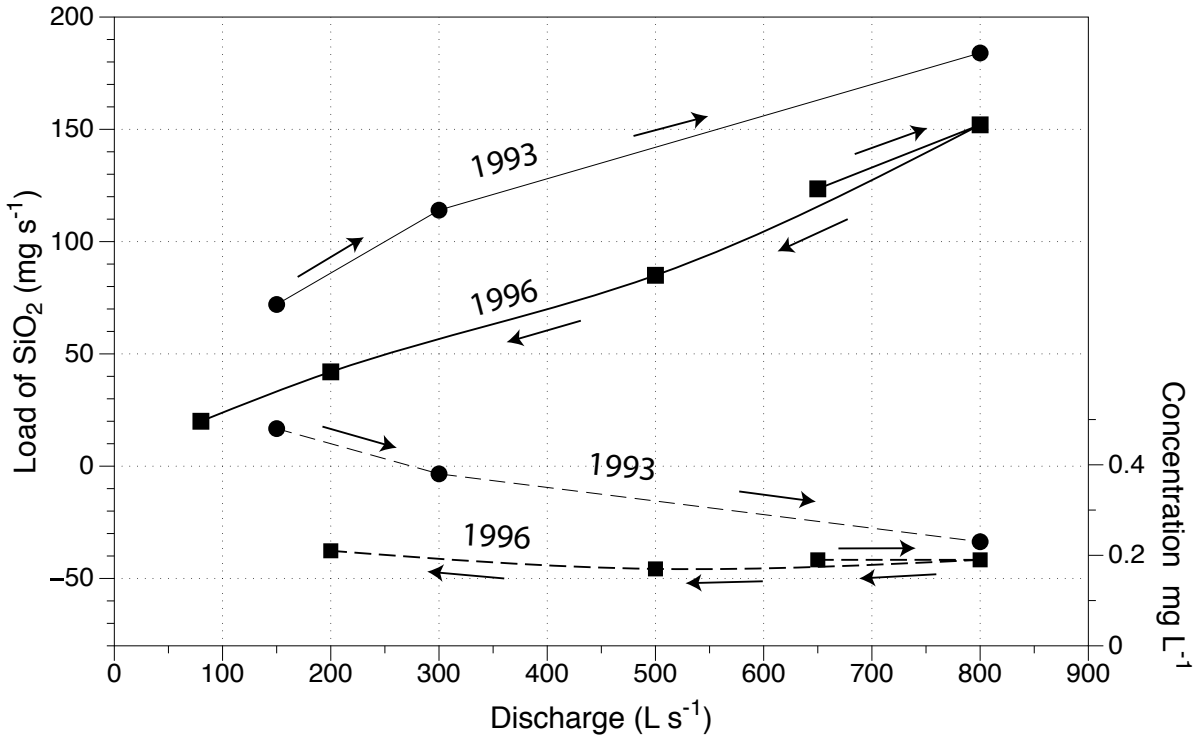

Fig. 11. Dissolved concentration (dashed line) and load (solid line) of SiO_2 versus discharge during two different flood events at Ali Primera resurgences in the Aonda System. While during growing discharge the dissolved silica concentration slightly decreases, its dissolved load follows an opposite path, considerably increasing. Arrows indicate time evolution.

system, less than 1 km long (Fig. 4), with concentration around 1.0 mg L^{-1}, was measured in a dry period with very low discharge coming from cave drippings and rivulets.

SiO_2 concentration in cave stream water varies also with discharge. The stream flowing through the Aonda cave was repeatedly measured at the Ali Primera resurgence under different discharge conditions (point 9, Fig. 5). The regular decrease of SiO_2 concentration was observed with the increase of discharge during storm events, nonetheless the dissolved silica load transported by the stream rose with the increase of the discharge (Fig. 11).

Cave drips and stagnant ponds

Thirty-eight samples were collected from drips and standing ponds. The analyses (Fig. 10 D-E-F) showed that cave drips can be divided in two groups based on dissolved silica concentrations, below or above 4 mg L^{-1}. The chemical characteristics of high silica drippings have the following features: a) transparency, b) very low EC, ranging from 4 to 13 µS cm^{-1}, c) relatively high pH, ranging from 5.0 to 6.5, and d) high dissolved SiO_2 concentration, ranging from 5.6 to 8.6 mg L^{-1} (water almost saturated with respect to quartz, sometimes dripping from opal speleothems). This last characteristic is unique, since no other type of water found in tepuis presents such a high dissolved silica content.

Low silica drippings are characterised by: a) transparency (with few exceptions), b) higher EC, ranging from 10 to 33 µS cm^{-1}, c) lower pH, ranging from 3.7 to 5.5, and d) relatively low dissolved SiO_2 concentrations, ranging from 0.15 to 3.40 mg L^{-1} (undersaturated with respect to quartz).

Drip rates are generally not correlated with silica concentration, although faster drips are often believed to contain lower silica contents.

The chemical analysis of a high silica drip in the Imawarì Yeuta cave forming a black-reddish flowstone revealed the presence of relatively high iron concentration (114 µg L^{-1}), low aluminium (34 µg L^{-1}), potassium (0.47 mg L^{-1}) and the highest content of barium documented among all the samples (7.7 µg L^{-1}). Standing pools that are fed by drippings in inactive branches of the Imawarì Yeuta cave system and Auchimpe have the highest content of SiO_2 documented in the cave water samples (8.6 and 8.1 mg L^{-1}), low EC values (11.0 and 4.1 µS cm^{-1}) and pH close to neutrality (6.1 and 6.6). The samples from these pools in Imawarì Yeuta cave showed also relatively high amounts of dissolved barium (2.8 and 6.5 µg L^{-1}), chlorides (1.1 mg L^{-1}) and sulphates (0.63 mg L^{-1}), while iron and aluminium were almost below the detection limit.

2.2.4.5 Chemical composition of the quartz-sandstones

The 10 samples of quartz-sandstones collected from the Mataui Formation on Roraima, Akopan and Auyan tepuis were observed in thin section under the polarized light microscope in order to identify their mineralogical composition. From a petrographic point of view these rocks are composed mainly

of detrital monocrystalline quartz grains with non-undulatory extinction and often with overgrowth, disposed in interlocked structures due to the burial metamorphism that affected the Roraima Group (Urbani et al., 1977) (Fig. 12 A-B). Detrital matrix is absent. In some samples the content of authigenic aluminium phyllosilicates (mostly pyrophyllite with minor kaolinite) is relevant. Kaolinite frequently grows on the expense of feldspars and white mica, during the early diagenesis at relatively low pressures and temperature. Pyrophyllite forms from precursor kaolinite and quartz through a dissolution-precipitation process (reaction isograd).

ID	Description	SiO_2	TiO_2	Al_2O_3	Fe_2O_3	MnO	MgO	CaO	Na_2O	K_2O	P_2O_5
AKT	Unweathered quartzite	96.03	0.05	3.28	0.10	0.001	0.005	0.017	0.419	0.059	0.015
ROR17	Unweathered quartzite	96.39	0.07	2.27	0.43	0.001	0.003	0.016	0.575	0.201	0.016
AK3B	Weathered quartzite	82.95	0.13	11.14	0.35	0.004	0.003	0.006	0.315	0.046	0.024
AK4	Weathered quartzite with dark bands	85.71	0.09	3.00	0.50	0.002	0.003	0.011	0.319	0.035	0.031
AK5A	Weathered quartzite with dark bands	73.85	0.51	22.59	2.01	0.021	0.012	1.011	0.428	0.460	0.105
AK5B	Weathered quartzite with dark bands	71.71	0.65	22.60	3.70	0.035	0.070	1.010	0.505	0.629	0.079
AK5C	Unweathered quartzite	85.00	0.07	14.21	0.17	0.004	1.085	1.085	0.297	0.158	0.072
AK3A	Weathered quartzite with dark bands	81.03	0.48	16.38	1.75	0.014	1.024	1.024	0.253	0.047	0.039
ROR16	Weathered quartzite	78.41	0.11	7.08	0.13	0.001	/	0.008	0.285	0.096	0.069
KC1	Arkose from Kukenan F.m.	52.99	0.17	9.86	21.93	0.027	0.352	/	0.169	0.888	0.247

Table 1. Bulk-rock composition of different quartz-sandstones (%). The symbol "/" means below the detection limit.

Sample ID	Ba	Ce	Cl	Cu	F	S	Sr	Th	U	V	W	Y	Zn	Zr
AKT	343.6	/	6	34.7	102.9	/	25.4	5.9	1.0	3.3	687.2	8.1	/	60.9
ROR17	359.8	/	6.7	29.3	137.9	/	38	6.2	2.3	5.7	722.3	6.1	/	194.3
AK3B	285.3	0.6	7.1	30.8	152.0	/	27.5	7.6	2.7	3.4	267.5	10.9	1.0	231
AK4	307.7	/	4.8	31.6	139.5	/	13.7	3.9	1.8	5.4	315.1	3.8	2.8	111.6
AK5A	376.7	117.0	113.0	34.2	249.5	/	81.6	20.5	7.2	14.2	95.8	28.6	15	816.4
AK5B	382.2	120.1	227.5	31.8	298.4	/	92.5	21.8	8.0	21.7	248.9	27.7	19.4	856.4
AK5C	487.9	/	34.7	29.9	174.8	/	26.8	5.5	1.2	2.7	167.8	7.9	0.5	104.4
AK3A	108.2	70	/	30.2	199.9	/	49	15.5	5.3	9.4	495.1	23.1	30.7	825.8
ROR16	395.9	23.9	21.5	28.9	134.5	/	33.7	8.0	2.4	3.5	319.3	8.4	1.4	139.1
KC1	161.5	50.5	56.9	38.1	946.1	232.5	31.2	19.7	10.5	107.2	117.9	11.4	70.6	125.7

Table 2. Trace element composition of different quartz-sandstones (ppm). The symbol "/" means below the detection limit.

The coexistence of kaolinite and pyrophyllite in the cement approximately marks the transition diagenesis-metamorphism (Bucher and Frey, 1994). In some cases they occur as a thin coating of aluminium phyllosilicates covering the interdigitated quartz grain rims (microstylolites), typical texture of pressure solution during burial metamorphism (Fig. 12 C). Thin veins of iron hydroxides cross the quartz-sandstone parallel to the stratification showing them to have migrated during the low grade burial metamorphism following fluid pressure cracks that cut the quartz grains (Fig. 12 D). In this facies, quartz grains are well rounded probably because of a higher phyllosilicate cement impeding grain contact and consequent pressure solution. Feldspars are very rare and were not found in most samples.

The WD-XRF analyses, performed on the same 10 samples to obtain their relative elemental concentration (Table 1-2), confirmed the petrographic observations. In general, the content of SiO_2 (which is almost totally quartz with only insignificant amounts of amorphous silica) is between 70 and 90% while the other major component is aluminium, with concentrations between 3 and 22% depending on the relative content of phyllosilicates such as pyrophyllite, muscovite, and kaolinite.

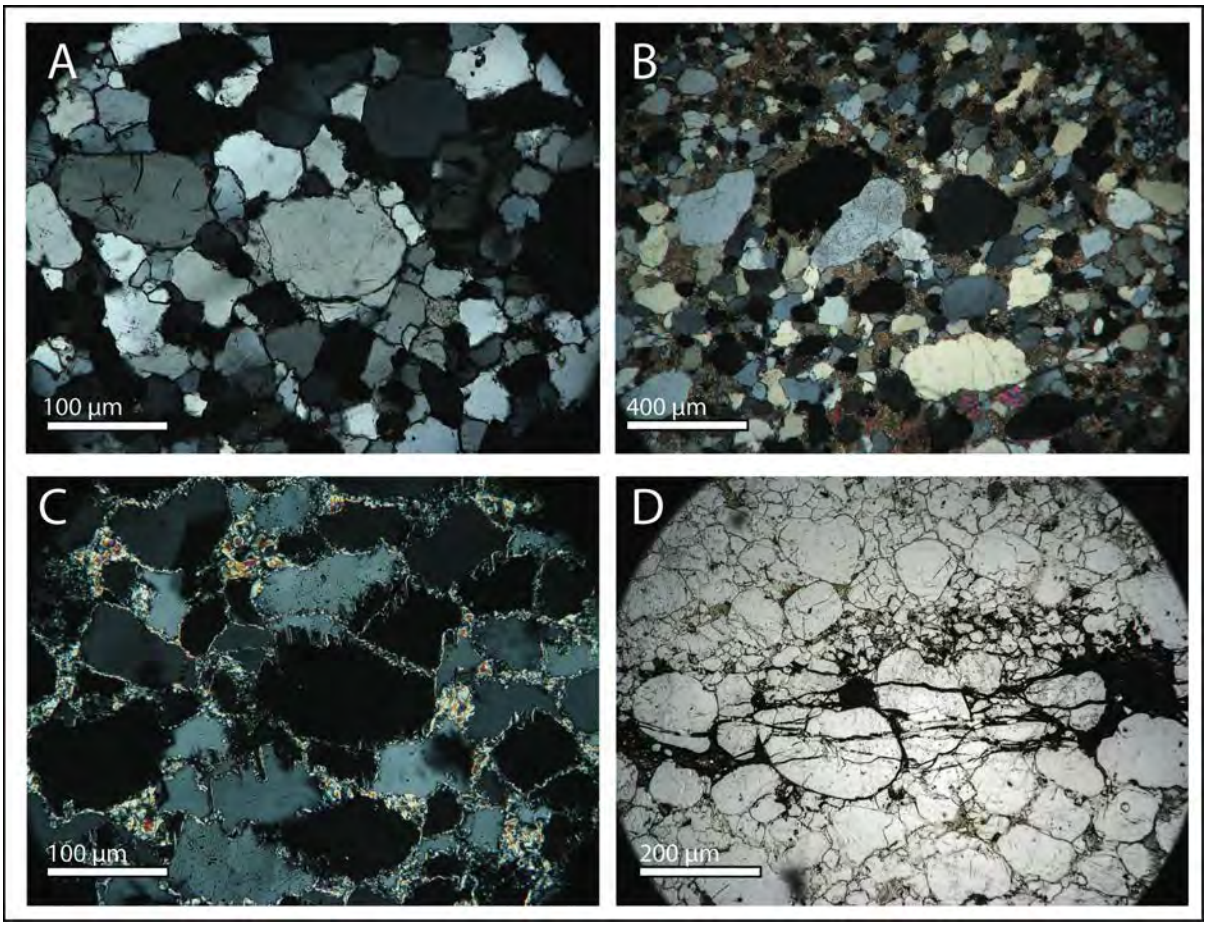

Fig. 12. Petrographic features observable in thin sections of the Mataui Formation samples: A) Typical quartz-sandstone composed almost totally by quartz monocrystalline grains with interlocked structure (X Nicols); B) Quartz-sandstone richer in pyrophyllite (X Nicols); C) A thin coating of phyllosilicates covers the interdigitated quartz grains (microstylolites) typical of pressure solution during burial metamorphism (X Nicols); D) Injected iron hydroxide provoking quartz grains cracking due to vertical fluid pressure (|| Nicols).

These phyllosilicates were already reported as common components of these rocks also by previous authors (Urbani, 1976; Aubrecht et al., 2011; Sauro et al., 2013a). Analyses performed also in the more arkosic beds, show low concentrations in K and Na, and almost no Ca and Mg, suggesting that the content of feldspar in these lithotypes is below 1-4%. Iron is present in the form of iron hydroxides such as goethite and limonite (determined by raman analyses, see Sauro et al., 2013c).
As regards the trace elements, barium reaches concentrations around 300-400 ppm and is normally present in sandstone as interstitial brines in form of soluble $BaCl_2$ salts (Pettijohn et al., 1987). Titanium, fluorine, tungsten, and zirconium are components of highly insoluble minerals such as detrital titanite, apatite, wolframite, and zircons (Pettijohn et al., 1987).
A sample (KC-1) collected from the Kukenán Formation at the foot of the Auyan Tepui showed a more ferric composition with only 53% of quartz, 10% of aluminium and 22% of iron oxides.

2.2.5 Discussion

2.2.5.1 The silica-water system

In the waters of the tepui environment, at low temperature (16-20 °C) and acidic pH (4-5), the content of dissolved silica depends on the very low kinetics of dissolution and precipitation of quartz, and the time of water-rock interaction plays a fundamental role. In these conditions, silica is present in solution mostly as orthosilicic acid, H_4SiO_4, or as colloidal polycyclic acids (Krauskopf, 1956). The reaction with water is the following:

$$SiO_{2(s)} + 2H_2O_{(l)} \rightarrow H_4SiO_{4(aq)}$$

In these waters the orthosilicic acid is almost undissociated and the effects of complexion, hydrolysis and polymerisation should be negligible.
Rimstidt (1997) calculated the saturation at nearly neutral pH to be 8.7 mg L^{-1} for quartz in pure water at 17 °C (the average temperature of water in tepui caves), and around 100 mg L^{-1} for amorphous silica. The rate of quartz dissolution (k+) depends on temperature and pH of the solution (Fig. 13, for T=25 °C). The k+ values for quartz were determined measuring dissolution far from equilibrium in laboratory, obtaining values ranging between $1 \cdot 10^{-12}$ and $1 \cdot 10^{-13}$ mol m^{-2} s^{-1} at 25 °C in the pH range of interest for tepui waters (Bandstra et al., 2008). Amorphous silica dissolves at a rate approximately ten times faster than quartz under comparable conditions (Brantley, 2008). However, the dissolution rate constant and the solubility of quartz at low temperature are quite difficult to measure by experimental testing in laboratory, because of the long time needed to reach equilibrium. As a consequence, the uncertainty associated with the measured values for the parameters of the rate equation is quite large. A challenging factor, when experimental results are

used for comparison with a natural environment, is the calculation of the reactive surface area of the dissolving mineral.

The ionisation of the orthosilicic acid only starts at neutral to basic pH (Harman, 1927; Govett, 1960), and at increasing alkaline conditions, with pH > 8-9, it undergoes up to four consecutive dissociations, significantly increasing the amount of quartz which can be dissolved (Ford and Williams, 2007), releasing H^+ ions according to reactions:

$$H_4SiO_{4(aq)} \rightarrow H_3SiO_4^- + H^+$$
$$H_3SiO_{4\,(aq)}^- \rightarrow H_2SiO_4^{2-} + H^+$$
$$H_2SiO_{4\,(aq)}^{2-} \rightarrow HSiO_4^{3-} + H^+$$
$$HSiO_{4\,(aq)}^{3-} \rightarrow SiO_4^{4-} + H^+$$

Another important dissolution process, which releases silicic acid in a natural water system, is the hydrolysis of silicate minerals such as feldspars:

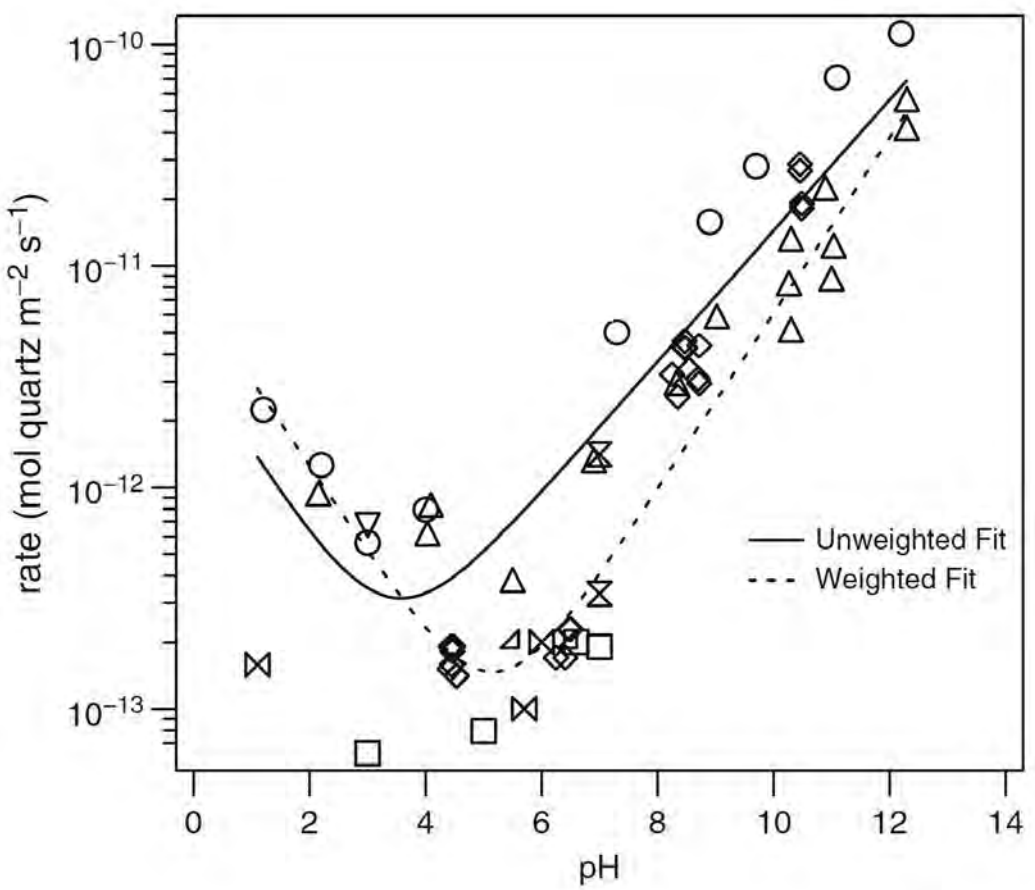

Fig. 13. Surface area-normalized quartz predicted dissolution rates at 25 °C as a function of pH, derived from the fitting of experimental data (symbols represents different experiments after Bandstra et al., 2008). Solid and dashed lines represent two non-linear fits of data.

$$2KAlSi_3O_{8(s)} + 2H_2CO_{3(aq)} + 9H_2O_{(l)} \rightarrow Al_2Si_2O_5(OH)_{4(s)} + 4H_4SiO_{4(aq)} + 2K^+ + 2HCO_3^-$$

$$2NaCaAl_3Si_5O_{16(s)} + 8H_2CO_{3(aq)} + 11H_2O_{(l)} \rightarrow 3Al_2Si_2O_5(OH)_{4(s)} + 4H_4SiO_{4(aq)} + 2Ca^{2+} + 2Na^+ + 8HCO_3^-$$

These reactions require dissolved CO_2 in the water system, release K and/or Na and/or Ca and form secondary minerals such as kaolinite, illite, and montmorillonite. Feldspars have dissolution rates increasing with rising H^+ activity at pH < 6, and rising OH^- activity above pH = 8.5 (Blum, 1994).
Moreover, silicic acid is released by the dehydroxylation-desilication dissolution-recrystallization reaction forming kaolinite from the metastable pyrophyllite in presence of water (Hurst and Könkle, 1985):

$$Al_2Si_4O_{10}(OH)_{2(s)} + 10H_2O \rightarrow 2Al^{3+} + 4H_4SiO_{4(aq)} + 6OH^-$$

$$2Al^{3+} + 2H_4SiO_4 + 6OH^- \rightarrow Al_2Si_2O_5(OH)_{4(s)} + 5H_2O$$

or the direct dissolution of kaolinite in case of acid pH, releasing also aluminium into the solution:

$$Al_2Si_2O_5(OH)_{4(s)} + 6H^+ \rightarrow 2Al^{3+} + H_2O + 2H_4SiO_4$$

All these reactions can contribute to the total amount of silicic acid in the water system and the signature of each process can be determined by the presence or absence of ions such as Al, K, Na, and Ca (Clayton, 1988).

2.2.5.2 Surface silica contribution

Unlike other measurements performed in other parts of the world (Hem, 1985; Rutherford, 1967), no dissolved silica was measured in rainwaters on tepuis. The average pH measured on tepuis was 5.4 (Fig. 9A), well comparable with the theoretical average value for rainwater, because of atmospheric dissolved carbon dioxide. Actually, the measured pH ranged from 3.8 to 7.0. That also is usual, since a very large volume of air passes through a storm system, rainfall characteristics are highly variable, not only from place to place but also from storm to storm in a single area (Hem, 1985). Rainwaters over the Gran Sabana region are not affected by anthropogenic sources of pollution neither by marine salt spray, showing therefore very low values of EC (1.3-23.5 $\mu S\ cm^{-1}$, Fig. 9A). Thus, rainwater is almost distilled water with minor dissolved elements related to atmospheric contributions (Sauro et al., 2013d).
When rainfall reaches the tepui surface, rainwater is in part drained by streams or retained over variable times in bushes, grass carpets and peat deposits. Because of decomposing vegetation, the water gets enriched in organic matter, giving its characteristic amber colour (Ertel et al., 1986).

Probably because of this enrichment in organic acids and dissolved organic CO_2, the pH decreases becoming more acid than that of rainwater (average pH 4.7). Small amounts of SiO_2 are dissolved from the quartz-sandstone substrate, producing an average concentration of 0.12 mg L^{-1}. The actual concentration of dissolved silica in the peat bogs and solution ponds varies depending on the time elapsed from the last rain event (time of water recharge in the ponds and swamps) and the local evaporation rate. A slight negative correlation between dissolved SiO_2 and pH was found (R^2 = -0.35, Fig. 9B), suggesting a correlation between the organic acids and the amount of silica in solution, as found in experimental studies (Bennet et al., 1988; Bennet, 1991).

Streams flowing on the tepui surfaces collect the waters seeping from the surrounding swamps and peat bogs, slightly enriched in dissolved silica, and also interact directly with the quartz-sandstone bedrock. The concentrations of dissolved SiO_2 measured in these streams are still very low, 0.2 mg L^{-1} in average. This could be due to the short time of water-rock interaction or locally to the formation of silica and iron hydroxide crusts on the rock surface because of evaporation processes. This case hardening shields the quartz rocks from subcutaneous dissolution and impedes the subcutaneous flow of seepage waters toward the external surfaces. For this reason, the mean denudation at the top of the tepuis calculated with ^{10}Be and ^{26}Al cosmogenic nuclides by Brown et al. (1992) is only of 1 mm ka^{-1} over the last several hundred thousand years, an order of magnitude lower compared to the 12 mm ka^{-1} measured on the surrounding lowlands in the Gran Sabana region (Yanes and Briceño, 1993).

2.2.5.3 Subsurface silica dissolution

In Roraima, Aonda and Imawarì Yeuta cave systems, the underground streams show a significant increase of silica concentration along their course. However, as observed for surface streams, the silica enrichment by direct dissolution along the wet streambeds is predictably almost insignificant. This is due to the very short time and little surficial area available for water-rock interaction. A calculation using the highest possible dissolution rate constant for quartz, outlined before, shows that environmental and physical conditions are insufficient even to produce a measurable increase in silica concentration in streams. The almost constant dissolved SiO_2 along less than 1 km in the main subterranean stream of Akopan-Dal Cin cave system (Fig. 4), with concentration around 1 mg L^{-1} measured in a dry period with very low discharge coming from cave drips, appears to confirm this hypothesis.

Consequently, the increase in silica concentration measured along most of the cave streams depends on contributions of dissolved silica from fractures, seepage waters, and condensation films on vadose conduit walls. For this reason the decrease in concentration during flood events (Fig. 11) is related to

an almost chemostatic behaviour because the dissolved silica derives mainly from seepage waters with slow infiltration rates instead of quick stream floodwaters sinking directly from the surface.

The low K concentration (slightly above the detection limit of 0.4 mg L^{-1} in only four samples out of fifteen) and the absence of Na and Ca (always lower than the detection limit of 0.4 mg L^{-1}) observed in both surface and underground waters of Imawarì Yeuta cave, and the extremely low EC, suggest that hydrolysis doesn't represent a relevant process controlling the silica concentration in the tepui waters. The aluminium solubility is very low at pH value ranging from 4 to 9 and its content doesn't change downstream, from peat and superficial streams through the cave system (Fig. 14A), keeping concentrations of around 50-60 µg L^{-1}. The presence of high aluminium concentrations (over 100 mg L^{-1}) and higher EC in some drippings reported by Aubrecht et al. (2012), and interpreted as a proof of laterisation, must be reconsidered to more appropriate values of 100 µg L^{-1}. In fact, considering the colorimetric kit that these authors used for their analyses, it is evident that there was an error in the notation of mg L^{-1} instead of the correct µg L^{-1}. Applying this correction to their data the aluminium concentrations are similar to our findings. In all cases the values of aluminium concentration documented by our research suggest that hydrolysis of feldspars and the dissolution of kaolinite can only be of local significance, in agreement with the general composition of the quartz-sandstones.

Because hydrolysis is generally negligible, the major contribution of dissolved silica must derive directly from dissolution of quartz, with probably minor amounts of pyrophyllite-kaolinite reactions affecting the composition of seepage waters in some beds.

Some insights in the SiO_2 dissolution process working in the subsurface are obtained examining the set of samples from drips and dripping-fed pools in caves. The two types of chemically distinct drip waters can be interpreted as fast seepage water (low silica drips), with probably several hours/days of residence time, and slow seepage water (high silica drippings), which probably is a mix of recent and old (possibly with even more than several years residence time) waters.

Although most of dripping waters probably come from infiltration of organic-rich waters (peat bogs), they are characteristically transparent. Virtually all suspended organic material is supposed to be filtered out during the slow descent through very thin microfracture systems, explaining their transparency (Fig. 7D).

The long residence time, i.e. of water-rock interaction, can explain the high dissolved silica concentration measured in many drips and standing pools. Local evaporation in the ventilated cavities might further increase the silica concentration.

The interaction with microbial communities producing ammonia on cave walls and rock pores, as suggested by Barton et al. (2009), could represent a mechanism for increasing pH and enhancing dissolution rates locally, but the higher values of pH documented in dripping waters are still not reaching the neutrality and their very low EC indicates that the silicic acid is almost undissociated.

Moreover ammonia and in general nitrates were not found in detectable concentration in any of the drip samples or standing pools. Therefore, if this process is really effective it has probably only local significance and does not affect the general composition of drip waters.

Condensation on cave walls provides a different source of water available for quartz dissolution. At a low flow rate the condensation water film is divided into thin threads or rivulets, and at even lower flow rates, the threads and rivulets break up into trains of sliding drops and blobs (Ghezzehei, 2004). In condensation water the pH values should be close to neutrality, being related to equilibrium with the atmospheric CO_2. Aubrecht et al. (2013) suggested that the group of drips closer to saturation is mainly related to originally strongly undersaturated, therefore highly aggressive, condensation water. However, the rate of downward movement of a condensation water film on a cave wall is far too fast, and the interaction time with the rock surface too short, to be consistent with the observed

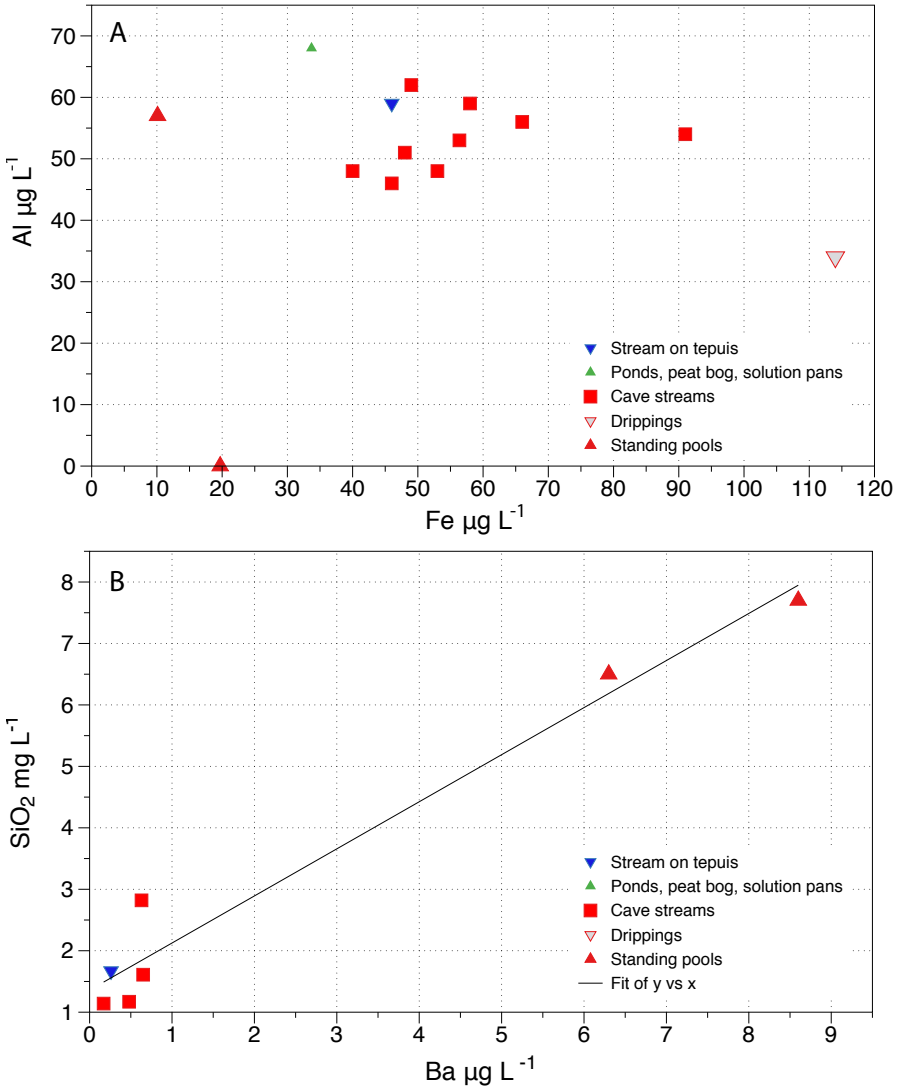

Fig. 14. A) Relationship between Al and Fe concentration (mg L^{-1}) in superficial and underground waters of the Imawarì Yeuta cave system: most of the samples have Al and Fe content around 40-60 µg L^{-1}, only a sample from a dripping water showed to be relatively enriched in Fe. B) Positive correlation between barium and SiO_2 content of cave waters revealing the seepage water contribution.

high concentration of silica in drippings.

Tokunaga and Wan (1997) have already demonstrated that film flow is a very important mechanism of flow in the vadose zone. Thus, the role of condensation water in further enlargement of pre-existing cave passages could be crucial to attain the impressive size of many subterranean conduits, given the extensive occurrence of films of strongly undersaturated water that line entire surfaces of ceilings and walls, continuously replaced by new condensation water.

When a film of water wets a cave wall, a process of solute diffusion could be active because of the different SiO_2 concentration existing between water in the wetting film (undersaturated and continuously renewed) and the water (supposed to be at the saturation point) in the intergranular porosity of the quartz-sandstone bedrock. Some silica molecules might be transported through diffusion from the rock pores to the film, causing pore water to become undersaturated with respect to quartz, reactivating dissolution on the surrounding grain surfaces. Once triggered, and given enough time (i.e., in geological stable conditions, absence of fast erosion of tepui plateaus and without a faster weathering mechanism of cave walls), the chemical potential due to solute diffusion could allow a slow but considerable removal of silica from inside the rock, producing the deeply arenised surfaces in the quartz-sandstone cave walls, as suggested by Piccini and Mecchia (2009).

The concept of arenisation in quartz-sandstones was explained first by Martini (1979) as due to dissolution along quartz grains boundaries, where the water circulates very slowly (advection). However, given the size of intergranular pores in unaltered rock (less than 1000 nm; Derjaguin and Churaev, 1986; Pettijohn et al., 1987), we do not think advection to be possible. On the other hand, aqueous diffusion is generally the dominant transport mechanism within the pores, and diffusion occurs along each mineral grain boundary interconnected with continuous paths (Garrels et al., 1949). Norton and Knapp (1977) experimentally determined the diffusion through some samples of unaltered quartzites, obtaining diffusion porosities of approximately 0.1%, a value that could be enough to start the arenisation process raising the general porosity in altered walls. The relatively high concentration of barium in the drips and dripping-fed pools closer to saturation (Fig. 14B) is also a clue giving information on the origin of these waters: barium, in fact, is typically present in the intergranular pores of the quartz-arenite in form of barium chloride (Pettijohn, 1987).

In general the concentrations of silica dissolved in streams and in the drips are in agreement with the few other studies on dissolved silica in surface and ground waters reported from other quartz-sandstone terrains like the Sydney Basin (Wray, 1995), Tchad (Mainguet, 1972), and Amem Land (Dames and Moore, 1981). Even though their precipitation regimes differ dramatically from those of the Gran Sabana, these similarities suggest that quartz dissolution and consequent arenisation is an important geomorphic process also in many other areas of the World.

2.2.5.4 Estimation of the subsurface dissolution

Even if the data are affected by large uncertainties because of the approximation in the discharge measurements and because the whole set is related only to the dry season, rough calculations can be made to estimate the subsurface dissolution contribution in the studied cave systems. Based on our data, the measured increase of dissolved silica concentration between inflow and outflow in Aonda, Roraima Sur and Akopan-Dal Cin cave systems were 0.08, 0.17 and 0.80 mg L^{-1}, respectively. Rough estimates of average discharges in the dry season (February-March) were 400, 500, and 90 L s^{-1}, respectively. Therefore, the load of dissolved silica added to the cave streams (downstream the inflow) and transported out of the system was of 32, 85 and 72 mg s^{-1}, respectively for the three caves. However, a small part of this load of silica comes from the dissolution on the surface of the tepuis (mainly in peat bogs and swamps). We can estimate this fraction considering our mean infiltration rate (i.e. effective precipitation) calculated for the months of February and March (65 mm/month). This infiltration rate can be changed into infiltration discharge by calculating the approximate areas of direct infiltration into the cave systems (downstream of the inflow), by means of the published cave surveys. We calculated catchments of about 0.8, 0.9 and 0.8 km^2 for Aonda, Roraima Sur, and Akopan-Dal Cin cave systems, respectively, obtaining similar infiltration discharges for the three systems (20-22 L s^{-1}, referred to the February-March period). Since the concentration of silica dissolved on the tepui plateaus was approximately 0.2 mg L^{-1} (surface streams), an average contribution of about 4-4.5 mg s^{-1} of dissolved silica (dry season) is expected from quartz dissolution on the tepui surfaces, before infiltration, in all three cave systems. These values can be compared with those estimated for the whole loads of dissolved silica added to the cave streams downstream of the inflow (i.e. 32, 85 and 72 mg s^{-1}, respectively) concluding that the dissolution of silica on the top surface of the tepuis contributes for only 5-13% of the total dissolved silica load. The remaining 87-95%, corresponding to 28, 81 and 68 mg s^{-1} for Aonda, Roraima Sur, and Akopan-Dal Cin cave systems respectively, would come from the underground dissolution of quartz in fractures, cave walls and streambeds. These values are referred to the dry season, when the rainfalls are less than 3 times lower than that of the average month. For correction to annual estimates of average quartz dissolution rates in these three cave systems, values at least double might be more realistic. Applying this correction, the quartz masses dissolved in the three systems would be around 1,800, 5,100 and 4,300 kg a^{-1}, corresponding to volumes of 0.7, 1.9 and 1.6 m^3 a^{-1}, respectively for Aonda, Roraima Sur, and Akopan-Dal Cin cave systems respectively. Runoff distribution is also invoked in the chemical weathering rate values obtained for the Carrao Basin, the Upper Caroni Basin and Gran Sabana region where surface rate values of 6,200, 6,900 and 6,600 kg km^{-2} a^{-1}, respectively have been observed (Yanes and Briceño, 1993).

These calculated amounts of SiO_2 removed from the cave systems, even if affected by large uncertainties, are surely relevant for speleogenesis, further considering that the dissolution of 20% of the rock is enough to cause a complete arenisation (Martini, 2000), breaking up the quartz-sandstone framework and consequently allowing mechanical erosion by turbulent streams. This means that for each 1,000 kg of silica (corresponding to 0.37 m^3 of quartz) removed through dissolution, around 1.8 m^3 of arenised quartz-sandstone might easily be removed by mechanical erosion afterward. These simple and rough calculations do not consider that rock can be eroded before being completely decemented and that running waters can also carry coarse (polygranular) sands and pebbles.

Considering the time span of weathering exposure for this area of South America (many tens of millions of years) (Briceño and Schubert, 1990; Piccini and Mecchia, 2009), even if the detected concentrations of SiO_2 are low, the effect of silica dissolution must be considered important in the geomorphic evolution. Furthermore, the variability of the climate during the past could have had an additional role: the process was surely decelerating during drier periods and accelerating during wetter periods.

However, our analyses do not exclude that other mechanisms of weathering might also be locally active along some beds, such as the dissolution of iron hydroxides, or the pyrophyllite-kaolinite re-equilibration reaction, with consequences on the rock hardness, further enhancing arenisation and the potential of mechanical erosion. These additional processes probably control the development of horizontal caves along specific layers.

In the streams flowing on the tepui pediments and the rivers of the surrounding lowlands the concentration of silica can reach the highest values of the entire set of samples. This because of the fact that along the pediments the streams flow on the arkosic sandstones of the Umaipé and Kukenán Formations where hydrolysis can give a relevant contribution of SiO_2, and also of Na, K, Ca, and Mg (see the chemical analysis for the tributaries of Caronì river in Edmond et al., 1995). The higher solubility of feldspars and amorphous silica with respect to quartz explains the abrupt increase of silica concentration (10-20 mg L^{-1}) measured along small streams flowing on the pediments below the Roraima tepui. Mainly for this reason the denudation rate calculated by previous studies on dissolved load mass balances of the Caronì river is around ten times higher than that of the tepui summit plateau (between 9 and 12 mm ka^{-1}; Yanes and Briceño, 1993; Edmond et al., 1995).

2.2.6 Conclusions

Even if the detected concentrations of SiO_2 are low, as expected from experimental studies, quartz dissolution appears to play a fundamental role in the formation of the tepui landscape. The presented geochemical data show that the majority of dissolved silica in surface and underground

waters of tepuis results from the dissolution of quartz while hydrolysis of other silicates only plays a minor role.

On the top surface of the tepuis the dissolution of silica is very slow contributing only for 5-13% of the total dissolved silica load. In the subsurface the major contribution of silica to the underground drainage, about 87-95% of the total dissolved silica load, is most likely given by slow percolation along vertical fissures and horizontal interlayers or laminar movements of condensed water films on cave walls. These waters could be enriched in SiO_2 not only from direct dissolution but mainly by chemical potential diffusion from the intergranular porosity-saturated waters. This process does not produce secondary minerals, such as clay minerals, which might seal the fractures and inhibit the water flow. The low content of K, Al, and Fe documented in some samples are probably related to local hydrolysis, dissolution of minor kaolinite and goethite in certain layers. All these chemical data suggest that arenisation, sensu Jennings (1983), is an active process.

In conclusion, weathering on the tepui table mountains works mainly underground causing the opening of deep fractures (*simas* and *grietas*) and the formation of extensive horizontal conduit networks. The tepui top surface is lowering mostly through collapses related to these underground processes, while scarp retreat is controlled by the higher weathering rate of the more arkosic formations constituting the base of the massifs.

Acknowledgements

We want to thank all participants of the many expeditions organised by La Venta on the tepuis over the last twenty years, and especially our Venezuelan members Raul Arias Betancourt and Freddy Vergara Castro for the logistic support. This research has benefited from the permit for speleological exploration and water analyses from the Instituto National de Parques (INParques) from Venezuela and from the economic support of many sponsors: Geotec S.P.A., Dolomite, Intermatica, Ferrino, Napapijri, and Allemano Metrology. Detailed chemical analyses on the waters sampled during the 2013 expedition to Auyan Tepui were sponsored by the Chelab s.r.l. laboratories, Treviso. WD-XRF analyses on rock samples were carried out by Lydia Zender of ETH-Zurich. FS, LP and MM wrote the main discussion, MM made the majority of the analyses with the help of JL, FV and all the other authors. LS and JDW highly contributed to the final text, while NT contributed with the petrographic and WDS analyses discussion.

Appendix Tables

Table A1. The whole set of 159 analyses divided in different groups of hydrodynamic conditions. The data set specifies collecting sites, date of sampling, temperature (°C), pH, EC (µS cm^{-1}), SiO_2 (mg L^{-1}), Discharge (L s^{-1}, or drops $minute^{-1}$ if underlined), colour.

	Samle ID		tepui massif	location	date	T °C	pH	EC uS/cm	SiO2 mg/L	Disch. (L/s - *drops/min*)	L = limpid A = amber
Table 1. Field analyses of rain water in Tepui area	A	0a	Auyantepui - Aonda Bench	Aonda Base Camp	20/02/93		4.6	15.90	0.00		
					21/02/93		5.0	5.70			
					24/02/93		6.5	4.30	0.00		
					01/03/93		5.6	1.30	0.00		
					05/03/93		3.8	4.70			
					24/02/96		5.6	6.30	0.00		
	A	0b	Auyantepui - Northern area	Auyantepui Northern Base Camp	22/02/93		3.8	2.10			
	C	0	Chimanta Massif -SE area	Village of Yunek	10/02/09		6.5	23.50	0.00		
					16/02/09		7.0	15.40	0.00		
	R	0a	Roraima Tepui - Southern area	"Base Camp"	28/01/12		5.4		0.00		
	R	0b	Roraima Tepui - Southern area	Sugre "Hotel"	31/01/12		5.5				
Table 2. Field analyses of water from streams and rivers around Tepuis	A	31	Auyantepui - Northern side	Carrao River above Canaima Waterfall	23/02/96		5.1	9.90	2.12	140000	A
	A	30	Auyantepui - Northern side	Carrao River at the rapids	23/02/96		5.1	16.80	2.65	139000	A
	A	29	Auyantepui - Northern side	Carrao River at Isla Orquidea	23/02/96		5.0	9.20	3.44	137000	A
	A	28	Auyantepui - Northern side	The river in Aonda Valley	03/03/93		4.7	9.60	0.76	30000	A
	C	1	Chimanta Massif - SE side	Yunek River at Yunek village	10/02/09	23.1	5.8	7.80	4.28	9000	A
					16/02/09		5.2	9.60	1.11	12500	A
					22/02/09		5.7	9.80	4.07	6500	A
	R	1	Roraima Tepui - Southern side	Rio Kanaupán (1st stream along Mt. Roraima trail)	27/01/12	19.5	7.1		21.0	2	-
	R	2	Roraima Tepui - Southern side	Rio Maturu (2nd stream)	27/01/12	20.2	7.1		20.0	0.8	-
	R	3	Roraima Tepui - Southern side	Rio Kiuri (3rd stream)	27/01/12	20.7	5.8		10.0	5	-
	R	4	Roraima Tepui - Southern side	4th stream	27/01/12	21.7	6.0		10.0	3	-
	R	5	Roraima Tepui - Southern side	Rio Tek (5th stream)	01/02/12		6.4		8.40	2000	-
	R	6	Roraima Tepui - Southern side	Rio Kukenán (6th stream)	27/01/12	21.8	6.1		5.00	8000	-
	R	7	Roraima Tepui - Southern side	Stream on "The Slope" after the "Base Camp"	28/01/12	14.8	4.7		0.74	50	-
Table 3. Field analyses of water from surface streams on Tepuis	A	3	Auyantepui - Plateau	The surface river upstream of Aonda Upper Waterfall	03/03/93	17.2	4.4	18.20	0.19	2500	A
					04/03/96		4.3	21.20	0.15	100	A
					04/03/96		4.3	21.40	0.17	100	A
	A	4	Auyantepui - Aonda Bench	The surface river below Aonda Upper Waterfall	01/03/96		4.2	21.30	0.19	400 ?	A
					02/03/96		4.2	21.10	0.16	400 ?	A
	A	10	Auyantepui - Aonda Bench	Surface stream that feed into Sima Aonda	20/02/93	19.4	3.6	18.00	0.27	0.1	A
					22/02/93	20.4	4.2	24.30	0.27	0.1	A
					24/02/93		4.3	23.10	0.40	1	A
					24/02/96		4.2	22.60	0.19	0.1	A
					25/02/96		4.2	26.50	0.18	60 ?	A
	A	7	Auyantepui - Aonda Bench	Cueva de la Cascada swallet stream	02/03/96		4.2	22.00	0.15	60	A
	A	33	Auyantepui - Northern area	Surface stream near Sima Ayuantepui Norte 2	21/02/93	19.1	4.4	17.00	0.21	4	
					21/02/93	17.8	4.4	16.40		4	
					22/02/93	18.2	3.6	17.00	0.21	16	
					22/02/93	18.8	3.6	17.30		16	
					23/02/93	17.5	3.6	17.10	0.21	50	
					24/02/93	17.4	3.6	16.90	0.24	50	
					24/02/93	17.8	3.6	17.50		16	

					25/02/93	17.7	3.5	17.10		5	
	A	34	Auyantepui - Northwestern area	Surface stream (Rio Pintado) near Sima Auyan. Noroeste	28/02/93	17.1	3.6	26.60			
					28/02/93	17.2	3.6	18.20			
					28/02/93	17.4	3.7	27.10			
	A	11y	Auyan Tepui - North-Eastern sector	Sima del Viento swallet	08/03/13	15.5	3.1	15.50	0.26	1	A
	C	6	Chimanta Massif - Churi Tepui	Surface stream 1 on the plateau	11/02/09	16.6	4.7	14.00	0.15	75	A
	C	9	Chimanta Massif - Churi Tepui	Surface stream 2 on the plateau	11/02/09	16.5	4.8	10.40	0.17	100	A
	C	13	Chimanta Massif - Churi Tepui	Surface stream 3. near Las Columnas Cave entrance	12/02/09		4.7	20.10	0.30	5	-
	C	14	Chimanta Massif - Churi Tepui	Las Columnas Cave - stream at cave entrance	12/02/09		4.8	18.80	0.30	2	-
	C	20	Chimanta Massif - Akopan Tepui	Surface stream on the plateau	13/02/09		4.8	18.30	0.28	20	A
	R	11	Roraima Tepui - Southern part	Swallet towards the Window	31/01/12		5.5		0.01	3000	
	R	13	Roraima Tepui - Southern part	Surface stream in the Crystal Valley	29/01/12	14.6	4.9		0.04	0.2	
	R	17	Roraima Tepui - Southern part	Ojo the Cristal swallet (Roraima Sur B3)	30/01/12	16.2	4.8		0.02	2	
Table 4. Field analyses of water from ponds, peat bogs and solution pans on Tepuis	A	12	Auyantepui - Aonda Bench	A pond	20/02/93	23.0	4.4	12.10	0.02	stagnant	A
					24/02/96		4.2	23.40	0.00	stagnant	turbid
	A	14	Auyantepui - Aonda Bench	Peat	29/02/96		4.1	26.90	0.19	1L/10s	A
	A	13a	Auyantepui - Aonda Bench	Solution pan "a"	03/03/96		4.5	13.80	0.15	stagnant	A
	A	13 b	Auyantepui - Aonda Bench	Solution pan "b"	03/03/96		4.4	15.90	0.13	1L/150s	A
	A	5	Auyantepui - Plateau	Peat	04/03/96		4.3	19.90	0.13	1L/100s	A
	A	6	Auyantepui - Plateau	A solution pan	04/03/96		4.5	14.10	0.02	stagnant	A
	A	25	Auyantepui - Northern area	A pond	21/02/93	18.3	3.7	26.90	0.43	stagnant	-
					25/02/93	18.1	3.6	28.90	0.43	stagnant	-
	A	12y	Auyan Tepui - North-Eastern sector	A solution pan near camp site	08/03/13	17.5	5.9	11.32	0.13	stagnant	-
	C	2	Chimanta Massif - Churi Tepui	A solution pan at the Tower of Radio-link	11/02/09	25.6	5.0	56.70	0.04	stagnant	A
	C	3	Chimanta Massif - Churi Tepui	Peat at the Tower of Radio-link	11/02/09	20.7	4.9	16.40	0.06	stagnant	L
	C	4	Chimanta Massif - Churi Tepui	Water inside vegetation. at the Tower of Radio-link	11/02/09				0.06	stagnant	L
	C	5	Chimanta Massif - Churi Tepui	Peat at the Tower of Radio-link	11/02/09	22.6	5.0	10.10	0.04	stagnant	L
	C	7	Chimanta Massif - Churi Tepui	A solution pan near Stream No. 1	11/02/09	22.0	4.6	19.80	0.17	stagnant	A
	C	8	Chimanta Massif - Churi Tepui	Peat near Stream No. 1	11/02/09	22.2	4.7	16.20	0.06	stagnant	A
	C	10	Chimanta Massif - Churi Tepui	Peat near Stream No. 2	11/02/09	17.7	4.7	20.50	0.13	stagnant	A
	C	11	Chimanta Massif - Churi Tepui	Peat near Stream No. 2	11/02/09	17.5	4.7	18.60	0.13	stagnant	A
	C	12	Chimanta Massif - Churi Tepui	A solution pan in the Western area of the plateau	11/02/09		5.2	21.40	0.09	stagnant	A
	C	15	Chimanta Massif - Churi Tepui	Peat near the Auchimpe Cave entrance	21/02/09		4.9	12.60	0.23	stagnant	A
	C	21	Chimanta Massif - Akopan Tepui	Peat near the sima of Akopan Cave (Lower Bench)	14/02/09		4.7	20.50	0.17	stagnant	A
	C	22	Chimanta Massif - Akopan Tepui	Peat near the sima of Akopan Cave (Lower Bench)	16/02/09		4.7	22.30	0.30	stagnant	A
	R	12	Roraima Tepui - Southern part	"Jacuzzi" pond	29/01/12	15.8	5.2		0.00	almost stagnant	-
	R	14	Roraima Tepui - Southern part	Pond "a" near Sugre "Hotel"	29/01/12	16.3	5.8		0.00	stagnant	-
	R	15	Roraima Tepui - Southern part	Pond "b" near Sugre "Hotel"	29/01/12	16.0	5.2		0.00	almost stagnant	-
	R	16	Roraima Tepui - Southern part	Peat near Ojo de Cristal Cave entrance	30/01/12	19.6	4.9		0.01	stagnant	-
Table 5. Field analyses of water from cave streams and	A	9	Auyantepui - Aonda Bench	Sima Aonda - Ali Primera Resurgence	01/03/93		3.9	21.40	0.48	150	A
					01/03/93		4.5	16.40	0.38	300	A
					04/03/93		4.4	19.30	0.23	800	A
					28/02/96		4.2	20.50	0.19	650	A
					29/02/96		4.2	21.20	0.19	800	A
					01/03/96		4.2	21.40	0.17	500	A

					04/03/96		4.3	19.80	0.21	200	A
	A	8	Auyantepui - Aonda Bench	Sima Aonda. upstream of Ali Primera Resurgence	06/03/96		4.3	21.50	0.25	80	A
	A	11	Auyantepui - Aonda Bench	Sima Aonda 2. cave stream	27/02/93		4.7	11.70	0.92	2	A
	A	27	Auyantepui - Aonda Valley	Aonda water downstream of Lower Waterfall/Resurgence	03/03/93	19.8	4.3	22.60	0.27	3500	A
	A	32	Auyantepui - Northern area	Sima Auyantepui Norte 2. stream below 300 m waterfall	20/02/93	17.2	3.7	13.40	0.21	10	-
	A	1y	Auyantepui - Northeastern area	Ymawarì Yeuta. beginning of Rio de Los Italianos	04/03/13	14.3	6.0	11.25	0.43	3	A
	A	2y	Auyantepui - Northeastern area	Ymawarì Yeuta. beginning of Rio de Los Guacharos	04/03/13	14.3	5.1	14.52	0.48	3	A
	A	3y	Auyantepui - Northeastern area	Ymawarì Yeuta. beginning of Rio de Los Venezuelanos	05/03/13	14.4	4.1	12.35	0.32	5	A
	A	5y	Auyantepui - Northeastern area	Ymawarì Yeuta. small stream (point 44AA Jp)	05/03/13	14.4	3.8	8.06	0.60	1	-
	A	6y	Auyantepui - Northeastern area	Ymawarì Yeuta. big stream (point 44B Jo)	05/03/13	14.2	3.9	8.08	0.75	5	-
	A	7y	Auyantepui - Northeastern area	Ymawarì Yeuta. Rio de Los Guacharos (point 66)	05/03/13	16.1	4.2	17.62	0.17	10	-
	A	8y	Auyantepui - Northeastern area	Ymawarì Yeuta. waterfall from fracture	05/03/13	14.6	4.0	10.85	0.65	1	
	A	9y	Auyantepui - Northeastern area	Ymawarì Yeuta. Rio de Las Columnas	05/03/13	14.5	3.9	8.12	0.65	15	-
	A	10 k	Auyantepui - Northeastern area	Ymawarì Yeuta. Collector de noroeste	11/03/13	14.7	3.0		0.63	30	A
	C	23	Chimanta Massif - Akopan Tepui	Akopan Cave - the stream near the resurgence	14/02/09	15.6	4.9	14.60	1.20	100	A
					15/02/09		4.8	13.70	0.90	70	A
					16/02/09		5.0	13.60	0.81	100	A
	C	24	Chimanta Massif - Akopan Tepui	Akopan Cave - 1st affluent stream	14/02/09		4.8	15.80	1.45	0.2	A
					15/02/09		4.9	12.10	1.54	0.1	A
	C	35	Chimanta Massif - Akopan Tepui	Akopan Cave - the stream before the sifon affluent	14/02/09		4.9	15.10	1.37	25	A
	C	38	Chimanta Massif - Akopan Tepui	Akopan Cave - 2nd affluent stream from the right	14/02/09		4.8	14.30	1.45	10	A
	C	39	Chimanta Massif - Akopan Tepui	Akopan Cave - 3nd affluent stream from the right	14/02/09		4.7	34.30	1.03	6	A
	C	40	Chimanta Massif - Akopan Tepui	Akopan Cave - the stream before the 3rd affluent	14/02/09		4.7	15.40	1.28	9	A
	C	16	Chimanta Massif - Churi Tepui	Auchimpe Cave - the stream near the entrance	20/02/09		4.9	14.10	0.11	<1	A
	C	17	Chimanta Massif - Churi Tepui	Auchimpe Cave - the stream at the great affluent	20/02/09		5.1	9.60	0.43	15	A
	C	18	Chimanta Massif - Churi Tepui	Auchimpe Cave - stream at the cave bottom	20/02/09		5.1	9.30	0.41	2	A
	R	20	Roraima Tepui - Southern part	Ojo de Cristal Cave - main stream at Lago Sangrado	30/01/12	13.8	5.0		0.09	2	-
	R	22	Roraima Tepui - Southern part	Ojo de Cristal Cave - affluent into Lago Sangrado	30/01/12		5.0		0.13	0.02	-
	R	19	Roraima Tepui - Southern part	Ojo the Cristal Cave. a pond fed by the stream only	30/01/12	13.7	4.9		0.04	stagnant	-
	R	23	Roraima Tepui - Southern part	Ojo the Cristal Cave - a pond fed by the stream only	30/01/12	13.9	5.0		0.10	stagnant	-
	R	10	Roraima Tepui - Southern part	De la Ventana Resurgence	31/01/12		5.5		0.04	3000	-
	R	9	Roraima Tepui - Southern part	Southern Wall Higher Resurgence	01/02/12		5.2		0.15	300	-
	R	8	Roraima Tepui - Southern part	Southern Wall Lower Resurgence	28/01/12	14.9	4.8		0.21	250	-
					01/02/12		5.2		0.19	250	-
Table 6. Field analyses of water dripping from cave walls and roofs	A	15	Auyantepui - Aonda Bench	Sima Aonda, Ali Primera tunnel, -300 m level	01/03/96		6.4		7.10	25	L
	A	16	Auyantepui - Aonda Bench	Sima Aonda 2, base of P285, -300 m level	23/02/93	17.4	3.7	13.40	1.60	0.6 L/min	L
	A	17	Auyantepui - Aonda Bench	Sima Aonda 2, -300 m level downstream of P285	27/02/93		4.6	14.10	0.92	rapid dripping	L
	A	18	Auyantepui - Aonda Bench	Sima Aonda 2, a solution pan fed by dripping, -300 m level	27/02/93		4.9	10.20	1.26	stagnant water	L
	A	19	Auyantepui - Aonda Bench	Sima Aonda 2, a solution pan fed by dripping, -300 m level	27/02/93		4.9	9.90	1.18	stagnant water	L
	A	20a	Auyantepui - Aonda Bench	Sima Aonda 3, -80 m level gallery	25/02/96		4.1	27.20	0.15	rapid dripping	L
	A	20 b	Auyantepui - Aonda Bench	Sima Aonda 3, -80 m level gallery	06/03/96		4.1	32.80	0.21	rapid dripping	L
	A	21a	Auyantepui - Aonda Bench	Sima O'trespolo , -80 m level gallery	26/02/96	16.7	4.5	16.00	0.34	200	L
	A	21 b	Auyantepui - Aonda Bench	Sima O'trespolo , -80 m level gallery	26/02/96	16.7			0.32	20	L
	A	22a	Auyantepui - Aonda Bench	Sima del Bloque, -80 m level gallery	03/03/96		4.1	28.40	0.35	9 L/min	A
					05/03/96		4.1	29.10	0.35	1L/min	L
	A	22 b	Auyantepui - Aonda Bench	Sima del Bloque, -80 m level gallery	03/03/96		4.2	28.00	0.60	14	L

	A	22c	Auyantepui - Aonda Bench	Sima del Bloque, -80 m level gallery	05/03/96		4.4	21.00	0.90	1	L
	A	22 d	Auyantepui - Aonda Bench	Sima del Bloque, -80 m level gallery	05/03/96		4.1	29.50	0.35	20	L
	A	22e	Auyantepui - Aonda Bench	Sima del Bloque, -80 m level gallery	05/03/96		4.1	30.00	0.35	60	L
	A	22f	Auyantepui - Aonda Bench	Sima del Bloque, -80 m level gallery	06/03/96		4.2	24.00	0.74	4	L
	A	4y	Auyantepui - Northeastern area	Imawarì Yeuta, pond fed by dripping, (Black gours)	13/03/13	14.4	5.0	9.80	6.30	0.1 L/m	turbid
	A	10y	Auyantepui - Northeastern area	Imawarì Yeuta, pond fed by dripping, (Laguna Blu)	13/03/13	14.8	6.1	10.98	8.60	0	Blu
	A	A1 4y	Auyantepui - Northeastern area	Imawarì Yeuta, pond fed by dripping, (fssil branch)	13/03/13	14.4	5.1	6.87	8.87	0	L
	A	15y	Auyantepui - Northeastern area	Imawarì Yeuta, dripping before Volcano's Land	13/03/13	14.8	6.1	5.37	7.48	0.1 L/m	L
	C	19	Chimanta Massif - Churi Tepui	Auchimpé Cave, a pond fed by dripping from opal stlagmite	20/02/09		6.6	4.10	8.13		L
	C	25	Chimanta Massif - Akopan Tepui	Cueva Akopan, beginning of the 1st affluent stream	14/02/09		5.4	7.50	6.85	44	L
					15/02/09		5.4	8.70	7.70	60	L
	C	26	Chimanta Massif - Akopan Tepui	Cueva Akopan, between 1st affluent stream and the sifon	14/02/09		5.3	8.50	5.99	12	L
	C	27	Chimanta Massif - Akopan Tepui	Cueva Akopan, between 1st affluent stream and the sifon	14/02/09				6.42	1.3	L
	C	28	Chimanta Massif - Akopan Tepui	Cueva Akopan, between 1st affluent stream and the sifon	14/02/09		5.5	7.30	6.42	41	L
	C	29	Chimanta Massif - Akopan Tepui	Cueva Akopan, between 1st affluent stream and the sifon	14/02/09		5.5	7.80	5.99	15	L
	C	30	Chimanta Massif - Akopan Tepui	Cueva Akopan, between 1st affluent stream and the sifon	14/02/09		5.4	8.00	5.56	112	L
	C	31	Chimanta Massif - Akopan Tepui	Cueva Akopan, between 1st affluent stream and the sifon	14/02/09		5.2	9.20	6.85	0.14 L/min	L
	C	32	Chimanta Massif - Akopan Tepui	Cueva Akopan, between 1st affluent stream and the sifon	14/02/09		5.2	9.20	6.85	0.14 L/min	L
	C	33	Chimanta Massif - Akopan Tepui	Cueva Akopan, between 1st affluent stream and the sifon	14/02/09				7.28	48	L
	C	34	Chimanta Massif - Akopan Tepui	Cueva Akopan, between 1st affluent stream and the sifon	14/02/09		5.0	12.60	7.28	15	L
	C	36	Chimanta Massif - Akopan Tepui	Cueva Akopan, in the tunnel upstream of the sifon	14/02/09		5.1	8.90	7.28	133	L
	C	37	Chimanta Massif - Akopan Tepui	Cueva Akopan, pond fed by dripping upstream of the sifon	14/02/09		5.1	10.50	6.85		L
	C	41	Chimanta Massif - Akopan Tepui	Cueva Akopan, at the base of the sima	14/02/09		4.6	24.70	1.97	120	A
	R	18	Roraima Tepui - Southern part	Ojo the Cristal Cave, in the 1st room	30/01/12		5.5		3.44	76	L
	R	21	Roraima Tepui - Southern part	Ojo the Cristal Cave, upstream of Lago Sangrado	30/01/12		5.5		5.60	60	L
	R	24	Roraima Tepui - Southern part	Ojo the Cristal Cave, pond fed by dripping	30/01/12	13.9	4.9		0.15		L

Table A2. Major and minor element concentrations of the water samples from Imawarì Yeuta cave system (the sign "/" means below the detection limit).

Station		Fe µg/L	Al µg/L	K mg/L	Ba µg/L	Cd µg/L	Cl mg/L	SO4 mg/L	NH4 mg/L
A	11y	46	59	/	/	/	/	/	/
A	12y	33.7	68	/	/	/	/	/	0.24
A	1y	46	46	/	1.67	/	/	/	0.2
A	2y	53	48	/	/	/	0.43	0.46	/
A	3y	40	48	/	/	/	/	/	/
A	5y	48	51	/	1.17	/	/	/	0.36
A	6y	91	54	/	/	/	/	/	0.5
A	7y	58	59	0.41	/	/	/	/	/
A	8y	49	62	0.68	/	/	/	/	0.39
A	9y	66	56	0.57	1.14	/	/	/	0.69
A	10k		53	/	/	/	/	/	/
A	4y	10.1	57	/	1.61	/	0.98	0.59	/
A	10y	/	/	/	2.82	/	1.15	0.63	/
A	A14y	19.7	/	/	6.5	1.07	0.69	0.66	/
A	15y	114	34	0.47	7.7	/	/	/	/

References

Aubrecht, R., Lánczos, T., Gregor, M., Schlögl, J., Smída, B., Brewer-Carías, Ch., Vlcek, L., 2011. Sandstone caves on Venezuelan tepuis: Return to pseudokarst? Geomorphology 132, 351-365.

Aubrecht, R., Barrio-Amorós, C.L., Breure, A.S.H., Brewer-Carías, C., Derka, T., Fuentes-Ramos, O.A., Gregor, M., Kodada, J., Kováčik, Ľ., Lánczos, T., Lee, N.M., Liščák, P., Schlögl, J., Šmída, B., Vlček L., 2012. Venezuelan tepuis: their caves and biota. Acta Geologica Slovaca Monograph, Comenius University, Bratislava, 168 p.

Aubrecht, R., Lánczos, T., Gregor, M., Schlögl, J., Šmída, B., Liščák, P., Brewer-Carías, Ch. & Vlček, L., 2013. Reply to the Comment on "Sandstone caves on Venezuelan tepuis: Return to pseudokarst?". Geomorphology 197, 197-202.

Bandstra, J.Z., Buss, H.L., Campen, R.K., Liermann, L.J., Moore, J., Hausrath, E.M., Navarre-Sitchler, A.K., Jang, J.-H., Brantley, S.L., 2008. Compilation of Mineral Dissolution Rates. In: Brantley, S.L., Kubicki J.D., White, A.F. (Ed.), Kinetics of Water-Rock Interaction, Springer Science, 737-823.

Brantley, S.L., 2008. Kinetics of Mineral Dissolution. In: Brantley, S.L., Kubicki, J.D., White, A.F. (Eds.), Kinetics of Water-Rock Interaction, Springer Science, 151-210.

Barton, H., Suarez, P., Muench, B., Giarrizzo, J., Broering, M., Banks, E., Venkateswaran, K., 2009. The alkali speleogenesis of Roraima Sur Cave, Venezuela. In: White, W.B. (Ed.), Proceedings of the 15th International Congress of Speleology, Kerrville, Texas, July 19-26 2009, 802-807.

Bennett, P.C., 1991. Quartz dissolution in organic-rich aqueous systems. Geochimica et Cosmochimica Acta 55, 1781-1797.

Bennett, P.C., Melcer, M.E., Siegel, D.I., Hassett, J.P., 1988. The dissolution of quartz in dilute aqueous solutions of organic acids at 25°C. Geochimica et Cosmochimica Acta 52, 1521-1530.

Blum, A. E., 1994. Feldspars in weathering. In: Parsons, I. (Ed.), Feldspars and their reactions. NATO ASI Series, Springer Netherlands, 595-630.

Brewer-Carías, C., Audy, M., 2011. Entrañas del mundo perdido. Charles Brewer-Carías ediciones, Altolitho, Caracas, 291 p.

Briceño, H.O., Paolini, J., 1992. Aspectos geoquímicos del macizo del Chimantá. In: Huber O. (Ed.), Chimantá. Escudo de Guayana, Venezuela. Un Ensayo Ecológico Tepuyano. Oscar Todtmann Editores, Caracas, 75-88.

Briceño, H.O., Schubert, C., 1990. Geomorphology of the Gran Sabana, Guyana Shield, Southeastern Venezuela. Geomorphology 3, 125-141.

Briceño, H.O., Schubert, C., Paolini, J., 1990. Table-mountain geology and surficial geochemistry: Chimantà massif, Venezuelan Guayana Shield. Journal of South America Earth Sciences 3(4), 179-194.

Brown, E. T., Stallard, R. F., Raisbeck, G. M., Yiou, F., 1992. Determination of the denudation of Mount Roraima, Venezuela using cosmogenic ^{13}Be and ^{26}Al. EOS 73, 170.

Bucher, K., Frey, M., 1994. Petrogenesis of metamorphic rocks. Springer, Berlin, 318 p.

Clayton, J. L., 1988. Some observations on the stoichiometry of feldspar hydrolysis in granitic soil. Journal of Environmental Quality 17(1), 153-157.

Dames and Moore Pty. Ltd., 1981. Statement of Environmental Baseline Conditions: Koongarra Uranium Project Koongarra, NT. Dames and Moore Pty. Ltd.

Derjaguin, B.V. and Churaev, N.V., 1986. Properties of water layers adjacent to interfaces. In C.A. Croxton, Ed., Fluid Interfacial Phenomena, p. 748. Wiley, New York.

Doerr, S. H., 1999. Karst-like landforms and hydrology in quartzites of the Venezuelan Guyana shield: Pseudokarst or "real" karst? Zeitschrift für Geomorphologie 43, 1-17.

Edmond, J. M., Palmer, M. R., Grant, B., Stallard, R. F., 1995. The fluvial geochemistry and denudation rate of the Guayana Shield in Venezuela, Colombia, and Brazil. Geochimica et Cosmochimica Acta 59(16), 3301-3325.

Ertel, J. R., Hedges, J. I., Devol, A. H., Richey, J. E., de Nazare Goes Ribeiro, M., Ribeiro, G., 1986. Dissolved humic substances of the Amazon River system. Limnology and Oceanography 31(4), 739-754.

Ford, D.C., Williams, P., 2007. Karst Hydrogeology and Geomorphology. Willey & Sons, Chichester, 562 p.

Galán, C., 1992. El clima del macizo del Chimantá. In: Huber, O. (Ed.), El Macizo del Chimantá – Escudo della Guayana, Venezuela – Un ensayo ecologico tepuyano. O. Todtman Editors, Caracas, 37-52.

Galán, C., Lagarde, J., 1988. Morphologie et evolution des cavernes et formes superficielles dans les quartzites du Roraima. Karstologia 11-12, 49-60.

Galán, C., Herrera, F.F., Astort, J., 2004a. Origin of Roraima Sur system, Venezuela, with notes about karst development in quartzites. Boletin Sociedad Venezolana de Espeleologia 38, 17-27.

Galán, C., Herrera, F.F., Carreño, R., 2004b. Geomorfología e hidrología del Sistema Roraima Sur, Venezuela, la mayor cavidad del mundo en cuarcitas: 10,8 km. Boletin Sociedad Venezolana de Espeleologia 38, 2-16.

Garrels, R.M., Dreyer, R.M., Howland, A.L., 1949. Diffusion of ions through intergranular spaces in water-saturated rocks, Bulletin of the Geological Society of America, 60, 1809-1828.

Ghezzehei T.A., 2004. Constraints for flow regimes on smooth fracture surfaces. Water Resources Research 40, W11503, doi:10.1029/2004WR003164.

Gibbs, A.K., Barron, C.N., 1993. The Geology of the Guyana Shield. Clarendon Press, Oxford, 246 p.

Gonzáles de Juana, C., Picard, X., Iturralde, J. M., 1980. Geologia de Venezuela y de sus cuencas petrolifera. Edic. Foninves, Caracas, 1031 p.

Govett, G.J.S., 1960. Critical factors in the colorimetric determination of silica. Analytica Chimica Acta 25, 69-80.

Harman, R.W., 1927. Aqueous solutions of sodium silicates. Journal of Physical Chemistry 31, 616.

Hem, J.D., 1985. Study and interpretation of the chemical characteristics of natural water. U.S Geological Survey, Water-Supply Paper 2254, 263 p.

Hurst, V.J., Könkle, A.C., 1985. Dehydroxylation, rehydroxylation, and stability of kaolinite. Clays & Clay Minerals 33, 1-14.

Ipiña, J.M., 1994. Aspectos físico-químicos de los tepuyes Acopan y Amuri. Macizo de Chimanta, Gran Sabana, Venezuela. Boletin Sociedad Venezolana de Espeleologia 28, 5-9.

IRSA-CNR, A.P.A.T., 2003. Metodi analitici per le acque Manuali e Linee guida 29/2003. Sez. 4000, 509-524.

Jennings, J.N., 1983. Sandstone pseudokarst or karst? In: Young, R.W., Nanson, G.C. (Eds.), Aspects of Australian Sandstone Landscape. Australia and New Zealand Geomorphology Group Special Publication, Wollongong, 21-30.

Krauskopf, K.B., 1956. Dissolution and precipitation of silica at low temperatures. Geochimica et Cosmochimica Acta 10, 1-26.

Long, D.G.F., 2002. Aspects of Late Palaeoproterozoic fluvial style: the Uairen Formation, Roraima Supergroup, Venezuela. In: Altermann, W., Corcoran, P.L. (Eds.), Precambrian sedimentary environments: a modern approach to ancient depositional systems. Blackwell Pub., 323-338.

Mainguet, M., 1972. Le Modele des Gres. Paris: Institut Geographique National, 657 p.

Marker, M.E., 1976. Note on some South African pseudokarst. Boletin Sociedad Venezolana Espeleologia 7(13), 5-12.

Martini, J.E.J., 1979. Karst in Black Reef quartzite near Kaapsehoop, Eastern transval. Annals of South African Geological Survey 13, 115-128.

Martini, J.E.J., 1985. Les phénomènes karstiques de quartzites d'Afrique du Sud. Karstologia 9, 45-52.

Martini, J.E.J., 2000. Dissolution of quartz and silicate minerals. In: Klimchouk, A.B., Ford, D.C., Palmer, A.N., Dreybrodt, W. (Eds.), Speleogenesis. Evolution of karst aquifers. National Speleological Society, Huntsville, 452-457.

Martini, J.E.J., 2004. Silicate Karst. In: Gunn, J. (Ed.), Encyclopedia of Caves and Karst Science. Fitzroy Dearborn, London, 1385-1393.

Mecchia, M., Piccini, L., 1999. Hydrogeology and SiO_2 geochemistry of the Aonda Cave system (Auyantepui, Bolivar, Venezuela). Bolletin Sociedad Venezolana de Espeleologia 33, 1-11.

Mecchia, M., Sauro, F., Corongiu, C., Crobu, V., 2009. Speleological explorations in the Chimanta massif quartzites (Gran Sabana, Venezuela). Supplement to Kur magazine 12, 1-16.

Nimer, E., 1989. Climatologia do Brasil. IBGE, Rio de Janeiro, 421 p.

Norton, D., Knapp, R., 1977. Transport phenomena in hydrothermal systems: the nature of porosity. American Journal of Science, 277, 913-936.

Palmer A.N., 1999. A statistical evaluation of the structural influence on solution-conduit patterns. In: Palmer A.N., Palmer M.V., Sasowsky I.D. (Eds.), Karst Modeling. Karst Waters Institute, Special Publication 5, 187-195.

Pettijohn, J., Potter, P.E., Siever, R., 1987. Sand and Sandstone. Springer, Berlin, 553 p.

Piccini, L., 1995. Karst in siliceous rock: karst landforms and caves in the Auyán-tepui massif (Est. Bolívar, Venezuela). International Journal of Speleology 24, 41-54.

Piccini, L., Mecchia, M., 2009. Solution weathering rate and origin of karst landforms and caves in the quartzite of Auyan-tepui (Gran Sabana, Venezuela). Geomorphology 106, 15-25.

Reid, A. R., 1974. Stratigraphy of the type area of the Roraima Group, Venezuela. Bolletin de Geologia, Venezuela, Pub. Especial 6, 343-353.

Rimstidt, J.D., 1997. Quartz solubility at low temperatures. Geochimica et Cosmochimica Acta 61, 2553-2558.

Rutherford, G.K., 1967. A preliminary study of the composition of precipitation in S.E. Ontario. Canadian Journal of Earth Sciences 4(6), 1151-1160.

Santos, J.O.S., Potter, P.E., Reis, N.J., Hartmann, L.A., Fletcher, I.R., McNaughton, N.J., 2003. Age, source, and regional stratigraphy of the Roraima Supergroup and Roraima-like outliers in northern South America based on U-Pb geochronology. Geological Society of America Bulletin 115, 331-348.

Sauro, F., Piccini, L., Mecchia, M., De Waele, J., 2013a. Comment on “Sandstone caves on Venezuelan tepuis: Return to pseudokarst?” by R. Aubrecht, T. Lánczos, M. Gregor, J. Schlögl, B. Smída, P. Liscák, Ch. Brewer-Carías, L. Vlcek, Geomorphology 132, 351-365. Geomorphology 197, 190-196.

Sauro, F., De Vivo, A., Vergara, F., De Waele, J., 2013b. Imawarì Yeuta: a new giant cave system in the quartz sandstones of the Auyan Tepui, Bolivar state, Venezuela. Filippi, M., Bosak, P. (Eds.), Proceedings of the 16th International Congress of Speleology, Brno 19-27 July 2013, Volume 2, 142-146 .

Sauro, F., Lundberg, J., De Waele, J., Tisato, N., Galli, E., 2013c. Speleogenesis and speleothems of the Guacamaya Cave, Auyan Tepui, Venezuela, Proceedings of the 16th International Congress of Speleology, Brno 19-27 July 2013, Volume 3, 298-304.

Sauro, F., Tisato, N., De Waele, J., Bernasconi, S.M., Bontognali, T.R.R., Galli, E., 2013d. Source and genesis of sulphate and phosphate–sulphate minerals in quartz–sandstone cave environment. Sedimentology, doi: 10.1111/sed.12103.

Sczerban, E., Urbani, F., 1974. Formas carsicas en areniscas Precambricas del Territorio Federal Amazonas y Estado Bolivar. Boletin Sociedad Venezolana Espeleologia 5 (1), 25-54.

Snow, J. W., 1975. The climates of northern South America. University of Wisconsin, Madison, 476 p.

Tokunaga, T.K., Wan, J.M., 1997. Water film flow along fracture surfaces of porous rock. Water Resources Research 33(6), 1287-1295.

Urbani, F. 1976. Opalo, Calcedonia y Calcita en la Cueva del Cerro Autano (Am 11), Territorio Federal Amazonas, Venezuela. Boletin Sociedad Venezolana Espeleologia 7, 129-145.

Urbani, F., Talukdar, S., Szczerban, E. , Colveé, P., 1977. Metamorfismo de las rocas del Grupo Roraima, Ediciones Bolívar y Territorio Federal Amazonas. Memorias V Congreso Geologico Venezolano, Caracas, 623-638.

White, W.B., Jefferson, J.L., Haman, J.F., 1966. Quartzite karst in Southeastern Venezuela. International Journal of Speleology 2, 309-314.

Wray R. A. L,. 1995. Solutional Landforms in Quartz Sandstones of the Sydney Basin. PhD thesis, University of Wollongong, 381 p.

Wray, R.A.L., 1997a. A global review of solutional weathering forms on quartz sandstones. Earth Science Reviews 42, 137-160.

Wray, R.A.L., 1997b. Quartzite dissolution: karst or pseudokarst? Cave and Karst Science 24, 81-86.

Wray, R.A.L., 2000. The Gran Sabana: The World's Finest Quartzite Karst? In: Migon, P. (Ed.), Geomorphological Landscapes of the World. Springer, Dordrecht, 79-88.

Wray, R.A.L., 2013, Solutional weathering and karstic landscapes on quartz sandstones and quartzite, in Frumkin, A. (Ed.), Treatise on Geomporphology - Vol. 6 Karst Geomorphology, Elsevier.

Yanes, C.E., Briceño, H.O., 1993. Chemical weathering and the formation of pseudo-karst topography in the Roraima Group, Gran Sabana, Venezuela. Chemical Geology 107, 341-343.

Zawidzki, P., Urbani, F., Koisar, B., 1976. Preliminary notes on the geology of the Sarisariñama plateau, Venezuela, and the origin of its caves. Boletin Sociedad Venezolana de Espeleologia 7, 29-37.

CHAPTER 2.3

Published in Geomorphology, 197, 190-196.

COMMENT ON "SANDSTONE CAVES ON VENEZUELAN TEPUIS: RETURN TO PSEUDOKARST?" BY R. AUBRECHT, T. LÁNCZOS, M. GREGOR, J. SCHLÖGL, B. SMÍDA, P. LISCÁK, CH. BREWER-CARÍAS, L. VLCEK, GEOMORPHOLOGY 132 (2011), 351-365

Francesco Sauro[1,3], Leonardo Piccini[2,3], Marco Mecchia[3], Jo De Waele [1,3]

1) Dipartimento di Scienze Biologiche, Geologiche e Ambientali, Italian Institute of Speleology, Via Zamboni 67, 40126, Bologna, (Italy)
2) Dipartimento di Scienze della Terra, Università di Firenze, Via La Pira 4, 50121, Firenze, (Italy)
3) La Venta Esplorazioni Geografiche Association, Via Priamo Tron 35/F, 31100, Treviso, (Italy)

Corresponding author: Francesco Sauro

Abstract

In the recent work of Aubrecht et al. (2011) the presence of "unlithified or poorly-lithified beds" of sands in the quartz-sandstone stratigraphic succession is proposed as a key factor for speleogenesis in the Venezuelan tepuis. In this comment we observe that in the cited work the geologic history of the region, in terms of sedimentation environment, diagenesis and low grade burial metamorphism, has not been considered. Furthermore, the peculiar "pillar flow" columns that Aubrecht et al. describe as a proof of the unlithification are lacking in many other different cave systems in the same area.

Four critical points are discussed: the burial metamorphism of the Mataui Formation, the significance of the Schmidt Hammer measurements, the cave morphologies and the role of SiO_2 dissolution. Finally we suggest that weathering, in its wider significance, is probably the triggering process in speleogenesis, and there is no need to invoke a differential diagenesis of the sandstone beds.

Keywords: quartz-sandstones, diagenesis, weathering, speleogenesis, karst, pseudokarst

2.3.1 Introduction

In the last twenty years many new cave systems have been discovered in different massifs (tepui) of the Guyana Shield (Venezuela and Brazil), formed in the Precambrian quartzite sandstones of the Roraima Supergroup. Although many authors already discussed the main factors controlling the speleogenesis in the quartz-sandstone environment (see the review of Wray, 1997a, but also Wray, 2000; Piccini and Mecchia, 2009; Young et al., 2009), these recent explorations have shown that the largest karst systems in these low-soluble siliceous rocks are controlled predominantly by stratigraphic rather than by tectonic factors.

Many studies on the petrographical composition and texture of the Mataui Formation were previously performed by several authors, showing evidence of weathering due to dissolution along the contact surfaces of grains (of silica cement or of the syntaxial quartz overgrowth) with consequent removal of quartz grains by mechanical erosion (White et al., 1966; Chalcraft and Pye, 1984; Pouylleau and Seurin, 1985; Doerr, 1999). Also the presence of phyllosilicate minerals, such as kaolinite and pyrophyllite, as cement in less cohesive beds was suggested as one of the factors enhancing mechanical erosion of these particular layers (Szczerban et al., 1977; Ipiña, 1994; Galan et al., 2004).

In their recent work Aubrecht et al. (2011) explained the stratigraphic control on the speleogenesis by the presence of “unlithified or poorly-lithified beds” of sands which can be easily removed by running water, forming underground conduits through a piping process. To demonstrate that the different cohesiveness is related to a non-homogeneous diagenesis of the Mataui Formation sequence rather than to a different weathering rate (arenization) Aubrecht et al. performed a detailed petrographical and rheological study of the different strata.

While we are delighted to see an original contribution to this important topic and appreciating very much the relevant work performed by Aubrecht et al., we would like to draw attention to some critical points in the above-mentioned article.

In their interpretation the presence of unlithified beds in the sandstone stratigraphic succession is proposed as a key factor for speleogenesis, but in order to confirm this hypothesis the geologic history of the region, in terms of sedimentation environment, diagenesis and low grade burial metamorphism, has not been considered. Furthermore, the peculiar “pillar flow” columns that they describe as a proof of the unlithification are lacking in many other different cave systems in the same area.

In our opinion, the question “Return to pseudokarst?” provoked by their studies must be discussed in a wider point of view, examining the morphology and the development of all the caves known in this

area, because different processes could interact with different intensity in the genesis of caves, depending on a wide range of factors, but also on the different stages of the cave development. Also the significance of the SiO_2 geochemistry of the underground and surficial streams has to be considered in different cases, with a wider set of data, taking into account also the peculiar geomorphologic and climatic history of the region.

In this comment we focus on four main topics that are in contrast with the interpretation of Aubrecht et al., but also suggest some aspects related to the lithological composition of the sandstones that need further and more detailed investigations. The work of Aubrecht et al. is mainly based on a previous study (Aubrecht et al., 2008) and, inevitably, our comments here refer to this earlier paper as well.

2.3.2 Geological problems of the "unlithified sands" theory

In their previous work, Aubrecht et al. (2008) explained the variability in cohesiveness between different beds of sandstones as "purely diagenetic", due to an inhomogeneous diffusion of diagenetic fluids through intergranular voids, related to the different hydraulic conductivity between coarse and fine grained sands. The origin of the remnant pillars of more resistant quartzite observed in the caves is explained by the migration of diagenetic fluids through delimited pathways in the form of "finger flows". In support to this hypothesis they referred to some experimental works (Liu et al., 1994; Bauters et al., 2000) where a process of water diffusion through "finger flow fields" was studied in sands of different grain size. These studies were performed in a surface P-T environment, and do not consider former diagenetic conditions. This process is not described in the most complete reviews on diffusion of diagenetic fluids in sandstones (Wolf and Chilingarian, 1975; Pettijohn et al., 1987; Taylor et al., 2010). Further, in the experiments of Liu et al. and Bauters et al., the finger flow diffusion works only in originally dry sands where the intergranular voids are filled with air. In Aubrecht et al. (2008) this vadose original condition is assumed also for the quartz-sandstones of the Roraima Supergroup, although this seems highly unrealistic for a sandy sequence deposited in a shallow marine foreland basin (Reid, 1974; Ghosh, 1985; Gibbs and Barron, 1993; Santos et al., 2003).

Moreover in the discussion on the diagenetic processes Aubrecht et al. (2008) did not consider the fundamental work of Urbani et al. (1977) regarding the burial metamorphism that affected the Mataui Formation. This was confirmed by the diffuse presence of pyrophyllite and by the petrographical evidence of pressure solution between the quartz grains and consequent quartz grain overgrowths (Urbani et al., 1977; but for pressure solution evidence see also Gibbs and Barron, 1993; Ipiña, 1994; Piccini and Mecchia, 2009; Lundberg et al., 2010). A pressure of at least 1 kbar of P_{H2O}

(partial pressure of water) and a T in the region of 320-400 °C is required for the kaolinite + quartz reaction that forms pyrophyllite (Haas and Holdaway, 1973), while pressure solution is considered to be starting at about 1500 m of burial depth (Füchtbauer, 1967; Angevine and Turcotte, 1983). For these reasons, Urbani et al. (1977) suggested that the Mataui Formation was buried under at least 3000 m of sediments that have been eroded in the last hundred millions of years. At these low metamorphism conditions the diffusion diagenetic process described by Aubrecht et al. (2008) is unrealistic because pore water is a brine and the porosity is strongly reduced.

Pressure solution showing interpenetrating quartz grains and re-precipitation of quartz cement is the major cause of cementation in such P-T environments (Weyl, 1959; Siever, 1962; Pettijohn et al., 1987; Renard et al., 1999). The cementation is driven by local pore-sized solution-precipitation reactions and cannot be related to vertical fluid movement driven by gravity such as that typical of the finger flow hypothesis.

Also the time of burial needs to be considered as a fundamental parameter in the diagenetic processes. The Roraima Supergroup is inferred to be deposited in the Late Proterozoic (Santos et al., 2003), and was presumably buried by other sediments in the same basin in an early stage (Gibbs and Barron, 1993). The erosional exposure of the Mataui Formation probably started at the end of the Jurassic (Briceño and Schubert, 1990), so the burial time of the Mataui formation is supposed to be of several hundreds of millions of years. The persistence of unlithified beds intercalated by harder well lithified ones, after such a long burial time in those conditions of P-T is considered to be unrealistic in many studies on sandstone diagenesis (Maxwell, 1964; Füchtbauer, 1967; Scherer, 1987; Taylor et al., 2010).

The diffuse presence of pyrophyllite has been observed by the team of Aubrecht et al. (2011), and they also reported pressure solution in both the presumed lithified and unlithified beds (Fig. 6C-D and Fig. 7A-B of their work) but they didn't discuss the implication of these observations. We suggest that other processes are needed to explain the loss of cohesiveness of these sandstones in order to answer the question of Aubrecht et al.: "Was the poor lithification of some beds primary or did they turn to neosandstone due to weathering?".

2.3.3 Interpretative problems with the Schmidt Hammer hardness measurements

As a proof of the different cohesiveness (interpreted as a "grade of different diagenesis") of beds and of the remnant pillars, Aubrecht et al. (2011) performed many measures of hardness making use of the Schmidt Hammer. This method gives the relative hardness value of the superficial layer of the rock; this can been interpreted as primary hardness related to diagenesis, but almost always has to

be considered as secondary hardness due to weathering (Williams and Robinson, 1983; Goudie, 2006). Only if the measures were done directly on fresh cut samples without weathered surface can the primary hardness be obtained. If the arenization processes affect at least the first centimetres of the cave wall surface, this method, as used by Aubrecht et al., is not useful for assessing the primary difference in hardness between the beds. In addition, the high variability of the strength in each of the three different situations they considered ("poorly lithified", "well lithified" and "pillar") suggests that there is no clear rheological diversification and that the three cases are smoothly passing from one to the other. This distribution is more consistent with weathering processes than with a primary different lithification (intrinsic of the rock before weathering exposure).

We believe the Schmidt Hammer method gives indications on which are the softer layers now, but it is not a proof for understanding if these layers originally had a different lithification grade or if the weathering was more pervasive in one or the other.

2.3.4 Morphology of the caves and field evidence: problems of the pillar flow hypothesis

In Aubrecht et al. (2011) the origin of the caves is interpreted as the result of infiltrating waters mechanically eroding the unlithified beds, leaving intact harder pillars formed by the "finger flow" diagenetic process. In this model the dissolution of the silica cement and the consequent "arenization" (Martini, 2000) plays only a minor role. A sketch is shown in Fig. 3 of Aubrecht et al. (2008), where remnant pillars are considered as morphological evidence of this mechanism.

Galan et al. (2004) gave a detailed morphological description of the Roraima Sur System (the same cave system named Ojo de Cristal by Aubrecht et al., 2011) showing that pillars are not so ubiquitous but are present only in some areas of the conduit network (Fig. 1c). Our field observations confirm this situation in this cave. In addition, if this mechanism is considered as the triggering process of speleogenesis in the Mataui Formation and other Roraima-like quartz-sandstones (in contrast with the classical model of "arenization" described by Martini, 1979, 1985, 2000), similar morphologies should also be found in the other stratigraphically controlled caves of the area. We also expected that stream mechanical erosion would develop a general maze or spongework pattern, laterally enlarging the conduits along the unlithified bed leaving wide sectors of remnant pillars.

In Table 1 the major cave systems known in this lithology are listed with some information on the general shape of the conduits (maze, main conduit, branchwork, etc.) and the documented presence of pillar morphologies. It is evident that most of these stratigraphically controlled caves do not show the morphologies expected by the hypothesis of Aubrecht et al. (2011).

Cave Systems	Dev.	Depth	Massif	Shape	Main control	"Pillars"	References
Roraima Sur	10820	-70	Ror.	H, B	Strat.	Yes, not frequent	Galan et al., 2004, Brewer-Carías and Audy, 2011
Sima de Los Guacharos	1194	-111	Ror.	V, N	Tect.	None	Carreño et al., 2002
Brewer System*	17500	110	Chim.	H, MC	Strat.	Yes, frequent	Aubrecht et al., 2011; Brewer-Carías and Audy, 2011
Arana-Eladio*	2500	70	Chim.	H, MC	Strat.	Yes, frequent	Aubrecht et al., 2011; Brewer-Carías and Audy, 2011
Cueva Zuna	2520	-85	Chim.	H, B	Strat.	Yes, frequent	Aubrecht et al., 2011; Brewer-Carías and Audy, 2011
Columnas	159	-16	Chim.	H, MC	Strat.	Yes, frequent	Mecchia et al., 2009; Sauro, 2009
Akopan-Dal Cin	2598	177	Chim.	H, B	Strat.	None	Mecchia et al., 2009; Sauro, 2009
Maripak	682	54	Chim.	H, MC	Strat.	None	Mecchia et al., 2009; Sauro, 2009
Escondida	152	4	Chim.	H, MC	Strat.	None	Mecchia et al., 2009; Sauro, 2009
Guacamaya	1082	57	Auy.	H, MC	Strat.	None	Sauro et al., 2011
Aonda System*	5600	-383	Auy.	V, H, N	Tect.-Strat.	Almost none	Piccini & Mecchia, 2009
Auyan Tepui Noroeste	2950	-370	Auy.	V, H, N	Tect.	Almost none	Piccini & Mecchia, 2009
Aguila	700	-180	Auy.	V, H, N	Tect.	None	Sauro, 2010
Guaiquinima*	2000	…	Guai.	H, MC	Strat.	None	Szczerban et al., 1977
Autana	635	40	Aut.	H, CL	Strat.	None	Colveé, 1973; Galán, 1982
Sima Mayor	405	-314	Sar.	V	Strat.	None	Zawidski et al., 1976; SVE, 1976
Sima Menor	989	-248	Sar.	V, H, MC	Strat.	None	Zawidski et al., 1976; SVE, 1976
Sima de la Lluvia	1352	-202	Sar.	V, H, MC	Strat.	None	Zawidski et al., 1976; SVE, 1976
Abisso Guy Collet	896	-670	Ar.	V, N	Tect.	None	Ayub, 2006

*Table 1. List of the main caves known in quartz-sandstones in the Roraima Supergroup or Roraima-like quartz-sandstones. The sign * represents not a single cave but different ones considered to be part of a single cave system. Ror. = Roraima; Chim. = Chimanta; Auy. = Auyan; Guai. = Guaiquinima; Aut. = Autana; Sar. = Sarisariñama; Ar. = Aracà; H = Horizontal; V = Vertical; N = Network; B = Branchwork; MC = Main Conduits; CL = Conduits labyrinth; Strat. = Stratigraphic; Tect. = Tectonic.*

In the following paragraphs we give some examples showing that pillar morphologies are not so frequent in the other known caves developed in the Mataui Formation:

- The Akopan-Dal Cin System is a 2.5 km-long, active cave with a branchwork pattern where the galleries, sometimes more than 30 m wide, have a circular, slightly rectangular or elliptic

cross-section (Fig. 1a, 1b; Mecchia et al., 2009; Sauro, 2009). No pillars were observed, and there is no evidence of collapses underneath which they could be hidden. However, the stratigraphical control is evident along interbeds and finer layered strata.

- The Guacamaya Cave in Auyan Tepui is a 1 km-long cave divided in two main branches. Pillars were not observed in the whole cave even though there are no collapses or reworking of original conduits at least in the inner part (Fig. 1f). The stratigraphic control in this case seems to follow the presence of a BIF-like bed of iron-hydroxides (goethite-limonite inter-layered with amorphous silica, see Sauro et al., 2011).
- Zawidzki et al. (1976) did not report pillar morphologies when describing the huge galleries underneath the big collapse sinkholes of the Sarisariñama plateau (Sima Menor and Sima de la Lluvia). The galleries are mainly single conduits without a maze pattern as expected in the speleogenetical conditions described by Aubrecht et al. (2011).
- The caves of Guaiquinima tepui described by Szczerban et al. (1977) also do not show pillar morphologies, whereas they are controlled stratigraphically by thick layers of "metalimonita" (clay minerals like pyrophyllite).
- The horizontal levels of the Aonda and Auyan Tepuy Noroeste System show only few examples of pillars (Fig. 1e) related to mechanical erosion of streams and anastomosing interstratal conduits (Piccini, 1995).

In the Autana Cave System, developed inside the Roraima-like sandstone of Cerro Autana in the Amazonas region, the galleries show spectacular rounded (probably phreatic) tube morphologies (Fig. 1d) without the presence of any pillars.

The pillars described by Aubrecht et al. (2011), but also by Doerr (1999), are often regularly spaced. This regular disposition cannot be explained by non-uniform lithification, but is more consistent with a regular disposition of fractures due to tectonic or gravitational load (Doerr, 1999; Yang et al., 2012). In many cases pillars are not vertical but inclined along low angles because related to anastomosing of sub-vertical parallel fractures (Fig. 1e, 2). Moreover they form local maze or spongework passages in areas of the caves that are frequently flooded (see for example the plan view of Cueva de Las Columnas in Mecchia et al., 2009, or of Cueva Kuekenan in Doerr, 1999) suggesting that their origin is related to mechanical and chemical processes similar to those described for caves in carbonate environments with allogenic recharge (Palmer, 2003).

Another case that is incongruent with the unlithified bed hypothesis is related to the deeply weathered walls of the deepest shafts ("simas") explored inside the Aonda bench in the Auyan Tepui (Piccini, 1995) but also in other tepuis like Chimantha (Sociedad Venezolana de Espeleologia, 1994),

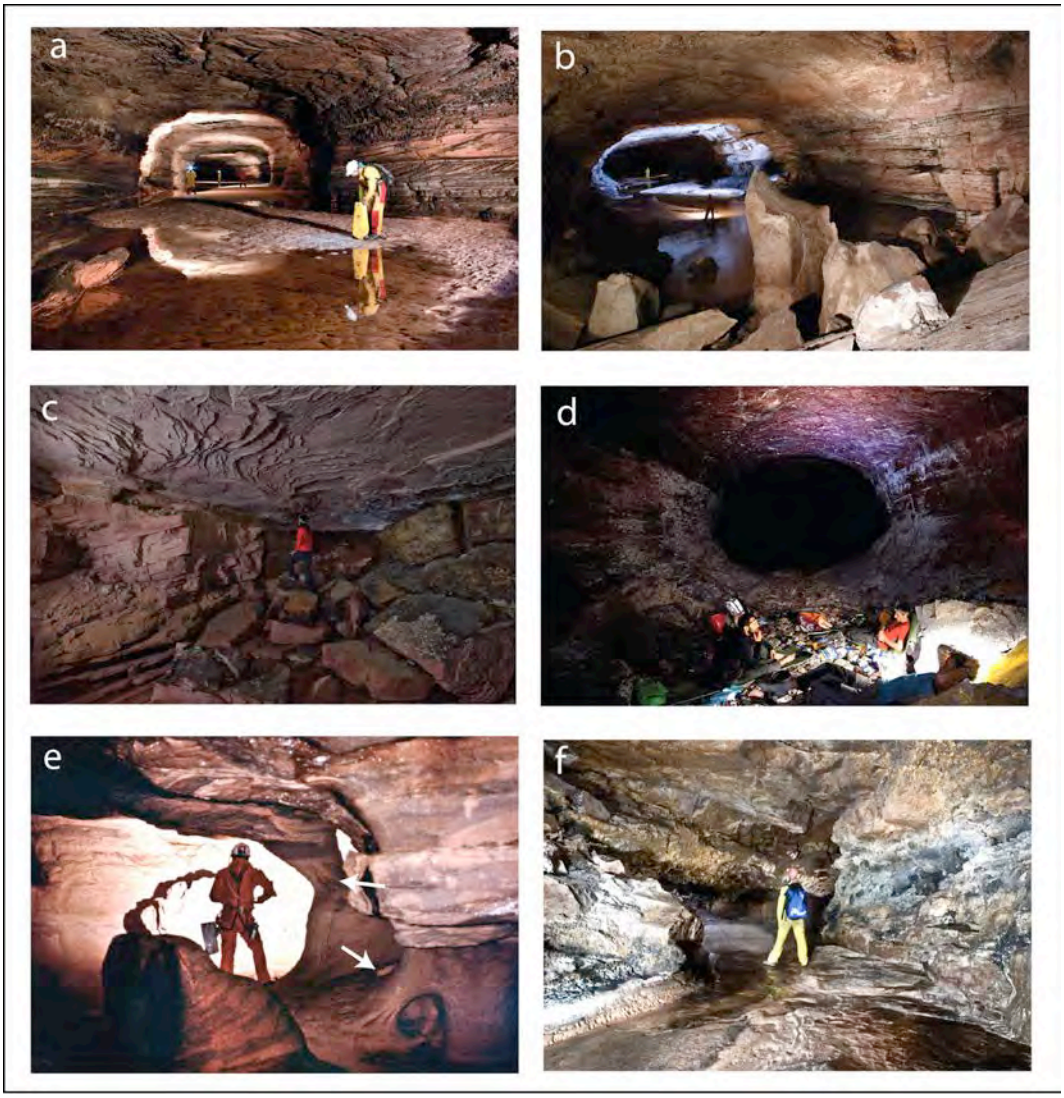

Fig.1. Some conduit morphologies that are not in accordance with the pillar flow hypothesis described by Aubrecht et al. (2011) a) b) The main gallery of Akopan-Dal Cin Cave System (Chimanta Tepui), with a rectangular (a) and elliptic (b) section, without pillars and lateral enlargement expected in the case of pillar flow hypothesis (Photographs by Vittorio Crobu). c) A gallery in the Roraima Sur System (Roraima Tepui) developed mainly along an interbed between cross-laminated sandstones. No pillars are present (Photograph by Francesco Sauro). d) A former phreatic tube morphology in Cueva Autana (Autana Tepui, Amazonas region) (Photograph by Alastair Lee/posingproduction.com). e) A gallery in the main horizontal active level of Auyan Tepui Noroeste Systems. Arrows show two oblique pillars at different heights related to mechanical stream erosion (Photograph by Paolo Pezzolato). f) An active corridor in Guacamaya Cave (Auyan Tepui), no pillars are evident while the conduits seem to be controlled by a layer of iron hydroxides (the grey bed on the right) (Photograph by Francesco Sauro).

Yuruani (Galan, 1991) and Wei Assipu (Carreño et al., 2002). Several speleological reports (Sociedad Venezolana de Espeleologia, 1984; Gori et al., 1993; Bernabei et al., 1993; AA.VV., 1994; Rigamonti, 1995) describe the occurrence of metres of "friable" rock on the walls of these deep shafts. These conditions usually occur more in the narrow deep shafts, where the walls are permanently wet by percolation or condensation waters. Conversely, on the exposed outside cliff walls at the same stratigraphical height the rock is frequently very hard. A similar situation of diffuse weathering along the walls was also found in the deepest quartzite cave of the world in the "Roraima-like" quartz sandstone of Aracà Tepui in Brazil (Guy Collet Abyss, 679 m deep; Ayub, 2006; Epis and Ayub, 2010).

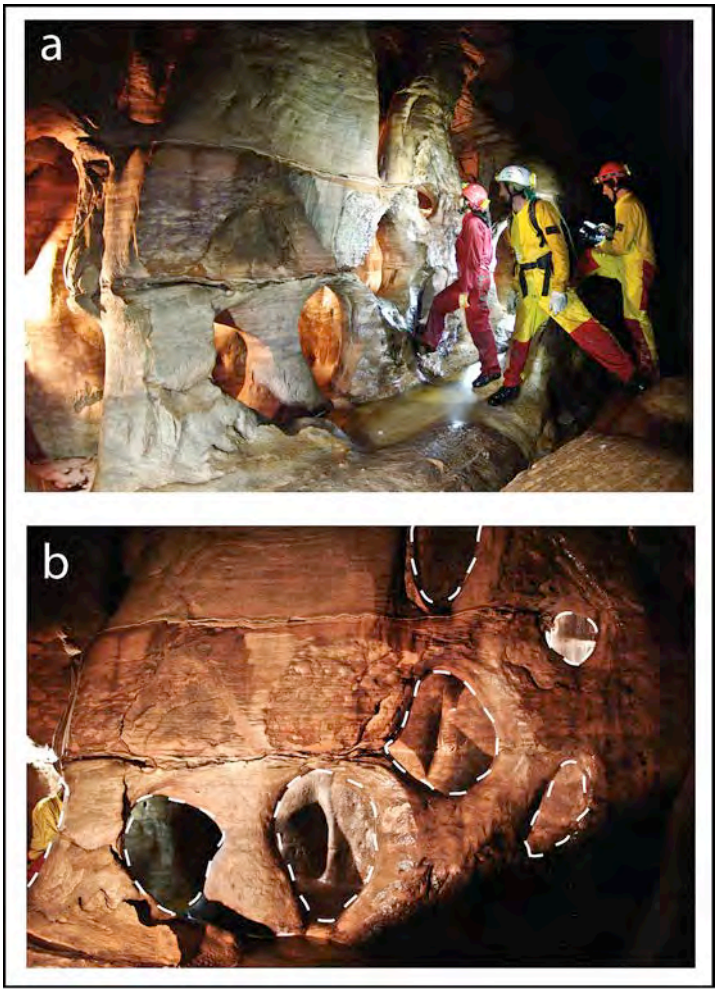

Fig.2. Example of pillar formation related to anastomosis of vertical fractures in a cave in Akopan Tepui. a) Behind the wall a waterfall is flowing along a fracture. b) Detailed view of the wall with highlighted the just formed pillars to the left and the upcoming oblique pillars and "oblò" to the right, also along different sandstone beds. (Photographs by Vittorio Crobu)

How can hundreds of metres of beds be unlithified in a shaft while along the bounding cliffs of the tepui the same beds appear as hard sandstones? Only some type of weathering process can explain this situation and it is evident that it is not possible that the entire stratigraphic sequence is unlithified in one place and a few hundreds of metres away it is not. This means that weathering processes are active today and that they have to be considered as a reliable speleogenetical process.

2.3.5 Petrographical problems and the role of SiO_2 dissolution

In some previous works on the weathering of the Mataui Formation, evidence of quartz dissolution was shown by thin sections and SEM in the weathered sandstones of the Roraima Tepui (Martini 1979; Chalchraft and Pye, 1984; Doerr, 1999), and also in the same site of Cueva Charles Brewer

related to photokarren morphologies (Lundberg et al., 2010). Contrarily Aubrecht et al. (2011) reported that "the most important point is that no signs of quartz dissolution were observed in any of the samples". We observe that dissolution morphologies like pits or notches on quartz grains are in the range of 1-2 μm (Burley and Kantorowicz, 1986) while the SEM images shown in Figs. 6 and 7 of Aubrecht et al. (2011) are one order of magnitude larger in scale, preventing recognition of the possible presence of these features. In addition SEM methods are unable to resolve features at the nanometric scale as highlighted by Pope (1995): his research with High Resolution TEM on apparently unweathered quartz grains demonstrated that most of the weathering processes act at a nanoscale, with sub-microscale crystalline disintegration, or amorphization, of exterior surfaces and internal fractures of the quartz grains.

However in the discussion of their article, Aubrecht et al. (2011) are in contradiction with their previous sentence when they say that the condensation of air moisture on the wall "causes corrosive dissolution due to strong undersaturation with respect to the SiO_2 of the precipitated water". In fact the values of the silica content of dripping waters are generally high: 2.3-3.3 mg/l in Aubrecht et al. (2011), an average of 1.0 mg/l in Piccini and Mecchia (2009) on the Auyan Tepui, and about 3.1 mg/l in Akopan Tepui (Mecchia et al., 2009), sometimes reaching up to 7-8 mg/l if the drip comes from

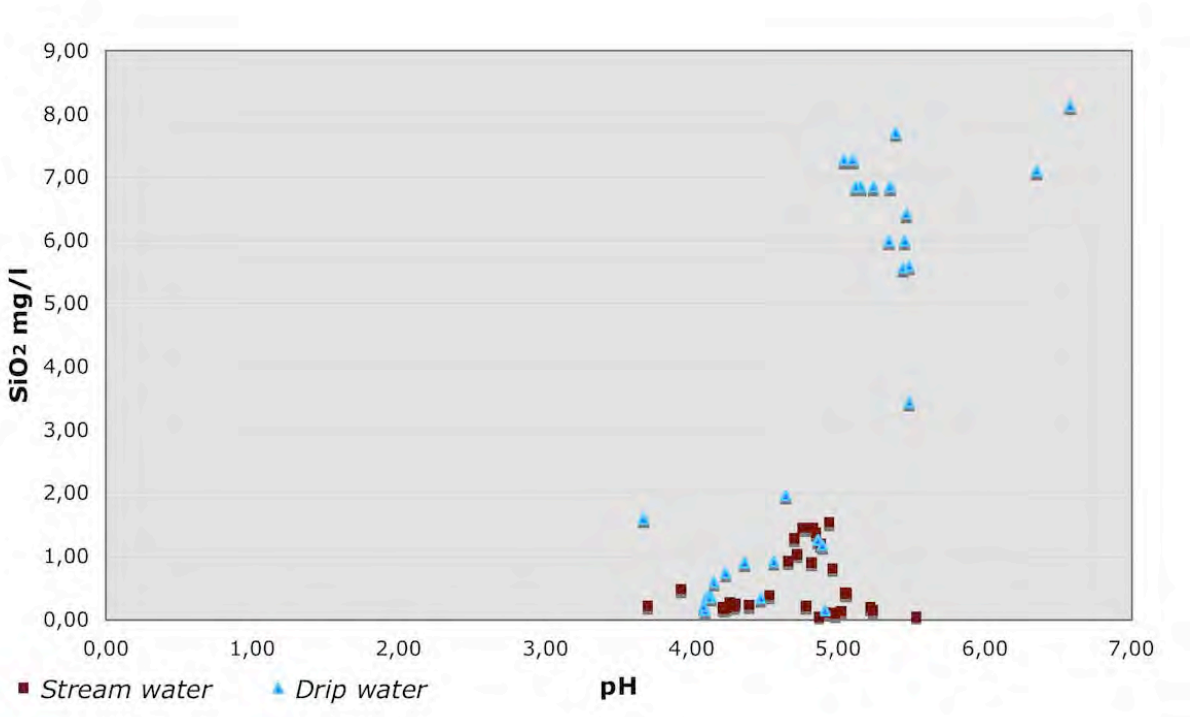

Fig. 3. SiO_2 content versus pH in dripping and stream waters, from four different cave systems (Aonda, Akopan-Dal Cin, Cueva Eladio, Roraima Sur).

opal speleothems. Analyses of waters from four different cave systems in Auyan, Chimantha and Roraima massifs show that the content of SiO_2 of dripping water is usually significantly higher than that of stream waters (part of these data and the analytical methods applied have been published in Piccini and Mecchia, 2009) (Fig. 3). We noted that besides condensation water on the walls, also the seepage water infiltrating into small cracks and fissures could play an important role in dissolution because the low solution rate of silica allows the water to remain undersaturated and chemically aggressive over long distances and time (Martini, 1979; Mecchia and Piccini, 1999). Further petrographical studies are needed, but if dissolution is present in the cave walls it has to play an important role also in the weathering of joints and microcracks.

2.3.6 Brief discussion: unlithified beds or neo-sandstones?

The stratigraphical control in the genesis of caves many km long within the Mataui Formation of the tepuis is evident. In many cases, like the two described by Aubrecht et al. (2011), the control is related to the presence of less cohesive layers of sandstones at well defined stratigraphical heights. In a succession of sandstone that underwent several hundred million years long burial metamorphism, the presence of beds with a different diagenetic grade is unrealistic. The cohesiveness of a rock depends not only on diagenetic processes but also on the mineralogical composition, texture, tectonic stresses, and above all chemical-biological weathering. This term has to be considered in its wider significance; of course dissolution of silica, but including also all the other processes on different mineralogical phases of the rock, like hydrolysis of silicates, leaching, oxidation of iron in diffused sulfides and others. In the work of Aubrecht et al. (2011) the main difference in the mineralogical composition between the softest and the hardest layers was for the first time clearly demonstrated, with the presence of major aluminosilicate and clay minerals like kaolinite (sometimes constituting the matrix of the rock). They noted that this reflects a more arkosic composition of these sandstones, in contrast to the almost pure quartz-sandstone around. They asserted also that the “red muds” are probably the remnants of “lateritisation” processes of the more arkosic beds, but they did not discuss the consequences in terms of disaggregation and weathering of these beds.

We suggest that the mineralogical composition and the petrographical features (grain size, sorting, depositional structures) of the different beds control the intensity of the weathering processes, i.e. the hardness of the different beds. If one or more types of weathering are the triggering processes controlling the cohesiveness, the softest layers are former neo-sandstones, as proposed by Martini (2004), and there is no need to invoke a differential diagenesis.

In general, if the conditions are favourable, the whole stratigraphical succession could be weathered in terms of the "arenization" theory (Martini, 2000), but only a few layers have different characteristics that boost the disintegration by other weathering processes, controlling the development of original inter-layer protoconduits which later evolve thanks to stream mechanical erosion, in true horizontal cave systems.

This situation was described in carbonate environment by Lowe (1992) and Filipponi et al. (2009) introducing the inception horizon hypothesis (IHH). Applying their definition we can assert that here the inception horizons are "layers especially favourable to the opening of proto-conduits through karstic or pseudo-karstic processes by virtue of physical, lithological or chemical deviation from the predominant quartz-sandstone facies".

The term karst or pseudo-karst finally has to be chosen depending on the predominant processes that allow the formation of the voids in the first phases of speleogenesis (Jennings, 1983; Urbani, 1991; Wray, 1997b). Further investigation, in different cave systems of the area, is needed to better define this problem.

References

AA.VV, 1994. Tepui 1993. Progressione 30, 120 p.

Angevine, C.L., Turcotte, D.L., 1983. Porosity reduction by pressure solution: A theoretical model for quartz arenites. Geological Society of America Bullettin 94, 1129-1134.

Aubrecht, R., Lánczos, T., Smída, B., Brewer-Carías, Ch., Mayoral, F., Schlögl, J., Audy, M., Vlcek, L., Kovácik, L., Gregor, M., 2008. Venezuelan sandstone caves: a new view on their genesis, hydrogeology and speleothems. Geologica Croatica 61, 345-362.

Aubrecht, R., Lánczos, T., Gregor, M., Schlögl, J., Smída, B., Brewer-Carías, Ch., Vlcek, L., 2011. Sandstone caves on Venezuelan tepuis: Return to pseudokarst? Geomorphology 132, 351-365.

Ayub, S., 2006. Geology and geomorphology aspects of the deepest quartzite cave in the world. Proceedings of the 10th International Symposium on Pseudokarst, Gorizia, 94-100.

Bauters, T.W.J., Di Carlo, D.A., Steenhuis, T.S., Parlange, J.Y., 2000. Soil water content dependent wetting front characteristics in sand. Journal of Hydrology 231/232, 244-254.

Bernabei, T., Mecchia, M., Pezzolato, P., Piccini, L, Preziosi, E., 1993: "Tepuy '93: ancora Venezuela!". Speleologia, Rivista della Società Speleologica Italiana 29, 8-23.

Brewer-Carías, C., Audy, M., 2011. Entrañas del mundo perdido. Charles Brewer-Carías (Ed.), Caracas, 290 p.

Briceño, H.O., Schubert, C., 1990. Geomorphology of the Gran Sabana, Guyana Shield, Southeastern Venezuela. Geomorphology 3, 125-141.

Burley, S.D., Kantorowicz, J.D., 1986. Thin section and S.E.M. textural criteria for the recognition of cement-dissolution porosity in sandstones. Sedimentology 33, 587-604.

Carreño, R., Nolla, J., Astort, J., 2002. Cavidades del Wei-Assipu Tepui, Macizo del Roraima, Brasil. Boletin Sociedad Venezolana de Espeleologia 36, 36-45.

Chalcraft, D., Pye, K., 1984. Humid tropical weathering of quartzite in southeastern Venezuela. Zeitschrift fur Geomorphologie 28, 321-332.

Colveé, P., 1973. Cuevas en cuarcitas en el Cerro Autana, Territorio Federal Amazonas. Boletin Sociedad Venezolana de Espeleologia 4/1, 5-13.

Doerr, S. H. 1999. Karst-like landforms and hydrology in quartzites of the Venezuelan Guyana shield: Pseudokarst or "real" karst? Zeitschrift fur Geomorphologie 43, 1-17.

Epis, L., Ayub, S., 2010. Abisso Guy Collet – la grotta in quarzite più profonda del mondo (Amazzonia, Brasile). Speleologia, Rivista della Società Speleologica Italiana 62, 59-67.

Filipponi, M., Jeannin, P., Tacher, L., 2009. Evidence of inception horizons in karst conduit networks. Geomorphology 106, 86-99.

Füchtbauer, H., 1967. Influence of different types of diagenesis in sandstone porosity. 7th World Petroleum Congress, Mexico, Proceedings, vol. 2, 353-369

Galán, C., 1982. Notas sobre la morfologia de la Cueva Autana y algunos comentarios generales sobre las formas pseudocarsicas desarrolladas en cuarcitas del Grupo Roraima, Guyana, Venezuela. Boletin Sociedad Venezolana de Espeleologia 10 (19), 115-128.

Galán, C., 1991. Expedición SVE a los tepuys Ilù, Tramen y Iuruaní. Boletin Sociedad Venezolana de Espeleologia 25, 47.

Galán, C., Herrera, F.F., Carreño, 2004. Geomorfología e hidrología del Sistema Roraima Sur, Venezuela, la mayor cavidad del mundo en cuarcitas: 10,8 km. Boletin Sociedad Venezolana de Espeleologia 38, 2-16.

Ghosh, S.K., 1985. Geology of the Roraima Group and its implication. Boletin de Geologia, Venezuela, Pub. Especial 10, 33-50.

Gibbs, A.K., Barron, C.N., 1993. The Geology of the Guyana Shield. Clarendon Press, Oxford, 246 p.

Gori, S., Inglese, M., Tognini, P., Trezzi, G., Rigamonti, I., 1993. Auyan-tepui, speleologia tropicale nelle quarziti. Speleologia, Rivista della Società Speleologica Italiana 28, 23-33.

Goudie, A.S., 2006. The Schmidt Hammer in geomorphological research. Progress in Physical Geography 30, 703-718.

Haas, H., Holdaway, M. J., 1973. Equilibria in the system Al_2O_3-SiO_2-H_2O involving the stability limits of pyrophyllite, and thermodynamic data of pyrophyllite. American Journal of Science 273, 449-464.

Ipiña, J.M., 1994. Aspectos físico-químicos de los tepuyes Acopan y Amuri. Macizo de Chimanta, Gran Sabana, Venezuela. Boletin Sociedad Venezolana de Espeleologia 28, 5-9.

Jennings, J.N., 1983. Sandstone pseudokarst or karst? In: Young, R.W., Nanson, G.C. (Eds.), Aspects of Australian Sandstone Landscape. Australia and New Zealand Geomorphology Group Special Publication, Wollongong, pp. 21-30.

Liu, Y., Steenhuis, T.S., Parlange, J.Y., 1994. Formation and persistence of fingered flow fields in coarse grained soils under different characteristics in sands. Journal of Hydrology 159, 187-195.

Lowe, D.J., 1992. The origin of limestone caverns: an inception horizon hypothesis. Manchester Metropolitan University, Ph.D. thesis, 512 pp.

Lundberg, J., McFarlane, D.A., Brewer-Carias, C., 2010. An extraordinary example of photokarren in a sandstone cave, Cueva Charles Brewer, Chimantá Plateau, Venezuela: biogeomorphology on a small scale. Geomorphology 121(3-4), 342-357.

Martini, J.E.J., 1979. Karst in Black Reef quarzite near Kaapsehoop, Eastern transval. Annals of South African Geological Survey 13, 115-128.

Martini, J.E.J., 1985. Les phénomènes karstiques de quartzites d'Afrique du Sud. Karstologia 9, 45-52.

Martini, J.E.J., 2000. Dissolution of quartz and silicate minerals. In: Klimchouk, A.B., Ford, D.C., Palmer, A.N., Dreybrodt, W. (Eds.), Speleogenesis-Evolution of karst aquifers. National Speleological Society, Huntsville, pp. 452-457.

Martini, J.E.J., 2004. Silicate Karst. In: Gunn, J. (Ed.), Encyclopedia of Caves and Karst Science. Fitzroy Dearborn, London, pp. 1385-1393.

Maxwell, J.C., 1964. Influence of depth, temperature, and geologic age on porosity of quartzose sandstone. AAPG Bulletin 48, 697-709.

Mecchia, M., Sauro, F., Corongiu, C., Crobu, V., 2009. Speleological explorations in the Chimanta massif quartzites (Gran Sabana, Venezuela). Supplement to Kur magazine 12, 16 p.

Mecchia, M., Piccini, L., 1999. Hydrogeology and SiO_2 geochemistry of the Aonda Cave system (Auyantepui, Bolivar, Venezuela). Boletin Sociedad Venezolana de Espeleologia 33, 1-11.

Palmer, A.N., 2003. Dynamics of cave development by allogenic water. Acta Carsologica 30/2, 14-32.

Pettijohn, J., Potter, P.E., Siever, R., 1987. Sand and Sandstone. Springer, Berlin, 553 p.

Piccini, L., 1995. Karst in siliceous rock: karst landforms and caves in the Auyán-tepui massif (Est. Bolívar, Venezuela). International Journal of Speleology 24, 41-54.

Piccini, L., Mecchia, M., 2009. Solution weathering rate and origin of karst landforms and caves in the quartzite of Auyan-tepui (Gran Sabana, Venezuela). Geomorphology 106, 15-25.

Pope, G.A., 1995. Newly discovered submicron-scale weathering in quartz: geographical implications. Professional Geographer 47/4, 375-387.

Pouylleau, M., Seurin, M., 1985. Pseudo-karst dans des roches gréso-quartzitiques de la formation Roraima. Karstologia 5, 45-52.

Reid, A. R., 1974. Stratigraphy of the type area of the Roraima Group, Venezuela. Bolletin de Geologia, Venezuela, Pub. Especial 6, 343-353.

Renard, F., Park, A., Ortoleva, P., Gratier, J.-P, 1999. An integrated model for transitional pressure solution in sandstones. Tectonophysics 312(2-4), 97-115.

Rigamonti, I., 1995. La roccia. In: "Venezuela 1992 - Spedizione speleologica italiana all'Auyantepuy", Il Grottesco, Bollettino Gruppo Grotte Milano CAI-SEM, num. speciale, 32-40.

Santos, J.O.S., Potter, P.E., Reis, N.J., Hartmann, L.A., Fletcher, I.R., McNaughton, N.J., 2003. Age, source, and regional stratigraphy of the Roraima Supergroup and Roraima-like outliers in northern South America based on U-Pb geochronology. Geological Society of America Bulletin 115, 331-348.

Sauro, F., 2009. Mondi Perduti, sugli altopiani quarzitici del Venezuela, Speleologia 61, 38-47.

Sauro, F., De Waele, J., Forti, P., Galli, E., Vergara, F., 2011. Speleogenesi e speleotemi di opale della Cueva Guacamaya, Auyan Tepui, Gran Sabana, Venezuela. Atti del XXI Congresso Nazionale di Speleologia, Trieste, in press.

Scherer, M., 1987. Parameters influencing porosity in sandstones: a model for sandstone porosity prediction. AAPG Bulletin 71, 485-491.

Siever, R., 1962. Silica solubility, 0-200° C and the diagenesis of siliceous sediments. Journal of Geology 70, 127-150.

Sociedad Venezolana de Espeleologia, 1984. Catastro Espeleologico National. Boletin Sociedad Venezolana de Espeleologia 22, 65-75.

Sociedad Venezolana de Espeleologia, 1994. Cavidades Estudiadas en la Expedición al Macizo de Chimanta, 1993. Boletin Sociedad Venezolana de Espeleologia 28, 34-51.

Szczerban, E., Urbani, F., Colveé, P., 1977. Cuevas y simas en cuarcitas y metalimolitas del Grupo Roraima, Meseta de Guaiquinima, Estado Bolivar. Boletin Sociedad Venezolana de Espeleologia 8, 127-154.

Taylor, T.R., Giles, M.R., Hathon, L.A., Diggs, T.N., Braunsdorf, N.R., Birbiglia, G.V., Kittridge, M.G., Macaulay, C.I., Espejo, I.S., 2010. Sandstone diagenesis and reservoir quality prediction: models, myths, and reality. AAPG Bulletin 94, 1093-1132.

Urbani, F., 1991. Algunos comentarios sobre terminología kárstica aplicada a rocas silíceas. Boletin Sociedad Venezolana de Espeleologia 24, 5-6.

Urbani, F., Talukdar, S., Szczerban, E., Colveé, P., 1977. Metamorfismo de las rocas del Grupo Roraima, Edo. Bolívar y Territorio Federal Amazonas. Memorias V Congreso Geologico Venezolano, Caracas, pp. 623-638.

Weyl, P.K., 1959. Pressure solution and the force of crystallization - a phenomenological theory. Journal of Geophysical Research, 64, 2001-2025.

White, W.B., Jefferson, J.l., Haman, J.F., 1966. Quartzite karst in Southeastern Venezuela. International Journal of Speleology 2, 309-314.

Williams, R.B.G., Robinson, D.A., 1983. The effect of surface texture on the determination of the surface hardness of rock using the Schmidt Hammer. Earth Surface Processes and Landforms 8, 289–292.

Wolf, K.H., Chilingarian, G.V., 1975. Diagenesis of Sandstones and Compaction. In: Developments in Sedimentology, Elsevier, Vol. 18, pp. 69-444.

Wray, R.A.L., 1997a. A global review of solutional weathering forms on quartz sandstones. Earth Science Reviews 42, 137-160.

Wray, R.A.L., 1997b. Quartzite dissolution: karst or pseudokarst? Cave and Karst Science 24, 81-86.

Wray, R.A.L., 2000. The Gran Sabana: The World's Finest Quartzite Karst? In: Migon, P. (Ed.), Geomorphological Landscapes of the World. Springer, pp. 79-88.

Yang, G., Tian, M., Zhang, X., Chen, Z., Wray, R.A.L., Ge, Z., Ping, Y., Ni, Z., Yang, Z., 2012. Quartz sandstone peak forest landforms of Zhangjiajie Geopark, northwest Hunan Province, China: pattern, constraints and comparison. Environmental Earth Sciences 65, 1877-1894.

Young, R.W., Wray, R.A.L., Young, A.R.M., 2009. Sandstone Landforms, Cambridge University Press, Cambridge, 314 p.

Zawidzki, P., Urbani, F., Koisar, B., 1976. Preliminary notes on the geology of the Sarisariñama plateau, Venezuela, and the origin of its caves. Boletin Sociedad Venezolana de Espeleologia 7, 29-37.

CHAPTER 2.4

Manuscript to be submitted to Geomorphology

THE PATTERN OF QUARTZ-SANDSTONE CAVES: EVIDENCES OF THE ARENISATION PROCESS

Francesco Sauro[1,3], Leonardo Piccini[2,3], Jo De Waele [1,3]

1) Dipartimento di Scienze Biologiche, Geologiche e Ambientali, Italian Institute of Speleology, Via Zamboni 67, 40126, Bologna, (Italy)
2) Dipartimento di Scienze della Terra, Università di Firenze, Via La Pira 4, 50121, Firenze, (Italy)
3) La Venta Esplorazioni Geografiche Association, Via Priamo Tron 35/F, 31100, Treviso, (Italy)

Corresponding author: Francesco Sauro

Abstract

A detailed petrographic, structural and morphometric investigation of different types of caves carved in the quartz-sandstones of the "tepui" table mountains allowed to identify the main speleogenetic factors guiding the cave patterns development and the formation of peculiar features commonly found in these caves like funnel shape pillars, pendants and floor bumps. Samples of fresh and weathered quartz-sandstone of the Mataui Formation (Roraima Supergroup) collected into the caves were characterised through WDS dispersive X-Ray chemical analyses, picnometer measurements, EDAX punctual analyses, SEM and thin sections microscopy observations. In all the caves an alternation of two compositionally different strata was identified: almost pure quartz-sandstones with content of silica over 95 % and high primary porosity (around 4 %), and phyllosilicate-rich quartz-sandstone with contents of aluminium over 10 % and low primary porosity (lower than 0.5 %). Phyllosilicates are mainly pyrophyllite and kaolinite. SEM images on weathered samples showed clear evidences of dissolution on quartz grains with characteristic features at different degree of development, depending on the frailty of the samples. Grain boundary dissolution increases the rock porosity and gradually releases the quartz grains showing that arenisation is a widespread weathering process in these caves. The primary porosity and the degree of fracturing of the quartz-sandstone beds result as the main factors controlling intensity and distribution of the arenisation

process. Arenisation along the inception horizons or strata-bounded fracture network predisposes the formation of caves in specific stratigraphic positions where the loose sands produced by weathering can be removed by piping, gradually anastomising the open fractures forming braided mazes, geometric networks, or main conduit patterns, depending on the local lithological and structural guidance on the weathering process.

This study clearly demonstrates that all the peculiar morphologies documented in the caves can be easily explained as results of arenisation, which is guided by layers with peculiar petrographic characteristics (primary porosity, content of phyllosilicates), different grade of fracturation (strata bounded fractures or continuous dilational joints), together with the hydrologic recharge conditions of the systems (floodwater injection or diffuse infiltration).

Keywords: quartz-sandstone, speleogenesis, arenisation, weathering, strata-bounded fractures, Tepui, Venezuela

2.4.1 Introduction

About thirty years ago cavers and karst scientists believed that speleogenesis of caves in quartz-sandstones was related to exceptional conditions and only of local importance because of the extremely low solubility and dissolution rate of quartz (Tricart, 1972; Wray, 1993). Since 2000, several huge horizontal cave systems have been explored in the “tepui” table mountains of Venezuela, showing a wide variety of morphologies and dimensions well comparable to the most developed cave systems in classic carbonate karst (Aubrecht et al., 2012; Sauro et al., 2013c).

This paradox of widespread, complex and kilometres long cave systems in one of the hardest and less soluble rocks obviously requires to rediscuss the speleogenetic processes responsible for their formation. Until now, most of the theories so far presented involve the formation of loose sands along some preferential bedding planes or fractures and their winnowing out (piping) by underground flowing waters (Sczerban and Urbani, 1974; Galán and Lagarde, 1988). The role in generating the “loose sands” has been assigned to rock dissolution by meteoric (Jennings, 1983; Martini, 2000; Wray, 2000; Piccini and Mecchia, 2009) or hydrothermal waters (Zawidzki et al., 1976) through a weathering dissolution process called “arenisation”. Other authors assign importance to microbially-driven alkaline dissolution (Marker, 1976; Barton et al., 2009), or refer to the existence of unlithified beds, also produced by dissolution and weathering of aluminosilicates (Aubrecht et al., 2008; 2011; 2012). All these theories are still under discussion and there is not yet a clear understanding of the main speleogenetic and morphogenetic factors involved. Sauro et al. (2013a)

pointed out some problems related to the "unlithified beds" speleogenetic model proposed by Aubrecht et al. (2011) which is not compatible with the geologic history of the Gran Sabana region and does not explain the presence of decimetres of "friable" rock on the walls of deep shafts cutting the entire stratigraphic sequence. Conversely, Sauro et al. (2013a, 2013b) suggested that, if the conditions are favourable and given enough time, the whole stratigraphic sequence could be weathered in terms of the "arenisation" theory (Martini, 2000), but the grade of fracturing, the mineralogical composition and the petrographical features (grain size, sorting, depositional structures, primary porosity), and not the diagenetic degree of the quartz-sandstone, probably control the intensity of the weathering processes along the strata.

The main discussion is focused on the presence of some peculiar morphologies, like funnel-shaped pillars and pendants, which are considered by Aubrecht et al. (2013) as channels of a descending silica-bearing diagenetic fluid flow, while for Sauro et al. (2013a) they represent secondary forms related to arenisation and erosion processes along fracture networks.

After the exploration of kilometre long caves in the Roraima and Chimantha massifs since 2005 (Aubrecht et al., 2012; Audy and Bouda, 2013) in April 2013 a new giant cave was discovered by a joint Italian-Venezuelan expedition on the Auyan Tepui in the Canaima National Park. This system was named Imawarì Yeuta (the Cave where the Gods live in Pemon Kamarakoto indian language), and reaches now over 15.5 km of development, being actually one of the longest quartzite caves in the world (Sauro et al., 2013c). Besides its dimensions, the scientific interest of this cave is very high and all the characteristic morphologies described by Aubrecht et al. (2011, 2012) for the quartz-sandstone caves of the Churì Tepui and Roraima are here well represented. During this expedition, detailed morphometric studies were performed, together with a detailed survey and focused sampling of weathered and unweathered quartz-sandstones. The data from Imawarì Yeuta were then coupled with further morphological observations and samples from other caves developed in the Mataui Formation: the Roraima Sur System in the Roraima Tepui (Galán et al., 2004; Aubrecht et al., 2012), Akopan-Dal Cin System in the Chimantha massif (Mecchia et al., 2009; Sauro, 2009), Guacamaya Cave in the western sector of Auyan Tepui (Sauro et al., 2013b) and the crevice networks of the Aonda and Auyan Tepui Noroeste systems (Piccini and Mecchia, 2009). The aim of this research is to identify the main factors guiding the formation of caves along specific layers, to explain the processes behind the formation of pillars and pendant morphologies, and finally understand the main controls on the different cave patterns. This study combines the following investigations: 1) mineralogical, chemical and petrographical characterisation of the quartz-sandstone beds; 2) SEM imaging to identify dissolution morphologies on the quartz grains and signs of other potential

weathering processes; 3) Morphometric measurements and statistics of quartz-sandstone pillars in the Imawarì Yeuta cave in order to explain their relationship with fracture sets and the degree of fracturation; 4) Detailed topographic survey of the caves in order to identify the stratigraphical and structural guidance features on the cave genesis.

The results are then discussed in order to evaluate the potential morphological expressions of the arenisation-weathering process and the potential lithological and structural guidance in the formation of these typical caves.

2.4.2 Regional setting

The Gran Sabana is a vast geographical region, part of the Guyana Shield, located in northern South America, between Venezuela and Brazil, crossed by several tributaries of the Rio Caroní, which in turn flows into the Orinoco River (Fig. 1). The main massifs of the Gran Sabana have the shape of large table mountains named "tepuis", the local Pemón word meaning “house of the Gods” or mountain according to the local indigenous language (Pemón). The tepuis are delimited by vertical to overhanging cliffs many hundreds of metres high surrounded by the lowlands of the Wonkén planation surface, which isolates the massifs from each other. The high plateaus consist of a series of stratigraphically controlled planar surfaces (in general grouped into the Auyan planation surface, between 2000 and 2900 m a.s.l., considered of Mesozoic age) divided by secondary scarps (Briceño

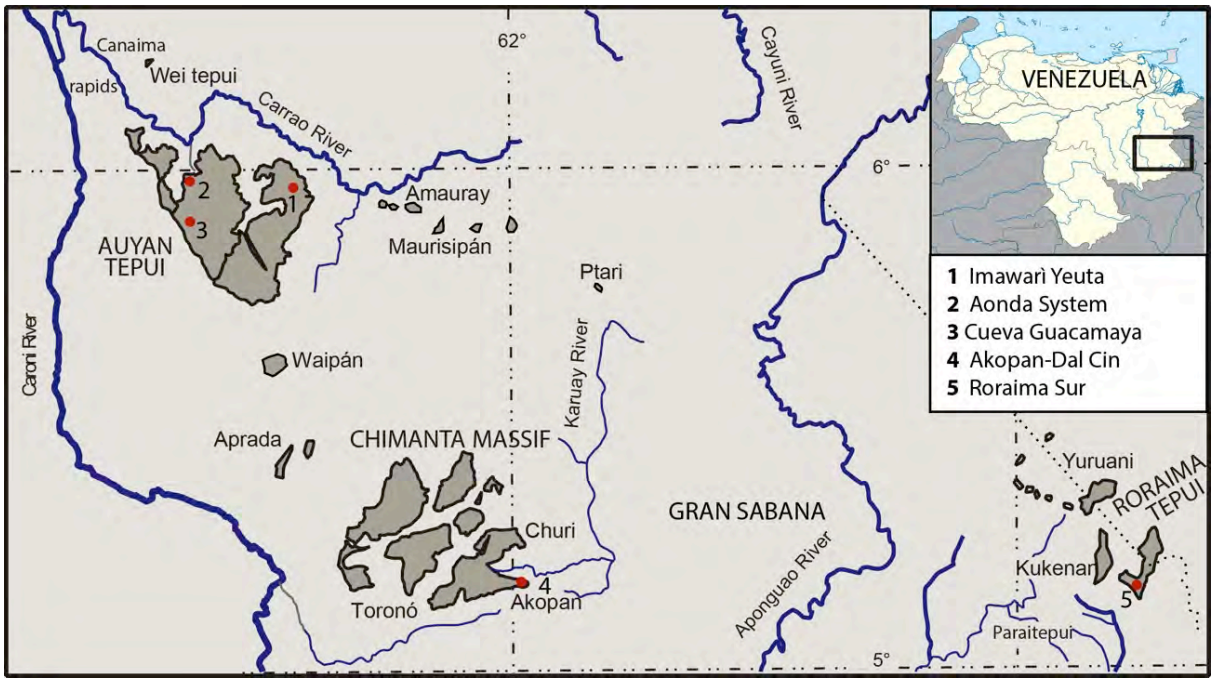

Fig.1. Geographic location of tepui massifs in the Gran Sabana Region and the investigated cave systems. In Auyan Tepui: Imawarì Yeuta, Guacamaya Cave, Aonda and Auyantepuy Noroeste systems. In the Chimantha massif: Akopan-Dal Cin System. In the Roriama Tepui: Roraima Sur System.

and Schubert, 1990). More than 60 tepuis are present in the Gran Sabana region but our research focused on the karst systems of the three most important massifs (Fig. 1): 1) Auyan tepui (700 km^2), one of the largest of the area, famous for the Angel waterfall, considered the highest in the world with its 975 metres of vertical drop, 2) Roraima Tepui (31 km^2) and 3) Akopan tepui, in the southeastern sector of the Chimantha Massif (composed of different tepuis with a total surface of 1470 km^2).

The igneous and metamorphic rocks in the northern portion of the Guyana Shield (Imataca-Bolivar Province, after González de Juana et al., 1980) have an age of 3.5 Ga. The siliciclastic rocks of the Roraima Group belong to the continental and pericontinental environment of the Roraima-Canaima Province (Reid, 1974). The age of this arenaceous group can be inferred only on the basis of the absolute dating of the granitic basement (2.3-1.8 Ga) and of the basaltic dykes and sills that cross the upper formation of the Roraima Group (1.4-1.8 Ga) (Briceño and Schubert, 1990; Santos et al., 2003). The Roraima Group was also intruded by Mesozoic basalts forming thin NE-trending dykes with ages of around 200 Ma (Hawkes, 1966; Teggin et al., 1985). A low-grade metamorphic overprint, leading to quartz grain overgrowths and pyrophyllite-muscovite formation in the more pelitic beds, is the result of the lithostatic load of ~3 km thick sediments which are now eroded (Urbani et al., 1977).

Caves are developed in the Mataui Formation, the youngest sediments of the Roraima Group. This formation is 600-900 m thick and ~1.5 Ga old, representing the highest part of the tepuis (Santos et al., 2003). The quartz grains composing these sandstones are well-sorted, between 30 and 200 µm in diameter, and cemented by syntaxial quartz overgrowths or by minor pore-filling phyllosilicates (pyrophyllite and/or kaolinite). Quartz commonly represents over 90% of the rock, giving the name "quartz-sandstone" (Martini, 2000; 2004). The slopes at the foot of the cliffs surrounding the tepuis are made of proto-quartzites, arkoses and graywackes, with beds of cherts, lutites and siltites (Uaimapué Formation; Reid, 1974). In the lowlands the main outcropping lithology is the Kukenán Formation, prevalently composed of siltites and shales.

From a structural point of view folding structures are absent, except for some wide folds at a very large scale. The bedding is normally horizontal, locally slightly inclined. Sets of mainly vertical fractures cut the plateaus, creating a regular network of quadrangular prisms. Important regional faults with relevant displacement have not been observed in the Gran Sabana area (Gibbs & Barron, 1993).

From a geomorphic point of view all the examined tepuis presents similar characteristics: 1) a slightly inclined pediment formed by detrital talus on the more erodible lithologies of the Uaimapué Formation; 2) an external vertical cliff (Mataui Formation), up to one thousand metres high,

presenting a few major ledges in specific stratigraphic positions; 3) an upper plateau divided in at least two secondary platforms with about 100-150 metres of altitude difference, controlled by specific stratigraphic layers. The lower platform is usually characterised by extensive fields of collapsed boulders, while the higher platform is more regular and flat without rock-piles, but often presenting wide fields of towers, crevices and rock cities.

The climate is tropical and the average annual rainfall is 3400-3600 mm. The average daily temperature is fairly constant all year round, with an estimated 13.9° C at 2200 m altitude, and a mean difference between day and night of 10° C (Galán, 1992).

The high rainfall supports a temperate vegetation; forests, sedges, grasses, and bromeliads grow in the sheltered locations, peat swamps and bogs are well-developed and often extensive, particularly where the substrate is characterised by weathered diabase sills (Briceño and Schubert, 1990). Quartz-sandstone outcrops are bare of vegetation except for mosses, lichens, and algae. The water flows on the plateaus, forming high waterfalls along the external cliffs, or sinking in fractures and cave systems to later resurge from springs scattered around the cliffs (Mecchia and Piccini, 1999).

2.4.3 The caves

2.4.3.1 The Imawarì Yeuta cave system

The Imawarì Yeuta cave is situated in the northeastern sector of the Auyan Tepui at an altitude of 2030 m a.s.l. (Fig. 1-1) The cave develops mainly at the stratigraphic elevation of the lower platform,

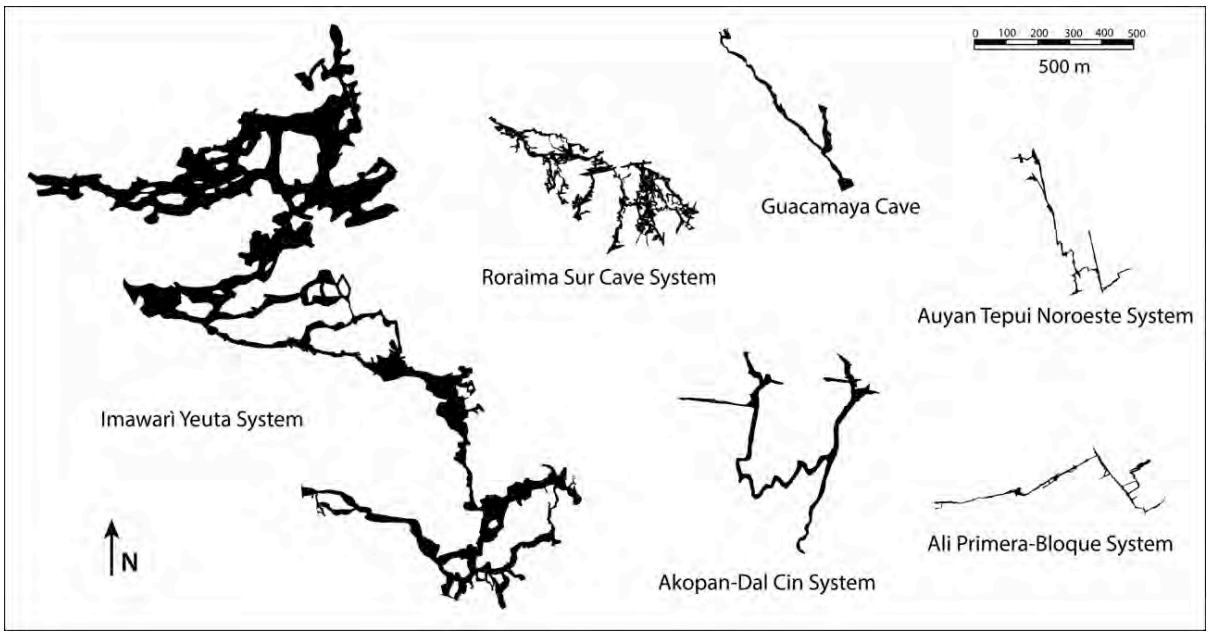

Fig. 2. Plan view and size/pattern comparison of the investigated cave systems. The survey of Roraima Sur is adapted from Aubrecht et al. (2013), all the others are from the La Venta Archive.

extending almost horizontally for more than 20 km (15.6 actually surveyed but at least additional 4 more explored) about 100-150 metres beneath the upper platform surface (Fig. 2 and 3a) (Sauro et al., 2013c). The main entrances to the system are situated at the base of the tepui internal cliff borders or at the bottom of deep giant collapse dolines and joint-controlled sinkholes opening in the inner part of the upper platform. The direction of drainage is in general from ESE to WNW following the gently dip of the quartz-sandstone beds. From a hydrological point of view the cave system consists of three independent collectors, two of them draining a big collapse dolina named Sima del Viento, while the most important one derives from the catchment area of a larger circular collapse dolina to the north, about five hundred metres wide, and of a nearby smaller sinkhole (Fig. 3a). Here a stream falls into the cave from the upper platform through an about 90 metres high waterfall. During the explorations, carried out during a particularly dry period, the first two streams had a minimum discharge of about 20 l/s, while the main river reaches a minimum of 100 l/s. From the signs left by water on the walls it was evident that this last river can probably reach several cubic metres per second during the rain season, flooding the lower sectors of the cave. A labyrinth network of inactive galleries, developed along a distinct bed, interconnects the different rivers. This “open” bed can reach impressive width (more than 300 metres in some sectors) creating huge environments where the ceiling is supported only by relict pillars and wide columns (Fig. 3b). This situation causes large collapse zones with a chaotic floor of fallen boulders. Some dry galleries situated some metres above the actual streams thalwegs show palaeo-phreatic rounded morphologies and are in general almost perpendicular to the present vadose drainage (Fig. 3c).

The most typical morphologies characterising the cave system are layer-bounded pillars (Fig. 3d). These features in Imawarì Yeuta are very similar to those described by Aubrecht et al. (2012) for the Churì and Roraima tepui caves and by Doerr (1999) in the Kukenan tepui, but with an even wider variety of forms and dimensions. Pillars are normally 1 to 3 metres high, often characterised by elliptical cross-sections with the major axes from a few centimetres to several metres long. They develop only along specific layers, bounded by more massive banks. The smaller pillars are characterised by a funnel shape with a vertical or, more often, slightly inclined axis and an elliptical rather than circular cross-section of the narrower central part up to 1 metre in diameter. At increasing size the funnel shape is less prominent becoming more cylindrical. In many cases the pillars have an elongated form in plan view, sometimes becoming a true septum dividing the cave passages in parallel corridors. At even bigger size (more than 5 metres in diameter) they constitute rough massive columns sometimes surrounded by minor funnel-shaped pillars. These morphologies are not widespread in the cave, but they are concentrated in specific locations, mainly on the lateral

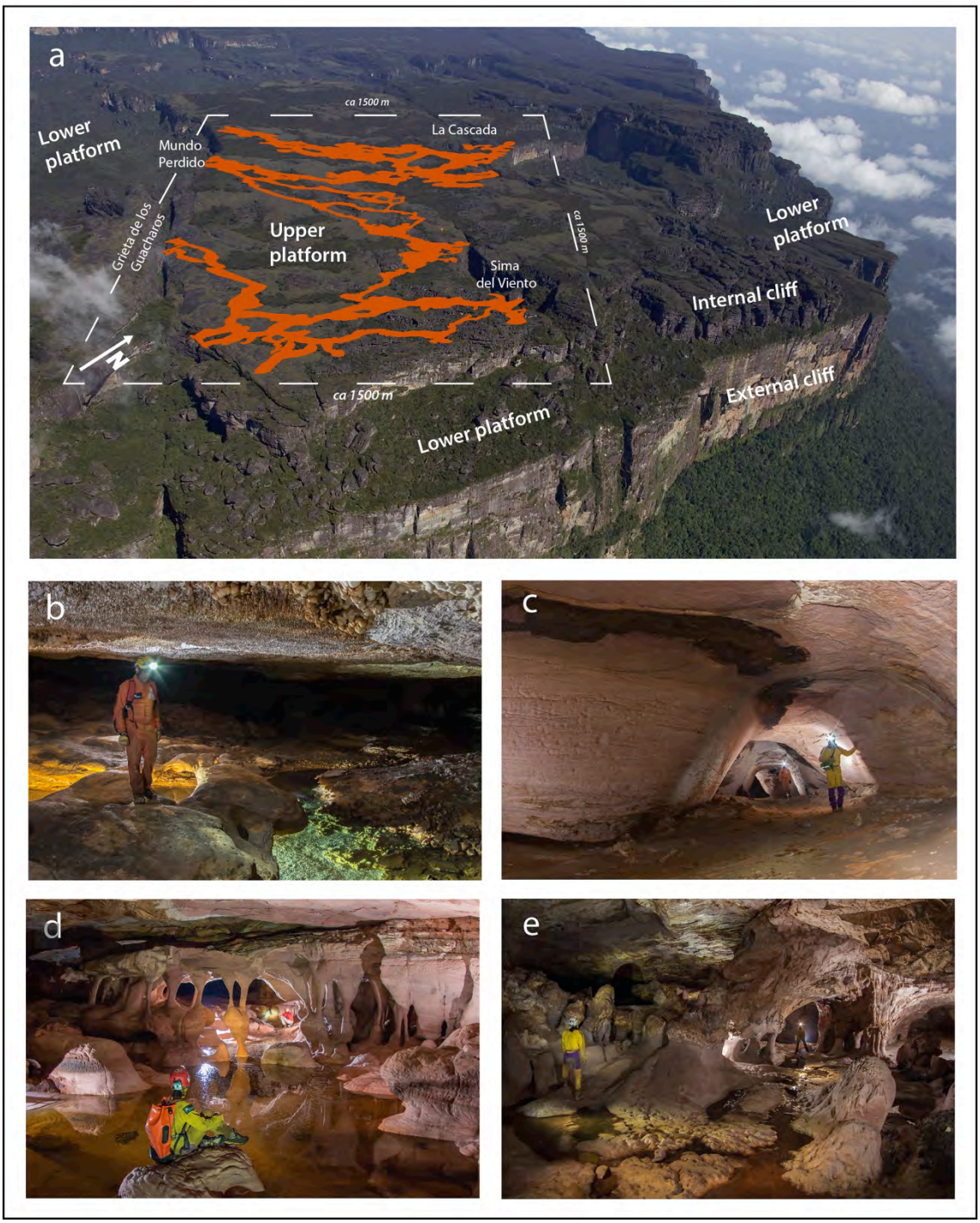

Fig. 3. Plan projection and typical morphologies of Imawarì Yeuta cave: a) cave system plan projection on the tepui surface: the cave develops at the height of the lower platform with the main entrances located in deep collapses, grietas or at the base of the cliff rims of the higher platform; b) hundred metres wide strata-bounded environments with flat ceilings characterise the cave system; c) conduits in the upper dry level of galleries of the system are characterised by rounded, probably paleo-phreatic cross-section; d) field of funnel-shaped pillars in the Galeria de las Mil Columnas, along one of the three main streams of the cave; e) complex environments with bumps rising from the floor, pendants, pillar and septums characterise the Universo del Silencio sector of the cave. Photos Vittorio Crobu, La Venta Geographic Explorations Team.

side of hydrologically active galleries. Small funnel-shaped pillars are particularly well developed (in groups of more than forty pillars in only a few tens of metres) along the outer convex walls of meanders and in the lower, often partially flooded, levels of the rivers beds. Other related typical morphologies are rounded or rhombohedral pendants protruding from the ceiling or similar bumps rising from the floor (Fig. 3e). Similar mammillary forms were also described by Aubrecht et al. (Fig. 2 A-B in 2013) in the Muchimuk Cave System. Likewise to the pillars, these features can have different sizes, and they are concentrated only in specific sectors of the cave.

In general the presence of pillars and septums of all size gives to the cave a general maze network, well recognisable in the topographic survey plan view (Fig. 2).

The cave is also characterised by the presence of spectacular silica speleothems and gypsum formations, and by iron hydroxide residual deposits. These “red-muds” in some cases flow out from the higher interlayers of the cave galleries, forming massive brownish flowstone on the floor, similar to other goethite speleothems described in other quartzite caves of the Sarisariñama and Chimantha tepuis (Zawidzki et al., 1976; Aubrecht et al., 2012).

2.4.3.2 The Guacamaya cave

Guacamaya cave represents the first horizontal cave discovered in the Auyan Tepui in 2009 (Sauro, 2009; Sauro et al., 2013b). Different from Imawarì Yeuta, this cave system presents a “main conduit” pattern (Fig. 2). The caves develops in the same stratigraphic position of Imawarì Yeuta, at the level of the lower platform, and in general the cave conduits are situated at shallow depth from the surface, only 20-30 metres below the upper platform in some places.

The main branch is a hydrologic through-passage about 350 metres long with a permanent stream of some litres per seconds crossing the cave from the highest entrance to the lower resurgence (Fig. 4a). About one hundred metres from the lower entrance, a lateral inactive branch develops straight to the south for 700 metres ending in a boulder choke close to the surface. The passage is of significant size, more than 30 metres wide and about 15 metres high in some sectors, with a great collapse room at the intersection of the two branches. Both the active and the dry branches are developed along a layer of iron hydroxides with minor amorphous silica, similar to typical Banded Iron Formations, from some decimetre to a metre thick (Fig. 4a-b). This guidance is evident in the cross-sections of the galleries showing an elliptical or keyhole profile developed along this stratum (Sauro et al., 2013b). Original small phreatic conduits entrenched by vadose canyons are recognisable. Pillars are very rare while only in the lower part of the hydrologically active tunnel, a few septums and bridges constituted by the hardest beds are recognisable in some sectors.

It is evident that the cave is part of a more extended system, now dissected and open to the surface: the valleys upstream and downstream of the cave represent the unroofed continuation of the main conduit, showing the same lithological control.

2.4.3.3 The Akopan-Dal Cin cave system

Akopan-Dal Cin system is situated in the Akopan Tepui, in the southern sector of the Chimantha massif. This is a cave of more than 2.7 km length (Fig. 2), draining the higher plateau of the mountain through a large, 105 m deep collapse doline (Mecchia et al., 2009). At the bottom of the shaft the stream follows a horizontal meandering gallery, collecting waters from two other sinks. The river flows down to the lower entrance called "Resurgencia Dal Cin" where the stream exits from the cave and forms a 200 m high waterfall on the external tepui cliff. Just before the waterfall, a dry passage at the same level leads to another big entrance opening on the tepui cliff, the Akopan cave (Fig. 4c).

In general, the cave passages present a rectangular cross-section of significant size, over 20x10 metres (Fig. 4c). During floods these galleries can be completely flooded as observed during an exceptional rain event in the expedition of February 2012. The main collector is a meandering passage following the shallow dip of the strata. The other branches, instead, are clearly controlled by vertical fractures and presents a straight line development. Vertical and inclined pillars, forming peculiar "oblò" passages between different parallel diaclases, are present only in the Tramo Tibia Rotta. These features were interpreted by Sauro et al. (2013) as anastomosis of parallel vertical fractures (see Fig. 2 in Sauro et al., 2013).

Also in the Akopan-Dal Cin System a unique stratum strictly controls the development of the conduits: all the galleries follow a quartz-sandstone centimetric bed characterised by millimetric bands of iron hydroxides (Sauro et al., 2014). This level of horizontal conduits is situated at the same height of the major ledge characterising the external cliff of the Akopan tepui.

2.4.3.4 The Roraima Sur cave system

The Roraima Sur cave system, known also as Ojo de Crystal cave system (Aubrecht et al., 2012) is a maze of low conduits developed at shallow depth from the surface, beneath the upper platform of the Roraima Tepui. Thin layers of siltstone and shale guide the whole cave where different collectors fed by sinking streams follow the gentle dip of the strata (Galán et al., 2004). The dimensions of the galleries is far less prominent than the other horizontal caves known in the other tepuis, rarely reaching more than 5 metres of width. Since a detailed map of the cave has not been published, the total length of the system is still debated (Aubrecht et al., 2012). Nonetheless, the complex networks

Fig. 4. Typical cave morphologies from other investigated systems of the Gran Sabana tepui: a) an active gallery in the Guacamaya cave with keyhole cross-section developed along a bed of iron-hydroxides; b) the BIF-like stratum guiding the galleries in the Guacamaya cave; c) entrance gallery of the Akopan cave with a rectangular cross-section guided by the intersection of an iron hydroxide layer and a major fracture (arrow on the ceiling); d) Fracture-controlled vertical narrow canyon in the Ali Primera Resurgence in the Aonda system; e) The Ojo de Cristal entrance in the Roraima Sur system: the cave is developed along a specific quartz sandstone stratum while massive banks form overhanging ledges. Photo Vittorio Crobu (a,b,c,e) and Tullio Bernabei (d), La Venta Geographic Explorations Team.

of galleries interconnected by narrow passages allowed surveying around 10 km of passages (Brewer-Carías and Audy, 2011). In general, the cave has an anastomotic pattern, with a few major collectors interconnected by dry side passages developed along the same geological bed. These conduits are characterised by non-excavated relicts of the strata in forms of flat columns. Funnel-shaped pillars are presents only in a few parts of the cave and are in general less developed than those

documented in Imawarì Yeuta. For a detailed description of the cave and the hydrological connections see Galán et al. (2004).

2.4.3.5 Fissure networks of the Aonda and Auyan Tepui Noroeste system

A different example of cave system in the quartz-sandstones of the Mataui Formation is given by the crevice network collectors explored along the rims of the Aonda Canyon in the northwestern sector of the Auyan Tepui (Fig. 1-3; Sociedad Venezolana de Espeleologia, 1984; Bernabei et al., 1993; Gori et al., 1993; AA.VV., 1994; Rigamonti, 1995), but also close to the rims of other tepuis like Chimantha (Sociedad Venezolana de Espeleologia, 1994), Yuruani (Galán, 1991) and Wei Assipu (Carreño et al., 2002). The two most extensive systems are those of Auyan Tepui Noroeste (2.9 km of development, -370 m of depth) and the Ali Primera-Sima del Bloque cave stream network (2 km of development) resurging at the bottom of the deep Sima Aonda (Fig. 2). These are vertical shafts named “simas” or “grietas”, up to three hundred metres deep, developed along vertical fractures opened by gravitative release close to the tepui rims. In plan view these caves have an elongated narrow shape following the guiding fracture, while in profile they develop vertically for hundred metres with only a few ledges in specific stratigraphic positions. Their walls are characterised by friable rock, commonly permanently wetted by percolation or condensation waters. Conversely, on the exposed outside cliff walls at the same stratigraphical height the rock is frequently very hard, suggesting that water derived from direct infiltration or condensation in the subsurface enhances the arenisation process responsible for weathering and consequent enlargement of the fracture walls (Piccini and Mecchia, 2009). At the bottom of the shafts, horizontal, narrow and high canyons collect the water toward the resurgences located along the external cliffs of the plateau. These conduits are developed mainly along the intersection between the dilational fractures and specific stratigraphic levels, mainly siltstones and shale layers. In these collectors, peculiar features are represented by septums with rare aligned pillar morphologies separating parallel corridors.

2.4.4 Methods

2.4.4.1 Petrography, mineralogy and chemical composition

Petrographic studies on several quartz-sandstone samples from the Mataui Formation collected in the Auyan, Akopan, Roraima Tepui, Aonda and Auyan Tepui Noroeste caves, pillars and massive banks collected in Imawarì Yeuta, with various degree of cohesion/hardness, fresh and weathered, were carried out by means of transmitted light microscopy thin section observations, SEM imaging,

EDAX chemical point analyses, WD-XRF chemical bulk analyses, XRD mineral determinations and porosity determination with gas displacement methods.

For SEM images we used a SEM Jeol JSM-5400 electron microscope, digitalized with an iXRF 550i video card and equipped with a Si-drift detector for Energy Dispersive X-ray Spectroscopy at the BIGEA Department at the University of Bologna.

For X-Ray Diffraction analyses (XRD) quartz-sandstone samples were ground to an ultrafine powder in an agate mortar and lightly pressed in a plastic sample holder. XRD patterns were recorded with a Philips PW 1050/25 and a PANalytical X'Pert PRO Diffractometer (experimental conditions 40Kv and 20 mA tube, CuKα Ni filtered radiation λ = 1.5418 Å) at the Department of Chemical and Geological Sciences of Modena-Reggio Emilia University.

The bulk chemical determinations of 11 samples collected from cave walls in all the caves and from pillars in Imawarì Yeuta were obtained by two wave dispersive X-ray fluorescence spectrometers (WD-XRF) (Panalytical Axios, XRF Laboratory, BIGEA – Bologna, and Panalytical Axios at the Institute for Mineralogy and Petrology - IMP of ETH – Zurich) on pressed powder pellets, following the matrix correction methods of Franzini et al. (1972), Leoni and Saitta (1976) and Leoni et al. (1982). Calibration is based on 35 international reference materials. The estimated precision and accuracy for trace-element determinations are better than 5%, except for elements at <10 ppm (10-15%). Volatile content was evaluated by thermogravimetric TG-DTG-DTA analysis (XRF Laboratory, BIGEA – Bologna) in air atmosphere using a Setaram Labsys double-furnace apparatus (temperature range 20-1050°C; heating rate 10°C/min; platinum crucibles; calcined Al_2O_3 as reference substance; flow rate of air 0.27 mL/s; temperature accuracy about ±1°C).

Porosity analyses on five dried cores collected in unweathered or slightly weathered quartz-sandstone samples from the Mataui Formation were performed at the Rock Deformation Lab of ETH (Zurich) with a helium picnometer (MicroMeritics-AccuPyc-1330), which measures the porosity by means of gas displacement and the sample volume/gas pressure relationship (Hartikainen et al., 1996).

2.4.4.2 Morphometric analyses

Morphometric measurements of 110 pillars were carried out in Imawarì Yeuta cave by means of a laser-distance meter Leica Disto D8 and the Cavesniper instrument (Megaplot SJ), a device equiped with an electronic compass integrated with a digital clinometer, whose readings are calculated with an ARM7TDMI processor. Those instruments allowed measuring quickly and with a high degree of precision (accuracy respectively 1 mm and 1°) the major (*M*) and minor axes (*m*) length of the central

section, the direction (*D*) of the main axis, the dip (*i*) and dip direction (*id*) of the pillar (Fig. 5). Columns characterised by an ellipticity *e* (*M/m*) of the central part of the pillar higher than 3 and dimension of the major axis exceeding 1.5 metres were avoided during the measurements because they were considered septums rather then proper pillars. The measurements were done in three different sectors of the cave: Rio de los Italianos, Rio de Los Venezuelanos and Galeria de las Mil Columnas. In addition, in the surrounding area of every station we measured fractures and bedding plane dips and directions by means of a geological compass.

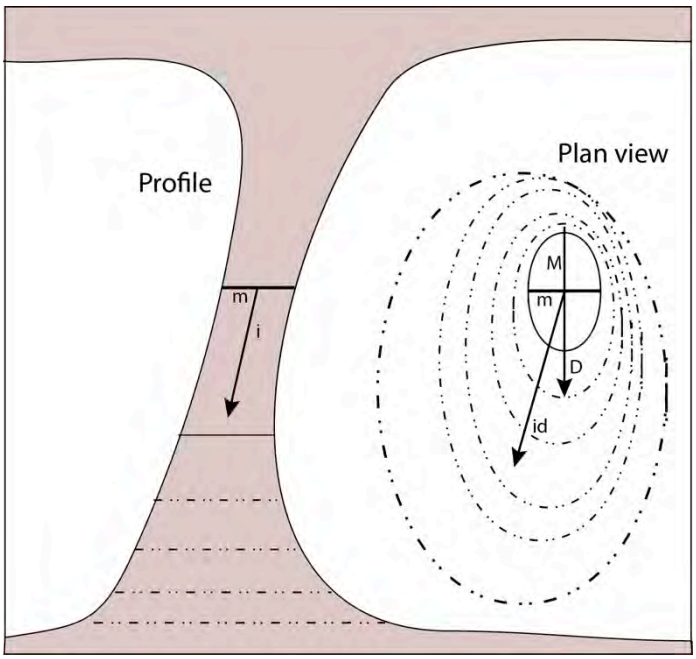

Fig. 5. Scheme showing the morphological measurements performed on the pillars in Imawarì Yeuta: minor axes (m), major axes (M), ellypses direction (D), pillar dip (i), dip direction (di)

2.4.5 Results and intepretation

2.4.5.1 Quartz-sandstone composition and petrography

In all the caves and in their surroundings two main petrographic groups can be clearly recognised by means of bulk compositional analyses (XRF): almost pure quartz-sandstone or quartz conglomerate with silica content ranging between 95-99 %, and aluminium phyllosilicate-rich quartz-sandstones with silica content around 70-90 % and aluminium over 10-20% (Table 1).

From a petrographic point of view the almost pure quartz-sandstones are composed mainly of detrital monocrystalline quartz grains with non-ondulatory extinction cemented by grain overgrowth, disposed in interlocked structures due to the burial metamorphism that evidently affected the Roraima Group (Urbani et al., 1977; Gibbs and Barron, 1993; Sauro et al., 2013a) (Fig. 6a). Conversely, in the second group the phyllosilicates are relevant and constitute a pore filling matrix (Fig. 6b). In some cases these phyllosilicates occur as a thin coating covering the interdigitated quartz grain rims (microstylolites), forming a typical texture of pressure solution during burial metamorphism (Sloss and Feray, 1948; Gratier et al., 2005; Fjellanger and Nystuen, 2007; Fig. 6c).

%	Sample	SiO_2	TiO_2	Al_2O_3	Fe_2O_3	MnO	MgO	CaO	Na_2O	K_2O	P_2O_5
Almost pure quartz-sandstones	**AKT**	96.03	0.05	3.28	0.10	0.001	0.005	0.017	0.419	0.059	0.015
	AK4	95.55	0.10	3.34	0.55	0.002	0.003	0.012	0.356	0.039	0.035
	R1	96.39	0.07	2.27	0.43	0.001	0.003	0.016	0.575	0.201	0.016
	V17	98.9	0.07	0.62	0.15	0.05	0.01	0.05	0	0.13	0.02
	V18	96.48	0.09	2.58	0.22	0.05	0.33	0.17	0.01	0.04	0.03
	V19	98.83	0.08	0.66	0.14	0.05	0.01	0.05	0	0.14	0.02
Aluminium phyllosilicate rich quartz-sandstone	**AK5A**	73.85	0.51	22.59	2.01	0.021	0.012	1.011	0.428	0.460	0.105
	AK5B	71.71	0.65	22.60	3.70	0.035	0.070	1.010	0.505	0.629	0.079
	AK5C	85.00	0.07	14.21	0.17	0.004	1.085	1.085	0.297	0.158	0.072
	AK3A	81.03	0.48	16.38	1.75	0.014	1.024	1.024	0.253	0.047	0.039
	ROR16	90.97	0.12	8.21	0.15	0.001	1.160	0.009	0.331	0.111	0.080

Table 1. Wavelength dispersive X-ray chemical analyses of different quartz-sandstone samples.

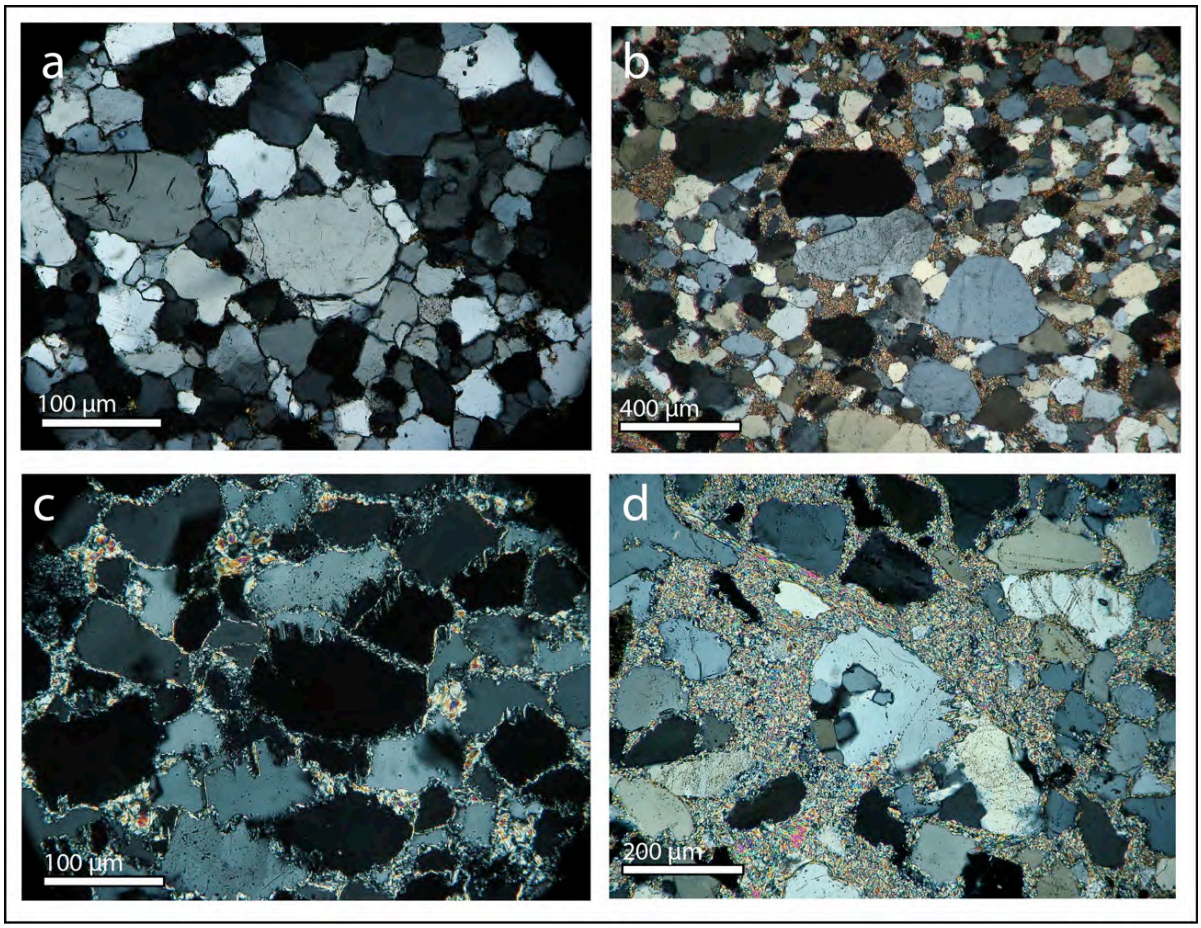

Fig. 6. Thin sections (at crossed nicols) of different unweathered quartz-sandstone samples: a) almost pure quartz-sandstone composed of quartz grains cemented by syntaxial overgrowths; b) quartz-sandstone characterised by a phyllosilicate matrix filling with evident overgrowths only at the direct contact between quartz grains; c) A thin coating of phyllosilicates (pyrophyllite) covers interdigitated quartz grains (microstylolites) typical of pressure solution during burial metamorphism; d) in presence of high pyrophyllite content the quartz grains result consumed because of the quartz-consuming kaolinite + quartz = pyrophyllite low grade metamorphic reaction (Hurst and Könkle, 1985).

With increasing phyllosilicate content, the quartz grains show strong corrosion in contact with pyrophyllite due to the quartz-consuming *kaolinite + quartz = pyrophyllite* low grade metamorphic reaction (Hurst and Könkle, 1985) (Fig. 6d). In these matrix-rich samples pressure solution with grain overgrowth is evident only at the direct contact between quartz grains.

Opal-A and feldspars, suggested to be minor components of these lithologies by Aubrecht et al. (2011), were not observed in all our samples.

Phyllosilicates were characterised through XRD analyses as pyrophyllyte ($A1_2Si_4O_{10}(OH)_2$), kaolinite ($Al_2Si_2O_5(OH)_4$), and rare muscovite ($KAl_2(AlSi_3O_{10})(F,OH)_2$). The first two minerals are the most abundant and can be easily distinguished also through SEM imaging and EDAX point analyses (Fig. 7). Pyrophyllite appears as fan-shaped or needle-like masses radiating in various directions, filling pores between quartz grains. Chemical EDAX counts on these masses show the peak of aluminium almost at half-height of the silica peak because of the chemical ratio Si/Al=2 in pyrophyllite. Conversely,

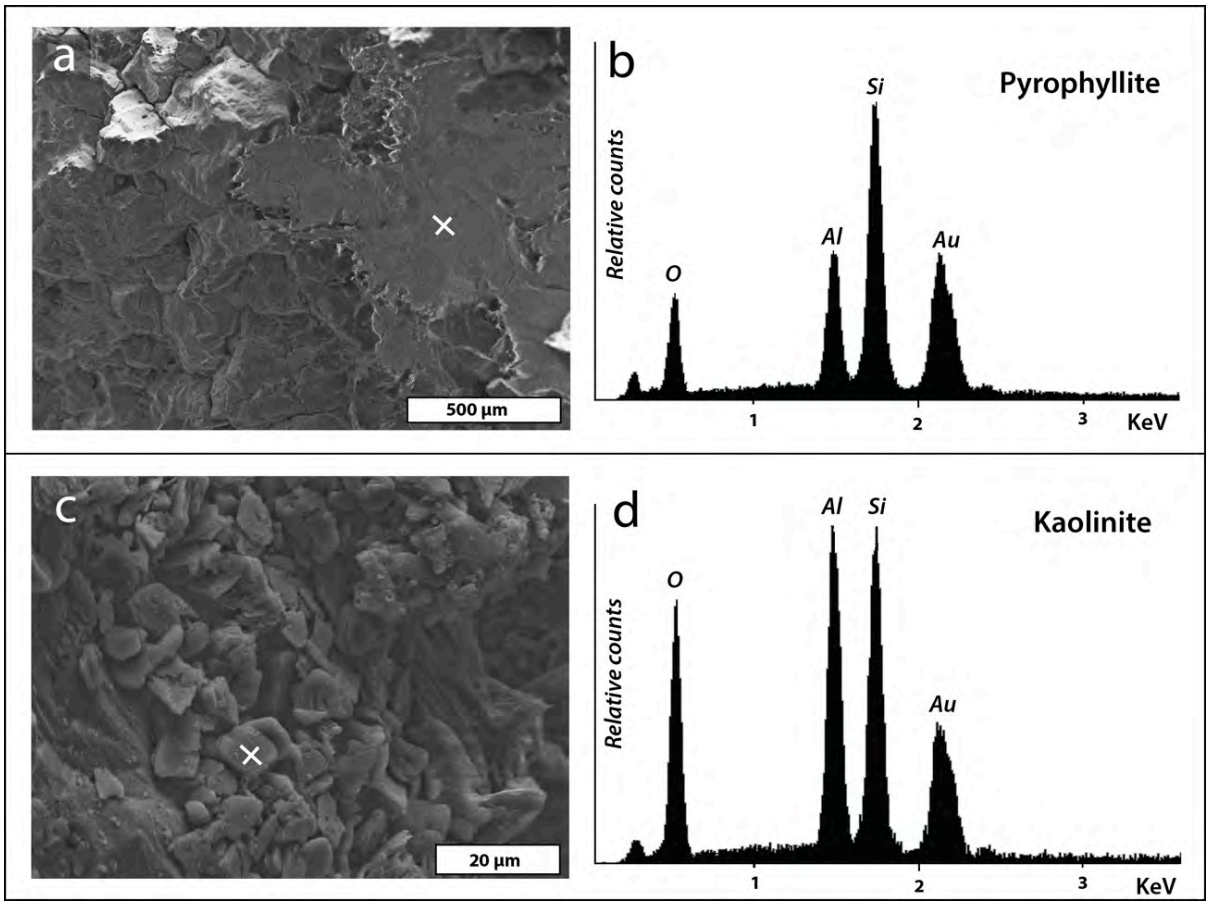

Fig. 7. SEM images and EDAX punctual analyses of pyrophyllite and kaolinite: a) fan-shaped plates of pyrophyllite filling pores between quartz grains; b) the EDAX counts on the cross shown in "a" reveal a ratio between silica and aluminium Si/Al=2 characterising pyrophyllite; c) pseudo-hexagonal clusters of plates of kaolinite covering quartz grains; d) the EDAX counts of aluminium on the kaolinite clusters (cross in "c") are almost the same of silica because of the chemical ratios Si/Al=1.

kaolinite occurs in the form of microscopic pseudo-hexagonal plates and clusters of plates covering quartz grains, often growing on pyrophyllite masses. On kaolinite, the EDAX counts of aluminium are almost the same of silica because of the chemical ratio Si/Al=1. Thus, the formation of the present phyllosilicate minerals can be ascribed to diagenetic mineral transformations in a more or less chemically closed system during the burial stage of the quartz-sandstone, or alternatively to subsequent weathering processes. What is evident at a first glance is that, in general, pyrophillite appears to be more abundant in fresh unweathered samples, while kaolinite is more common in weathered low cohesive ones.

The aluminium phyllosilicate-rich group constitutes the hardest and massive banks, with a glassy appearance and conchoidal fracture in fresh samples, while the almost pure quartz-sandstone represents often the more weathered and low-cohesive strata, showing an earthier fracturing. The pillars mainly develop in this latter lithology.

The picnometer measurements performed on fresh unweathered samples (Table 2) show a primary porosity one order of magnitude higher in almost pure quartz-sandstone respect to the alluminum phyllosilicate-rich ones. The primary porosity is also controlled by anisotropies, like parallel and cross bedding, varying in dependence of their orientation.

Sample	Direction	Por. %	Tepui	Description
R1	perp.	4.64	Roraima	Fresh almost pure quartz-sandstone with cross bedding
	parallel	6.98		
GS7	perp.	3.41	Auyan	Fresh almost pure quartz-sandstone with parallel bedding
	parall.	7.69		
AKT	perp.	6.53	Akopan	Slightly weathered almost pure quartz-sandstone with cross bedding
	parall.	11.11		
IY11	perp.	6.85	Auyan	Slightly weathered almost pure quartz-sandstone with cross bedding
	parall.	10.33		
IY10	perp.	0.58	Auyan	Fresh phyllosilicate-rich quartz-sandstone with parallel bedding
	parall.	0.24		

Table 2. Primary porosity of unweathered samples of quartz-sandstones.

2.4.5.2 Evidences of the arenisation weathering process

SEM imaging was performed on seven quartz-sandstone samples collected in the caves. Samples collected from roofs, floors and from the inner part of funnel-shaped pillars are characterised by different cohesiveness. Despite some authors noticed the absence of evident dissolution morphologies on samples collected from the Roraima Sur and Muchimuk cave systems (the latter in the Chimantha massif; Aubrecht, et al. 2011; 2012; 2013), in our case most of the samples from all the investigated caves showed clear evidences of dissolution, with characteristic features at different degree of development (Fig. 8). These findings are in agreement with the previous studies of Chalchraft and Pye (1984) and Ghosh (1985) on samples collected on the Roraima tepui. The more

cohesive samples show abundant welding between the grains by a pervasive syntaxial quartz overgrowth, on the contrary the weathered, less cohesive samples show a wide network of voids between the grains. In these last samples, the surfaces of the quartz grains are also characterised by pervasive pitting (Fig. 8 a,b,c). In most of these cases dissolution along the quartz grains/overgrowths appears to be "surface controlled" (Burley and Kantorowicz, 1986) producing features typical of slow kinetics, such as well defined v-shaped pits (Fig. 8c2). Dissolution shows to be more active at high energy sites like face edges, corners and triple junctions of the quartz overgrowths (White and Peterson, 1990), gradually releasing the grain contacts (Fig. 8d-e).

Dissolution features are more evident in the almost pure quartz-sandstone than in the aluminium-phyllosilicate rich ones. However they are often present also on quartz grains partially covered by kaolinite masses. Another process that affects the cohesiveness of the rock is the neoformation of kaolinite on the expenses of pyrophyllite masses (Fig. 9). This happens through the dissolution-recrystallization reaction involving the metastable pyrophyllite in presence of water described by Hurst and Könkle (1985). The neoformation is easily recognisable in the phyllosilicate-rich quartz-sandstone samples, suggesting that the majority of the kaolinite is neoforming during the exhumation or directly during the weathering process in subsurface conditions. Therefore there is no need to invoke a diagenetic fluid extremely rich in H_4SiO_4 at low temperatures to explain the co-existence of these minerals as supposed by Aubrecht et al. (2013). Very similar weathering processes (producing also illite) were found to be active in the weathering of the phyllosilicate-rich quartz-sandstone of the Varanger Peninsula in northern Norway (Fjellanger and Nystuen, 2007).

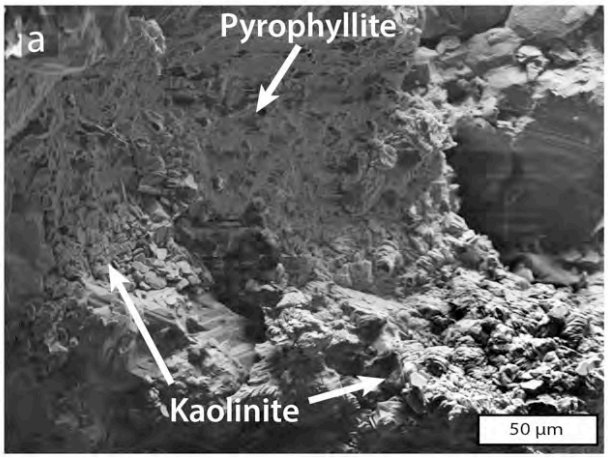

Fig. 9. a) Neo-forming kaolinite at the expenses of pyrophyllite through the dissolution recrystallization reaction described by Hurst and Könkle (1985): this reaction increases the porosity of the rock and favours access of water and dissolution of quartz: note the highly corroded quartz grain surface at the right in b).

These results clearly show that the different degree of cohesiveness of the samples is related to the weathering degree and the consequent arenisation. The gradual release of grains and the increasing porosity of the quartz-sandstone are due mainly to the direct dissolution of the quartz grains, and only marginally to the neoformation of kaolinite at the expenses of pyrophyllite in the phyllosilicate-rich strata.

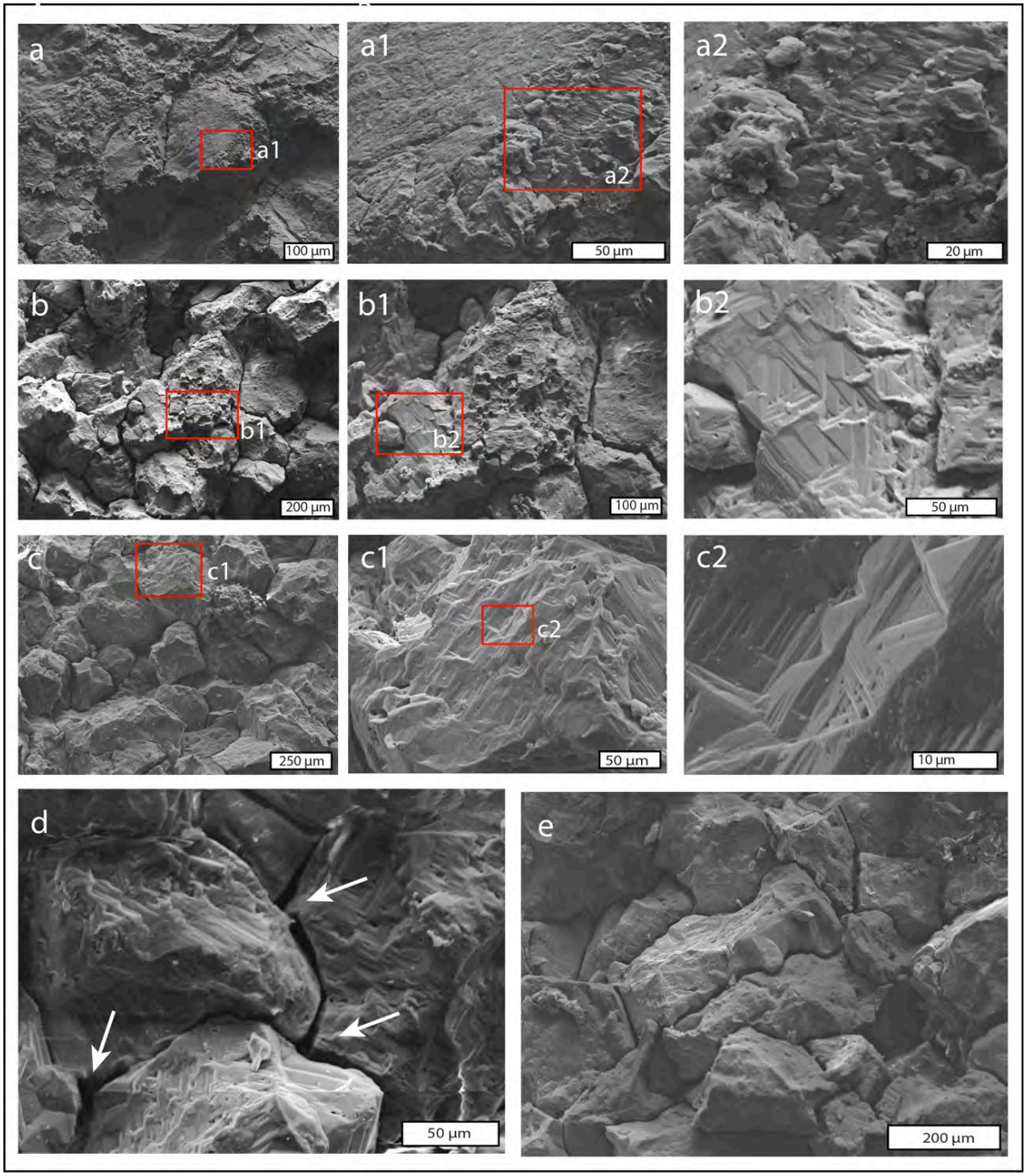

Fig. 8. SEM images of quartz sandstone samples with different degree of cohesiveness: a) cohesive sample with abundant welding between the grains by a pervasive syntaxial quartz overgrowth: at low magnification there are not evident signs of dissolution while at increasing magnification it is possible to observe small dissolution features starting to affect the grain surface (a1, a2); b) low cohesive samples showing a high porosity between the quartz grains that are clearly characterised by dissolution morphologies like pitting (b1) and v-shapes (b2); c) almost non-cohesive sample with high intergranular porosity: all the grain surfaces are characterised by diffused v-shaped dissolution features; d) highly weathered sample showing higher dissolution porosity at the triple junctions between quartz overgrowths: note the diffuse dissolution features on the whole surface of the grains; e) highly weathered sample showing how the quartz grains are gradually released from the interlocked structure.

2.4.5.3 Morphometry of pillar and mammillary features

The morphological measurements of pillars in Imawarì Yeuta cave are report in table 3. The data clearly show that the horizontal cross-section of the narrower central part of these columns is in most of cases an elongated ellipse rather than a circle. The length of the major axes (M) range between 10 and 130 cm, while the mean ellipticity *e* in the whole set of measurements is 1.9. Similar values of *e* are maintained even considering different major axes dimensional classes: 130 cm < *e* = 2.11 > 50 cm, 50 cm < *e* = 2.29 > 30 cm, 30 cm < *e* = 1.56 > 15 cm, 15 cm < *e* = 1.63. Plotting the axes directions (ellipses) for each station of measurements in a rose diagram it is clear that the pillars are characterised by specific orientations, often at angles of 15°, 30° and 60° between them (Fig. 10). In the majority of cases in each station these ellipses are not oriented along the stream flow direction, so they cannot be interpreted as the result of mere directional mechanical erosion. Conversely, with respect to the fracture sets documented at each station (red lines in Fig. 9), the major axes of the ellipses are oriented at 10-15° or approaching the bisector between the major conjugate fractures. Furthermore only 15% of the measured pillars are vertical while the majority of

	M	m	D	i	id	M	m	D	i	id
Galeria Mil Columnas at point 53	25	15	273	-63	357	55	19	247	-61	159
	35	21	172	-74	91	70	38	244	-55	146
	22	18	187	-65	6	14	10	269	-75	14
	14	14	/	-79	104	20	10	173	-15	138
	70	47	100	-57	4	23	14	270	-90	/
	35	24	95	-65	3	29	24	256	-90	/
	21	13	90	-65	13	28	20	250	-90	/
	8	8	/	-67	7	58	40	260	-64	166
	15	8	29	-66	18	35	23	270	-71	172
	13	8	256	-81	20	42	15	200	-80	216
	30	13	76	-59	102	31	18	290	-62	218
Rio de los venezuelanos at points S2-S4	27	80	261	-69	169	26	20	250	-79	314
	10	20	252	-70	183	70	30	226	-71	155
	37	15	240	-76	210	33	12	266	-84	332
	13	8	260	-75	199	35	24	250	-80	145
	7	5	232	-72	185	40	21	245	-80	210
	35	18	244	-72	183	25	29	262	-73	223
	37	20	261	-73	146	52	36	243	-75	185
	22	14	251	-82	202	25	20	234	-72	222
	23	20	295	-74	238	14	9	246	-76	185
	16	7	246	-77	339	22	10	221	-81	218
	34	16	259	-90	/	20	30	256	-82	190
	19	7	218	-77	277	40	25	217	-72	286
	15	8	195	-78	259	44	24	253	-77	221
	12	5	253	-75	317					
Rio de los italianos at point 33	75	30	228	90	/	35	6	280	-67	191
	60	25	237	90	/	37	12	290	-57	204
	30	22	260	90	/	21	17	315	-58	225
	32	15	224	90	/	25	22	280	-73	171
	20	13	266	90	/	7	6	280	-60	159
	33	17	275	-70	7	43	20	263	-69	175
	38	25	258	-75	350	35	20	220	-72	114
	130	40	280	90	/	37	21	267	-80	149
	130	60	290	90	/	54	26	270	-83	277
Galeria Mil Columnas at point 65-71	54	26	358	-83	91	30	16	292	-73	168
	22	11	357	-83	334	38	25	165	-83	352
	24	11	0	-70	266	18	14	319	-76	46
	31	5	1	-79	263	28	18	244	-74	173
	50	26	350	-74	344	30	28	252	-90	/
	32	5	357	-73	215	19	18	252	-90	/
	24	12	320	-67	298	70	26	279	-90	/
	20	15	67	-64	318	15	8	316	-90	/
	16	9	11	-77	81	10	9	280	-77	198
	39	20	19	-68	119	25	17	36	-73	321
	25	11	49	-90	/	22	12	44	-59	320
	19	10	93	-90	/	28	15	193	-71	225
	11	6	21	-82	240	20	17	97	-78	235
	21	9	12	-90	/	15	10	199	-48	24
	70	42	196	-90	/	27	16	123	-67	221
	36	15	10	-90	/	20	16	111	-79	205
	10	4	14	-90	/	30	17	120	-72	210
	30	26	280	-61	180	16	13	89	-72	303
	62	38	280	-90	/	10	13	329	-79	303

Table 3. Morphological measurements of funnel-shape pillars in Imawarì Yeuta divided in measurements station.

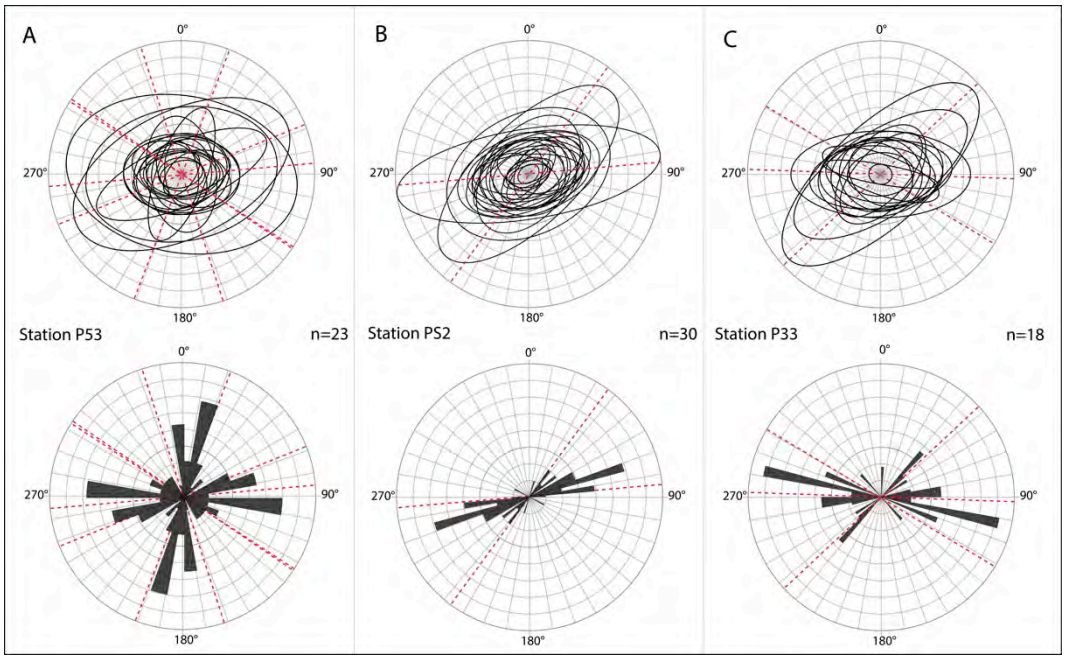

Fig. 10. Major and minor axes of the central pillar cross-section from three stations of measurements in Imawarì Yeuta cave: the major and minor axes are simplified as ellipses in the upper rose diagram, while the lower rose diagrams represents only the frequency directions of the major axes and the relationship with the fracture sets directions measured in the surroundings (red dotted lines).

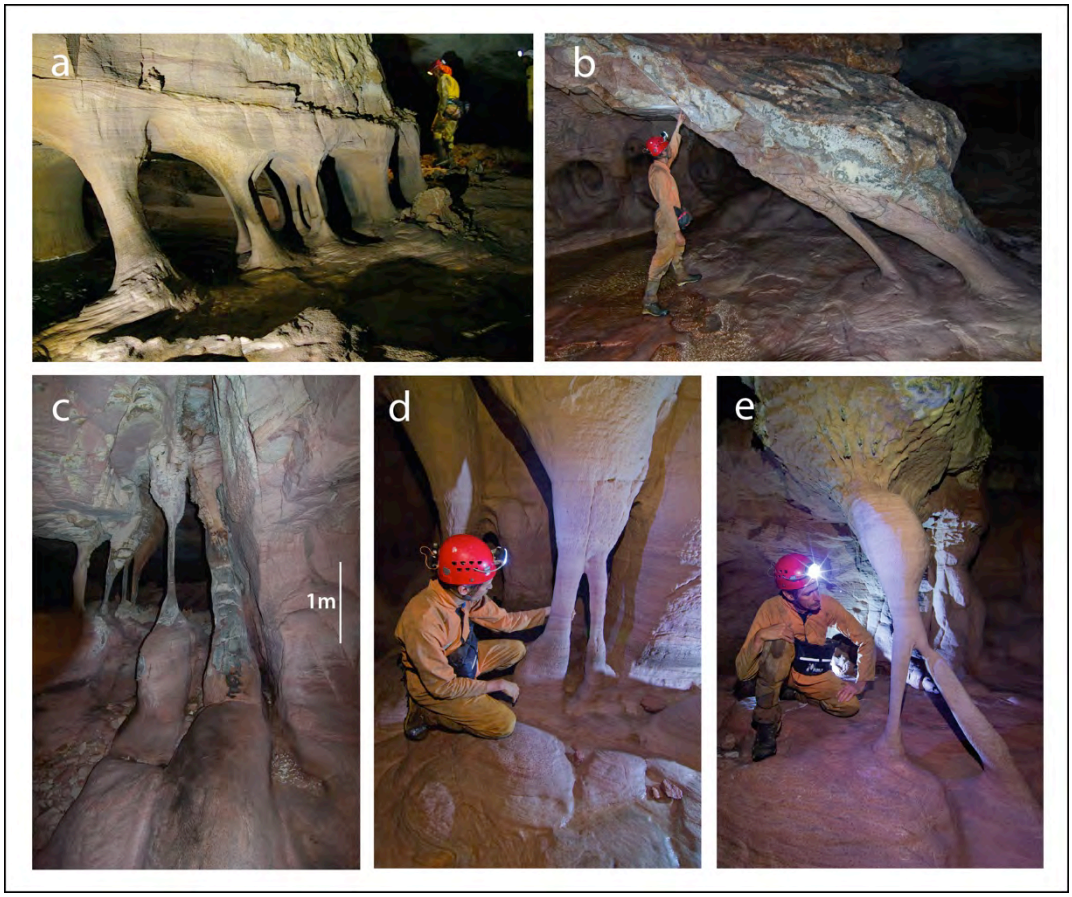

Fig. 11. Pillar morphologies related to local fracturing: a) set of aligned pillars inclined along local fractures; b) two highly inclined pillars evolved parallel to evident low angle fractures on the ceiling (above the speleologist); c) pillars formed along parallel fracture septums. d) pillar splitting controlled by the enlargement of an evident vertical fracture; e) pillar splitting in two differently inclined branches. Photos Francesco Sauro, La Venta Geographic Explorations Team.

them are inclined, from only a few degrees up to 50°. In many cases specific inclinations are clearly related to fracture sets with the same dipping (Fig. 11 a-b) and characterise big groups of pillars in the same area. In addition, pillars are often in line with septums oriented parallel to evident major fractures (Fig. 11 c).

Another documented morphology is the splitting of pillars in two or even more branches often with different inclinations (Fig. 11 d-e). In most of the cases these splittings are related to secondary fractures observable at the junction (Fig. 11 d).

The morphometric analysis of the mammillary morphologies (or pendants) on the ceilings and floor

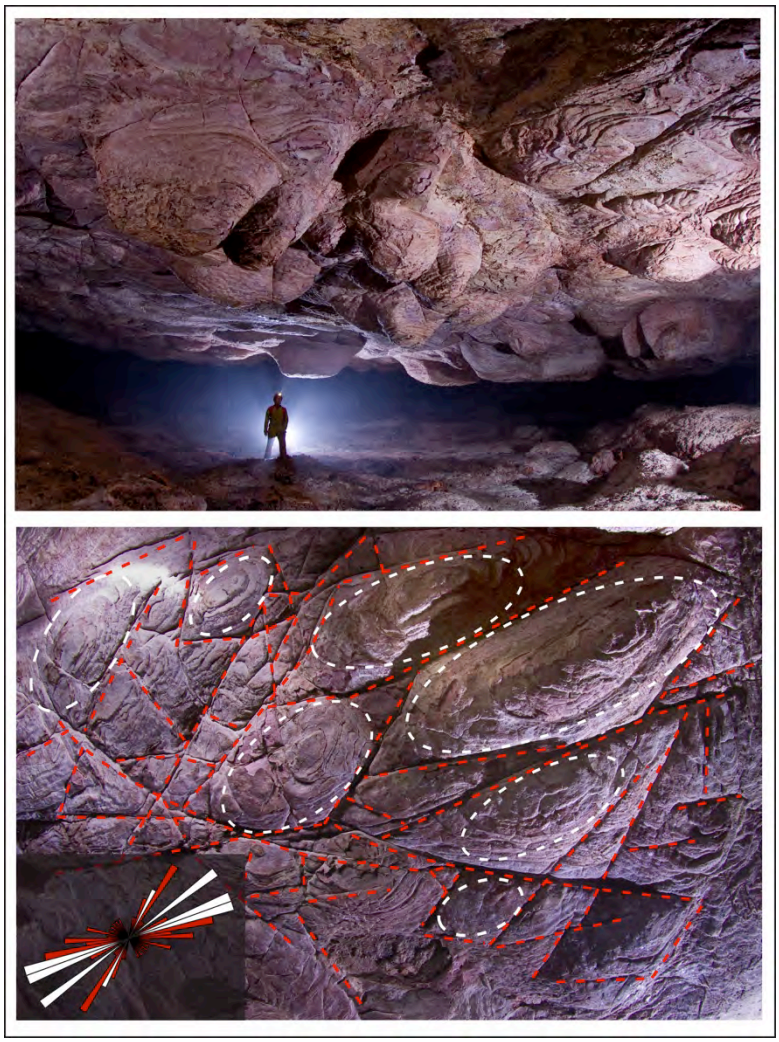

Fig. 12. Pendant morphologies protruding from the ceiling of Imawarì Yeuta cave: a) Pendants are elongated presenting an elliptic section like the majority of the pillars ; b) the relationship between pendants and the fracture network is evidenced in a zenital photo of the ceiling: the ellipses of the pendants develop mainly along the bisector of the conjugated fractures or along the secondary joint sets (see the rose diagram on the left).

of the cave passages shows almost the same relationship with the fracture sets (Fig. 12). Each pendant is delimited by a complex network of conjugate fractures and the associated ellipse's major axes result at 10-15° or approach the bisector between the conjugate sets.

All these geometries suggest a strict relationship between fractures and pillar/mammillary formation.

2.4.6 Discussion

2.4.6.1 Strata-bounded fractures: the origin of pillars and maze network caves

Along the cliffs delimiting the upper platforms from the lower ones, both in Roraima, Auyan and Chimantha Tepui, a repetition of massive banks forming overhanging and protruding strata and more fractured carved ones often characterized by half-pillar morphologies is evident (Fig. 13 but see also Fig. 47-48 in Aubrecht et al., 2012). These latter strata are frequently characterised by honeycomb features showing to be more prone to weathering than the overlying and underlying massive beds (Fig. 13 A-A1). The same situation is present also inside the caves, where the passages are often developed along specific strata where pillars are often formed, while roofs and floors are constituted by massive and less fractured strata.

Previous authors (Aubrecht et al., 2008, 2011, 2013) interpreted this alternation of soft and harder beds as "purely diagenetic", i.e. due to an inhomogeneous diffusion of late diagenetic fluids through intergranular voids, related to the different hydraulic conductivity between coarse- and fine-grained sands. The funnel pillar morphologies would be related to the migration of these diagenetic fluids through delimited channels in the form of "finger flows". Therefore half-pillars would represent the harder lithified parts while the surrounding softer rock would have remained unlithified, and would have thus been readily removed by erosion because of its softness.

Conversely, the results presented in this paper points to a different interpretation where the fracturing density-spacing and the primary porosity of the different strata are the main factors controlling the intensity and distribution of the arenisation process driving the formation of pillar morphologies and caves in specific stratigraphic positions. Strata-bound intense fracturing is typical of alternating strata with different petrographic and rheologic characteristics. These fractures can be related to regional stresses distributed along strata with different thickness (Pollard and Segall, 1987), or to local fluid overpressure during the diagenesi (hydro-fracturation; Gudmundsson and Brenner, 2001; Brenner and Gudmundsson, 2004; Philipp et al., 2006). Joints spacing, aperture variations and arrest depend primarily on the mechanical properties of the host rock and on the strata thickness (Shackleton et al. 2005). If the stratigraphic sequence is composed of an alternation of anisotropic banks with different composition, and therefore different Young's modulus, fractures can develop only along specific strata while

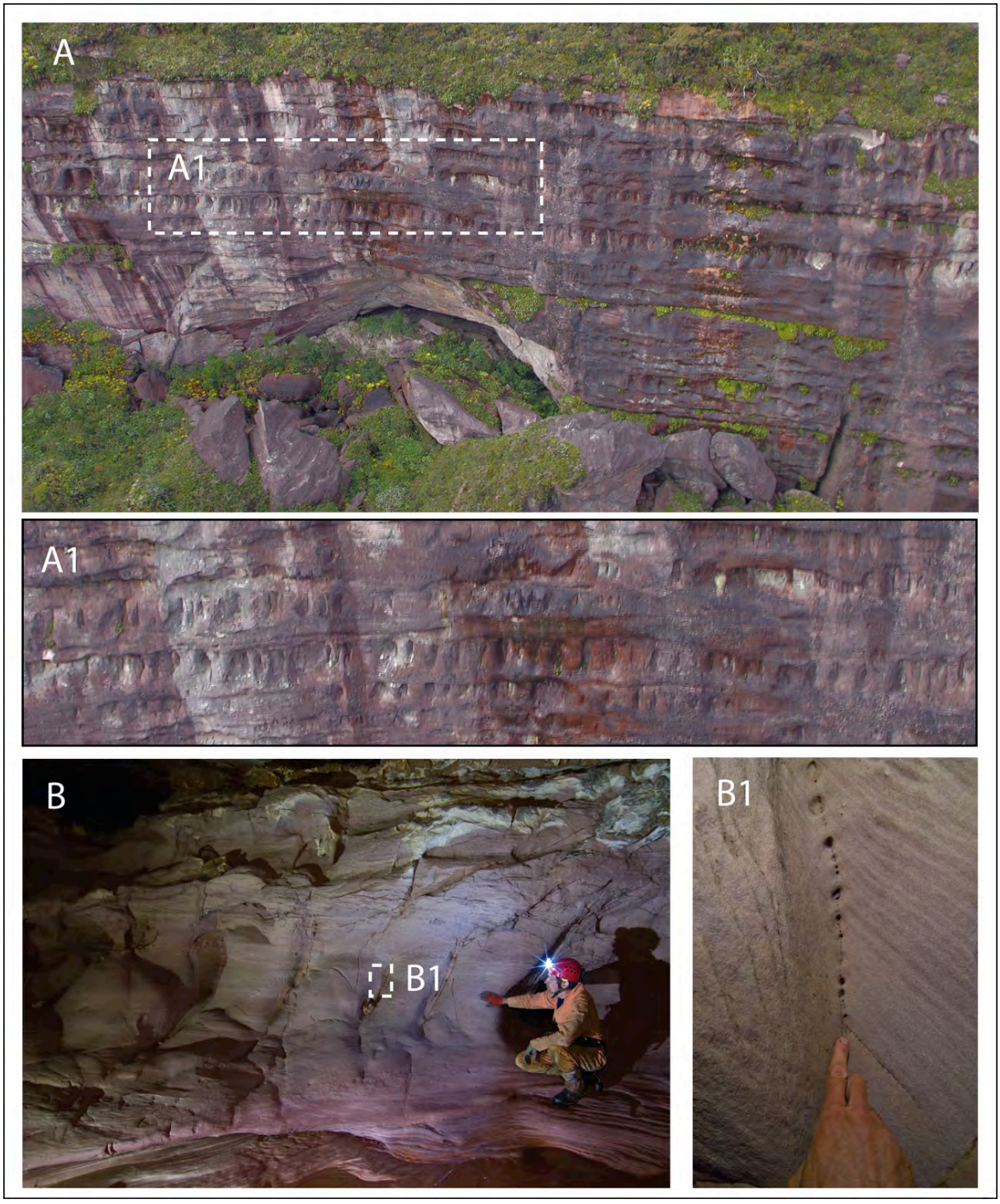

Fig. 13. Strata-bounded fractures: A) alternation of massive banks forming overhangings and fractured strata with half pillar morphologies on the cliff above the entrance "Sima del Viento" in Imawarì Yeuta cave: this regular alternation is clearly shown in A1; B) strata-bounded fractures along the cave walls: each fracture is wider in the central part and tapers away toward the overlying bed; B1) every fracture is clearly arenised and show centimetric dissolution and piping tubes. Photos Francesco Sauro, La Venta.

others arrest or limit their propagation (Brenner and Gudmundsson, 2004). These vertically confined fractures form networks that are interconnected mainly horizontally.

The chemical and petrographical analyses showed that in the tepui massifs the protruding homogeneous banks are composed mainly of phyllosilicate-rich quartz-sandstones, while the weathered highly fractured strata are almost pure quartz-sandstones. This difference in composition, and therefore in mechanical properties, resulted in the propagation of the fractures only in the latter, pure quartz-sandstone strata, with a dense spacing. The evidence of this typical layer-bounded fractures is clearly found also in the cave walls (Fig. 13 B), where joints become more inclined and thinner and finally taper away and come to arrest toward the overlying banks.

Such strata-bounded fracturing increases the surface area available for arenisation in these pure quartz-sandstone strata. When the undersaturated meteoric waters from the surface (Piccini and Mecchia, 2009; Mecchia et al., 2014) enter in this dense network of layer-bounded joints, dissolution initiates and propagates. This process is effective even after hundreds of metres long fracture pathways because of the extremely slow reaction kinetics of quartz dissolution allowing the water to remain undersaturated over long times and distances causing arenisation of great volumes of rocks (Mecchia et al., 2014). Thus, arenisation works mainly underground along the more fractured layers, without necessary involving surface lowering. Some authors called this process in general "phantomisation" (Quinif, 1999; Häuselmann and Tognini, 2005), because weathering predisposes the rock mass for the formation of caves that are afterward opened through piping and mechanical erosion.

The effectiveness of the arenisation process in these strata is clearly demonstrated by our SEM observations, with diffused pitting and V-shaped features on the quartz grains, typical of slow dissolution kinetics, and increasing porosities at the grain contacts.

The arenisation process is more effective in the almost pure quartz-sandstone mainly because of the following reasons:

- A higher primary porosity than the phyllosilicate-rich strata. A more porous sandstone displays a higher potential for the penetration of undersatured water and for diffusion/dissolution transport between the quartz grains with subsequent deep weathering (Young, 1988; Wray, 1997b; Mecchia et al., 2014).
- The presence of a wide network of strata-bounded fractures that do not propagate into the phyllosilicate-rich strata. This complex macro- and microfracture system allows the penetration of undersatured water in these strata with consequent arenisation.

- Absence of residual clay minerals. In these strata the arenisation can work without producing residual clays that would clog the fractures and inhibit the process (Mecchia et al., 2014).

Definitely the almost pure quartz-sandstones in general are more prone to the arenisation process than the surrounding strata, but the degree of fracturing controls the distribution of the process in the rock mass, and therefore the presence or absence of pillar morphologies. However, also the aluminium phyllosilicate-rich strata can be weathered by means of quartz-dissolution and pyrophyllite-kaolinite or kaolinite dissolution reactions but the effectiveness of these processes is limited because of the low primary porosity. In addition, arenisation does not develop deep into these strata because they are not fractured.

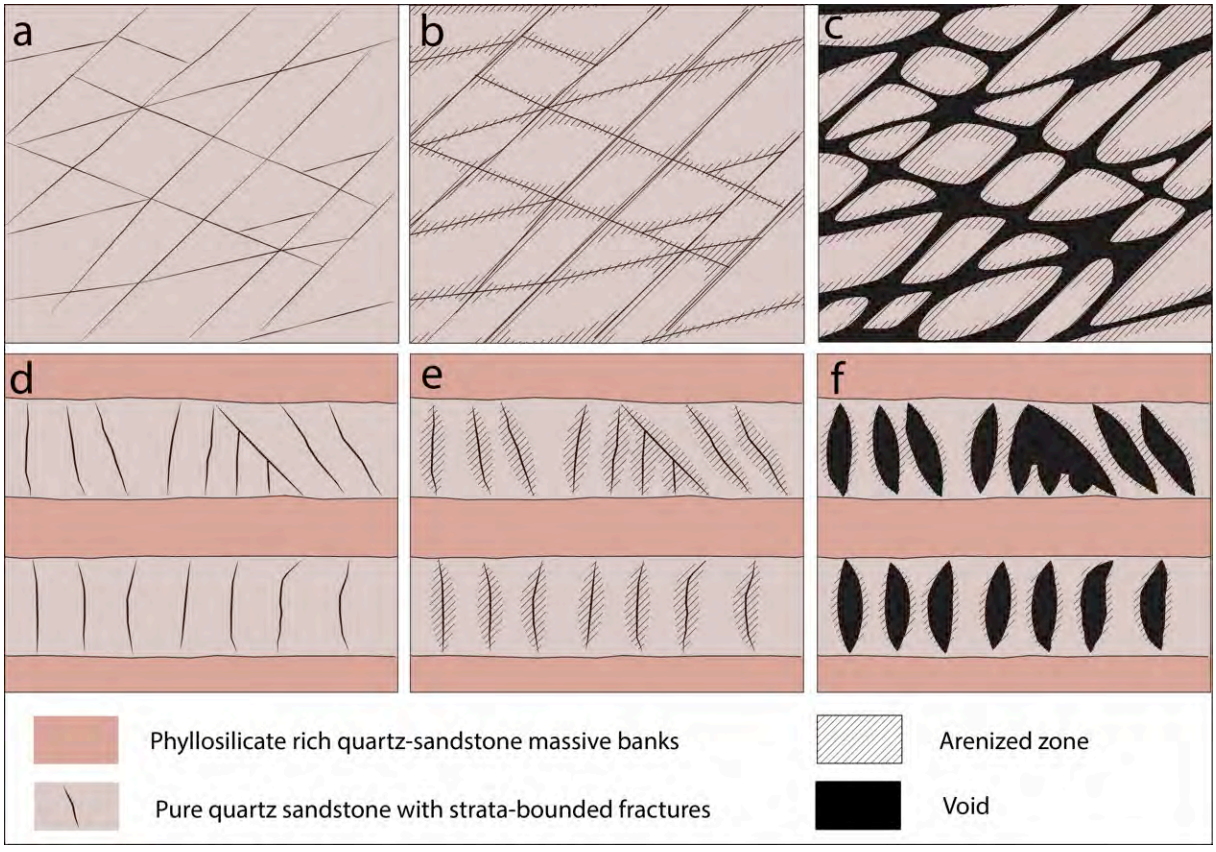

Fig. 14. Schematic model of the anastomosis of strata-bounded fractures through the arenisation process. In plan view: a) the fractured stratum is represented by a set of major and minor conjugate joints; b) arenisation propagates into the fractures being more intense at fracture intersections; c) piping removes the loose sand produced by the arenisation process and frees the pillar morphologies that show a rhombohedral elliptic cross-section because of the strata-bounded fracture network geometry and of the enhanced arenisation at the fracture intersections. In vertical view: d) The fracture network is bounded in the almost pure quartz sandstone layers, with the fracture aperture more prominent in the middle of the bed tapering away approaching the surrounding phyllosilicate-rich beds; e) arenisation propagates starting and being more effective where the fracture aperture is wider in the middle of the bed; f) piping removes the loose sand produced by the arenisation process and frees the funnel-shaped pillars that continue to be arenised during seasonal floods and by surface films of water due to condensation processes.

In the almost pure quartz-sandstone strata, the arenisation gradually decomposes the rock in between the existing fractures starting from the larger ones, or in the site where the initial aperture of these joints is wider, normally in the middle part of the bed (Fig. 14). In a more advanced stage, the loose sand produced by weathering is removed by piping and the open fractures are gradually anastomised developing empty spaces between relict septa and pillars (Fig. 14c). The dimensions of this network and the presence of funnel-shaped pillars or wider massive remnants depend on the spacing between the initial fractures. The geometry of the weathering relics is easily predictable because these remnants will be aligned roughly along the major fracture sets or along rhombohedrical conjugate joints (Fig. 14c). These relationships between joint families and pillars or pendants are clearly recognisable in the morphometric measurements reported from Imawarì Yeuta cave (Fig. 10-12).

2.4.6.2 The inception hypothesis and the cave pattern guidance in quartz-sandstones

As proposed by Martini (1985), arenisation is promoted mainly by undersaturated water seepage along the fracture network. However, if the fracture network is layer-bounded, like in the case described for Imawarì Yeuta, water can penetrate from the surface only when the stratum will be open to the outside by surface lowering, tectonic continuous fractures or scarp retreat. If one of these strata is unroofed on the plateau surface, fields of towers develop on the tepui platforms (Fig. 15). When the strata is dissected laterally by secondary continuous fractures due to gravitational release or collapses along the cliffs, half pillars and honeycomb features alternated with overhanging massive banks develop on these vertical walls (Fig. 12 A, B). Conversely, only in presence of some specific pathways conveying the water flow into the subsurface, arenisation is able to work along the whole strata predisposing the development of extensive horizontal strata-bounded cave systems.

Therefore the main question in the formation of the widest maze network systems on the tepuis, such as Imawarì Yeuta and Roraima Sur caves, remains the following: along which pathways the water penetrated inside a continuous fractured strata? In carbonate environment these layers particularly favourable for the development of the primary cave conduits were debated in the Inception Horizon Hypothesis (IHH) proposed by Lowe (1992) and then investigated in detail by Filipponi et al. (2009). Applying their definition to the quartz-sandstone environment we can assert that here the inception horizons could be “layers especially favourable to the opening of proto-conduits through karstic or pseudo-karstic processes by virtue of physical, lithological or chemical deviation from the predominant quartz-sandstone facies” (Sauro et al., 2013a). Therefore the answer to the question above has to be investigated verifying the presence of some specific layers

characterising the cave system development, other than solely fractured beds that are common in the stratigraphic sequence.

In the majority of the investigated caves speleologists noticed the presence of residual iron hydroxide deposits (mainly goethite; Sauro et al., 2014) or even continuous layers of iron hydroxides guiding the gallery development like those described in the Guacamaya cave and in the Akopan-Dal Cin cave system. These layers are difficult to identify being often absent because more prone to erosion and dissolution than the surrounding quartz-sandstones. In the Guacamaya cave the iron hydroxide beds have all the characteristics of a Banded Iron Formation, locally folded and stretched because of shear related to the lithostatic load and the stronger rigidity of the overlying beds of quartz-sandstones (Sauro et al., 2013b). In addition, in all the caves it is possible to observe iron hydroxides flowing out from interstrata forming massive brownish flowstone, similar to other goethite speleothems described in other quartzite caves of the Sarisariñama and Chimantha tepuis (Zawidzki et al., 1976; Aubrecht et al., 2011).

Reardon (1979) suggested that iron-silicate complexes (like Fe-H_2SiO_4) might increase the silicic acid solubility. This supposition was lately confirmed by the studies of Morris and Fletcher (1987) and Serezhnikov (1989) showing that in ferrous iron solutions under oxidising conditions the potential solubility of quartz increases by a factor 10 over that of amorphous silica. Therefore, iron hydroxide layers located in only a few stratigraphic positions could have been a favourable stratigraphic pathway for the formation of proto-conduits in local phreatic settings, promoting the infiltration of meteoric water in the surrounding fractured strata.

Fig. 15. When strata bounded fractures open to the surface a wide field of towers and pseudo-rhombic or elliptic bumps develops on the platform surface (Roraima). Photo Vittorio Crobu, La Venta Geographical Explorations Team.

Moreover, also local layers of shales and silt could have been preferential pathways working either as acquiclude or acquitard allowing water to infiltrate along specific stratigraphic surfaces. Galán et al. (2004) noticed the presence of centimetric layers of shale and siltstone guiding the development of the conduits in the Roraima Sur Cave System. Szczerban et al. (1977) described a horizontal cave system in the Guaiquinima Tepui whose development is clearly guided by siltstone layers.

Fig. 16. The effect of floodwater injection along strata-bounded fractures is evident in the sink of El Foso in the Roraima Tepui: the sidewalls of the cavity remain flooded for most of the year showing well developed pillar morphologies. Photo Vittorio Crobu, La Venta Geographical Explorations Team.

Similar lithological controls were described also by Piccini (1995) and Piccini and Mecchia (2009) in the Aonda and Auyan Tepui Noroeste fissure systems with thin layers of silts guiding the formation of major ledges along deep *simas* and controlling the horizontal collectors at the bottom of the shafts. In fact, gravitational release fractures along the peripheral rims could have also focused the water flow deep into the rock mass, concentrating at certain stratigraphic horizons that can work also as sliding surfaces during the dilation movements. These fractures represent true "tectonic inceptions" from which the development of a crevice-like cave system can start (Sauro et al., 2012).

Until now only few authors have debated the initial speleogenetic phases and the formation of proto-conduits in quartz-sandstones (Wray, 2009). The presence of rounded tubes in the upper dry level of Imawarì Yeuta cave suggests that in the first phases the cave network developed under local shallow phreatic conditions, evolving to vadose conditions only when the proto-conduit network became able to evacuate great amounts of loose sand. These local epiphreatic/temporary-flooded conditions are still maintained during flood events and probably persist for long times during the rain season. In these zones of the cave the floodwater injection (Palmer, 2007) into the fractured strata on the side cave walls further propagates the arenisation process. Once arenised, the whole strata is gradually excavated by mechanical erosion creating huge strata-bounded cave environments and ceiling collapses.

The floodwater injection process is particularly effective in zones of concentrated water flow like bends in the main underground streams, that often evolve into extremely wide meanders whose convex side is characterised by the most spectacular pillar morphologies (Sauro et al., 2013c). Because of this, the majority of the weathering areas evolving in pillar fields are situated in the low, frequently flooded, areas of the cave. Clear examples of these settings in surface conditions are the sinkhole of El Foso (Fig. 16) and the closed depression of Lake Gladis in Roraima tepui, whose flooded sidewalls are also characterised by well developed pillar morphologies as observed also by Aubrecht et al. (2012; Fig. 54).

Cave System	Sratigraphic guid.	Tectonic guid.	Recharge type	General Morphologies	General Pattern
Imawarì Yeuta, (Muchimuk?, Arana?)	Iron hydroxide layer (inception horizon)	Closely spaced strata-bounded fractures	Sinking streams, great fluctuation discharge, floodwater injection	Strata bounded environments, funnel-shaped pillars, wide columnar relicts, septums, pendants and bumps, vast collapse zones	**ANASTOMOTIC STRATA-BOUNDED**
Roraima Sur (Guayquinima?)	Shale-Silt layer (inception horizon)	Widely spaced strata-bounded fractures	Sinking streams, great fluctuation discharge, floodwater injection	Strata bounded, massive metres wide columns, locally funnel-shaped pillars	**ANASTOMOTIC STRATA-BOUNDED**
Guacamaya, Akopan-Dal Cin	Iron hydroxide/ BIF layer (inception horizon)	Major tectonic and gravitational release continuous fractures	Sinking streams, great fluctuation discharge, floodwater injection	Strata entrenched, conduit rectangular or keyhole section, rare septums	**MAIN CONDUIT/ BRANCHWORK**
Aonda System, Auyan Tepui Noroeste	Few Silt layers	Major gravitational release continuous fractures	Diffused along vertical fractures, point sinking streams	Hundred metres deep "grietas", high and narrow canyons, fracture-controlled fissures, long septums between parallel fractures	**GEOMETRIC ANGULAR NETWORK**

Table 4. Summary of cave patterns and general morphologies in relation to the tectonic and stratigraphic guidance.

Therefore, also the type of recharge has a great influence on the evolution of the systems, where a concentrated inflow with frequent flood events favors the formation of maze caves, while the diffuse infiltration along networks of mainly tectonic fissures open to the surface promote a diffuse arenisation only along vertical fractures evolving in deep and long "*grietas*" like the spectacular ones of the Aonda area.

The interaction between inception features (either stratigraphic and tectonic), the presence of fractures, their continuity and spacing, together with the hydrologic and recharge conditions, guide the general shape of the different cave systems, as resumed in Table 4. It is evident that the formation of the giant anastomotic cave systems like Imawarì Yeuta, Roraima Sur, and probably also Muchimuk (Aubrecht et al., 2012), is related to a combination of favourable

conditions like the presence of prominent inception horizons and dense strata-bonded fracturation. Smaller caves like Guacamaya and Akopan-Dal Cin have a main conduit pattern because of a less prominent influence of the strata-bounded fractures but still following stratigraphical inception horizons. On the other hand, if only continuous dilation fractures without major stratigraphical control guide the infiltration, deep "*grietas*" and fracture-controlled high and narrow canyon collectors as those described for the Aonda and Auyan Tepui Noroeste Systems develop (Piccini and Mecchia, 2009).

2.4.7 Conclusions

This study demonstrates that the arenisation process proposed by Martini (1979) and Jennings (1983) works with different intensities depending on the petrographical characteristics of the quartz-sandstone, being effective only where meteoric water can access the rock through specific stratigraphic or tectonic pathways. Arenisation well explains all the morphologies found in the caves of the tepui massif. Pillars and pendants clearly are the relics of weathering anastomosis between strata-bounded fractures and there is no need to invoke peculiar diagenetic conditions that do not seem to fit into the geologic history of the area as proposed by Aubrecht et al. (2011, 2012).

The primary porosity and the degree of fracturing of the quartz-sandstone beds result as the main factors controlling the intensity and the distribution of the arenisation process, together with peculiar inception horizons and the recharge conditions of the systems.

While mechanisms other than true dissolution, like piping and mechanical erosion, largely modelled the landscape and finally carved the caves of the tepui into the weathered rock, quartz dissolution evidently plays an essential and triggering role. Thus, these processes could be effectively considered as “true karst” as proposed by many authors (Wray, 2000; Young et al., 2009).

However, because of the complexity and specificity of caves and surface morphologies found in the tepui mountains and in other similar quartz-sandstone landscapes of the world, we suggest to use solely the specific term “arenisation” that much better focalises the whole weathering process and its consequences on the speleogenesis and morphogenesis (Eberhard and Sharples, 2013).

References

AA.VV, 1994. Tepui 1993. Progressione 30, 1-120.

Aubrecht, R., Lánczos, T., Smída, B., Brewer-Carías, Ch., Mayoral, F., Schlögl, J., Audy, M., Vlcek, L., Kovácik, L., Gregor, M., 2008. Venezuelan sandstone caves: a new view on their genesis, hydrogeology and speleothems. Geologica Croatica 61, 345-362.

Aubrecht, R., Lánczos, T., Gregor, M., Schlögl, J., Smída, B., Brewer-Carías, Ch., Vlcek, L., 2011. Sandstone caves on Venezuelan tepuis: Return to pseudokarst? Geomorphology 132, 351-365.

Aubrecht, R., Barrio-Amorós, C.L., Breure, A.S.H., Brewer-Carías, C., Derka, T., Fuentes-Ramos, O.A., Gregor, M., Kodada, J., Kováčik, Ľ., Lánczos, T., Lee, N.M., Liščák, P., Schlögl, J., Šmída, B., Vlček L., 2012. Venezuelan tepuis: their caves and biota. Acta Geologica Slovaca Monograph, Comenius University, Bratislava, 168 p.

Aubrecht, R., Lánczos, T., Gregor, M., Schlögl, J., Šmída, B., Liščák, P., Brewer-Carías, Ch., Vlček, L., 2013. Reply to the Comment on "Sandstone caves on Venezuelan tepuis: Return to pseudokarst?". Geomorphology 197, 197-202.

Audy, M., Bouda, R., 2013. Quartz-sandstone caves on table mountains of Venezuela. In: Filippi, M., Bosak, P. (Eds.), Proceedings of the 16th International Congress of Speleology, Brno 19-27 July 2013, Volume 2, 20-23 .

Barton, H., Suarez, P., Muench, B., Giarrizzo, J., Broering, M., Banks, E., Venkateswaran, K., 2009. The alkali speleogenesis of Roraima Sur Cave, Venezuela. In: White, W.B. (Ed.), Proceedings of the 15th International Congress of Speleology, Kerrville, Texas, 19-26 July 2009, 802-807.

Bernabei, T., Mecchia, M., Pezzolato, P., Piccini, L, Preziosi, E., 1993. Tepuy '93: ancora Venezuela!. Speleologia, Rivista della Società Speleologica Italiana 29, 8-23.

Brenner, S. L., Gudmundsson, A., 2004. Arrest and aperture variation of hydrofractures in layered reservoirs. Geological Society, London, Special Publications 231(1), 117-128.

Brewer-Carías, C., Audy, M., 2011. Entrañas del mundo perdido. Charles Brewer-Carías (Ed.), Caracas, 290 p.

Briceño, H.O., Schubert, C., 1990. Geomorphology of the Gran Sabana, Guyana Shield, Southeastern Venezuela. Geomorphology 3, 125-141.

Burley, S.D., Kantorowicz, J.D., 1986. Thin section and S.E.M. textural criteria for the recognition of cement-dissolution porosity in sandstones. Sedimentology 33, 587-604.

Carreño, R., Nolla, J., Astort, J., 2002. Cavidades del Wei-Assipu Tepui, Macizo del Roraima, Brasil. Boletin Sociedad Venezolana de Espeleologia 36, 36-45.

Chalcraft, D., Pye, K., 1984. Humid tropical weathering of quartzite in southeastern Venezuela. Zeitschrift fur Geomorphologie 28, 321-332.

Doerr, S. H. 1999. Karst-like landforms and hydrology in quartzites of the Venezuelan Guyana shield: pseudokarst or "real" karst? Zeitschrift fur Geomorphologie 43, 1-17.

Eberhard, R.S., Sharples, C., 2013. Appropriate terminology for karst-like phenomena: The problem with 'pseudokarst'. International Journal of Speleology 42(2), 109-113.

Filipponi, M., Jeannin, P., Tacher, L., 2009. Evidence of inception horizons in karst conduit networks. Geomorphology 106, 86-99.

Fjellanger, J., Nystuen, J. P., 2007. Diagenesis and weathering of quartzite at the palaeic surface on the Varanger Peninsula, northern Norway. Norwegian Journal of Geology 87(1/2), 239-251.

Franzini, M., Leoni, L., Saitta, M., 1972. A simple method to evaluate the matrix effects in X-Ray fluorescence analysis. X-Ray Spectrometry 1, 151-154.

Galán, C., 1991. Expedición SVE a los tepuys Ilù, Tramen y Iuruaní. Boletin Sociedad Venezolana de Espeleologia 25, 47.

Galán, C., 1992. El clima del macizo del Chimantá. In: Huber, O. (Ed.), El Macizo del Chimantá – Escudo della Guayana, Venezuela – Un ensayo ecologico tepuyano. O. Todtman Editors, Caracas, 37-52.

Galán, C., Lagarde, J., 1988. Morphologie et evolution des cavernes et formes superficielles dans les quartzites du Roraima. Karstologia 11-12, 49-60.

Galán, C., Herrera, F.F., Carreño, 2004. Geomorfología e hidrología del Sistema Roraima Sur, Venezuela, la mayor cavidad del mundo en cuarcitas: 10,8 km. Boletin Sociedad Venezolana de Espeleologia 38, 2-16.

Ghosh, S.K., 1985. Geology of the Roraima Group and its implication. Boletin de Geologia, Venezuela, Pub. Especial 10, 33-50.

Gibbs, A.K., Barron, C.N., 1993. The Geology of the Guyana Shield. Clarendon Press, Oxford, 246 p.

González de Juana, C., Picard, X., Iturralde, J. M., 1980. Geologia de Venezuela y de sus cuencas petrolifera. Edic. Foninves, Caracas, 1031 p.

Gori, S., Inglese, M., Tognini, P., Trezzi, G., Rigamonti, I., 1993. Auyan-tepui, speleologia tropicale nelle quarziti. Speleologia, Rivista della Società Speleologica Italiana 28, 23-33.

Gratier, J., Muquet, L., Hassani, R., Renard, F., 2005. Experimental microsylolites in quartz and modeled application to natural stylolitic structures. Journal of Structural Geology 27, 89-100.

Gudmundsson, A., Brenner, S. L., 2001. How hydrofractures become arrested. Terra Nova 13(6), 456-462.

Hartikainen, K., Hautojärvi, A., Kuoppamäki, K., Timonen, J., 1996. Helium gas methods for rock characteristics and matrix diffusion. Posiva Ed., Helsinki, Report number 96-22, 58 p.

Häuselmann, P., Tognini, P., 2005. Kaltbach Cave (Siebenhengste, Switzerland): phantom of the sandstone? Acta Carsologica 34(2), 383-396.

Hawkes, D.D., 1966. Differentiation of the Tumatumari-Kopinang Dolerite Intrusion, British Guiana. Geological Society of America Bulletin 77(10), 1131-1158.

Hurst, V.J., Könkle, A.C., 1985. Dehydroxylation, rehydroxylation, and stability of kaolinite. Clays & Clay Minerals 33, 1-14.

Ipiña, J.M., 1994. Aspectos físico-químicos de los tepuyes Acopan y Amuri. Macizo de Chimanta, Gran Sabana, Venezuela. Boletin Sociedad Venezolana de Espeleologia 28, 5-9.

Jennings, J.N., 1983. Sandstone pseudokarst or karst? In: Young, R.W., Nanson, G.C. (Eds.), Aspects of Australian Sandstone Landscape. Australia and New Zealand Geomorphology Group Special Publication, Wollongong, pp. 21-30.

Leoni, L., Saitta, M., 1976. X-ray fluorescence analysis of 29 trace elements in rock and mineral standards. Rendiconti Società Italiana di Mineralogia e Petrologia 32, 497-510.

Leoni, L., Menichini, M., Saitta, M., 1982. Determination of S, Cl, and F in silicate rocks by X-Ray fluorescence analyses. X-Ray Spectrometry 11, 156-158.

Lowe, D.J., 1992. The origin of limestone caverns: an inception horizon hypothesis. Manchester Metropolitan University, Ph.D. thesis, 512 pp.

Marker, M.E., 1976. Note on some South African pseudokarst. Boletin Sociedad Venezolana Espeleologia 7(13), 5-12.

Martini, J.E.J., 1979. Karst in Black Reef quartzite near Kaapsehoop, Eastern transval. Annals of South African Geological Survey 13, 115-128.

Martini, J.E.J., 1985. Les phénomènes karstiques de quartzites d'Afrique du Sud. Karstologia 9, 45-52.

Martini, J.E.J., 2000. Dissolution of quartz and silicate minerals. In: Klimchouk, A.B., Ford, D.C., Palmer, A.N., Dreybrodt, W. (Eds.), Speleogenesis: Evolution of karst aquifers. National Speleological Society, Huntsville, pp. 452-457.

Martini, J.E.J., 2004. Silicate Karst. In: Gunn, J. (Ed.), Encyclopedia of Caves and Karst Science. Fitzroy Dearborn, London, pp. 1385-1393.

Mecchia, M., Piccini, L., 1999. Hydrogeology and SiO_2 geochemistry of the Aonda Cave system (Auyantepui, Bolivar, Venezuela). Boletin Sociedad Venezolana de Espeleologia 33, 1-11.

Mecchia, M., Sauro, F., Corongiu, C., Crobu, V., 2009. Speleological explorations in the Chimanta massif quartzites (Gran Sabana, Venezuela). Supplement to Kur magazine 12, 16 p.

Mecchia, M., Sauro, F., Piccini, L., De Waele, J., Sanna, L., Tisato N., Lira, J., Vergara, F., 2014. Geochemistry of surface and subsurface waters in quartz-sandstones: significance for the geomorphic evolution of tepui table mountains (Gran Sabana, Venezuela). Journal of Hydrology (in print).

Morris, R. C., A. B. Fletcher, 1987. Increased solubility of quartz following ferrous–ferric iron reactions. Nature 330, 558-561.

Palmer, A. N., 2007. Cave geology. Cave Books, Dayton, OH, 454 p.

Philipp, S. L., Hoffmann, S., Bartelsen, T., Oelrich, A., Gudmundsson, A., 2006. Field studies and numerical models of hydrofracture propagation in mechanically layered rocks. Geophysical Research Abstracts 8, abstract number 06374.

Piccini L. (1995) - Karst in siliceous rocks - Karts landforms and caves in the Auyàn-tepui Massif (est. Bolivar, Venezuela). International Journal of Speleology, 24 ,(Phys.) 1-4, 41-54.

Piccini, L., Mecchia, M., 2009. Solution weathering rate and origin of karst landforms and caves in the quartzite of Auyan-tepui (Gran Sabana, Venezuela). Geomorphology 106, 15-25.

Pollard, D. D., Segall, P., 1987. Theoretical displacements and stresses near fractures in rock: with applications to faults, joints, veins, dikes, and solution surfaces. Fracture mechanics of rock, 277(349), 277-349.

Quinif, Y., 1999. Fantômisation, cryptoaltération et altération sur roche nue, le triptyque de la karstification. Etudes de géographie physique, suppl. XXVIII, 159-164.

Reardon, E. J., 1979. Complexing of silica by iron (III) in natural waters. Chemical Geology 25(4), 339-345.

Reid, A. R., 1974. Stratigraphy of the type area of the Roraima Group, Venezuela. Bolletin de Geologia, Venezuela, Pub. Especial 6, 343-353.

Rigamonti, I., 1995. La roccia. Il Grottesco, Bollettino Gruppo Grotte Milano CAI-SEM, num. speciale, 32-40.

Santos, J.O.S., Potter, P.E., Reis, N.J., Hartmann, L.A., Fletcher, I.R., McNaughton, N.J., 2003. Age, source, and regional stratigraphy of the Roraima Supergroup and Roraima-like outliers in northern South America based on U-Pb geochronology. Geological Society of America Bulletin 115, 331-348.

Sauro, F., 2009. Mondi Perduti, sugli altopiani quarzitici del Venezuela, Speleologia 61, 38-47.

Sauro, F., Zampieri, D., Filipponi, M., 2013. Development of a deep karst system within a transpressional structure of the Dolomites in north-east Italy, Geomorphology, 184, 51-63.

Sauro, F., Piccini, L., Mecchia, M., De Waele, J., 2013a. Comment on “Sandstone caves on Venezuelan tepuis: Return to pseudokarst?” by R. Aubrecht, T. Lánczos, M. Gregor, J. Schlögl, B. Smída, P. Liscák, Ch. Brewer-Carías, L. Vlcek, Geomorphology 132, 351-365. Geomorphology 197, 190-196.

Sauro, F., Lundberg, J., De Waele, J., Tisato, N., Galli, E., 2013b. Speleogenesis and speleothems of the Guacamaya Cave, Auyan Tepui, Venezuela. In: Filippi, M., Bosak, P. (Eds.), Proceedings of the 16th International Congress of Speleology, Brno 19-27 July 2013, Volume 3, 298-304.

Sauro, F., De Vivo, A., Vergara, F., De Waele, J., 2013c. Imawarì Yeuta: a new giant cave system in the quartz-sandstones of the Auyan Tepui, Bolivar state, Venezuela. In: Filippi, M., Bosak, P. (Eds.), Proceedings of the 16th International Congress of Speleology, Brno 19-27 July 2013, Volume 2, 142-146 .

Sauro, F., Tisato, N., De Waele, J., Bernasconi, S., Bontognali, R.R T., Galli, E., 2014. Source and genesis of sulphate and phosphate-sulphate minerals in quartz-sandstone cave environment. Sedimentology, doi: 10.1111/sed.12103

Serezhinikov, A. I., 1989. Silica in acid natural solutions. In Transactions (Doklady) of the USSR Academy of Sciences, Earth Science Section, 298, 134-138.

Shackleton, J. R., Cooke, M. L., Sussman, A. J., 2005. Evidence for temporally changing mechanical stratigraphy and effects on joint-network architecture. *Geology*, *33*(2), 101-104.

Sloss, L. L., Feray, D. E., 1948. Microstylolites in sandstone. Journal of Sedimentary Research 18(1), 3-13.

Sociedad Venezolana de Espeleologia, 1984. Catastro Espeleologico National. Boletin Sociedad Venezolana de Espeleologia 22, 65-75.

Sociedad Venezolana de Espeleologia, 1994. Cavidades Estudiadas en la Expedición al Macizo de Chimanta, 1993. Boletin Sociedad Venezolana de Espeleologia 28, 34-51.

Szczerban, E., Urbani, F., 1974. Formas carsicas en areniscas Precambricas del Territorio Federal Amazonas y Estado Bolivar. Boletin Sociedad Venezolana Espeleologia 5 (1), 25-54.

Szczerban, E., Urbani, F., Colveé, P., 1977. Cuevas y simas en cuarcitas y metalimolitas del Grupo Roraima, Meseta de Guaiquinima, Estado Bolivar. Boletin Sociedad Venezolana de Espeleologia 8, 127-154.

Teggin, D., Martinez, M., Palacios, G., 1985. Un estudio preliminar de las diabasas del estado Bolivar, Venezuela. Memorias VI Congreso Geologico Venezolano. Caracas, pp. 2159-2206.

Tricart, J., 1972. The landforms of the humid tropics, forests and savannas. Longman. London, 306 p.

Urbani, F., Talukdar, S., Szczerban, E., Colveé, P., 1977. Metamorfismo de las rocas del Grupo Roraima. Edo. Bolívar y Territorio Federal Amazonas. Memorias V Congreso Geologico Venezolano, Caracas, pp. 623-638.

White, A. F., Peterson, M., 1990. The role of reactive surface areas in chemical weathering. Chemical Geology 84, 334-336.

Wray, R.A.L., 1993. Solutional Landforms on Silicates; largely ignored or largely unrecognised? 19th Bienial Conference Australian Speleological Federation, Launceston, 110 p.

Wray, R.A.L., 1997a. A global review of solutional weathering forms on quartz-sandstones. Earth Science Reviews 42, 137-160.

Wray, R.A.L., 1997b. Quartzite dissolution: karst or pseudokarst? Cave and Karst Science 24, 81-86.

Wray, R.A.L., 2000. The Gran Sabana: The World's Finest Quartzite Karst? In: Migon, P. (Ed.), Geomorphological Landscapes of the World. Springer, pp. 79-88.

Wray, R. A., 2009. Phreatic drainage conduits within quartz-sandstone: evidence from the Jurassic Precipice Sandstone, Carnarvon Range, Queensland, Australia. Geomorphology 110(3), 203-211.

Young, R W., 1988. Quartz etching and sandstone karst: examples from the East Kimberleys, Northwestern Australia. Zeitschrift fur Geomorphologie 32, 409-423.

Young, R.W., Wray, R.A.L., Young, A.R.M., 2009. Sandstone Landforms. Cambridge University Press, Cambridge, 314 p.

Zawidzki, P., Urbani, F., Koisar, B., 1976. Preliminary notes on the geology of the Sarisariñama plateau, Venezuela, and the origin of its caves. Boletin Sociedad Venezolana de Espeleologia 7, 29-37.

CHAPTER 2.5

Published in Geomorphology, doi: 10.1016/j.geomorph.2013.12.031

HYPOGENIC SPELEOGENESIS IN QUARTZITE: THE CASE OF CORONA 'E SA CRABA CAVE (SW SARDINIA, ITALY)

Francesco Sauro[1], Jo De Waele[1], Bogdan P. Onac[2], Ermanno Galli[3], Yuri Dublyansky[4], Eleonora Baldoni[1], Laura Sanna[5]

1) Department of Biological, Geological and Environmental Sciences, Bologna University, Via Zamboni 67, 40126 Bologna, Italy, jo.dewaele@unibo.it; cescosauro@gmail.com

2) Department of Geology, University of South Florida, 4202 E. Fowler Ave., SCA 528, Tampa, FL 33620, USA, bonac@usf.edu

3) Department of Chemical and Geological Sciences, University of Modena and Reggio Emilia, Largo S. Eufemia 19, 41121 Modena, Italy, gallier@unimore.it

4) Institute of Geology and Paleontology, Leopold Franzens Universität Innsbruck, Austria, juri.dublyansky@uibk.ac.at

5) Institute of Biometeorology, National Research Council of Italy, Traversa La Crucca 3, 07100 Sassari, Italy, speleokikers@tiscali.it

Corresponding author: Francesco Sauro

Abstract

Detailed morphologic and petrographic investigation in Corona 'e Sa Craba, a quartzite cave in SW Sardinia, revealed clear evidence of quartz dissolution morphologies, without signs of mechanical erosion by running waters. On the cave walls, extremely well-developed boxworks of quartz veinlets that project out of the quartzite bedrock argue for active differential solution processes, probably also in subaerial conditions. Thin section microscopy and scanning electron microscope (SEM) images show pervasive dissolution morphologies, namely pits and notches on quartz crystals causing the deep arenization of the cave walls.

The study of secondary cave minerals and the sulfur isotopic composition of sulfates and sulfides, coupled with data on fluid inclusion temperatures, allowed reconstructing the peculiar speleogenetic history of this hypogenic hydrothermal quartzite cave.

The cave formed by reduced hydrothermal fluids at temperatures above 130°C, probably under basic-neutral pH in phreatic conditions. The presence of abundant cations of Ba^{2+} in reduced Cl-rich

fluids enhanced the quartz dissolution rate, allowing the formation of the void in deep settings. During the Late Oligocene uplift of the area, the hydrothermal fluids in the cave reached oxygen-rich conditions, thus a minerogenetic phase started with the deposition of barite. The presence of cinnabar crusts in the lower part of the cave walls and on the boulders suggests a later volcanic phase with Hg-rich vapors ascending from below. Other minerals such as alunite, basaluminite, gypsum and halloysite (typical of an acid sulfate alteration environment), and phosphates were formed in a final, much more recent stage.

The $\delta^{34}S$ values of the cave sulfate minerals indicate that S is derived from the remobilization of original Precambrian Pb-Zn Mississippi Valley Type ores.

All these observations make Corona 'e Sa Craba the world's first hypogenic cave in quartzites where the speleogenetic mechanisms have been studied and reconstructed in detail using a variety of modern methods. This study confirms that dissolution of quartz by hot and alkaline fluids at depth can also give rise to large dissolutional porosity in the apparently poorly soluble quartzite rocks.

Keywords: quartzite karst; mineralogy; sulfur stable isotopes; speleogenesis; hypogenic cave

2.5.1 Introduction

Caves in quartzites are generally not very common because of quartz's low solubility and solution rates under surface conditions (Wray, 1997; Martini, 2000). Most of the quartzite caves documented in the world are small, and commonly form along tectonic fractures. Prominent exceptions are the large quartzite caves which have been documented in the last thirty years in South Africa (Martini, 1979, 1985), Brazil (Carreño et al., 2002; Ayub, 2006; Willems et al., 2008), and Venezuela (Chalcraft and Pye, 1984; Wray, 2000; Piccini and Mecchia, 2009; Aubrecht et al., 2011; Brewer-Carías and Audy, 2011). The discovery of extensive horizontal cave systems in the Venezuelan tepuis has re-opened the debate on whether these caves form via typical karst solutional or mainly erosional processes (Aubrecht et al., 2011; 2013; Sauro et al., 2013a).

Quartzite caves can be peculiar minerogenetic environments, very different from classical carbonate rocks, and in some cases the study of cave minerals can help understanding the speleogenetic processes that formed the hosting cavities (Zawidzki et al., 1976; Urbani, 1980; Hill and Forti 1997; Onac and Forti, 2011a; Galli et al., 2013; Sauro et al., 2013b). In classical carbonate settings the most illustrative cases of mineralogical studies unraveling the speleogenesis of caves are those of hypogenic caves formed by sulfuric acid speleogenesis (SAS; e.g. Hill, 1987; Polyak and Güven, 1998; Onac et al., 2011; Plan et al., 2012). Here minerogenesis and speleogenesis are strictly linked and the presence of many sulfates and other minerals typical of an extremely acid environment helps to understand the original processes responsible for the creation of the voids (Onac et al., 2009).

To date, only few hypogenic caves were reported from silicate rocks. The studies of Ermakov (1958), focusing on deposits of piezo-optical quartz in Russia, reported solutional cavities developed in zones of schistosity in quartzites and, less frequently, in tectonically disturbed thick quarzite veins, as well as in association with bedding and partition planes of the acidic rocks. Mineralized solution cavities were also described in jaspers associated with Sb-Hg mineralization in southern Kirghizstan by Leven (1961) and Kornilov (1978). Also Lovering et al. (1978) reported small dissolution voids in quartzites associated with Pb-Ag ores in Colorado. Generally these voids are rather small, but in the northern part of the Krivoy Rog iron ore basin (Ukraine) an ~1500 m long, 25 m wide, and 350 m deep cave was documented in carbonized quartzites (Tsykin, 1989). These large voids would have formed in hydrothermal conditions characterised by the circulation of hot alkaline fluids.

The presence of dissolution voids in quartzites is believed to be common at depth, where the solubility of quartz is greater due to higher temperatures and alkalinity of the solutions, as suggested by Zawidzki et al. (1976), Lovering et al. (1978), Andreychouk et al., (2009), and Klimchouk (2012).

Corona ‘e Sa Craba Cave, in southwest Sardinia (Italy), presents typical corrosion features with boxwork morphologies and pervasive arenization of the quartzite, showing also an exceptional variety of secondary mineral phases, most of them sulfates, but also sulfides and phosphates.

The detailed geomorphological and mineralogical study of this quartzite cave, scanning electron microscope (SEM) and Wavelength Dispersive X-ray Fluorescence (WD-XRF) investigations on the hostrock, analyses of S stable isotopes, and fluid inclusions in barite crystals, suggest this cave is of hydrothermal hypogenic origin.

This study confirms that large hypogenic caves are formed not only in carbonates but also in silicic rocks, opening new perspectives for future studies on silicate karst in deep speleogenetic settings.

2.5.2 Geological setting of the area

Corona ‘e Sa Craba Cave is situated in a quartzite ridge in southwest Sardinia, near the small town of Barbusi (Carbonia, Italy) (Fig. 1). This area of Sardinia is characterised by the outcropping of the oldest sedimentary rocks of Italy, composed of Early Cambrian to Upper Carboniferous metasediments. A first sedimentary cycle (Lower Cambrian-Lower Ordovician) is separated by the Sardinian Unconformity from a second cycle (Upper Ordovician-Upper Carboniferous). The oldest sedimentary sequence is composed of metasandstones and shales of the Nebida Group deposited in a shallow marine coastal environment where rivers delivered large amounts of terrigenous material. Toward the top of this succession some oolitic limestone bars testify the evolution toward a more arid climate and the establishment of a coastal plain. This commenced the deposition of the Gonnesa Group (dolostones and limestones) in sabkha and Bahamas-like carbonate platform environments, respectively. These shallow water deposits abruptly change toward epicontinental nodular

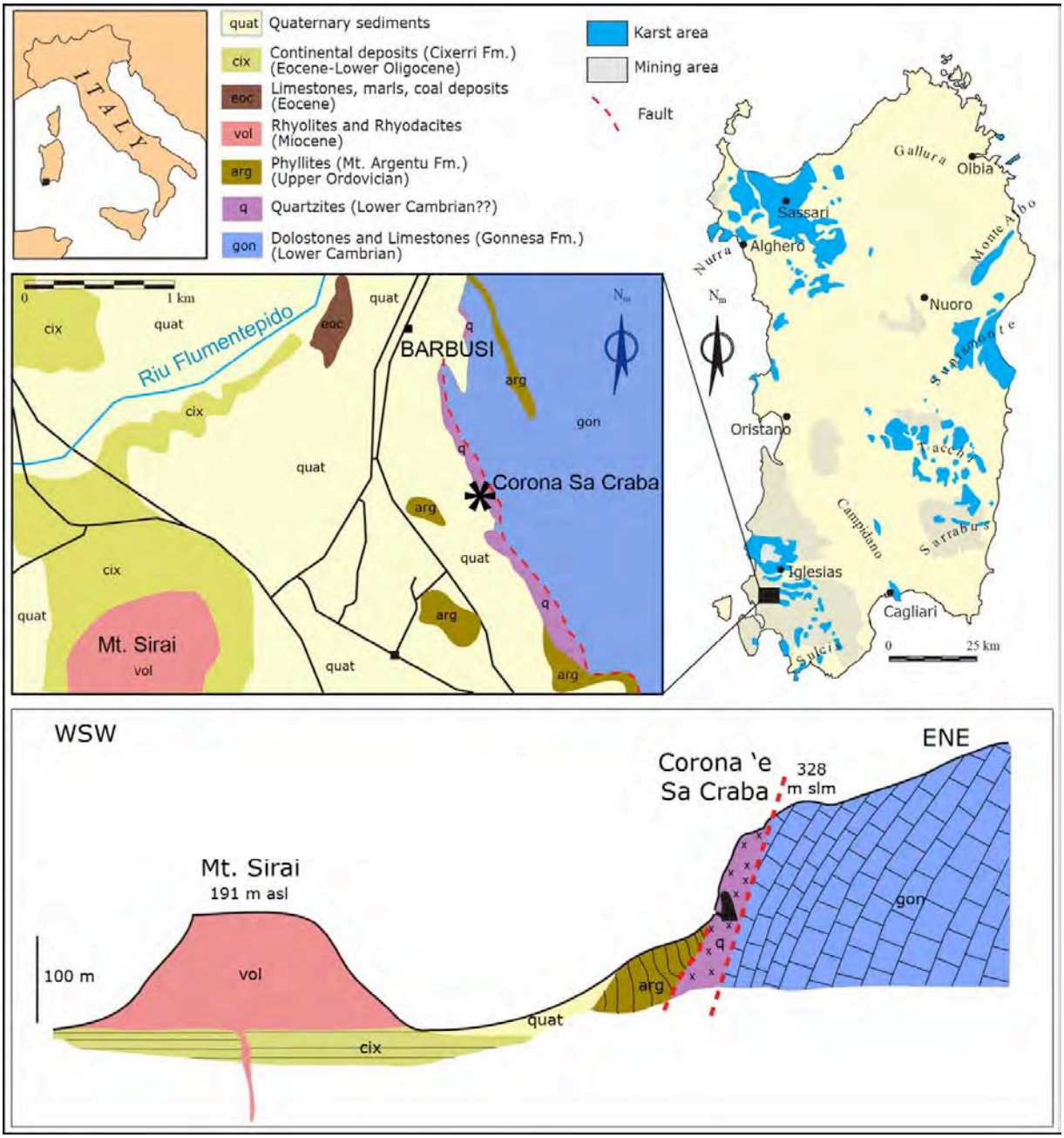

Fig. 1. Location of the study area, geological schematic sketch map, and schematic geological cross-section of the surroundings of Corona 'e Sa Craba Cave (modified from Assorgia et al., 1993).

limestones and pelagic metashales of the Iglesias Group (Pillola, 1989; Bechstadt and Boni, 1996; Carmignani et al., 2001). At the end of Cambrian-Early Ordovician, during a continental period (Sardinian Unconformity) part of these older sediments were eroded away. Later, the transgressive sediments (conglomerates and shales) of the Monte Argentu Formation (Middle Ordovician) accumulated. Quartzite bodies in the form of lenses or major ridges are widespread near to the unconformity. They are interpreted as products of supergene silicification processes affecting the upper part of the Cambrian sediments during the long continental period related to the Sardinian Unconformity (Padalino et al., 1973; Boni and Amstutz, 1982). Other authors (Piovan and Violo, 1965)

argued that the quartzite bodies formed originally as syngenetic chert beds during the sedimentation of shales and carbonates, with later silica remobilization by hydrothermal fluids. More recent studies (Boni et al., 1992) suggest a tectonic-hydrothermal nature of at least some parts of these quartzites. This observation is supported by their alignment along the main NNW-SSE structural features of the area (i.e., Barbusi thrust in Fig. 1). In addition, the quartzites usually represent silicified tectonic breccias of the original Gonnesa dolostones enclosing fragments of the Monte Argentu shales. This type of quartzites (consisting of quartz crystals of 100 μm to 1 cm across) formed along the Variscan tectonic structures as a product of hydrothermal fluid discharge. Diffuse sulfide mineralization, considered post-Variscan in age, is typical for the limestones and dolostones around the quartzite bodies. However, such mineralizations are less important in the quartzite bodies, indicating that probably the same late silica-bearing fluids remobilized sulfides along these hydrothermal pathways (Boni et al., 1992).

Most likely, the Middle Triassic transgression never reached the Barbusi area, nor did the Tertiary transitional sediments; thus the Paleozoic rocks of the area have undergone subaerial erosion since Late Paleozoic. The Tertiary sediments are composed of littoral limestones and coal seams (Paleocene-Middle Eocene), and the very thick continental sedimentary succession of the Cixerri Fm (Middle Eocene-Upper Oligocene) deposited in the nearby slowly subsiding area west of Barbusi (Bechstadt and Boni, 1996; De Waele et al., 2013).

During the Oligocene-Lower Miocene the area was subjected to two compressive tectonic phases that were partially imposed on inherited Variscan structures. The first, characterised by N-S trending folds and thrust faults that affect the Mesozoic and Early Tertiary sediments of Southwest Sardinia, is related to the formation of the Pyrenees before the complete separation of the Sardinian-Corsican block from the South-European margin (Lower Oligocene). The second phase has typical E-W trending folds (Narcao and Cixerri basins) and thrust faults associated with NW-SE dextral strike-slip faults, and is related to the rifting of the Sardinian-Corsican microplate (Carmignani et al., 2004). This complex geodynamic period was characterised by the emplacement of volcanic products, mainly rhyolites and rhyodacites of Burdigalian-Langhian age (ca. 15 Ma ago), outcropping some kilometers southwest of Barbusi (Mt. Sirai, Fig. 1).

2.5.3 The Corona ‘e Sa Craba Cave

Corona ‘e sa Craba Cave opens at an altitude of 260 m asl, immediately southeast of the small village of Barbusi (Carbonia, SW Sardinia, Italy) (Fig. 1). Its small entrance, located at the base of a quartzite ridge, has been enlarged by mining activities in the early 1970s. The first visitors to the cave were mineral collectors, who exploited the natural void for its beautiful bluish barite crystals. Barite was present especially in the entrance part of the cave, along a NNW fracture that is also the cause of the

large rockfall that divides the cave in two parts. This mineral entirely covers walls and parts of cemented collapsed boulders, suggesting these latter ones are rather old. In 1971, cavers of the Gruppo Ricerche Speleologiche E.A. Martel of Carbonia (GRSEAM) explored the cave, but unfortunately it was too late to try and protect this exceptional mineralogical site. The Speleo Club Cagliari and the GRSEAM of Carbonia carried out a complete survey of the cave some years later.

The cave is composed of a series of rooms (Fig. 2) carved in dark grey to brownish quartzite. The floor of most of the cave is covered with breakdowns, particularly along the first 50 m from the entrance, which is at least partially the result of the excavations carried out by mineral collectors. The first room, semi-circular in plan (Fig. 2 point b), is separated from the rest of the cave by a large rockfall. Further behind the rockfall (Fig. 2 point d), the cave continues with a sizeable gallery (30 m wide and 20 m high) for another 100 m in a NW direction (Fig. 3). The centre of this large, elongated chamber hosts an important bat colony during spring-early summer. The floor below these roosts is covered with a large heap of old and fresh bat guano of a thickness of several meters. From the lowest part of this room the cave continues as an 8 m wide and 10 m high passage, clearly developed along a

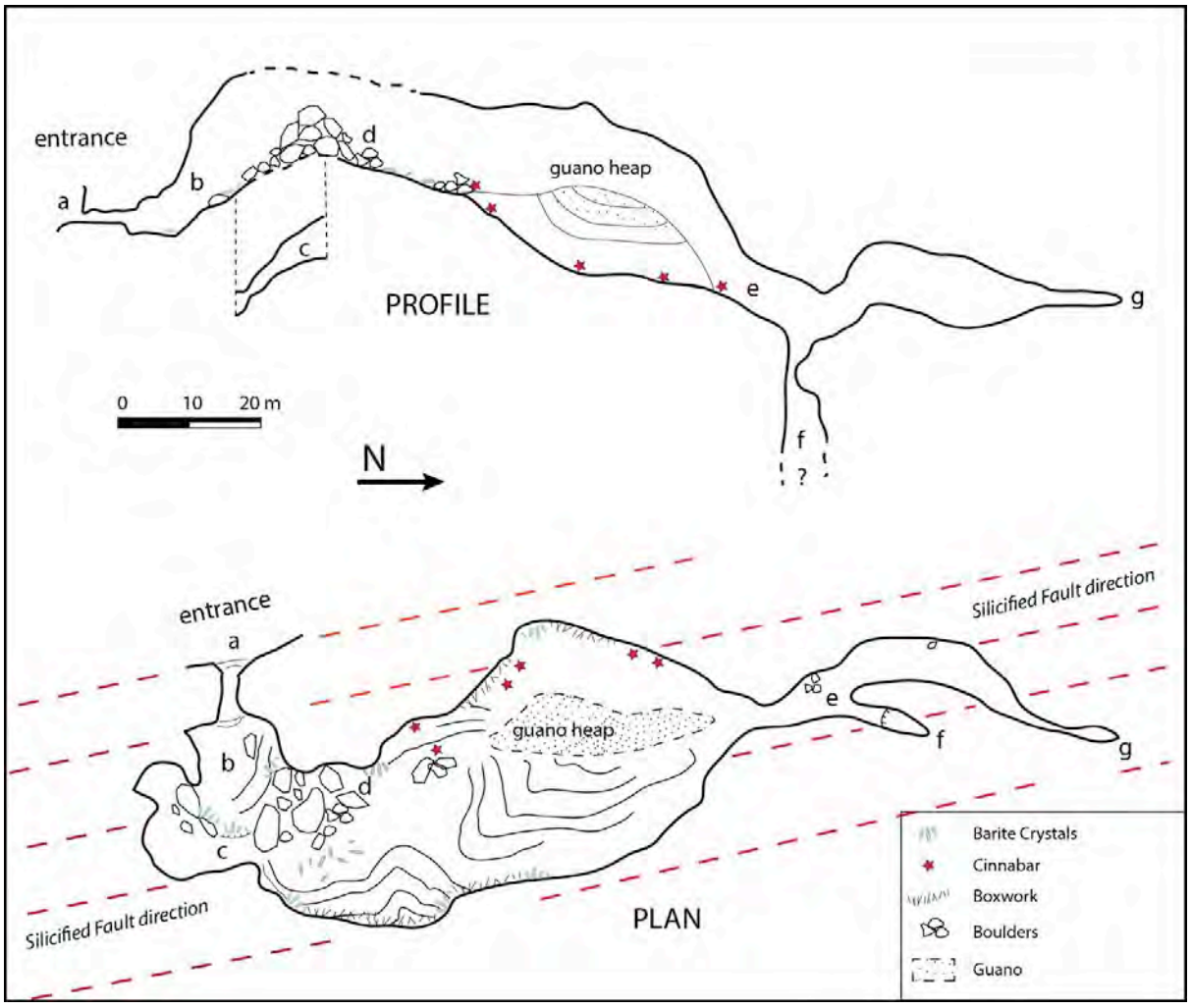

Figure 2. Plan and profile of the Corona 'e Sa Craba Cave (survey courtesy of GRSEAM caving Club, Carbonia).

fracture (Fig. 2 point e). Over the last 60 meters the cave gallery narrows progressively before becoming inaccessible (Fig. 2 point g). About 40 meters before the end, a passage on the right leads to a partially unexplored shaft developed along a fracture (Fig. 2 point f). The total development of the cave is 250 meters. It is devoid of typical vadose speleothems (i.e., stalactites, stalagmites, etc.) commonly decorating carbonate caves.

Of particular interest are the corrosion forms present on the cave walls (Fig. 4). In several places mm-thick dark brown quartz veinlets project out of the bedrock by several decimeters up to a meter, forming boxworks. The bedrock is composed of microcrystalline quartz, whereas the veinlets are

Figure 3. The large underground chamber in the middle part of the cave. The photo is taken from the rockfall (point d) looking north to point e of Fig. 2 (photo V. Crobu).

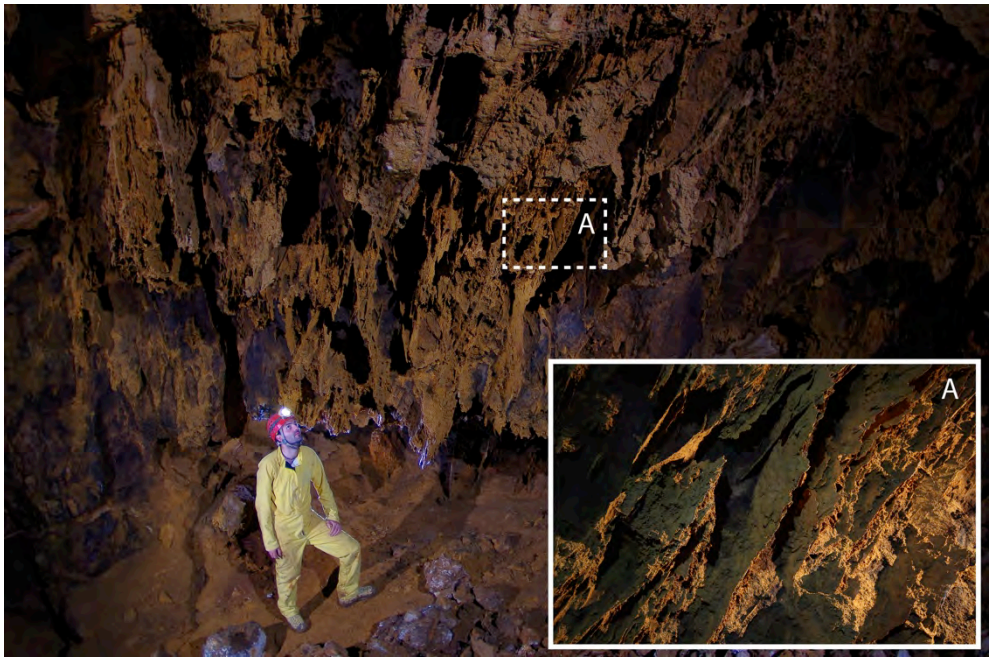

Figure 4. Quartz boxwork veins protruding from the quartzite bedrock by more than half a meter (inset A for details) (cave wall east of point d) (photo V. Crobu, inset R. De Luca).

built up of bigger quartz crystals. Between some of the veinlets, pasty and fine-grained black or very dark-brown material composed of poorly crystallized Mn and Fe oxides resides.

2.5.4 Methods

Cave mineral and rock samples were collected by means of a steel spoon or a geological hammer placing a few grams of material in small plastic cylindrical containers or sampling bags. Galena was sampled in an abandoned underground quarry in mineralized dolostones 500 meters north from the cave entrance.

Chemical determinations were obtained by a wave dispersive X-ray fluorescence spectrometer (WD-XRF) (Philips PW 1480, XRF Laboratory, BIGEA Bologna) on pressed powder pellets, following the matrix correction methods of Franzini et al. (1972), Leoni and Saitta (1976) and Leoni et al. (1982). Calibration is based on 35 international reference materials. The estimated precision and accuracy for trace-element determinations are better than 5%, except for elements at <10 ppm (10-15%). The high barium concentration was evaluated using in house artificial standards. Volatile content was evaluated by thermogravimetric TG-DTG-DTA analysis in air atmosphere using a Setaram Labsys double-furnace apparatus (temperature range 20-1050°C; heating rate 10°C/min; platinum crucibles; calcined Al_2O_3 as reference substance; flow rate of air 0.27 mL/s; temperature accuracy about ±1°C).

Detection of all the different phases was achieved by combining röntgenographic with semi-quantitative chemical analyses. X-ray analyses were performed either on a Philips PW1050/25 diffractometer available at the Department of Chemical and Geological Sciences of Modena and Reggio Emilia University, when the material was sufficient and sufficiently homogeneous, or on Gandolfi cameras (Ø 114.6 mm, 24/48 h standing time), when the material was scarce and difficult to separate. In both cases experimental conditions were set at: 40 kV, 20mA, filtered CuKα Ni radiation, λ = 1.5418 Å. All the samples, and in particular the fragments used in Gandolfi cameras, were characterized by means of semi-quantitative chemical analyses and high resolution frames from a scanning electron microscope (ESEM Philips XL40) equipped with EDS – EDAX 9900 microprobe, available at the Centro Interdipartimentale Grandi Strumenti (C.I.G.S.) of Modena and Reggio Emilia University.

Additional mineralogical analyses were performed on the University of South Florida's Bruker Analytical X-Ray System, Inc. D8 Endeavor X-Ray diffractometer (XRD). Samples were scanned from 5º to 75º 2θ with a step increment of 0.02º, a scan speed of 0.5 s/step (analytical conditions: 50 kV, 40 mA, Cu Kα radiation, line source filtered with a Ni foil). Mineral identification and abundance was evaluated semi-quantitatively by determining peak intensities (peak height) of the X-ray diffraction results with DIFFRAC^{Plus} EVA V.8.0 software.

A Philips 515 SEM equipped with an electronic microprobe EDAX DX4 detector for Energy Dispersive X-ray Spectroscopy was used to obtain chemical information and images of etched quartz surfaces at the BIGEA Department (University of Bologna).

The $^{34}S/^{32}S$ ratios of S-bearing minerals were measured on a Delta V Isotope Ratio Mass Spectrometer coupled with an Elemental Analyzer Costech ECS 4100 (EA-IRMS) at the University of South Florida Stable Isotope Lab following the method described in Grassineau et al. (2001). The results reported in standard d-notation were normalized to CDT (Cañon Diablo Troilite) using $\delta^{34}S$ values of the four IAEA standards (IAEA, International Atomic Energy Agency, S-2, $\delta^{34}S$ = 22.7‰ and IAEA S-3, $\delta^{34}S$ = −32.3‰, for sulfides and IAEA SO-5, $\delta^{34}S$ = 0.5‰, and IAEA SO-6, $\delta^{34}S$ = −34.1‰ for sulfates). The reproducibility between replicate standards in each run was better than ± 0.1‰ (1σ).

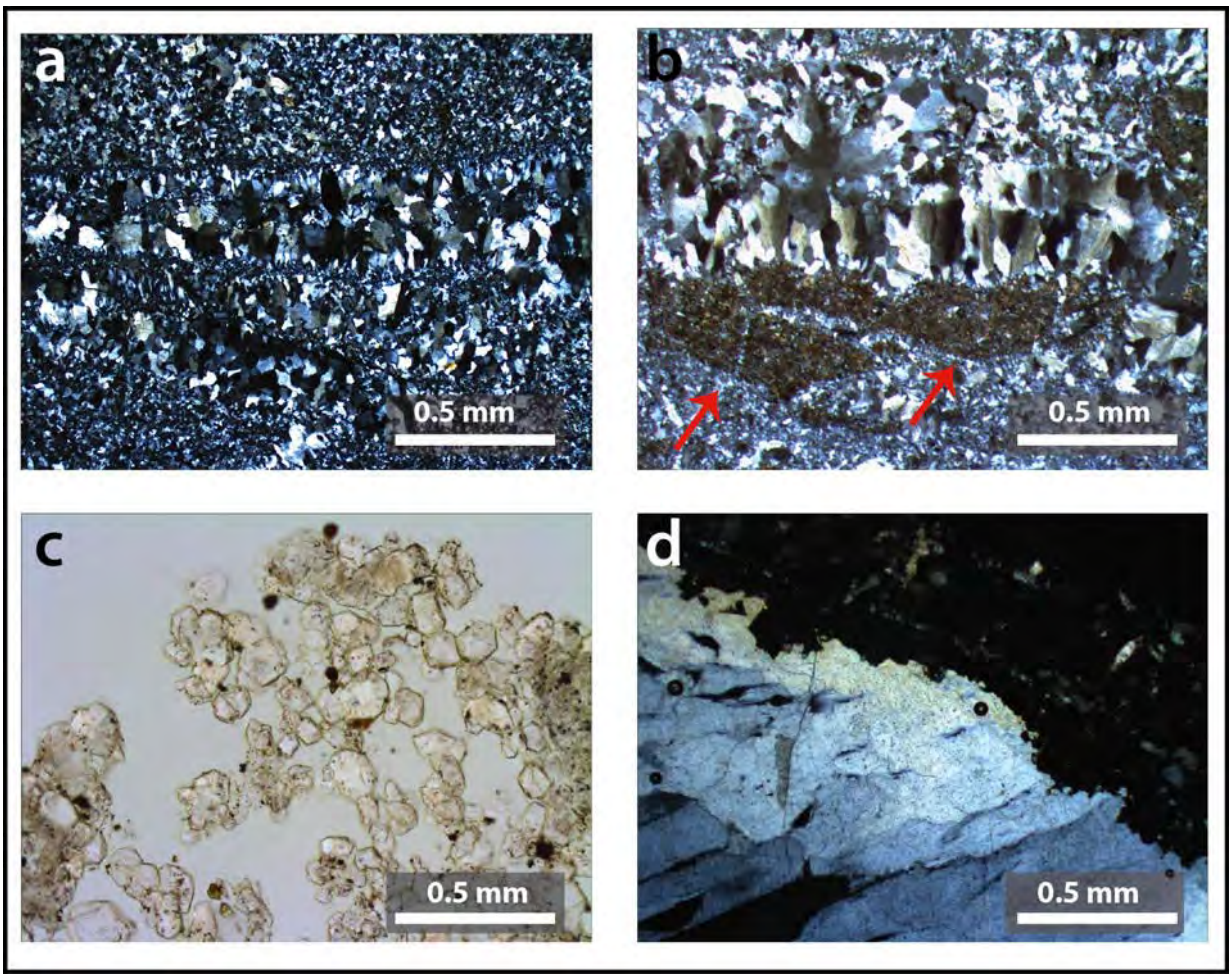

Fig. 5. Thin sections of quartzite from Corona 'e Sa Craba Cave: a) Typical texture composed of a matrix of small-size interlocked crystals and veinlets built of larger crystals with comb structure (polars X); b) Relics of dolomite replaced by quartz (arrows; polars X); c) Arenized quartzite in which the general framework is destroyed and singular grains are loosened (polars II); d) Quartz vein made of large isochroic quartz crystals with visibly dissolved and corroded rims (polar X).

2.5.5 Results

2.5.5.1 Composition of the quartzite and evidences of quartz dissolution

A detailed chemical and petrographic study was carried out on the quartzite rocks hosting the cave. Both WD-XRF chemical analysis and microscope observations suggest that quartzites are the result of a pervasive silicification of an original dolomitic tectonic breccia. In thin sections, the constituent quartz grains (sometimes euhedral crystals) develop an interlocked mosaic structure (Fig. 5a). Agglomerates of fine quartz crystals host a network of quartz veinlets composed of somewhat coarser crystals assembled in a comb structure (Fig. 5a-b). Rare crystals or rhombohedral pseudomorphs of the original dolomite can be observed in the inner part of some clasts (Fig. 5b).

The dissolution along crystal faces tends to separate each crystal grain of the interlocked texture, leading to the so-called arenization (sensu Jennings, 1983) described by Martini (2000) (Fig. 5c). Weathered samples from the cave surface appear to be deeply arenized, with individual crystals losing cohesion with neighbours. The effect of dissolution is more severe in the fine-grained matrix of

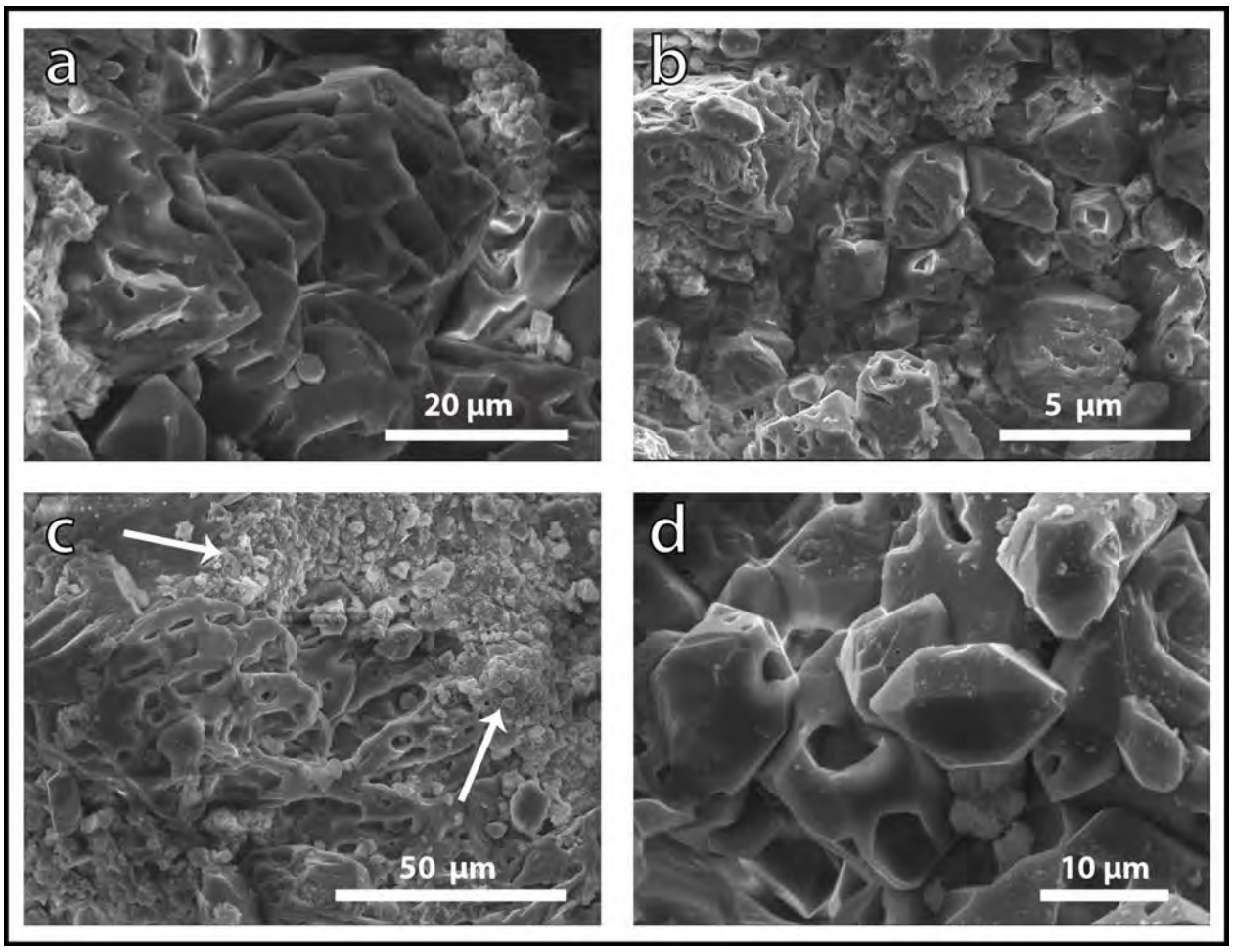

Figure 6. SEM images of dissolved quartzite: a-b) Severe dissolution along quartz crystal faces releases single crystals from the quartzite rock; c) Dissolution of larger crystals does not affect much of quartzite's cohesion and consequently less friable material is released from the rock; the lighter grey grains in the upper right part of the image are iron hydroxides and phosphates (arrows); d) Deep corrosion pits on euhedral quartz crystals.

the rock, whereas the coarse-crystalline veinlets appear to be more refractory (Fig. 5c-d). However, in contrast to quartzite caves in Venezuela and other epigenic quartzite caves (Doerr, 1999), at Corona 'e Sa Craba this speleogenetic mechanism requires much more pervasive intergranular corrosion, which needs to completely release quartz crystals from the rock. This is because running waters and related erosional processes, facilitating speleogenesis in most epigenic quartzite cave settings, are not available in this cave. Because of that, accumulations of sand composed of these loose grains are common directly below the most arenized parts of the quartzite walls.

The degree of silicification of the dolomite is usually around 90 %, and the quartzite typically contains only 1 to 2 mass % of Mg (Table 1). In only one case have we found a massive slab of rock (dolomite sample collected in the lowermost part of the cave, covered by Mn-hydroxides, see Table 1), which retained the original dolomitic composition with only minor silicification. It can be expected, therefore, that the tectonic dolomitic breccia was silicified incompletely, and some less fractured blocks could have successfully resisted silicification.

Chemical analyses of the dolomite sample described above showed that the original Cambrian dolomite is enriched in metals, with major concentrations in Zn and Ba. In contrast, quartzite contains much lower amounts of these elements. This suggests that the silica-bearing fluids were also responsible for the mobilization (removal) of the metallic ions present in the original dolomite.

Quartzite on cave walls exhibits weathering morphologies such as boxwork and extensive arenization (Fig. 4). SEM images (Fig. 6) of arenized samples show widespread pits and V-shaped notches on the crystal faces, characteristic of severe etching (Burley and Kantorowicz, 1986). Pitting and corrosion depressions generally range in size from 1 to 20 µm, but can also completely obliterate the crystal habit. Pits appear to occur irregularly, both on crystal faces and on terminations (Fig. 6d). In places, the arenized quartzite is covered by Mn- and Fe-hydroxides, probably formed during a later stage of the pervasive phreatic corrosion (Fig. 6c).

2.5.5.2 Mineralogy

Our research documented 24 mineral species in Corona 'e Sa Craba cave (Table 2): most of them are phosphates (7) related to the presence of bat guano and sulfates (6). In addition, oxyhydroxides (4), carbonates (3), silicates (3), and one sulfide were identified. Some of these minerals, namely spheniscidite and lizardite are for the first time reported from a cave environment (Onac and Forti, 2011b).

Sulfates

The sulfates are among the most common minerals in Corona 'e Sa Craba Cave. Besides barite, forming very beautiful and big bluish, reddish and yellowish euhedral crystals (Fig. 7a), we also found

basaluminite (Fig. 7b), alunite (Fig. 7c), natroalunite, walthierite, and gypsum. Walthierite is a rather rare barium-aluminum sulfate often associated with alunite. It normally forms by the interaction of hydrothermal fluids with barite. Gypsum is a common product of reaction between carbonates (in this case dolomite) and sulfuric acid-rich solutions resulted from the oxidation of H_2S (Hill, 1987; Galdenzi and Maruoka, 2003; Onac et al., 2011b). Similarly, alunite, basaluminite, and natroalunite form by the reaction between sulfuric acid and aluminum-bearing minerals (Khalaf, 1990; Polyak and Güven, 1996). Alunite, basaluminite, and gypsum are either precipitated directly over the quartzite bedrock or cover the cinnabar coatings.

Phosphates

Here we report seven phosphate minerals, all related to the massive accumulation of bat guano in the Corona 'e Sa Craba Cave. Taranakite and hydroxylapatite are rather common minerals in cave environments (Hill and Forti, 1997), whereas Al-strengite and vashegyite are less common (Onac et al., 2006). Robertsite is a very rare cave phosphate, recently discovered in a tropical limestone cave (Lion's Cave) in the St. Paul's Underground River National Park, Palawan, Philippines (Billi et al., 2013). Spheniscidite, is a hydrated phosphate containing hydroxyl precipitated from the reaction of ammonium-rich fresh guano leaches with K^+, Fe^{3+}, and Al^{3+} in cave sediments (Fig. 7d). This is the first reported occurrence of this mineral in a cave environment.

Berlinite, a very rare anhydrous phosphate might be present in this cave, considering that some of the XRD peaks positively match the reference mineral. However, compared to the other described phosphates, all of supergene origin, this mineral requires rather high temperature to form (over 350°C; Muraoka and Kihara, 1997; Onac and White, 2003; Onac and Effenberger, 2007). Further investigations are needed to verify the presence of berlinite in Corona 'e Sa Craba Cave.

Sulfides

Besides galena and sphalerite, occurring in the nearby ore deposits but present only as rare crystals in the quartzite hosting cave, the only identified sulfide we have found in Corona 'e Sa Craba is cinnabar (Fig. 7e-g). This mineral is usually deposited by epithermal ascending aqueous solutions or vapors deriving from deep igneous sources or as oxidation product of sphalerite in the gossan-like surface environment (Koski, 2012). In Corona 'e Sa Craba Cave it occurs as sub-millimeter thick bright red powdery coatings on walls in the lower part of the cave and particularly on the overhanging rock walls and boulders. It has also been seen covering barite crystals. This characteristic occurrence suggests that cinnabar originated from vapors or hydrothermal fluids rising from below between the boulders. Cinnabar is sometimes covered by typical SAS minerals (alunite, basaluminite, halloysite, and gypsum).

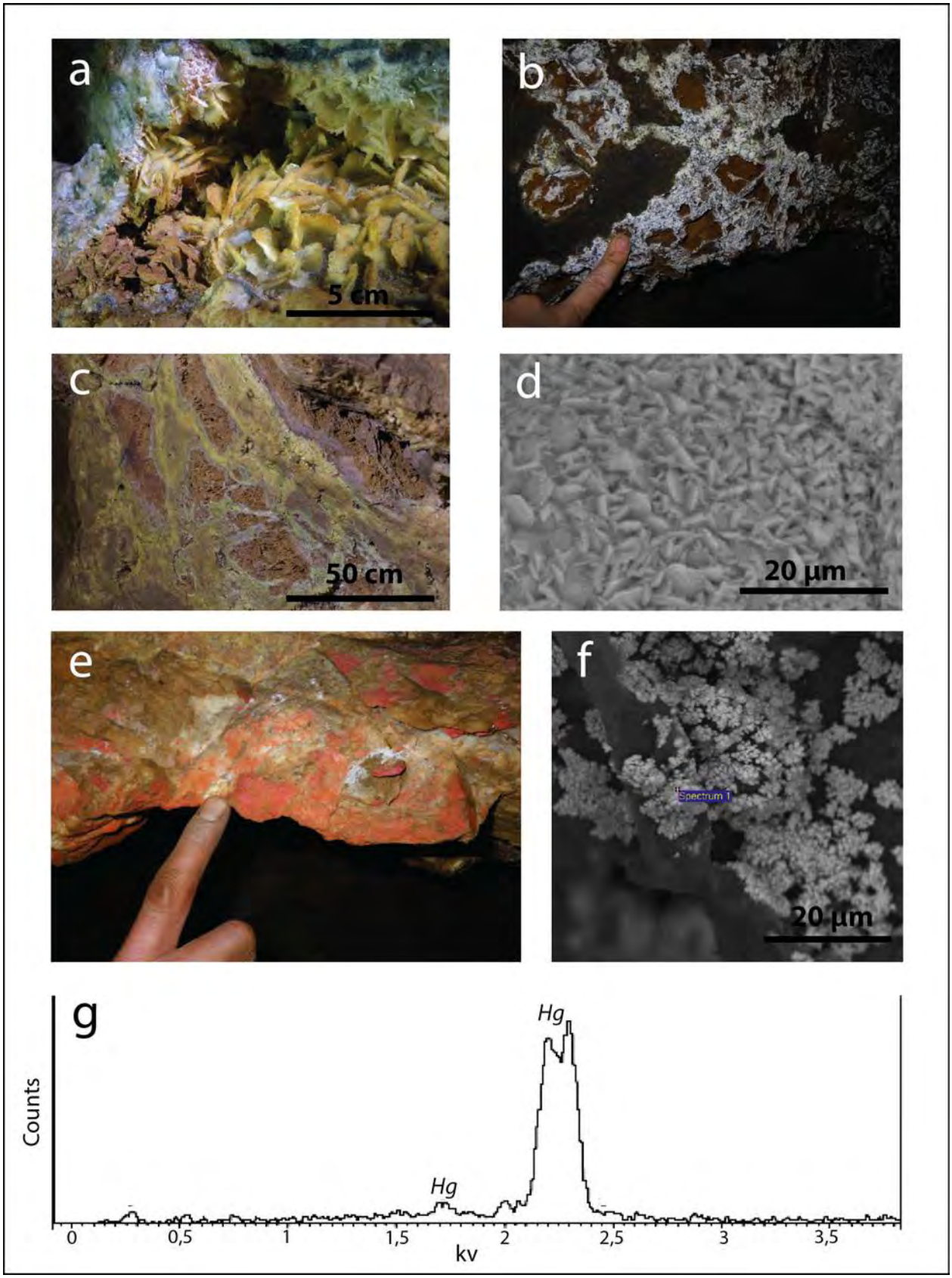

Fig. 7. In situ pictures, SEM microphotographs, and a diffractogram of some minerals from Corona 'e Sa Craba Cave: a) Yellow, green and blue barite crystals; b) Basaluminite on a weathered quartzite wall; c) Alunite covering a weathered quartzite wall; d) SEM image of spheniscidite; e) Cinnabar crusts on sharp edges of lower face of boulders; f-g) SEM image and WDX spectrum of cinnabar.

Oxides and hydroxides

Four oxides and hydroxides have been positively identified, namely hematite, pyrolusite, goethite, and todorokite. They occur as dark-colored coatings and crusts on the rock walls. These are common minerals derived from sulfide oxidation or leaching of silicate minerals.

Carbonates

Being common minerals in carbonate caves, calcite, and aragonite are rare in quartzite caves. Calcite was found in a powdery material covering the western wall of the canyon-like passage of the cave (Fig. 2 point e). It appeared as translucent yellowish-white crystals composed of pure calcite. This calcite can be related to weathering of incompletely silicified parts of the original dolomitic bedrock. Another possible source is the percolation of meteoric waters that have crossed the nearby or the overlying Cambrian limestones and dolostones.

Silicates

Besides quartz, and some common detrital clay minerals such as smectite and illite, two silicates are worth discussing. Halloysite is a typical hydrothermal mineral that forms in highly acidic environments (Polyak and Güven, 1996; Perruchot et al., 1997; Melka et al., 2000; De Waele et al., 2008). Lizardite usually forms by hydrothermal alteration of Mg-rich minerals such as olivine (serpentinitization). Prior to this work, lizardite was only reported from the hypogenic SAS-type cave of Cupp Couttun in Turkmenistan (Maltsev, 1997).

2.5.5.3 Sulfur Isotopes

The $\delta^{34}S$ values of the S-bearing cave minerals from the cave and of galena samples representing the nearby mineralized dolostones are given in Table 3. The $\delta^{34}S$ values range between +15.0 ‰ and +20.8 ‰ for the sulfate minerals (barite, basaluminite, and gypsum) and show relatively uniform compositions for galena (between +20.9 and +22.2 ‰). The cave cinnabar yielded enriched $\delta^{34}S$ (+31.5 ‰).

These results are in good agreement with the previously reported data for sulfur isotopic composition of sulfate and sulfide ore minerals from the Iglesiente and Sulcis areas (De Vivo et al., 1987; Boni et al., 1988; Cortecci et al., 1989; Ludwig et al., 1989; Vollmer et al., 1989). Galena shows values very similar to those reported by Jensen and Dessau (1966), consistent with sulfides derived from bacteria-reduced Cambrian seawater sulfates.

The isotopic signature of barite, basaluminite, and gypsum fits well with a population of sulfates distinguished in this area by Cortecci et al. (1989). These sulfates are considered to have formed via non-equilibrium oxidation of reduced sulfur from Cambrian-Ordovician sulfide ores in warm-hot

fluids. The reduced sulfur could have been derived from either sulfide minerals within the host rock or from ascending HS^- or H_2S-rich brines. These hypotheses are supported by the fact that the Corona 'e Sa Craba barite (and the other sulfates) and ore galena have nearly identical $\delta^{34}S$ values: the fractionation factors involved during oxidation are generally very small (Canfield, 2001), therefore the expected isotopic composition of sulphate produced by this mechanism should ultimately track the source of sulphide minerals.

In contrast, the higher $\delta^{34}S$ value of cinnabar suggests that this mineral has a different origin compared to both sulfate and ore galena samples. This peculiar mineralization found only on the lower parts of boulders and overhanging cave walls does not seem to have formed underwater, and might be related to a more recent thermal subaerial (vapor) phase.

2.5.6 Speleogenesis and mineral deposition

Both quartz solubility and rate of dissolution increase with temperature (Rimstidt, 1997), meaning that as the temperature drops the solubility decreases exponentially (Fig. 8a). Another parameter controlling these factors is the pH: solubility and dissolution rate are nearly constant at pH < 7-8 and increase at greater pH values (Siever, 1962; Bennet et al., 1988; Brady and Walther, 1989). In strongly alkaline conditions (pH > 9), silicic acid undergoes up to four consecutive dissociations, releasing H^+ ions according to reactions:

$$H_4SiO_{4(aq)} \rightarrow H_3SiO_4^- + H^+$$

$$H_3SiO_4^-{}_{(aq)} \rightarrow H_2SiO_4^{2-} + H^+$$

$$H_2SiO_4^{2-}{}_{(aq)} \rightarrow HSiO_4^{3-} + H^+$$

$$HSiO_4^{3-}{}_{(aq)} \rightarrow SiO_4^{4-} + H^+$$

significantly increasing the amount of quartz which can be dissolved (Ford and Williams, 2007).

Some authors argue the possibility that this process could happen also at low pH (Krauskopf, 1956; Füchtbauer, 1988; see also the diagram in Doerr, 1999), but the studies of Knauss and Wolery (1988) and Brady and Walther (1989) do not confirm such hypothesis (Fig. 8b). Furthermore, the numerical modeling by Aubrecht et al. (2011) does not evidence an increasing solubility at low pH values either.

In the case of Corona 'e Sa Craba Cave, the petrographical studies showed ubiquitous corroded quartz grains, leading subsequently to the arenization of the quartzite bedrock, confirming that an earlier dissolution process must have been active, allowing the formation of primary voids within the quartzites. Because the solution rate of quarzt is high only at alkaline pH, we expect that the speleogenetic phase be characterized by different fluid conditions with respect to the subsequent minerogenetic phases that show the typical signature of a highly acidic environment.

Barium, because of its very low solubility, can be mobilized in form of barium chloride only in a highly reducing environment where the sulphate ion is almost completely reduced (Hanor, 2000).

Precipitation of barite can be triggered by changing (from reduced to oxidative) conditions of the fluid. Therefore, information on the speleogenetic phase can be deduced taking into account the potential source of the barium, the conditions necessary for the barite precipitation and the related fluid inclusion data. The $^{87}Sr/^{86}Sr$ isotopic ratios and the total Sr contents of barite crystals from Corona 'e Sa Craba and other deposits in the area (Barbieri et al., 1984) suggest that these "karst" barites originate from recycling of deep-seated stratiform barites of seawater origin (Cambrian Punta Pipixedda stratiform barite; Padalino et al., 1973) by action of a highly reduced hydrothetmal fluid. Furthermore, if Cl^- is present in the system, the mobilization of barium could happen in the form of barium chloride, which is much more soluble than barium sulfate. Therefore, we hypothesize a phase during which the hydrothermal fluids circulating along the tectonic features and responsible for re-mobilization of barium were reduced and probably had an alkaline to neutral pH. Dove and Elston (1992) and Dove and Rimstidt (1994 and references therein) demonstrated that adding low concentrations of alkali cations (of both groups IA and IIA) may enhance the dissolution rates and solubility of quartz with cation-specific effects. Dove and Nix (1997) demonstrated that Ba^{2+} has the greatest quartz dissolution rate-enhancing effect above all other cations: a 0.005 molal Ba^{2+} solution enhances the dissolution rates and solubility of quartz as much as forty times compared to deionized water in a range between 20° to 200°C in near neutral-pH solutions (Fig. 8c).

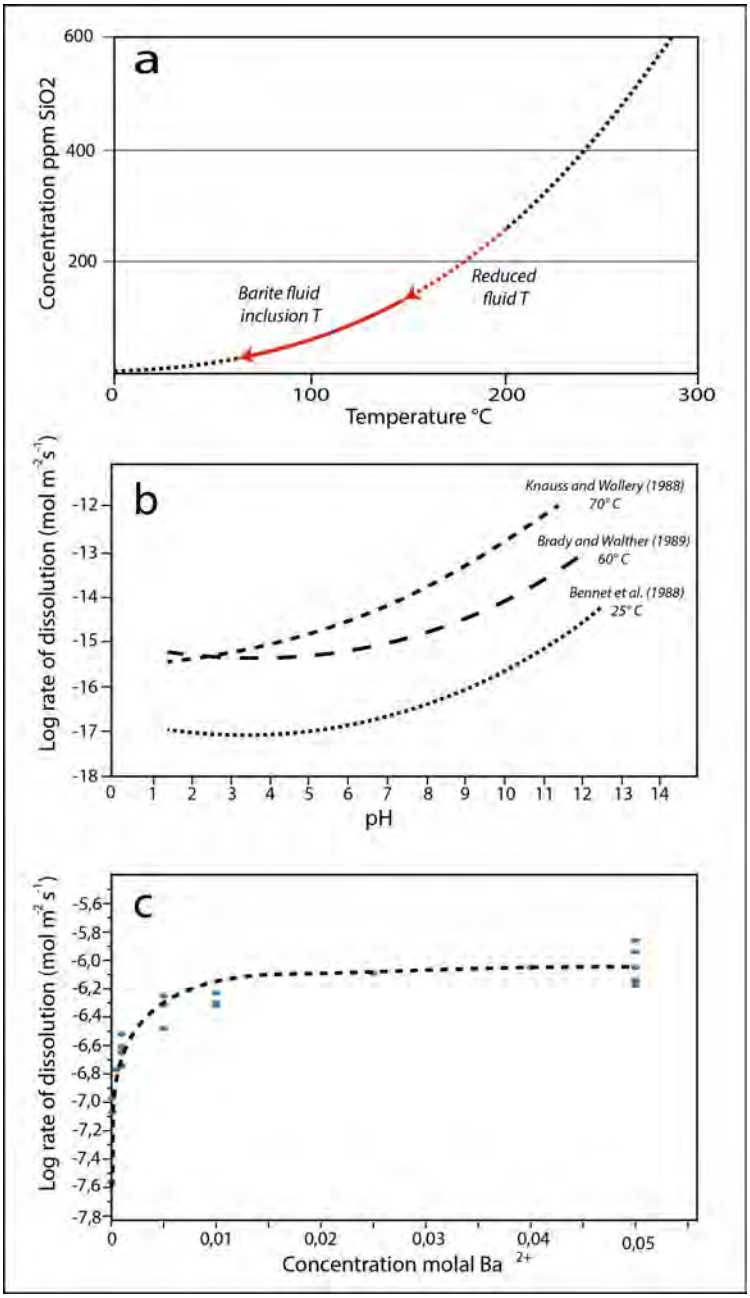

Fig. 8. Main parameters controlling the solubility of quartz in hydrothermal conditions: a) Dependence of quartz solubility from temperature (Rimstidt, 1997): the red solid line represents the range of T documented for the fluid inclusions in barites (Cortecci et al., 1989), therefore we expect a higher temperature during the earlier speleogenetic phase. b) Dependence of quartz dissolution rate on the pH at different temperatures (Bennet et al., 1988; Knauss and Wolery, 1988; Brady and Walther, 1989). c) Effect of Ba^{2+} on the dissolution rate of quartz (Dove, 1999).

It is reasonable to assume that the phreatic phase preceding the precipitation of barite was characterized by temperatures exceeding 130°C (the highest temperature as documented in barite fluid inclusion by Cortecci et al., 1989), high pH, and high Ba^{2+} concentrations. Under such conditions, the hydrothermal fluids were capable of dissolving the quartzites and generating the primary cave void (Fig. 9a). The corrosion resulted not only in opening of the cavity but also affected the integrity of cave walls, so that the quartzite bedrock can now be easily broken with bare hands. The corrosion acted directly upon quartz crystal boundaries weakening the overall quartzite cohesion (Martini, 2000). This process mostly affected the finer texture of quartzite and significantly less the veinlets built up of larger quartz crystals. This texture-selective corrosion caused by different surface energy of crystals with drastically different dimensions (Iler, 1955; Stumm and Morgan, 1981) produced the boxwork morphologies. The enlargement of the void lasted as long as the pH remained high and fluids were rather hot: almost no deposition of cave minerals took place at this stage, except for the coatings of Mn- and Fe-hydroxides.

Deposition of secondary cave minerals started only in the second phase, when fluids circulating through the cave became oxidizing due to the lowering of the local water level. The infiltration of oxygenated water along the fault line caused the oxidation of dissolved H_2S and sulfides in the bedrock to sulfuric acid, boosting the release of H^+ and therefore lowering the pH (Fig. 9b). Quartzite dissolution abruptly slowed down in this acidic and cold environment. However, we cannot exclude that during this phase the dissolution of un-silicified dolomite blocks within the quartzite breccia contributed to the enlargement of the cave. Because of the sulfide oxidation, the formation of sulfate ions resulted in precipitation of barite crystals on the cave walls, consequently lowering the Ba^{2+} concentration in the fluids. The newly formed, quasi-uniform coating of barite also shielded the quartzite bedrock from the ongoing, albeit very slow dissolution processes.

Because of further lowering of the (thermal) water table the cave drained and acquired subaerial conditions. At this stage, hot acidic vapors continued to rise from depth along some fractures (Fig. 9c). In this late phase condensation-corrosion processes were responsible for rejuvenating the weakening of quartzite, slowly enlarging the cave walls (see the dotted contour in Fig. 9c) but mostly reworking and increasing the boxwork size at specific sites. Evaporation-corrosion is considered a reliable process for limited amount of quartzite weathering even in epigenic conditions (Aubrecht et al., 2012). During this stage, cinnabar is deposited on the overhanging faces of boulders and walls by rising vapors.

The typical suite of SAS minerals (gypsum, basaluminite, alunite, and halloysite) formed in this subaerial stage by reaction of H_2SO_4 with the host rock and Al-Fe-Mg-rich cave sediments, probably related to quartzite and dolomite weathering residues. The phosphates, on the other hand, are clearly related to the presence of the bat guano deposit and the reaction between its phosphoric acid

leaches with the bedrock and cave sediments/deposits. All these minerals (barite, cinnabar, the SAS minerals, and the phosphates) are thus unrelated to the cave formation phase.

Although no data is available to numerically constrain different hydrothermal and vadose phases, the data and observations presented in this paper allow us to delineate a preliminary hypothesis on the speleogenetic history of this quartzite cave. As suggested by Boni et al. (1992), the quartzite of Corona 'e Sa Craba and other ridges in the Iglesiente area formed through silicification of a pre-existing Variscan tectonic breccia of dolomite clasts, probably by fluids derived from deep-seated leucogranites. This process could have happened during the late Permian or alternatively at the beginning of the Pyrenean-Alpine tectonic phase in the Lower Oligocene. This last reactivating tectonic phase pumped reduced hydrothermal fluids through the inherited Variscan structures and mobilized Cambrian-Ordovician sulfides and Ba^{2+} from deep-seated stratiform barite ores. The speleogenesis started in this phase because of the high aggressiveness of these fluids with respect to

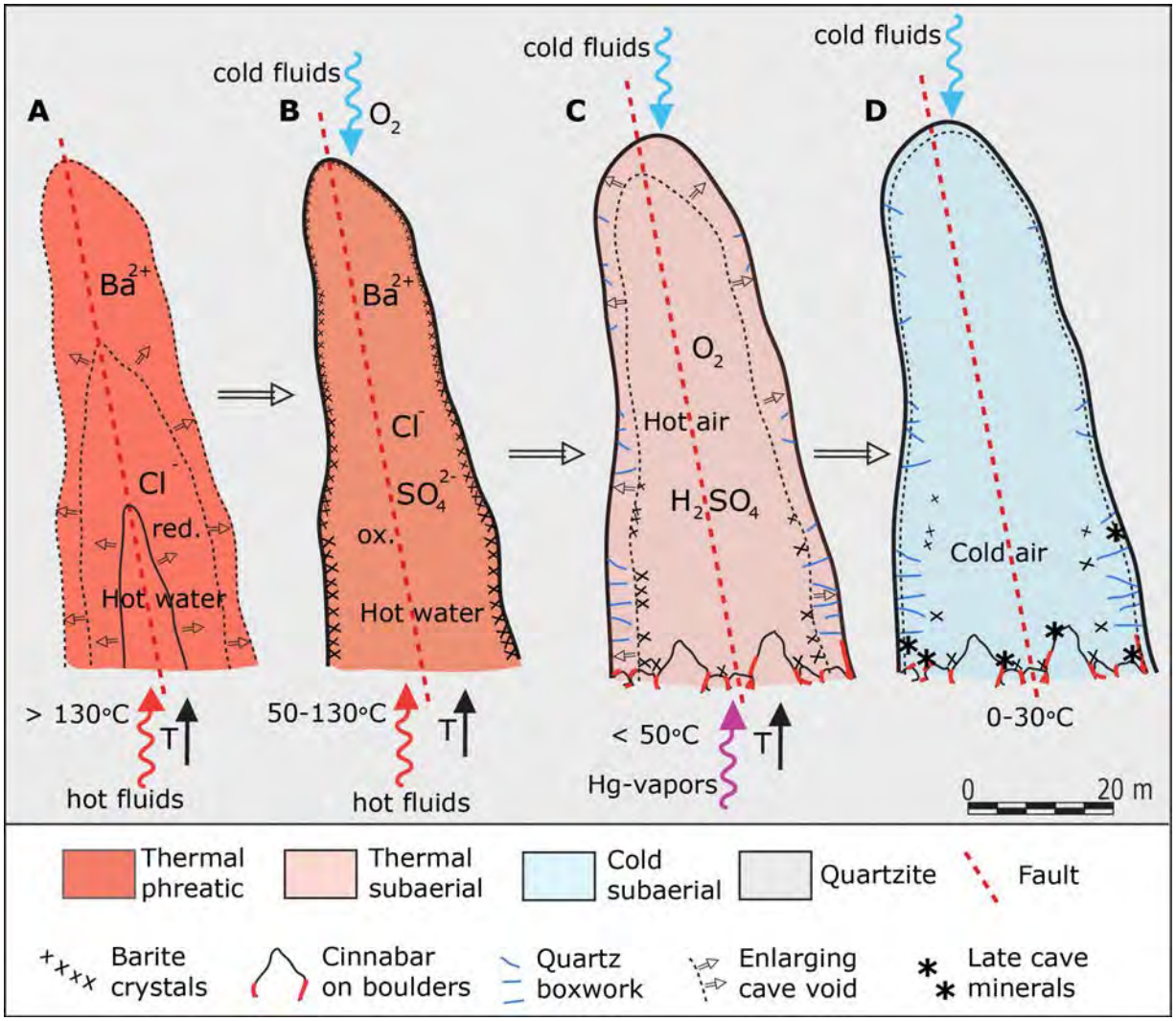

Fig. 9. Conceptual model of development and mineralization of Corona 'e Sa Craba cave (see discussion in the text).

quartzite. The dissolving capacity was primarily due to the relatively high temperatures (higher than 130°C), the neutral to alkaline pH, and the presence of Ba^{2+} in solution.

In the next phase, probably associated with the Early Miocene tectonic-volcanic activity, the cave environment became oxidizing due to the lowering of the water table in the area. This caused barite to precipitate in phreatic oxidative and thermal conditions. Later, the fluids drained out, leaving an air-filled cavity in which acid vapors related to the volcanic phase of the nearby Sirai volcanic complex (of Burdigalian-Langhian age) continued to outgas along a system of deep fractures. These vapors were responsible for the deposition of cinnabar, probably in the late volcanic stage (Langhian). The typical SAS-minerals (gypsum, basaluminite, alunite, and halloysite), instead, were deposited in an acid-sulfate alteration environment later, since they often cover the cinnabar coatings. The condensation-corrosion of vapors on the cave walls is responsible for the further slow widening of the void and for dramatically shaping the boxwork in both size and morphology.

Since the cave never accommodated underground streams or turbulent waters, it preserved the original corrosion morphologies for millions of years.

2.5.7 Conclusions

Corona 'e Sa Craba Cave is a relatively large hydrothermal hypogenic cave in silicate rock. Its genesis is related to the high aggressiveness of the hydrothermal fluid with respect to quartzite, in turn caused by the relatively high temperature of the fluid (more than 130°C), the high pH, and the presence in solution of Ba^{2+}.

The morphological characteristics of the cave and the hosted mineralogical association suggest that the circulating fluids reached an oxidative phase, with the consequent precipitation of barite, only when the cave was already formed. The isotopic composition of sulfates strongly suggests their origin from oxidation of reduced sulfur from Cambrian-Ordovician ores, either as sulfide minerals within the host rock or as H_2S ($\pm$ HS^-) carried by fluids from depth.

Thus, speleogenesis and mineral deposition were controlled by two different hydrothermal phases, the first related to reduced, and the second to oxidized conditions.

The formation of the cave probably dates back to the Lower Oligocene while the barite deposition is probably related to the Early Miocene when the uplift of the area gave rise to the oxidation. Cinnabar was deposited as the latest stage-mineral, related to sulfide oxidation by thermal vapors during the later subaerial period, probably contemporary to the volcanic activity reported in the area (Langhian). The typical SAS minerals formed mostly after the deposition of cinnabar, and might still be forming today. Also cave phosphates are forming presently by interaction of fresh guano with the bedrock and the cave sediments.

This study confirms once more that dissolution of quartzites can take place a deep-seated settings, where fluids can attain aggressiveness by hot temperatures, at basic to neutral pH and in the presence of inorganic cations in the solutions. This might open new perspectives for the study of deep karstified reservoirs in non-carbonate rocks.

Acknowledgements

Many thanks Mauro Messina and Alberto Muntoni for their assistance during field work, Riccardo De Luca, Vittorio Crobu, and Carla Corongiu for their wonderful cave pictures, and Mauro Villani for assembling the historical information on Corona 'e Sa Craba Cave and the mining operations in the area. WD-XRF analyses were carried out at BIGEA (University of Bologna) with the help of Enrico Dinelli. SEM pictures were taken with the assistance of Giorgio Gasparotto (BIGEA) and Massimo Tonelli (C.I.G.S. of Modena and Reggio Emilia University).

References

Andreychouk, V., Dublyansky, Y., Ezhov, Y., Lisenin, G., 2009. Karst in the Earth's Crust: its distribution and principal types. University of Silezia – Ukrainian Institute of Speleology and Karstology, Sosnovec-Simferopol, 72 p.

Assorgia, A., Fadda, A., Perna, G., Ottelli, L., 1993. Carta Geologica del Bacino Carbonifero del Sulcis, Carta in scala 1:25000, Carbosulcis S.p.A., In: Fadda, A., Ottelli, L., Perna., G., (Eds.), Il bacino carbonifero del Sulcis: Geologia, idrologia, miniere. Carbosulcis, Cagliari.

Aubrecht, R., Lánczos, T., Gregor, M., Schlögl, J., Smída, B., Brewer-Carías, Ch., Vlcek, L., 2011. Sandstone caves on Venezuelan tepuis: Return to pseudokarst? Geomorphology 132, 351-365.

Aubrecht, R., Barrio-Amorós, C.L., Breure, A.S.H., Brewer-Carías, C., Derka, T., Fuentes-Ramos, O.A., Gregor, M., Kodada, J., Kováčik, Ľ., Lánczos, T., Lee, N.M., Liščák, P., Schlögl, J., Šmída, B., Vlček L., 2012. Venezuelan tepuis: their caves and biota. Acta Geologica Slovaca Monograph, Comenius University, Bratislava, pp. 168.

Aubrecht, R., Lánczos, T., Gregor, M., Schlögl, J., Šmída, B., Brewer-Carías, Ch., Vlcek, L., 2013. Reply to the Comment on "Sandstone caves on Venezuelan tepuis: Return to pseudokarst?". Geomorphology (DOI: 10.1016/j.geomorph.2012.11.017).

Ayub, S., 2006. Geology and geomorphology aspects of the deepest quartzite cave in the world. Proceedings of the 10th International Symposium on Pseudokarst, Gorizia, 94-100.

Barbieri, M., Masi, U., Tolomeo, L., 1984. Strontium geochemical evidence for the origin of the barite deposits from Sardinia, Italy. Economic Geology 79(6), 1360-1365.

Bechstadt, T., Boni, M., 1996. Sedimentological, stratigraphical and ore deposits field guide of the autochtonous Cambro-Ordovician of Southwestern Sardinia. Memorie descrittive della Carta Geologica d'Italia 48, 1-390.

Bennett, P.C., Melcer, M.E., Siegel, D.I., Hassett, J.P., 1988. The dissolution of quartz in dilute aqueous solutions of organic acids at 25°C. Geochimica et Cosmochimica Acta 52, 1521-1530.

Billi, S., Forti, P., Galli, E., Rossi, A., 2012. Robertsite: un nuovo fosfato scoperto nella Tagusan Cave (Palawan – Filippine). Atti del XXI Congresso Nazionale di Speleologia, Trieste, pp. 193-199.

Boni, M., Amstutz, G.C., 1982. The Permo-Triassic paleokarst ores of south-west Sardinia (Iglesiente-Sulcis): an attempt at a reconstruction of paleokarst conditions. In: Amstutz, G.C., Gorsy, A., Frenzel, G., Kluth, C., Moh, G., Wauschkuhn, A., Zimmerman, R.A., (Eds.), Ore genesis the state of the art. Berlin, Springer Verlag, 73-82.

Boni, M., Iannace, A., Pierre, C., 1988. Stable-isotope compositions of lower Cambrian Pb Zn Ba deposits and their host carbonates, Southwestern Sardinia, Italy. Chemical Geology: Isotope Geoscience section 72(3), 267-282.

Boni, M., Iannace, A., Köppel, V., Früh-Green, G., Hansmann, W., 1992. Late to Post-Hercynian hydrothermal activity and mineralization in Southwest Sardinia (Italy). Economic Geology 87, 2113-2137.

Brady, P.V., Walther, J.V., 1989. Controls on silicate dissolution rates in neutral and basic pH solutions at 25°C. Geochimica et Cosmochimica Acta 53, 2823-2830.

Brewer-Carías, C., Audy, M., 2011. Entrañas del mundo perdido. Charles Brewer-Carías (Ed.), Caracas, 290 p.

Burley, S.D., Kantorowicz, J.D., 1986. Thin section and S.E.M. textural criteria for the recognition of cement-dissolution porosity in sandstones. Sedimentology 33, 587-604.

Canfield, D.E., 2001. Biogeochemistry of sulfur isotopes. Reviews in Mineralogy and Geochemistry 43, 607-636.

Carmignani, L., Oggiano, G., Barca, S., Conti, P., Salvadori, I., Eltrudis, A., Funedda, A., Pasci, S., 2001. Geologia della Sardegna. Note illustrative della Carta Geologica della Sardegna a scala 1:200.000. Memorie Descrittive della Carta Geologica d'Italia, Istituto Poligrafico e Zecca dello Stato, Rome, pp. 1-283.

Carmignani, L., Funedda, A., Oggiano, G., Pasci, S., 2004. Tectono-sedimentary evolution of southwest Sardinia in the Paleogene: Pyrenaic or Apenninic Dynamic? Geodinamica Acta 17, 275-287.

Carreño, R., Nolla, J., Astort, J., 2002. Cavidades del Wei-Assipu Tepui, Macizo del Roraima, Brasil. Boletin Sociedad Venezolana de Espeleologia 36, 36-45.

Chalcraft, D., Pye, K., 1984. Humid tropical weathering of quartzite in south eastern Venezuela. Zeitschrift für Geomorphologie 28, 321-332.

Cortecci, G., Fontes, J.C., Maiorani, A., Perna, G., Pintus, E., Turi, B., 1989. Oxygen, sulfur, and strontium isotope and fluid inclusion studies of barite deposits from the Iglesiente-Sulcis mining district, southwestern Sardinia, Italy. Mineralium Deposita 24(1), 34-42.

De Vivo, B., Maiorani, A., Perna, G., Turi, B., 1987. Fluid inclusion and stable isotope studies of calcite, quartz and barite from karstic caves in the Masua Mine, southwestern Sardinia, Italy. Chemie der Erde 46(3-4), 259-273.

De Waele, J., Forti, P., Naseddu, A., 2013. Speleogenesis of a complex example of an exhumed sulphuric acid karst in Cambrian carbonates (Mount San Giovanni, Sardinia). Earth Surface Processes and Landforms, DOI: 10.1002/esp.3375.

De Waele, J., Frau, F., Muntoni, A., Cannas, C., 2008. Ritrovamento di Halloysite nella Grotta Eraldo (Barega, Iglesias, Sardegna sud-occidentale). Atti del XX Congresso Nazionale di Speleologia (Iglesias, Sardinia), Memorie dell'Istituto Italiano di Speleologia II(21), 245-254.

Doerr, S. H. 1999. Karst-like landforms and hydrology in quartzites of the Venezuelan Guyana shield: Pseudokarst or "real" karst? Zeitschrift fur Geomorphologie 43, 1-17.

Dove, P. M., 1999. The dissolution kinetics of quartz in aqueous mixed cation solutions. Geochimica et Cosmochimica Acta 63(22), 3715-3727.

Dove, P.M., Elston, S.F., 1992. Dissolution kinetics of quartz in sodium chloride solutions: Analysis of existing data and a rate model for 25°C. Geochim. Cosmochim. Acta 56, 4147-4156.

Dove, P.M., Nix, C.J., 1997. The influence of the alkaline earth cations, magnesium, calcium, and barium on the dissolution kinetics of quartz. Geochimica et Cosmochimica Acta 61(16), 3329-3340.

Dove, P.M., Rimstidt, J.D., 1994. Silica-water interactions. In "Silica: Physical Behavior, Geochemistry, and Materials Applications", ed. P.J. Heaney et al., pp. 1-40.

Ermakov, N.P., 1958. Genetic basis for classification of the deposits of crystal-optic raw materials. Memoirs of VNIIP, T.2, V.1, 5-12. (In Russian)

Ford, D.C., Williams, P., 2007. Karst Hydrogeology and Geomorphology. Willey & Sons, 562 p.

Franzini, M., Leoni, L., Saitta, M., 1972. A simple method to evaluate the matrix effects in X-Ray fluorescence analysis. X-Ray Spectrometry 1, 151-154.

Füchtbauer, H., 1988. Sedimente und Sedimentgesteine (Vol. 2). Schweizerbart'sche Verlagsanstalt, Stuttgart, 1141 pp.

Galdenzi, S., Maruoka, T., 2003. Gypsum deposits in the Frasassi caves, Central Italy. Journal of Cave and Karst Studies 65, 111-125.

Galli, E., Brigatti, M.F., Malferrari, D., Sauro, F., De Waele, J., 2013. Rossiantonite, $Al_3(PO_4)(SO_4)_2(OH)_2(H_2O)_{10}.4H_2O$, a new hydrated aluminium phosphate-sulfate mineral from Chimantha massif, Venezuela: description and crystal structure. American Mineralogist (in press).

Grassineau, N., Nisbert, E., Bickle, M., Fowler, C., Lowry, D., Mattey, D., Abell, P., Martin, A., 2001. Antiquity of the biological sulfur cycle: evidence from suflur and carbon isotopes in 2700 million year-old rocks of the Belingwe Belt, Zimbabwe. Proceedings of the Royal Society of London B 268, 113-119.

Hanor, J. S., 2000. Barite–celestine geochemistry and environments of formation. Reviews in Mineralogy and Geochemistry 40(1), 193-275.

Hill, C. A., 1987. Geology of Carlsbad cavern and other caves in the Guadalupe Mountains, New Mexico and Texas. New Mexico Bureau of Mines and Mineral Resources 117, 150 p.

Hill, C., Forti, P., 1997. Cave minerals of the world, second edition, National Speleological Society, Huntsville, 463 p.

Iler, R.K., 1955. The colloid chemistry of silica and silicates. Cornell University Press, Ithaca, New York, 324 p.

Jennings, J.N., 1983. Sandstone Pseudokarst or Karst? In: Young, R.W., Nanson, G.C. (Eds), Aspects of Australian Sandstone Landscapes. Australian and New Zealand Geomorphology Group Special Publication No.1, Wollongong, University of Wollongong: 21-30.

Jensen, M.L., Dessau, G., 1966. Ore deposits of south-western Sardinia and their sulphur isotopes. Economic Geology 61, 917-932.

Khalaf, F.I., 1990. Diagenetic alunite in clastic sequences, Kuwait, Arabian Gulf. Sedimentology 37, 155-164.

Klimchouk, A., 2012. Speleogenesis, Hypogenic. In: White, W.B., Culver, D.C., 2012. Encyclopedia of caves. Academic Press. New York: 748-765.

Knauss, K.G., Wolery, T.J., 1988. The dissolution kinetics of quartz as a function of pH and time at 70°C. Geochimica et Cosmochimica Acta 52, 43-53.

Kornilov, V.F., 1978. The temperature regime of formation of the mercury-antimony mineralization (Southern Kirghizia). In: Ermakov, N.P. (Ed.), Thermobarogeochemsitry of the Earth's Crust. Moscow, Nauka: 155-161. (In Russian)

Koski, R.A., 2012. Supergene ore and gangue characteristics in volcanogenic massive sulfide occurrence model. U.S. Geological Survey Scientific Investigations Report 2010-5070-C, chap. 12, 6 p.

Krauskopf, K.B., 1956. Dissolution and precipitation of silica at low temperatures. Geochimica et Cosmochimica Acta 10, 1-26.

Leoni, L., Saitta, M., 1976. X-ray fluorescence analysis of 29 trace elements in rock and mineral standards. Rendiconti Società Italiana di Mineralogia e Petrologia 32, 497-510.

Leoni, L., Menichini, M., Saitta, M., 1982. Determination of S, Cl, and F in silicate rocks by X-Ray fluorescence analyses. X-Ray Spectrometry 11, 156-158.

Leven, J.A., 1961. Problems of origin of optical-quality fluorite from deposits of the Zeravshan-Gissar Mountains. Transactions of The Samarkand University 16, 35-51. (In Russian)

Lovering, T.S., Tweto, O., Loweing, T.G., 1978. Ore deposits of the Gilman District, Eagle Country, Colorado. U.S. Geological Survey Professional Paper 1017, 90 p.

Ludwig, K.R., Vollmer, R., Turi, B., Simmons K.R., 1989. Isotopic constraints on the genesis of base-metal ores in southern and central Sardinia. European Journal of Mineralogy 1, 657-666.

Maltsev, V., 1997. Cupp-Coutunn Cave, Turkmenistan. In: Hill, C., Forti, P. (Eds.), Cave minerals of the world, 2nd ed., National Speleological Society, Huntsville, pp. 323-328.

Martini, J.E.J., 1979. Karst in Black Reef quarzite near Kaapsehoop, Eastern transval. Annals of South African Geological Survey 13, 115-128.

Martini, J.E.J., 1985. Les phénomènes karstiques de quartzites d'Afrique du Sud. Karstologia 9, 45-52.

Martini, J.E.J., 2000. Dissolution of quartz and silicate minerals. In: Klimchouk, A.B., Ford, D.C., Palmer, A.N., Dreybrodt, W. (Eds.), Speleogenesis. Evolution of karst aquifers. National Speleological Society, Huntsville, pp. 171-174.

Melka, K., Suchy, V., Zeman, A., Bosàk, P., Langrovà, A., 2000. Halloysite from karst sediments of the Koneprusy area: evidence for acid hydrothermal speleogenesis in the Bohemian karst, Czech Republic. Acta Universitatis Carolinae Geologica 44(2-4), 117-124.

Muraoka, Y., Kihara, K., 1997. The temperature dependence of the crystal structure of berlinite, a quartz-type form of $AlPO_4$. Physics and Chemistry of Minerals 24 (4), 243-253.

Onac, B.P., Effenberger, H.S., 2007. Re-examination of berlinite ($AlPO_4$) from the Cioclovina Cave (Romania). American Mineralogist 92, 1998-2001.

Onac, B.P., Forti, P., 2011a. Minerogenetic mechanisms occurring in the cave environment, an overview. International Journal of Speleology 40 (2), 1-20.

Onac, B.P., Forti, P. 2011b. State of the art and challenges in cave minerals studies. Studia UBB Geologia, 56, 33-42.

Onac, B.P., White, W.B., 2003. First reported sedimentary occurrence of berlinite ($AlPO_4$) in the phosphate bearing sediments from Cioclovina Cave (Romania). American Mineralogist 88, 1395-1397.

Onac, B.P., Zaharia, L., Kearns, J., Vereș, D., 2006. Vashegyite from Gaura cu Muscă Cave (Locvei Mountains, Romania): a new and rare phosphate occurrence. International Journal of Speleology 35(2), 67-73

Onac, B.P., Sumrall, J., Tămaş, T., Povară, I., Kearns, J., Dârmiceanu, V., Vereș, D., Lascu, C., 2009. The relationship between cave minerals and H_2S-rich thermal waters along the Cerna Valley (SW Romania). Acta Carsologica 38(1), 27-39.

Onac, B.P., Wynn, J.G., Sumrall, J.B., 2011. Tracing the sources of cave sulfates: a unique case from Cerna Valley, Romania. Chemical Geology 288, 105-114.

Padalino, G., Pretti, S., Tamburrini, D., Tocco, S., Uras, I., Violo, M., Zuffardi, P., 1973. Ore deposition in karst formations with examples from Sardinia. In: Amstutz, G.C., Bernard, C., (Eds.), Ores in sediments. Berlin, Springer Verlag, pp. 209-220.

Perruchot, A., Dupuis, C., Brouard, E., Niçaise, D., Ertus, E.T.R., 1997. L'halloysites karstique: comparaison des gisements types de Wallonie (Belgique) et du Perigord (France). Clay Minerals 32(2), 271-287.

Piccini, L., Mecchia, M., 2009. Solution weathering rate and origin of karst landforms and caves in the quartzite of Auyan-tepui (Gran Sabana, Venezuela). Geomorphology 106, 15-25.

Pillola, G.L., 1989. Trilobites du Cambrien inférieur du SW de la Sardaigne, Italie. Paleontographica Italica 78, 1-174.

Piovan, U., Violo, M., 1965. Contributo alla conoscenza delle "Quarziti della zona di Iglesias". Atti Symposium AMS, sez I, 1-23.

Plan, L., Tschegg, C., De Waele, J., Spötl, C., 2012. Corrosion morphology and cave wall alteration in an Alpine sulfuric acid cave (Kraushöhle, Austria). Geomorphology 169/170, 45-54.

Polyak, V.J., Güven, N., 1996. Alunite, natroalunite and hydrated halloysite in Carlsbad Cavern and Lechuguilla Cave, New Mexico. Clays and Clay Minerals 44(6), 843-850.

Rimstidt J.D., 1997. Quartz solubility at low temperatures. Geochimica et Cosmochimica Acta 61, 2553-2558.

Sauro, F., Piccini, L., Mecchia, M., De Waele, J., 2013a. Comment on "Sandstone caves on Venezuelan tepuis: Return to pseudokarst?" by R. Aubrecht, T. Lánczos, M. Gregor, J. Schlögl, B. Smída, P. Liscák, Ch. Brewer-Carías, L. Vlcek, Geomorphology 132, 351-365. Geomorphology, http://dx.doi.org/10.1016/j.geomorph.2012.11.015

Sauro, F., Tisato, N., De Waele, J., Bernasconi, S.M., Bontognali, T.R.R., Galli, E., 2013b. Origin of sulphates and rare sulphate-phosphate minerals in the quartz-arenite caves of the tepuis table mountains, Bolivar State, Venezuela. Earth and Planetary Science Letters (submitted)

Siever, R., 1962. Silica solubility, 0-200° C and the diagenesis of siliceous sediments. Journal of Geology 70, 127-150.

Stumm, W., Morgan, J.J., 1981. Aquatic chemistry. 2nd ed., Wiley and Sons, 780 p.

Tsykin, R.A., 1989. Paleokarst of the Union of Soviet Socialistic Republics. In: Bosák, P., Ford, D.C., Głazek, J., Horáček, I. (Eds.). Paleokarst: a systematic and regional review, Vidala Academia, Praha, pp. 253-295.

Urbani, F., 1980. Lista de minerales secundarios encontrados en cuevas de Venezuela. El Guácharo 21, 44.

Vollmer, R., Turi, B., Simmons, K.R., Perna, G., 1989. Isotopic constraints on the genesis of base-metal ores in southern and central Sardinia. European Journal of Mineralogy 1, 657-666.

Willems, L., Rodet, J., Pouclet, A., Melo, S., Rodet, M.J., Compère, Ph., Hatert, F., Auler, A.S., 2008. Karsts in sandstones and quartzites of Minas Gerais, Brazil. Cadernos Lab. Xeolóxico de Laxe 33, 127-138.

Wray, R.A.L., 1997. A global review of solutional weathering forms on quartz sandstones. Earth Science Reviews 42, 137-160.

Wray, R.A.L., 2000. The Gran Sabana: The World's Finest Quartzite Karst? In: Migon, P. (Ed.), Geomorphological Landscapes of the World. Springer, pp. 79-88.

Zawidzki, P., Urbani, F., Koisar, B., 1976. Preliminary notes on the geology of the Sarisariñama plateau, Venezuela, and the origin of its caves. Boletin Sociedad Venezolana de Espeleologia 7, 29-37.

SECOND SECTION

SECONDARY CAVE MINERALS

CHAPTER 3.1

Published In American Mineralogist, 98, 1906-1913

ROSSIANTONITE, $AL_3(PO_4)(SO_4)_2(OH)_2(H_2O)_{10}\cdot 4H_2O$, A NEW HYDRATED ALUMINIUM PHOSPHATE-SULFATE MINERAL FROM CHIMANTA MASSIF, VENEZUELA: DESCRIPTION AND CRYSTAL STRUCTURE

Ermanno Galli[1], Maria Franca Brigatti[1]*, Daniele Malferrari[1], Francesco Sauro[2,3] and Jo De Waele[2,3]

1) Dipartimento di Scienze Chimiche e Geologiche - Università di Modena e Reggio Emilia. Largo S. Eufemia 19, I-41121, Modena, Italy

2) Dipartimento di Scienze Biologiche, Geologiche e Ambientali, Italian Institute of Speleology. Via Zamboni 67, 40126, Bologna, Italy

3) Associazione di Esplorazioni Geografiche La Venta, Via Priamo Tron 35/F, 31100, Treviso, Italy

Corresponding Author: Maria Franca Brigatti

Abstract

Rossiantonite, ideally $Al_3(PO_4)(SO_4)_2(OH)_2(H_2O)_{10}\cdot 4H_2O$, triclinic (space group *P*-1), *a* = 10.3410(5), *b* = 10.9600(5), *c* = 11.1446(5) Å, α = 86.985(2), β = 65.727(2), γ = 75.064(2)º, *V* = 1110.5(1) $Å^3$, *Z* = 2, is a new mineral from the Akopan-Dal Cin cave system in the Chimanta massif (Guyana Shield, Venezuela). The mineral occurs as small (≤ 0.15 mm) and transparent crystals in a white to slightly pink fine-grained sand, filling spaces between boulders of weathered quartz sandstone. Associated phases are gypsum, sanjuanite, rare alunite, quartz and micro-spherules of amorphous silica.

Rossiantonite is colorless with a white streak and vitreous luster. The mineral is brittle with irregular to sub-conchoidal fracture and it shows a poorly developed cleavage. Rossiantonite is biaxial and not pleochroic, with mean refractive index of 1.504.

The calculated density is 1.958 g cm^{-3}. Electron microprobe analyses, with H_2O measured by thermogravimetric analysis, provided the following empirical formula based on 28 O *apfu*: $Al_{2.96}Fe_{0.03}P_{1.01}S_2H_{30.02}O_{28.}$ The five strongest lines in the X-ray powder diffraction pattern, expressed as *d* (Å), *I*, (*hkl*), are: 4.647, 100, (210); 9.12, 56, (100); 4.006, 53, (220); 8.02, 40, (110); 7.12, 33, (011).

The crystal structure, refined using 3550 unique reflections to *R* = 0.0292, is constituted by P and Al rings, originating complex chains along the **b** by sharing the OH-OH edge belonging to the Al(3)

polyhedron. Three symmetrically independent Al sites can be identified, namely: Al(1), Al(2) and Al(3). Tetrahedral sites, occupied by P, share all their apexes with Al. Not shared octahedral apexes are occupied by water molecules. Four more water molecules are placed in between the previously identified chains. Two tetrahedra, occupied by S atoms, are connected along the chains by means of weak hydrogen bonding. Rossiantonite structure show similarities with minerals belonging to the sanjuanite-destinezite group

Keywords: rossiantonite, aluminium-phosphate-sulfate, Chimanta massif, crystal chemistry, crystal structure.

3.1.1 Introduction

Rossiantonite is a new mineral species that has been found in the Akopan-Dal Cin cave system. This latter is located in Chimanta massif, a sandstone table mountain of the Guyana Shield outcropping in the protected area of the Canaima National Park (Venezuela). The mineral is genetically closely associated to sanjuanite [$Al_2(PO)_4(SO)_4OH{\cdot}9H_2O$] (De Abeledo et al., 1968; Colombo et al., 2011) and shows the same essential chemical elements of hotsonite (Beukes et al, 1985), kribergite (Du Rietz, 1945) and of the unnamed mineral UM1940-01-SO: AlHP (Smith and Nickel, 2007), differing substantially, however, from all of these because of its peculiar stoichiometry.

The mineral is named after Antonio Rossi (1942 –2011), professor of Sedimentary Petrology at Modena and Reggio Emilia University and a precursor of scientific speleology in Italy, to further recognize his constant and precious efforts devoted to the study of minerals and, especially, of cave minerals.

The new mineral and mineral name were approved by the Commission on New Minerals, Nomenclature and Classification, IMA no. 2012-056 . The holotype material is deposited at the British Museum (registration number BM 2012,99), at the “Museo Mineralogico e Geologico Estense, GEMMA1786” of Modena and Reggio Emilia University, Italy (registration number 2/2012) and at ETH Mineralogical collection (Zurich), catalogue number 20130.

3.1.2 Occurrence and paragenesis

The mineral was collected by one of the authors (F.S.) inside the Akopan-Dal Cin cave system in the Akopan Tepui, representing the southern sector of the Chimanta massif (5°10'52''N 61°57'50''W; Mecchia et al., 2009). The cave develops inside the quartz sandstone of the Roraima Group. The sedimentary formations of this Group show continental to pericontinental facies with an age of approximately 1.8 Ga (Briceño and Schubert, 1990; Santos et al., 2003). Low grade metamorphism, with quartz–pyrophyllite paragenesis in the more arkosic beds, is interpreted as the result of the lithostatic load of the overburden from ~3 km thick sediments which are now eroded (Urbani, 1996).

Metamorphism is responsible for quartz overgrowth between the grains thus imparting saccharoidal texture to the quartz sandstone. The cave originated with the Mataui Formation, consisting of orthoquartzites and subarkoses with subordinate medium- to fine-grained lithic rocks.

The cave originated from a weathering process involving: dissolution of silica cements or quartz grain overgrowths and consequent “arenisation” of the orthoquarzites; piping and mechanical erosion; transport of the loose quartz grains (Wray, 1997; Martini, 2000).

Sample containing rossiantonite was collected on the floor of a dry passage near the entrance of Cueva Akopan. This sample is a white to slightly pink, fine-grained, light sand, composed of grains of different minerals, between boulders of weathered quartz sandstone, also containing gypsum, sanjuanite, rare alunite, quartz and micro-spherules of amorphous silica. The ceiling above sampling spot shows many silica speleothems, similar to those described by Aubrecht et al. (2008), probably originating, after breaking, previously mentioned microspherules of amorphous silica.

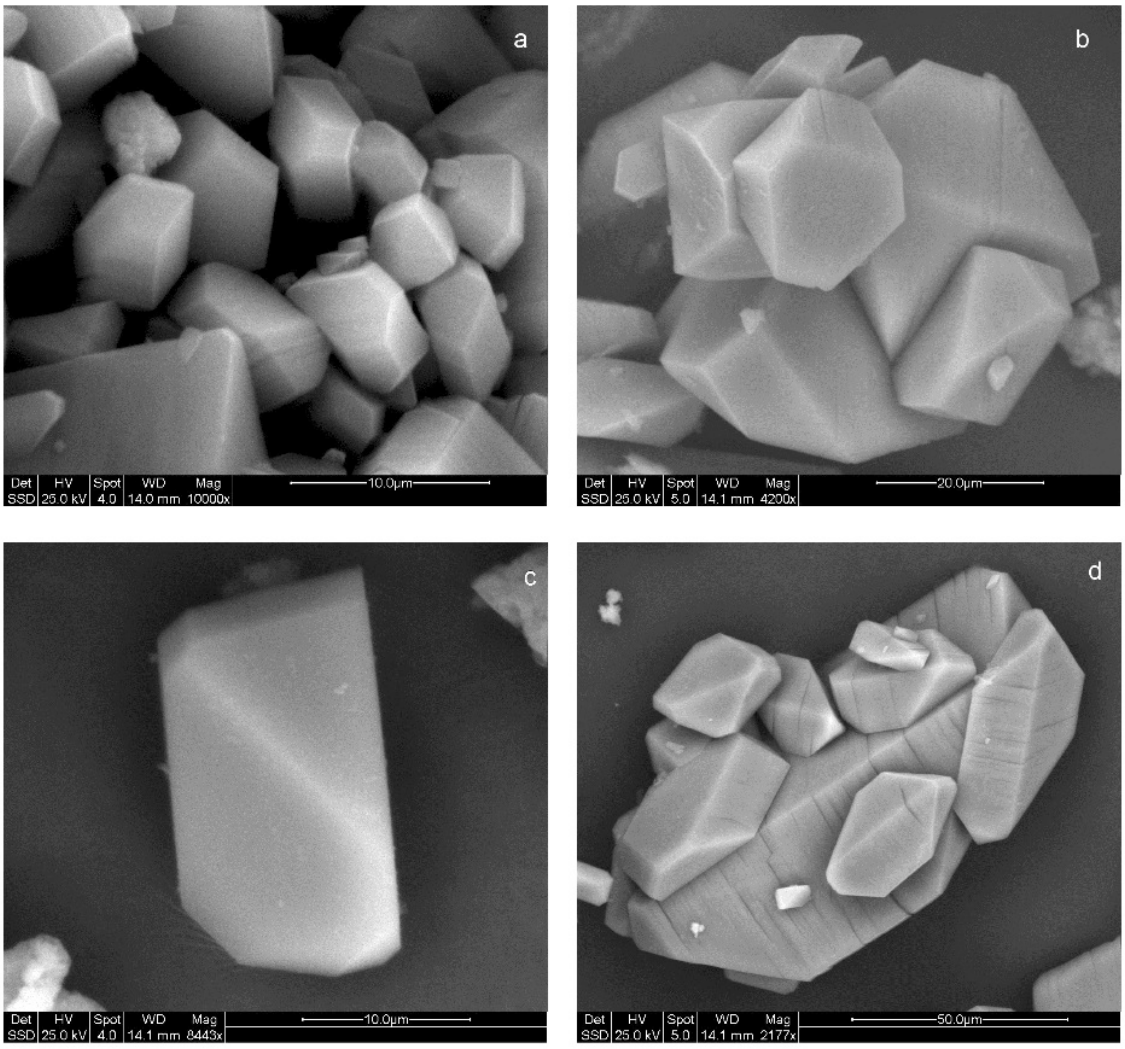

Fig. 1. SEM image of rossiantonite from the Akopan-Dal Cin cave system, Chimanta massif, Guyana Shield, Venezuela. a and b) crystal aggregates; c) individual crystals; d) crystal aggregates evidencing the damage produced by H_2O loss after exposure to electron beam.

3.1.3 Physical and optical properties

Rossiantonite forms aggregates of prismatic euhedral crystals, approximately 0.15 mm in size (Figure 1). The mineral is colorless and shows a white streak. Crystals are transparent with vitreous luster. Under ultraviolet light, the mineral shows dim green color, regardless of excitation frequency. The tenacity is brittle, the fracture is irregular or sub-conchoidal, and crystals exhibit no cleavage. No twinning is observed. Density and hardness could not be measured because of experimental limitations in separating pure single grains large enough for the purpose. The calculated density is 1.958 g cm^{-3} (on the basis of the empirical formula). Rossiantonite dissolves very easily in cold, dilute HCl/H_2O (1:1).

The optical properties could not be fully determined because of the small size of the crystals. Under plane-polarized reflected light, rossiantonite appears moderately birifrangent and not pleochroic with a mean refractive index, $\overline{n}$ = 1.504.

The Gladstone-Dale compatibility index, as defined by Mandarino (1981), provides an assessment of consistency for the average index of refraction, calculated density, and chemical composition. The compatibility index $[1 – (K_P/K_C)]$ for rossiantonite is 0.012 (superior). The mineral is biaxial. Extinction is approximately parallel to the direction of prism elongation and the interference colors vary from light grey to light cyan.

3.1.4 Chemical composition

The chemical composition of rossiantonite was measured with a Cameca SX 50 electron microprobe (EDS mode) on several crystals. A preliminary examination with successive 10 s analytical intervals revealed that the mineral was sensitive to the electron beam, with a monotonic increase in S, P and Al concentrations with time, possibly because of partial dehydration of the crystals during the experiments. Therefore, the sample was analyzed with a low beam current (2 nA), a scanning beam of 1μm on both standards and sample and short counting times (10 s). The following standards were used: synthetic Al_2O_3 (Al), synthetic Fe_2O_3 (Fe), barite (S), apatite (P).

The point analyses from a same fragment and among different fragments were observed to be homogeneous. The value of H_2O = 41.30 wt%, reported in the chemical analysis, was experimentally determined by means of thermogravimetric analysis, including evolved gas mass spectrometry, and thus associated to mass loss specifically related to H_2O.

Degassing under vacuum, following electron beam action in the microprobe chamber, is well documented for hydrated minerals. The sum obtained adding the experimentally determined H_2O value to the oxide percentages is usually greater than 100%. For the investigated mineral, the sum obtained for (Al_2O_3+ Fe_2O_3 + SO_3 + P_2O_5) is 74.96 instead of 58.70 wt%. For this reason the oxide

percentages, without water, were recalculated to 58.70wt%. Recalculation was carried out for all analytical points (11 point analysis) before averaging. Analytical data are given in Table 1.

The empirical formula (based on 28 O apfu) is $Al_{2.96}$ $Fe_{0.03}$ P S_2 $H_{30.02}$ $O_{28.}$ The structural formula is $Al_3(PO_4)(SO_4)_2(OH)_2(H_2O)_{10}{\cdot}4H_2O$, which requires Al_2O_3 = 23.37, P_2O_5 = 10.85, SO_3 = 24.47, H_2O = 41.31, total 100.00 wt%.

Table 1. Chemical composition of rossiantonite. Note: The wt% were recalculated to match results from microprobe and thermal analysis. See text for details. σ = standard deviation

Constituent	wt%	Range	σ
Al_2O_3	23.07	22.72-23.41	0.16
Fe_2O_3	0.30	0.17-0.50	0.01
SO_3	24.44	23.92-24.93	0.11
P_2O_5	10.89	10.60-11.09	0.02
H_2O	41.30		
Total	100.00		

3.1.5 Thermal analysis

Thermogravimetry (TG), differential thermal analysis (DTA) and derivative thermogravimetric curves (Figure 2a) were obtained simultaneously and were performed with a Seiko SSC 5200 thermal analyzer equipped with a quadrupole mass spectrometer (ESS, GeneSys Quadstar 422) to analyze gases evolved during thermal reactions. This device samples gases via an inert, fused silicon capillary system, heated to prevent gas condensing. Analyses of evolved gas phases were carried out in Multiple Ion Detection mode (MID), which allows the qualitative determination of evolved masses *vs*. temperature or time. The ion current curves of the evolved phases are shown in Figure 2b. The heating rate and the temperature range were set at 10°/min and 20-1200°C, respectively. The total weight loss was 64.8%. Two ranges of weight loss can be identified from the TG curve:

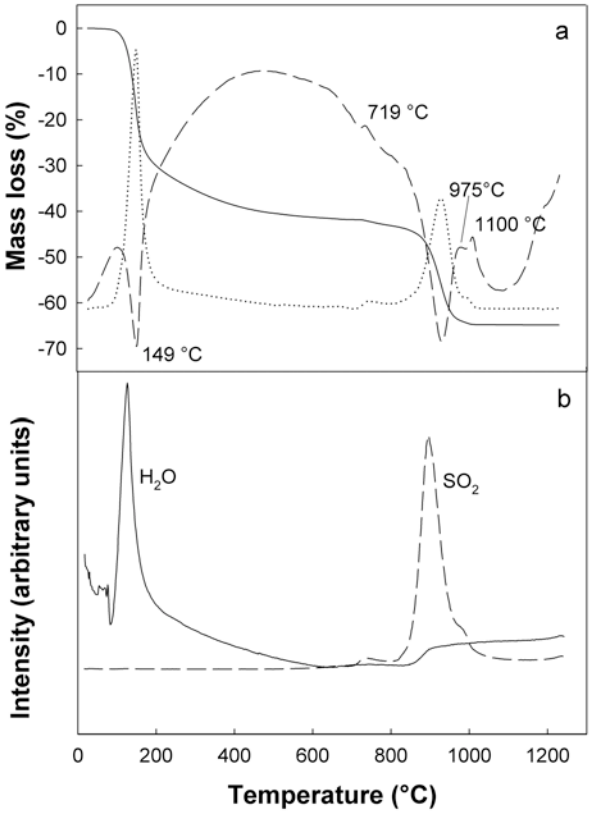

Fig. 2. (a) Thermogravimetric (solid line), derivative thermogravimetric (pointed line) and thermodifferential (dashed line) curves for rossiantonite. (b) Mass spectra of evolved gases during thermal analysis. Solid line H_2O (mass/charge ratio 18 uma); dashed line SO_2 (mass/charge ratio 64 uma).

the first interval (20-500°C) evidences a very strong endothermic reaction with a maximum at 149°C attributed, as confirmed by mass spectrometry, to water molecules only. The related weight loss is 41.30 wt%. The second interval shows a reaction at 719°C, connected to the formation of $Al_2(SO_4)_3$ (millosevichite-like structure), as indicated by powder X-ray diffraction on sample heated at 780°C, and a strong maximum at 975°C, giving a reduction of 21.0 wt %, associated to the release of SO_2 (Figures 2). The endo-exothermic reaction between 975 and 1100°C corresponds to the formation of $AlPO_4$ (berlinite-like structure). All these conclusions were confirmed by XRD analysis on phases generated after each thermal reaction.

3.1.6 Infrared spectroscopy

Infrared spectrum was recorded with an ATR Golden Gate (BRUKER - VERTEX 70) in the range 4000-600 cm^{-1} (Figure 3). The mineral contains four vibrational spectroscopically distinct units, namely phosphate, sulfate and hydroxyl units as well as water. Each one of these groups shows its own characteristic spectrum, which is generally different from the spectra of other units. The infrared spectrum of the hydroxyl stretching region (2400-3800 cm^{-1}) of rossiantonite is complex with a series of overlapping bands.

In the region 2400-3800 cm^{-1} infrared bands are observed at 2968, 3148, 3349, 3454, and 3519 cm^{-1}. The band at 3519 cm^{-1} can be assigned to the OH stretching vibration of the hydroxyl units. The effects at 3454, 3349, and 3148 cm^{-1} are related to the stretching mode $\nu_3(H_2O)$ of the two types of H_2O in the structure (i.e. H_2O related to Al centred octahedra and H_2O between tetrahedral and octahedral chains). The band at a lower wavenumber (2968 cm^{-1}) is attributed to strongly hydrogen-bonded water (Frost and Palmer, 2011).

The shoulder at 1608 and the band at 1672 cm^{-1} represent weakly hydrogen and strongly hydrogen bonded water (Frost and Palmer, 2011). In the region 650-1200 cm^{-1}, the spectrum is dominated by the band at 986 cm^{-1} assigned to the $(PO_4)^{3-}$ ν_1 symmetric stretching band. The band observed at 1042 cm^{-1} is assigned to the $(SO_4)^{2-}$ ν_1 symmetric stretching mode. As observed by Frost and Palmer (2011), the sulfate and phosphate stretching modes are possibly coupled, thus giving the intense band at 986 cm^{-1}. The bands at 1109 and 1143 cm^{-1} are attributed to

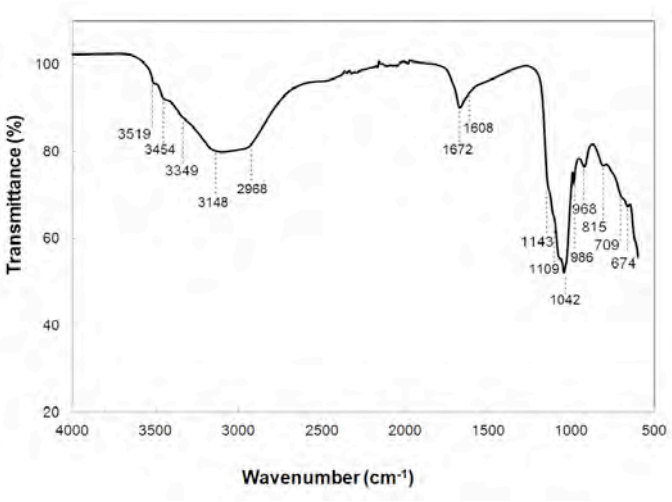

Fig. 3. Infrared spectrum of rossiantonite in the range 4000-600 cm^{-1}

the ν_3 antisymmetric stretching modes of $(PO_4)^{3-}$ and $(SO_4)^{2-}$. These values well match data reported for other phosphate-sulfate minerals (Colombo et al., 2011). Bands at 709 and 674 cm^{-1} are associated to vibrational modes involving H_2O molecules in a crystalline environment (Assaoudi and Ennaciri, 1997). The sharp band at 1042 cm^{-1} and that at 815 cm^{-1} are related to $\nu_3(PO_4)^{3-}$ and to Al-O-P antisymmetric stretching, respectively.

TABLE 2. X-RAY POWDER DIFFRACTION DATA FOR ROSSIANTONITE.

I_{REL}	2θ	D_{OBS}	D_{CALC}	*HKL*	I_{REL}	2θ	D_{OBS}	D_{CALC}	*HKL*
11	8.34	10.61	10.57	0 1 0	4	34.458	2.603	2.602	2 -1 4, -1 -4 1
32	8.71	10.16	10.14	0 0 1	2	35.357	2.539	2.536	4 1 1
56	9.69	9.12	9.11	1 0 0	1	35.602	2.522	2.523	3 0 4, 3 -2 1, 0 4 1
10	10.00	8.84	8.82	1 0 1	4	35.927	2.500	2.500	0 -1 4, 4 0 2, 2 4 2
40	11.04	8.02	8.00	1 1 0	4	36.373	2.470	2.471	1 4 2, 4 1 3
16	11.70	7.56	7.55	0 -1 1	3	36.362	2.432	2.433	0 1 4, 1 -2 4
33	12.43	7.12	7.11	0 1 1	1	37.194	2.417	2.417	-3 1 1
2	14.31	6.19	6.19	1 -1 1	3	37.406	2.404	2.403	0 -4 2, 1 -4 1, 4 0 3
22	15.50	5.72	5.71	-1 0 1	2	37.768	2.382	2.378	1 -4 0
6	16.11	5.50	5.49	1 0 2	3	38.305	2.350	2.347	3 4 2
2	16.74	5.30	5.28	0 2 0	4	38.631	2.331	2.332	-2 -1 3
3	17.49	5.07	5.07	1 1 2	3	39.327	2.291	2.287	0 4 2
29	17.74	5.00	4.99	2 0 1, 1 2 1	2	39.573	2.277	2.277	4 0 0
12	18.423	4.816	4.806	0 -2 1	4	39.895	2.260	2.257	4 -1 1
100	19.101	4.647	4.642	2 1 0	3	40.303	2.238	2.239	4 3 3, -1 4 1, 0 2 4
14	19.371	4.582	4.575	0 2 1	3	40.562	2.224	2.224	-1 -1 4
5	19.834	4.476	4.469	0 1 2	2	41.21	2.191	2.193	3 4 3, 1 4 3, 1 5 0
2	20.111	4.416	4.408	2 0 2	2	41.716	2.165	2.162	-2 -4 2
3	20.503	4.332	4.324	-1 -2 1	2	42.309	2.136	2.136	1 -1 5, 1 1 5
7	21.110	4.209	4.202	2 2 1	2	42.984	2.103	2.101	4 4 2, -2 -3 3
7	21.495	4.134	4.126	2 -1 1, 1-2 0	3	43.192	2.095	2.095	0 -5 1, -3 1 2
53	22.190	4.006	4.001	2 2 0	3	43.826	2.066	2.065	2 -4 0
18	23.149	3.842	3.836	2 -1 0	< 1	44.798	2.023	2.025	4 4 3
27	23.321	3.814	3.808	2 -1 2, -1 0 2	10	45.285	2.003	2.002	0 3 4, 5 1 1
28	23.528	3.781	3.774	2 2 2, 0 -2 2	2	46.112	1.969	1.966	-1 2 4
5	23.960	3.712	3.706	1 0 3, -2 -1 1	3	46.858	1.939	1.937	5 0 1, -3 -1 3, -2 4 1
12	24.468	3.638	3.633	-2 0 1	1	47.443	1.915	1.915	3 -3 4, -3 -2 3
15	25.235	3.529	3.523	0 3 0, 1 3 1	2	47.646	1.909	1.907	-2 0 4
8	25.501	3.493	3.487	2 0 3	4	48.405	1.881	1.881	4 -1 5

9	25.749	3.460	3.455	2 1 3	3	49.098	1.856	1.857	0 2 5, 2 0 6, -4 -4 1
12	25.991	3.428	3.423	-1 1 2	2	50.023	1.823	1.827	-1 0 5
15	26.372	3.380	3.381	0 0 3, -2 -2 1	2	50.491	1.808	1.805	-1 -4 4
5	26.587	3.353	3.352	3 1 2	1	51.041	1.789	1.790	2 -5 1, -1 3 4, -1 -2 5
9	27.200	3.279	3.278	0 -1 3	6	51.932	1.761	1.761	2 6 2
2	27.487	3.245	3.240	2 -2 1	2	53.244	1.719	1.718	0 6 1, 6 2 3
5	27.742	3.216	3.217	-2 1 1	2	53.485	1.713	1.712	-2 2 4
3	28.454	3.137	3.133	3 2 2	3	54.39	1.687	1.685	0 -1 6
7	28.815	3.098	3.097	1 3 2	2	55.083	1.667	1.668	5 -2 4, 2 6 3
4	29.412	3.037	3.036	3 0 0	< 1	55.553	1.654	1.655	4 3 6, 0 1 6, -3 -2 4
24	29.888	2.990	2.988	3 2 0	< 1	56.109	1.639	1.638	5 1 6, -2 -1 5
9	30.335	2.947	2.942	3 -1 1	3	57.413	1.605	1.607	-4 0 3, 3 5 5, -2 4 3
5	30.769	2.906	2.903	-2 -1 2	< 1	58.3	1.583	1.583	0 2 6, 2 5 5
4	31.345	2.854	2.850	1 -3 2	1	59.036	1.563	1.563	-5 -1 2
21	31.849	2.810	2.807	3 3 1	1	59.25	1.560	1.559	2 -1 7, 2 7 1, -2 5 2, -2 -3 5
2	32.328	2.769	2.765	-1 3 1	< 1	60.096	1.540	1.539	4 -4 0
4	32.569	2.749	2.747	-2 -2 2	2	60.764	1.523	1.524	-4 -4 3
4	33.524	2.673	2.673	1 1 4	2	60.99	1.519	1.518	3 7 0
7	34.085	2.630	2.630	-1 -2 3, 2 4 1	2	61.428	1.509	1.510	0 7 0, 6 5 2

3.1.7 X-Ray diffraction

3.1.7.1 Powder diffraction

The X-ray powder-diffraction pattern (Table 2) was recorded on a PANalytical X'Pert PRO diffractometer using monochromatic Cu$K\alpha_1$ radiation and calibrated with silicon as internal standard. Reflections were indexed using the results of the single-crystal study. The intensities of calculated powder lines, based on the structure determination, demonstrate generally good agreement between the observed and calculated patterns. Similarly, unit cell parameters, refined by least-square routine using the whole pattern, confirmed a triclinic cell a triclinic cell with a = 10.3415(3), b = 10.9580(3), c = 11.1445(3) Å, α = 86.968(4), β = 65.757(3), γ = 75.055(3)º, V = 1110.57(4) Å^3 in close agreement with parameters obtained from single-crystal study.

3.1.7.2 Single-crystal diffraction

Some rossiantonite crystals, optically homogeneous and inclusion-free, were selected for single-crystal X-ray study and analyzed with a Bruker X8 APEX four circle diffractometer combined with APEX 4K CCD detector, flat graphite monochromator and Mo$K\alpha$-radiation from a fine focus sealed tube. Unit-cell dimensions, determined by least-squares refinement of the setting angles of 25 high-θ reflections (15 < θ < 22°), show nearly identical values among investigated crystals. Data collection

Table 3. Data collection and structure refinement details for rossiantonite

Crystal size (mm)	0.12× 0.07×0.03
Diffractometer	Bruker X8 APEX
X-ray radiation/power	Mo*K*α (λ = 0.71075)(Å)/30kV, 52mA
Temperature (K)	298(2)
Structural formula	$Al_3(PO_4)(SO_4)_2(OH)_2(H_2O)_{10}\cdot 4H_2O$
Space group	$P\bar{1}$
Unit-cell dimensions	*a* = 10.3410(5) Å *b* = 10.9600(5) Å *c* = 11.1446(5) Å α = 86.985(2)° β = 65.727(2)° γ = 75.064(2)º
Volume (Å^3)	1110.5(1)
Z	2
Measured reflections	15073
Reflection with I>2σ(I)	3550
Refined parameters	438
θ range	1.93-24.25°
Index ranges	-11 ≤ *h* ≤ +11 -12 ≤ *k* ≤ +12 -12 ≤ *l* ≤ +10
Completeness to θ = 24.25° (%)	99.1
R_{int}	0.0449
Refinement method	Full-matrix least-squares on F^2
R [F^2>2σ(I)]	0.0292
wR (F^2)	0.0643
Goodness of Fit	0.944

was carried out on the crystal showing the best diffraction quality. The SMART system of programs was used for unit-cell determination and X-ray data collection. Redundant data were collected for an approximate sphere of reciprocal space and processed using the Bruker AXS program SAINT+ (Bruker, 1999). A Gaussian absorption correction was performed using a linear absorption coefficient (μ) of 1.90 mm^{-1}. The absorption correction, space group determination, and data merging were performed using XPREP, a part of the SHELX-97 software package (Sheldrick, 1997). The details of the data collection and the final structure refinement are provided in Table 3.

The structure was solved by direct methods using SIR2004 (Burla et al. 2005). SHELXL-97 software (Sheldrick, 2008) was used, with neutral atom scattering factors, for the refinement of the structure. The *E* statistics indicate that the structure is centrosymmetric. The structure was solved and refined in space group $P\bar{1}$. Direct methods provided the locations of all cation sites and of several O sites. The other O sites and all H sites were located on difference-Fourier maps.

The structure was refined by a combination of least-squares refinement and difference-Fourier synthesis to an *R* index of 0.0292 using soft constraints for the O–H distances. The maximum and minimum residual electron-density peaks are 0.52 and –0.27 e/Å^{-3} respectively. Final atomic parameters are listed in Table 4, selected interatomic distances are given in Table 5. Table 6[1] gives bond-valence values calculated from the parameters of Brown and Altermatt (1985).

3.1.8 Description of the structure

3.1.8.1 Overview of structure topology

Figure 4a represents a projection of the polyhedral structure down the **c***. Figure 4b details the chain developing along **b**. From these images it is well evident that the rossiantonite structure is dominated by chains extending parallel to **b**.

The repeating subunit of the chain consists of three symmetry-independent AlX_6 octahedra (X = O, OH, H_2O) and a PO_4 tetrahedron. $Al(1)X_6$ and $Al(2)X_6$ octahedra share a common vertex (i.e., O(5)h). The PO_4 tetrahedron shares one vertex with Al(2) and Al(3) octahedra, i.e., O2 and O1 anion sites, respectively, and two vertices with the Al(1) octahedron (i.e., O(3) and O(4) anions) forming three-member polyhedral rings. These rings form ideally infinite chains by sharing one edge (i.e., O(13)h-O(13)h octahedral edge), of two adjacent Al(3) octahedra (Figure 4b). The structure is completed by two symmetrically independent SO_4

tetrahedra and by four H_2O sites (Figure 4a).

The topology of the chain in rossiantonite appears to be unique, based on our review on sulfate and phosphate structures. However the pattern, where a tetrahedron occupied by P forms 3-membered ring subunits with octahedra occupied by Al, constituting chains developing indefinitely, is observed in other sulfate and phosphate structures, such as those of destinezite and sanjuanite (Peacor et al., 1999; Colombo et al., 2011).

3.1.8.2 Cation sites

The rossiantonite polyhedral structure is constituted by a tetrahedral P position, by two tetrahedral S [(S(1) and S(2)] positions and by three symmetrically distinct octahedral Al positions, namely Al(1),

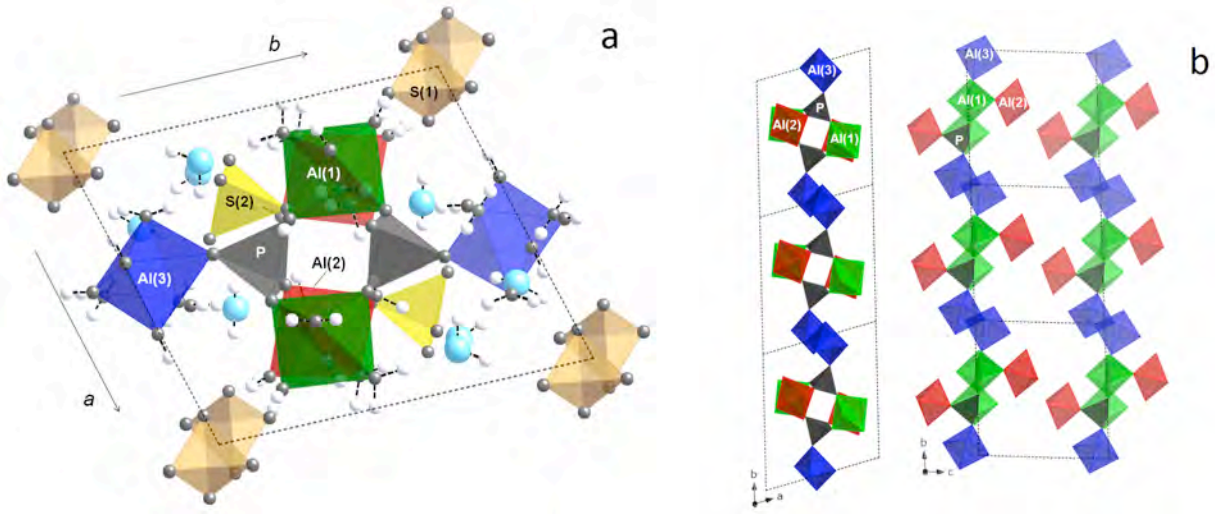

Fig. 4. (a) Projection of the structure along [001]. Filled polyhedra: green [Al(1)], red [Al(2)], blue [Al(3)], grey (P), orange [S(1)], yellow [S(2)]. Spheres: grey (oxygen atoms), light blue (water molecules), white (hydrogen atoms). Hydrogen bonds are shown as thin black dashed lines. (b) chain development in the structure. S polyhedra and water molecules were omitted.

Al(2) and Al(3).

The P site is completely occupied by P and coordinated by four O atoms, i.e., O(1), O(2), O(3), O(4), showing an average ⟨P-O⟩ distance of 1.527 Å (range 1.520(2) - 1.542(2) Å, Table 5), which is similar to with the average ⟨P-O⟩ distance of 1.537 (range 1.439-1.625 Å) given by Huminicki and Hawthorne (2002) for well-refined phosphate minerals. Bond valence calculation (Table 6[1]) and bond lengths (Table 5) strongly indicate a complete occupancy of this site by P.

Bond-length and bond-valence values suggest that the Al(1) octahedron $[Al(1)O_2(OH)(H_2O)_3]$ is coordinated by two oxygen atoms [O(3) and O(4)] shared with a PO_4 tetrahedron, by an OH group i.e., O(5)h, shared with the Al(2) octahedron and by three water molecules at the unshared corners, i.e., O(6)w, O(7)w and O(8)w positions (Tables 5 and 6[1]). The ⟨Al(1)-O ⟩ distance is 1.896 Å, with bond lengths ranging from 1.853(2) to 1.937(2) Å. The Al(1) complex coordination pattern produces a distorted polyhedron (bond length distortion, BLD = $\langle[(Al\text{-}O)_i - \langle Al\text{-}O\rangle]\rangle/\langle Al\text{-}O\rangle \times 100 = 1.34$). The three longer distances are related to Al(1)-OH_2 bonds.

The Al(2) octahedron $[Al(2)O(OH)(H_2O)_4]$ is coordinated by one oxygen atom [O(2)] shared with the PO_4 tetrahedron, by one OH group [O(5)h] that is shared with the Al(1) octahedron, as previously indicated, and by four H_2O molecules, namely O(9)w, O(10)w, O(11)w, and O(12)w positions. The ⟨Al(2)-O ⟩ is 1.893 Å, with bond lengths ranging from 1.807(2) to 1.964(2) Å and bond length distortion, BLD = 2.34%.

The Al(3) octahedron $[Al(3)O(OH)_2(H_2O)_3]$ is coordinated by one oxygen atom [O(1)] shared with the PO_4 tetrahedron, by two OH group [O(13)h], which constitute the edge shared between two adjacent Al(3) octahedra, and by three water molecules, namely O(14)w, O(15)w and O(16)w. The ⟨Al(3) – O⟩ distance is 1.889 Å, with bond lengths ranging from 1.842(2) to 1.948(2) Å. The calculated bond length distortion BLD is 1.92%. The octahedron showing greatest distortion is Al(2), which is also characterized by sharing four water molecules instead of three, as observed for Al(1) and Al(3).

The structure contains two S sites, i.e., S(1) and S(2) coordinated by four oxygen atoms in a quite regular tetrahedral arrangement. ⟨S-O⟩ distances are 1.467 Å (range 1.461-1.481 Å) and 1.473 Å (range 1.458-1.484 Å), for S(1) and S(2) tetrahedra, respectively. These values are in agreement with the average ⟨S-O⟩ length of 1.473 Å commonly observed for a sulfate ion (Louisnathan et al., 1977). Bond valence calculation and bond lengths are consistent with the complete occupancy of the site by S. Each S polyhedron is, surrounded by H ions, with distances from its apices ranging from approximately 1.79 to 1.95 Å. Hydrogen atoms are coordinated to octahedral oxygen atoms, forming OH and H_2O groups.

3.1.9 Minerogenesis

The origin of sulphates and rare sulphates-phosphates in the quartz sandstone caves of the tepuis is

discussed by Sauro et al (accepted in Sedimentology). However the minerogenesis of rossiantonite is still not clear. The mineralogical association (gypsum, alunite, sanjuanite) is very similar to that described for the sanjuanite occurrence in Argentina (De Abeledo et al., 1968), developing however under remarkably different environments: Carboniferous-Ordovician limestone bedrock and arid climate, in Argentina, and Precambrian quartz sandstone under tropical wet conditions, in Venezuela. De Abeledo et al. (1968) suggested a hydrothermal origin for sanjuanite with ascending acidic solutions. Colombo et al. (2011) suggested instead that the origin of sulfur in sanjuanite could be related to the weathering under arid conditions of syngenetic sulfides like pyrite in pelites or in Fe^{3+} oxy-hydroxide veins.

In the case of rossiantonite, WDS analysis demonstrated that the residual "red muds", consisting of Fe^{3+} oxy-hydroxides (hematite and goethite), observed along the wall and on the floor of the cave, are almost completely depleted in sulfur (below 10 ppm) and therefore cannot be considered the source for this element. On the other hand isotopic data on sulfur and oxygen from sulphates and sulphates-phosphates collected in many quartz sandstone caves of Venezuelan tepuis (for a detailed discussion and data see Sauro et al., submitted) suggest that sulfur originates from marine spray from the Atlantic Ocean, with possible contributions of dimethyl sulphide (DMS) and microbially reduced sulfur from the forests or peatbogs within the watershed. This spray, after having been conveyed inside the caves for hundreds of thousands following air currents, may thus account for the formation of sulphates and sulphates-phosphates. Dissolved phosphorus and/or decomposed organic matter, carried into the cave by water, may well account for the presence of this element. Aluminum is instead likely related to the presence of clay minerals documented in the cave (kaolinite and pyrophyllite). The association with alunite suggests a highly acidic minerogenetic environment (Khalaf, 1990; Wray, 2011).

Acknowledgements: This research is supported by the Italian Ministero dell'Istruzione Università e Ricerca (MIUR). We kindly thank Dr. Pier Luigi Fabbri for his valuable support in collecting ESEM images at the Centro Interdipartimentale Grandi Strumenti (CIGS), Università di Modena e Reggio Emilia. Associate Editor Fernando Colombo, Annibale Mottana and an anonymous reviewer significantly contributed to increase the quality of this contribution by sharing constructive remarks. This research was developed within the "Tepui Project" of "La Venta Esplorazioni Geografiche". We would like to thank all our Venezuelan collaborators, most of all Raul Arias Betancourt and Freddy Vergara Castro, for their logistic support in Venezuela. The finding of the new mineral was possible thanks to the collaboration with "In Parques Venezuela", "Raul Elicopteros" and "Elements Adventure". The expedition to Chimanta has benefited from the official support of the Ambassador of the Bolivarian Republic of Venezuela in Italy, Julian Isaias Rodriguez Diaz.

Table 4. Fractional coordinates and atom displacement parameters ($Å^2 \times 10^3$). Standard deviation in parenthesis.

Atom	*x*	*y*	*z*	Ueq	U11	U22	U33	U23	U13
P	0.5169(1)	0.6628(1)	0.0611(1)	12(1)	13(1)	11(1)	12(1)	1(1)	-5(1)
Al(1)	0.2508(1)	0.6175(1)	0.0287(1)	12(1)	12(1)	11(1)	13(1)	0(1)	-6(1)
Al(2)	0.2686(1)	0.6219(1)	0.3303(1)	14(1)	14(1)	16(1)	13(1)	2(1)	-6(1)
Al(3)	0.5557(1)	0.9431(1)	0.0933(1)	13(1)	15(1)	13(1)	14(1)	1(1)	-7(1)
S(1)	0.9545(1)	0.0474(1)	0.2582(1)	19(1)	18(1)	20(1)	17(1)	0(1)	-7(1)
S(2)	0.7454(1)	0.6453(1)	0.3275(1)	17(1)	16(1)	17(1)	16(1)	2(1)	-7(1)
O(1)	0.5849(2)	0.7740(2)	0.0446(2)	15(1)	14(1)	12(1)	18(1)	1(1)	-7(1)
O(2)	0.4415(2)	0.6399(2)	0.2062(2)	17(1)	14(1)	24(1)	15(1)	2(1)	-6(1)
O(3)	0.4034(2)	0.6926(2)	0.0003(2)	15(1)	17(1)	14(1)	18(1)	3(1)	-10(1)
O(4)	0.3621(2)	0.4525(2)	0.0155(2)	17(1)	14(1)	12(1)	20(1)	-1(1)	-4(1)
O(5)h	0.1804(2)	0.6365(2)	0.2137(2)	17(1)	12(1)	22(1)	15(1)	1(1)	-4(1)
O(6)w	0.1251(2)	0.7794(2)	0.0270(2)	23(1)	26(1)	21(1)	20(1)	-5(1)	-14(1)
O(7)w	0.6929(2)	0.3868(2)	0.1600(2)	22(1)	29(1)	19(1)	18(1)	-1(1)	-11(1)
O(8)w	0.0937(2)	0.5460(2)	0.0478(2)	21(1)	16(1)	21(1)	26(1)	-1(1)	-8(1)
O(9)w	0.1113(2)	0.5784(2)	0.4734(2)	20(1)	16(1)	22(1)	18(1)	6(1)	-3(1)
O(10)w	0.1735(2)	0.7943(2)	0.3898(2)	23(1)	34(1)	17(1)	18(1)	-1(1)	-15(1)
O(11)w	0.3450(3)	0.4378(2)	0.2952(3)	25(1)	24(1)	19(1)	25(1)	1(1)	-4(1)
O(12)w	0.3621(2)	0.6150(2)	0.4500(2)	22(1)	20(1)	30(1)	17(1)	9(1)	-9(1)
OH(13)h	0.3809(2)	1.0061(2)	0.0768(2)	16(1)	10(1)	20(1)	16(1)	4(1)	-3(1)
O(14)w	0.4662(3)	0.9136(2)	0.2753(2)	23(1)	27(1)	17(1)	18(1)	-1(1)	-8(1)
O(15)w	0.7472(2)	0.8864(2)	0.0953(2)	21(1)	22(1)	18(1)	27(1)	5(1)	-14(1)
O(16)w	0.5546(2)	1.1076(2)	0.1525(2)	25(1)	43(1)	17(1)	24(1)	4(1)	-21(1)
O(17)	0.0988(2)	1.0009(2)	0.2612(2)	38(1)	24(1)	48(1)	39(1)	14(1)	-13(1)
O(18)	0.9536(2)	1.1532(2)	0.1728(2)	38(1)	40(1)	46(1)	39(1)	21(1)	-25(1)
O(19)	0.9144(2)	0.9463(2)	0.2116(2)	41(1)	41(1)	34(1)	44(1)	-15(1)	-14(1)
O(20)	0.8423(2)	0.0913(2)	0.3931(2)	29(1)	29(1)	33(1)	21(1)	-7(1)	-7(1)
O(21)	0.8065(2)	0.6617(2)	0.1846(2)	22(1)	22(1)	24(1)	16(1)	4(1)	-6(1)
O(22)	0.6712(2)	0.5414(2)	0.3532(2)	25(1)	32(1)	26(1)	27(1)	8(1)	-17(1)
O(23)	0.6333(2)	0.7620(2)	0.3965(2)	27(1)	25(1)	25(1)	21(1)	-4(1)	-6(1)
O(24)	0.8619(2)	0.6151(2)	0.3743(2)	25(1)	24(1)	29(1)	30(1)	10(1)	-18(1)
W(1)	0.1245(3)	0.3117(2)	0.1365(2)	29(1)	25(1)	27(1)	31(1)	-3(1)	-5(1)
W(2)	0.2845(3)	1.0876(2)	0.4652(2)	33(1)	39(1)	30(1)	24(1)	-1(1)	-5(1)
W(3)	0.4048(3)	0.7884(2)	0.6555(2)	31(1)	28(1)	43(1)	20(1)	-4(1)	-10(1)
W(4)	0.1551(2)	0.2942(2)	0.3651(2)	31(1)	32(1)	30(1)	28(1)	-3(1)	-12(1)
H(5)	0.110(3)	0.631(3)	0.247(3)	24(11)					
H(6)	0.896(3)	1.198(3)	0.036(3)	40(11)					
H(6')	0.072(3)	0.825(3)	0.094(3)	25(9)					
H(7)	0.700(4)	0.436(3)	0.204(4)	59(13)					
H(7')	0.672(4)	0.331(4)	0.205(4)	59(14)					
H(8)	0.004(4)	0.583(3)	0.082(3)	40(11)					
H(8')	0.102(3)	0.466(3)	0.075(3)	47(11)					
H(9)	0.122(4)	0.510(3)	0.518(3)	54(11)					

H(9')	0.027(4)	0.625(4)	0.528(4)	73(14)
H(10)	0.168(3)	0.826(3)	0.455(3)	33(10)
H(10')	0.156(3)	0.849(3)	0.342(3)	38(10)
H(11)	0.290(4)	0.390(3)	0.312(3)	51(13)
H(11')	0.392(4)	0.426(3)	0.230(3)	38(13)
H(12)	0.458(4)	0.602(3)	0.414(3)	54(12)
H(12')	0.347(3)	0.567(3)	0.506(3)	31(10)
H(13)	0.302(3)	1.009(3)	0.127(3)	22(9)
H(14)	0.513(4)	0.864(3)	0.303(3)	53(13)
H(14')	0.417(3)	0.967(3)	0.328(3)	26(10)
H(15)	0.757(4)	0.819(4)	0.124(3)	45(13)
H(15')	0.783(4)	0.930(4)	0.120(4)	64(14)
H(16)	0.561(4)	1.136(3)	0.217(4)	57(12)
H(16')	0.571(3)	1.171(3)	0.102(3)	38(10)
HW1	1.072(3)	1.259(3)	0.144(3)	38(10)
HW1'	0.215(4)	0.274(3)	0.075(4)	56(12)
HW2	0.222(3)	0.043(3)	0.525(3)	46(10)
HW3	0.332(4)	0.823(4)	0.635(4)	73(14)
HW3'	0.471(4)	0.763(3)	0.587(4)	42(12)
HW4	0.143(4)	0.286(3)	0.296(4)	65(13)
HW4'	0.186(4)	0.223(4)	0.401(4)	73(13)

Note. Labels: P = phosphorous site; Al(1), Al(2), Al(3) = three symmetrically independent aluminum sites; S = sulfur site; O = anionic oxygen sites; H = hydrogen sites; W = oxygen position related to free H_2O. Label h identifies octahedral OH sites, label w identifies octahedral sites occupied by H_2O.

Table 5. Selected bond distances (Å) in rossiantonite.

P – O(1)	1.524(2)	S(1) – O(17)	1.461(2)	S(2) – O(21)	1.472(2)
P – O(2)	1.520(2)	S(1) – O(18)	1.461(2)	S(2) – O(22)	1.484(2)
P – O(3)	1.542(2)	S(1) – O(19)	1.465(2)	S(2) – O(23)	1.476(2)
P - O(4)	1.520(2)	S(1) – O(20)	1.481(2)	S(2) – O(24)	1.458(2)
<P – O>	1.527	<S(1) – O>	1.467	<S(2) – O>	1.473
Al(1) – O(3)	1.871(2)	Al(2) – O(2)	1.807(2)	Al(3) – O(1)	1.872(2)
Al(1) – O(4)	1.853(2)	Al(2) – O(5)h	1.851(2)	Al(3) – O(13)h	1.842(2)
Al(1) – O(5)h	1.887(2)	Al(2) – O(9)w	1.899(2)	Al(3) – O(13)h’	1.843(2)
Al(1) – O(6)w	1.915(2)	Al(2) – O(10)w	1.902(2)	Al(3) – O(14)w	1.902(2)
Al(1) – O(7)w	1.937(2)	Al(2) – O(11)w	1.964(2)	Al(3) – O(15)w	1.925(2)
Al(1) – O(8)w	1.911(2)	Al(2) – O(12)w	1.932(2)	Al(3) – O(16)w	1.948(2)
<Al(1) – O>	1.896	<Al(2) – O>	1.893	<Al(3) – O>	1.889
		O – H bonds			
O(5)h – H(5)	0.69(2)	O(11)w - H(11)	0.83(3)	W(1) - H(W1)	0.90(3)
O(6)w – H(6)	0.82(3)	O(11)w - H(11)	0.68(3)	W(1) - H(W1)’	0.88(3)
O(6)w– H(6)’	0.82(2)	O(12)w - H(12)	0.88(3)	W(2) - H(W2)	0.93(3)
O(7)w – H(7)	0.78(3)	O(12)w - O(12)’	0.78(3)	W(2) - (W2)’	0.83(3)
O(7)w– H(7)’	0.79(3)	O(13)h – H(13)	0.77(3)	W(3) - H(W3)	0.79(4)
O(8)w – H(8)	0.84(3)	O(14)w – H(14)	0.77(3)	W(3) - H(W3)’	0.86(4)
O(8)w – H(8)’	0.90(3)	O(14)w – H(14)’	0.76(3)	W(4) - H(W4)	0.84(3)
O(9)w – H(9)	0.89(3)	O(15)w - H(15)	0.79(4)	W(4) - H(W4)’	0.90(3)
O(9)w – H(9)’	0.87(3)	O(15)w - H(15)’	0.80(4)		
O(10)w-H(10)	0.80(3)	O(16)w - H(16)	0.83(3)		
O(10)w-H(10)’	0.82(3)	O(16)w- H(16)’	0.88(3)		

Table 6. Bond-valence analysis for rossiantonite (values are expressed in valence units). Deposited.

Atom	P	S(1)	S(2)	Al(1)	Al(2)	Al(3)	H'	H''	Σ
O1	1.289					0.506			1.795
O2	1.300				0.602				1.902
O3	1.221			0.512					1.733
O4	1.300			0.533					1.833
O5h				0.483	0.537		0.870		1.89
O6w				0.446			0.780	0.780	2.006
O7w				0.425			0.830	0.730	1.985
O8w				0.455			0.750	0.703	1.908
O9w					0.469		0.730	0.740	1.939
O10w					0.467		0.790	0.782	2.039
O11w					0.395		0.782	0.879	2.056
O12w					0.429		0.766	0.774	1.969
O13h						1.104	0.810		1.914
O14w						0.467	0.734	0.825	2.026
O15w						0.437	0.734	0.825	1.996
O16w						0.413	0.774	0.758	1.945
O17		1.558							
O18		1.554							
O19		1.533							
O20		1.468							
O21			1.508						
O22			1.464						
O23			1.488						
O24			1.554						
Σ	5.110	6.113	6.014	2.854	2.899	2.927			

References

Assaoudi, H. and Ennaciri, A. (1997) Vibrational spectra and structure of rare earth orthophosphates, weinschenkite type. Spectrochimica Acta, A53, 895-902.

Aubrecht, R., Brewer-Carías, C., Smída, B., Audy, M. and Kovácik, L. (2008) Anatomy of biologically mediated opal speleothems in the world's largest sandstone cave Cueva Charles Brewer, Chimanta Plateau, Venezuela. Sedimentary Geology, 203, 181-195.

Barton, H., Suarez, P., Muench, B., Giarrizzo, J., Broering, M., Banks, E. and Venkateswaran, K. (2009) The alkali speleogenesis of Roraima Sur Cave, Venezuela. In W.B. White Ed., 2009 ICS Proceedings of the 15th International Congress of Speleology, Vol. 1, Symposia, Part 1, p. 802-807. International Union of Speleology, Kerrville, Texas, USA.

Beukes, G.J., Schoch, A.E., Van der Westhuizen, W.A., Bok, L.D.C. and De Bruiyn, H. (1984) Hotsonite, a new hydrated aluminum-phosphate-sulfate from Pofadder, South Africa. American Mineralogist, 69, 979-983.

Brewer-Carías, C. and Audy, M. (2011) Entrañas del Mundo Perdido. Carlos Capriles de Altolitho C.A., Caracas (in Spanish).

Brown, I.D. and Altermatt, D. (1985) Bond-valence parameters from a systematic analysis of the inorganic crystal structure database. Acta Crystallographica, B41, 244–247.

Briceño, H.O. and Schubert, C. (1990) Geomorphology of the Gran Sabana, Guyana Shield, Southeastern Venezuela. Geomorphology, 3, 125-141.

Bruker AXS (1999) SAINT+ (version 6.01). Bruker AXS Inc, Madison, Wisconsin, USA

Burla, M.C., Caliandro, R., Camalli, M., Carrozzini, B., Cascarano, G.L., De Caro, L., Giacovazzo, C., Polidori, G., and Spagna, R. (2005) SIR2004: an improved tool for crystal structure determination and refinement. Journal of Applied Crystallography, 38, 381–388.

Colombo, F., Rius, J., Pannunzio-Miner, E.V., Pedregosa, J.C., Camì, G.E. and Carbonio, R.E. (2011) Sanjuanite: ab-initio crystal-structure solution from laboratory powder-diffraction data, complemented by FTIR spectroscopy and DT-DG analyses. Canadian Mineralogist, 49, 835-847.

De Abeledo, M.E.J., Angelelli, V., De Benyacar, M.A.R. and Gordillo, C.E. (1968) Sanjuanite, a new hydrated basic sulfate–phosphate of aluminum. American Mineralogist, 53, 1-8.

du Rietz, T. (1945): Kribergite, ett nyt mineral från Kristinebergs gruva I Västerbottens lan. Geologiska Foereningens i Stockholm Foerhandlingar, 67, 78-9 (in Swedish).

Frost, R.L. and Palmer S.J. (2011) A vibrational spectroscopic study of the mixed anion mineral sanjuanite $Al_2(PO_4)(SO_4)(OH)\cdot 9H_2O$. Spectrochimica Acta, A79, 1210–1214.

Huminicki, D.M.C. and Hawthorne, F.C. (2002) The Crystal Chemistry of the Phosphate Minerals. Reviews in Mineralogy and Geochemistry, 48, 123-253.

Khalaf, F.I. (1990) Diagenetic alunite in clastic sequences, Kuwait, Arabian Gulf. Sedimentology 37, 155-164.

Louisnathan, S.J., Hill, R.J. and Gibbs, G.V. (1977) Tetrahedral bond length variations in sulfates. Physics and Chemistry of Minerals, 1, 53-69.

Mandarino, J.A. (1981) The Gladstone-Dale relationship: Part IV. The compatibility concept and its application. Canadian Mineralogist, 19, 441–450.

Martini, J.E.J. (2000) Dissolution of quartz and silicate minerals. In: A.B. Klimchouk, D.C. Ford, A.N. Palmer and W. Dreybrodt, Eds., Speleogenesis-Evolution of Karst Aquifers, p. 452-457, National Speleological Society, Huntsville, Alabama, USA.

Mecchia, M., Sauro, F., Corongiu, C. and Crobu, V. (2009) Speleological explorations in the Chimanta massif quartzites (Gran Sabana, Venezuela). Supplement to Kur Magazine, 12, 1-16.

Peacor, D.R., Rouse, R.C., Coskren, T.D. and Essene, E.J. (1999) Destinezite ("diadochite"), $Fe_2(PO_4)(SO_4)(OH)\cdot 6H_2O$: its crystal structure and role as a soil mineral at Alum Cave Bluff, Tennessee. Clays and Clay Minerals, 47, 1-11.

Santos, J.O.S., Potter, P.E., Reis, N.J., Hartmann, L.A., Fletcher, I.R. and McNaughton, N.J. (2003) Age, source, and regional stratigraphy of the Roraima Supergroup and Roraima-like outliers in northern South America based on U-Pb geochronology. Geological Society of America Bulletin, 115, 331-348.

Sauro, F., De Waele, J., Forti, P., Galli, E. and Vergara, F. (2011) Speleogenesi e speleotemi di opale della Cueva Guacamaya, Auyan Tepui, Gran Sabana, Venezuela. Atti del XXI Congresso Nazionale di Speleologia, Trieste, 291-297 (in Italian).

Sauro, F., Piccini, L., Mecchia, M. and De Waele, J. (2012) Comment on "Sandstone caves on Venezuelan tepuis: Return to pseudokarst?" by R. Aubrecht, T. Lánczos, M. Gregor, J. Schlögl, B. Smída, P. Liscák, Ch. Brewer-Carías and L. Vlcek, Geomorphology 132 (2011), 351–365. Geomorphology in press, http://dx.doi.org/10.1016/j.geomorph.2012.11.015

Sheldrick GM (1997) SHELX-97, program for crystal structure determination. University of Göttingen, Germany.

Sheldrick, G.M. (2008) SHELXL-97—Program for the refinement of crystal structures. University of Göttigen, Germany.

Smith, D.G.W. and Nickel, E.H. (2007) A system for codification for unnamed minerals: report of the Subcommittee for Unnamed Minerals of the IMA Commission on New Minerals, Nomenclature and Classification. Canadian Mineralogist, **45**, 983-1055.

Urbani, F. (1996) Venezuelan cave minerals: a review. Boletín de la Sociedad Venezolana de Espeleología, **30**, 1-13.

Wray, R.A.L. (1997) A global review of solutional weathering forms on quartz sandstones. Earth Science Reviews, 42, 137-160.

Wray R.A.L. (2011) Alunite formation within silica stalactites from the Sydney Region, South-eastern Australia. International Journal of Speleology, 40, 109-116.

CHAPTER 3.2

Part of this chapter is published in Sedimentology, doi: 10.1111/sed.12103,

with the exception of the data related to Imawarì Yeuta Cave

SOURCE AND GENESIS OF SULPHATE AND PHOSPHATE-SULPHATE MINERALS IN A QUARTZ-SANDSTONE CAVE ENVIRONMENT

Francesco Sauro (1, 3), Nicola Tisato (2), Jo De Waele (1, 3), Stefano M. Bernasconi (2), Tomaso R.R. Bontognali (2), Ermanno Galli (4)

1) Dipartimento di Scienze Biologiche, Geologiche ed Ambientali, Università di Bologna, Via Zamboni 67, 40126, Bologna, (Italy)

2) ETH Zurich, Geological Institute, Soneggstrasse 5, 8092 Zurich (Switzerland)

3) Associazione di Esplorazioni Geografiche la Venta, Via Priamo Tron 35/F, 31030, Treviso

4) Dipartimento di Scienze Chimiche e Geologiche, Università di Modena e Reggio Emilia. Largo S. Eufemia 19, I-41121, Modena, Italy

Corresponding author: Francesco Sauro

Abstract

Gypsum ($CaSO_4 \bullet 2H_2O$), alunite ($KAl_3(SO_4)_2(OH)_6$), and rare phosphates-sulphates sanjuanite $Al_2(PO_4)(SO_4)(OH) \bullet 9(H_2O)$ and rossiantonite ($Al_3(PO_4)(SO_4) \bullet 2(OH)_2(H_2O)_{14}$) have been recently identified as secondary mineral deposits in different quartz-sandstone caves in the Gran Sabana region, Venezuela. Due to the extended timescale required for speleogenesis development in the hard and barely soluble quartz-sandstone lithology, these caves are considered to be as old as 20-30 My. The study of these peculiar secondary mineral deposits potentially reveals important insights for understanding the interaction between deep, superficial and atmospheric processes, during thousand to even millions of years. In this research we use chemical and petrographic analyses of potential host rock sources, sulphur and oxygen isotope ratios, and meteorological, hydrological and geographic data to investigate the origin of sulphates and phospho-sulphates. Our results suggest that the deposition of sulphates in these caves is not linked to the quartz-sandstone host-rock. Most probably these mineral deposits originate from an external atmospheric sulphate source, with potential contributions of marine non-sea salt (nss) sulphates, terrestrial dimethyl sulphide (DMS), and microbially reduced H_2S from the forests or peatbogs within the watershed. Air currents within the caves are the most plausible means of transport for aereosols, driving the accumulation of

sulphates and other secondary minerals in specific locations over millions of years. Moreover, the studied sulphate minerals often co-occur with silica speleothems of biological origin. Although this association would suggest a possible biogenic origin for the sulphates as well, direct evidence proving that microbes are involved in their formation remains to be found. Nonetheless, this study demonstrates that these quartz-sandstone caves accumulate and preserve allogenic sulphates, playing a yet unrecognized role in the sulphur cycle of tropical environments.

Keywords: Sulphates deposition, Rossiantonite, Sanjuanite, Quartz-sandstone caves, Sulphur isotopes, Tepui Table Mountains, Gran Sabana, Venezuela

3.2.1 Introduction

Over 300 secondary minerals have been found in cave environments (Hill and Forti, 1997; Onac and Forti, 2011), with sulphates and phosphates being probably the most common after carbonates. The presence of sulphates, mostly gypsum ($CaSO_4 \bullet 2H_2O$) and alunite ($KAl_3(SO_4)_2(OH)_6$), has been documented from numerous, globally distributed, cave environments. Generally, the presence of secondary minerals can provide important information regarding the weathering processes that originated the hosting cavities (Polyak *et al.*, 1998; Jagnow *et al.*, 2000; Audra *et al.*, 2007; Klimchouk, 2009). The occurrence of abundant gypsum in cave environments is often related to hypogenic sources of H_2S (Hose et al., 2000, Galdenzi & Maruoka, 2003), whereas alunite typically forms by reaction between aluminium-bearing minerals and sulphuric acid (Khalaf, 1990; Polyak & Güven, 1996). Cave phosphates are usually related to bat guano deposits that are rich in nitrogen and phosphorus, or to the decomposition of organic matter transported underground by percolating water (Onac & Veres, 2003).

Secondary sulphates and phosphates are common in caves developed in carbonates and gypsum bearing rocks (Hill, 1982), but also in basalt lava tubes (Forti, 2005) and in cavities within granites (Hill & Forti, 1997, Twidale and Vidal Romaní, 2005; and references therein).

During the past twenty years many new cave systems have been discovered in different “tepuis” (table mountains) of the Guyana Shield (Venezuela and Brazil), formed in the Precambrian quartz-sandstones of the Roraima Supergroup (Piccini & Mecchia, 2007; Sauro, 2009; Aubrecht *et al.*, 2011; Sauro *et al.*, 2013). The formation of caves and karst features in quartzitic rocks was considered exceptional given the low solubility and dissolution rates of quartz (Wray, 1997a, 1997b). Many authors discussed the different weathering processes that could be responsible for speleogenesis in this lithology (Zawidzki et al., 1976; Martini, 2000; Piccini & Mecchia, 2009; Aubrecht *et al.*, 2011;), however a clear understanding is still lacking (Sauro *et al.*, 2013). The slow dissolution rate of SiO_2, results from geochemical analyses of dissolved silica in cave waters, and the geomorphic history of

the region brought many authors to agree on placing the formation of these caves at 20-30 My ago (Doerr, 1999; Wray, 2000; Piccini & Mecchia, 2009).

The first studies on secondary minerals in quartz-sandstone karst environments, were carried out by Urbani (1980, 1981, 1996). The presence of gypsum was documented in the big shafts of the Sarisariñama and Auyan tepuis (Zawiszki *et al.*, 1976; Forti, 1994), and recently even in the Muchimuk cave system in Chimantha tepui (Aubrecht *et al.*, 2012). Quartz-sandstone caves have never been considered a favourable environment for the deposition of sulphates due to the very low sulphur content (in the form of sulphate or sulphide) of the bedrock, which is almost entirely composed of quartz with minor clay minerals, and the lack of a significant source of sulphur nearby (Forti, 1994, Wray, 2011).

However, gypsum and other sulphates were recently found in four different tepuis (Roraima, Chimantha, Auyan and Sarisariñama) in the major cave systems of the Gran Sabana area, hence demonstrating they have a widespread occurrence even in the quartz-sandstone environment. Moreover, an exceptional association of sulphates and phosphates was collected in a cave of the Akopan-Dal Cin System, in the Chimantha massif. Besides gypsum and alunite, the rare sanjuanite $Al_2(PO_4)(SO_4)(OH)\bullet 9H_2O$ and rossiantonite $Al_3(PO_4)(SO_4)_2(OH)_2(H_2O)_{10}\bullet 4H_2O$ were also observed. Sanjuanite was previously described from only two other places in the world (Argentina and Yakutia) but never from caves (De Abeledo *et al.*, 1968; Lazebnik *et al.*, 1998), whereas the latter represents a newly described mineral (Galli *et al.*, 2013). After this first recognition, sanjuanite was found in large quantities associated with minor aluminite ($Al_2(SO_4)(OH)_4\cdot 7H_2O$) also in the Imawarì Cave System recently discovered in the eastern sector of Auyan Tepui.

The relationship between these secondary minerals, the peculiar speleogenesis of cave systems in quartz-sandstone lithologies and the influence of other environmental factors can be inferred from the study of sulphur and oxygen isotopes (Holt & Kumar, 1991; Onac *et al.*, 2011). The sulphate can originate from various different sources, such as: 1) oxidation of sulphides (in ore deposits or disseminated in the host rock); 2) primary marine sulphate hosted in sedimentary rocks; 3) sea-water/atmospheric aerosols; 4) volcanic rocks; 5) oxidation of H_2S from deep magmatic bodies or oil reservoirs; 6) guano. Analysis of stable oxygen isotopes of the sulphate ion can provide information on its origin and on mineralization processes (Clark & Fritz, 1997).

This study documents the S, O and P potential sources of sulphates and phosphates found in “tepuis” caves. The study approach adopted combines i) chemical analyses of the host rock and of the chemical deposits (silica biospeleothems and minerals) present in the caves; ii) scanning electron microscopy (SEM); and iii) sulphur and oxygen stable isotope analyses of sulphate ions.

3.2.2 Geographical, geological and hydrogeological settings

The Gran Sabana is a vast geographical region, part of the Guyana Shield, located in northern South America, between Venezuela and Brazil, crossed by several tributaries of the Rio Caroní, which in turn flows into the Orinoco River (Fig. 1). The main massifs of the Gran Sabana have the shape of large table mountains named "tepuis" in the local Pemon indigenous language. The tepuis are delimited by vertical to overhanging cliffs many hundreds of meters high, surrounded by the lowlands of the Wonkén planation surface, which isolates the massifs from one another (Briceño & Schubert, 1990). More than 60 tepuis are present in the Gran Sabana region but our research focused on the karst systems of the most important ones: the Auyantepui (700 km^2), the Chimantha group (1470 km^2), and Roraima (31 km^2).

The igneous and metamorphic rocks in the northern portion of the Guyana Shield (Imataca-Bolivar Province, after González de Juana et al., 1980) have an age of 3.5 Ga. The siliciclastic rocks of the Roraima Group belong to the continental and pericontinental environment of the Roraima-Canaima

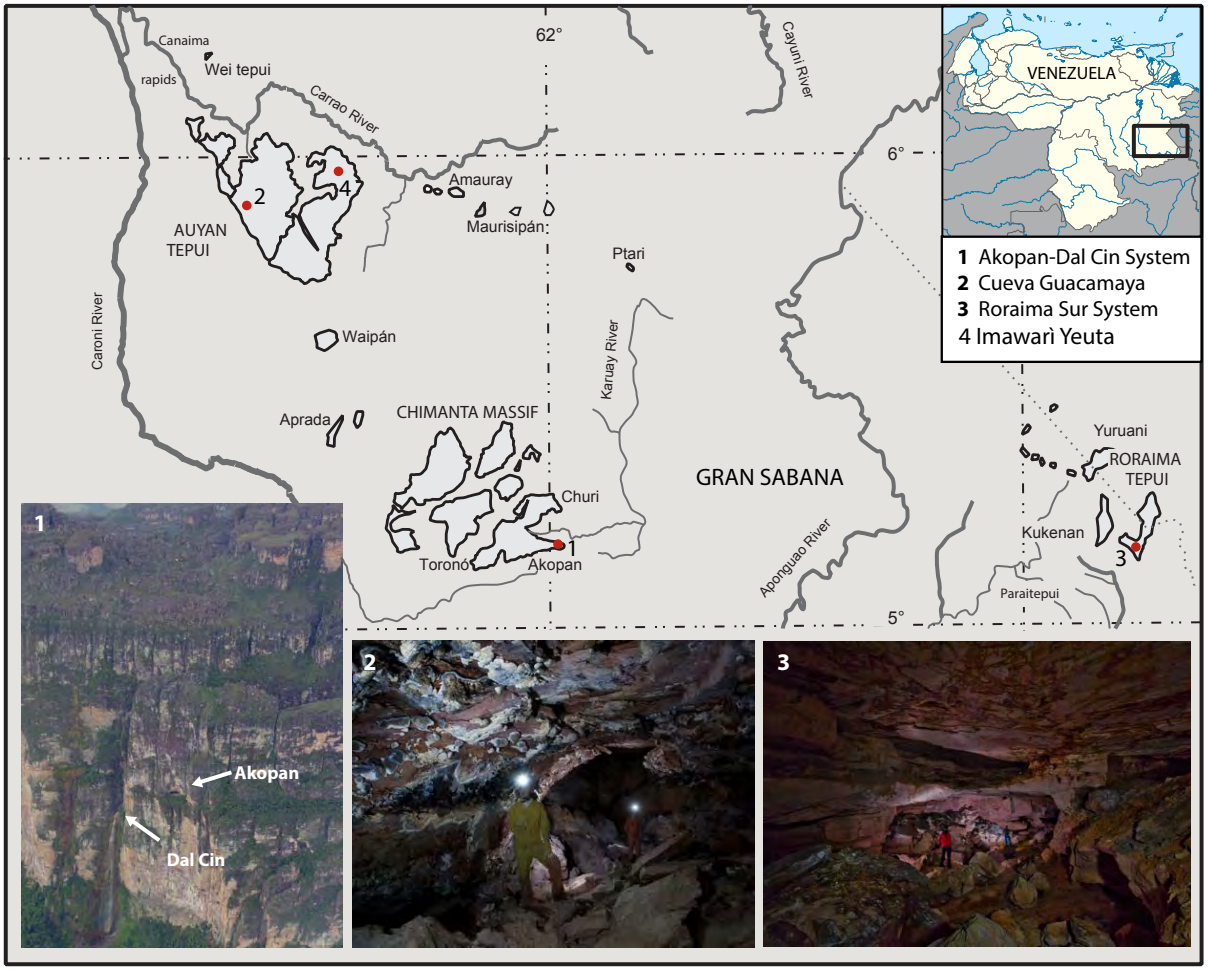

Fig. 1. Geographical map showing the Gran Sabana area and tepui Auyan, Chimantha and Roraima with the related sampling sites. In photos: 1) The dry entrance of Cueva Akopan and the waterfall of Resurgencia Dal Cin, the wall is approximately 650 meters high (photograph by Vittorio Crobu); 2) The dry passage of "Tramo de Los Opales" in Guacamaya Cave (photograph by Francesco Sauro); 3) A fossil gallery in the Roraima Sur System (photograph by Francesco Sauro).

Province (Reid, 1974). The age of this arenaceous group can be inferred only on the basis of the absolute dating of the granitic basement (2.3-1.8 Ga) and of the basaltic dykes and sills that cross the upper formation of the Roraima Group (1.4-1.8 Ga) (Briceño & Schubert, 1990; Santos *et al.*, 2003). The Roraima Group was also intruded by Mesozoic diabases forming thin NE-trending dykes with ages of around 200 Ma (Hawkes, 1966; Teggin *et al.*, 1985). A low-grade metamorphic overprint, leading to quartz grains overgrowth and pyrophyllite formation in the more pelitic beds, is the result of the lithostatic load of ~3 km thick sediments, which are now eroded (Urbani *et al.*, 1977).

All the investigated karst systems are developed in the Mataui Formation, the youngest sediments of the Roraima Group. This formation, which represents the highest part of the tepuis, is 600-900 m tick, and ~1.5 Ga-old (Santos *et al.*, 2003). The quartz grains composing these sandstones are well sorted, between 30 and 100 μm in diameter, and cemented with quartz or minor phyllosilicates (kaolinite and/or pyrophyllite). Quartz represents well over 90% of the whole rock, giving it the name "quartz-sandstone" (Martini, 2000, 2004). The slopes underlying the cliffs surrounding the Tepuis are made of proto-quartzites, arkoses and graywackes, with beds of cherts, lutites, and siltites (Uaimapué Formation; Reid, 1974). In the lowlands the main outcropping lithology is the Kukenán Formation, prevalently composed of siltites and shales.

From a structural point of view folding structures are absent, except for some wide folds at a very large scale. The bedding is normally horizontal, slightly inclined locally. Sets of mainly vertical fractures cut the plateaus, creating a regular network of quadrangular prisms. Regional faults with relevant displacement have not been observed in the Gran Sabana area (Gibbs & Barron, 1993).

The climate is tropical and on the Chimantha and Auyan tepuis the average annual precipitation is of 3400-3600 mm. The average daily temperature is fairly constant all year round, with an estimated 13.9°C at 2200 m altitude, and a mean difference between day and night of about 10° C (Galán, 1992).

The high levels of precipitation support a temperate type of vegetation; forests, sedges, grasses, and bromeliads grow in sheltered locations, peat swamps and bogs are well-developed and often extensive, particularly where the substrate is characterized by weathered diabase sills (Briceño *et al.*, 1990). Apart from the presence of moss, lichen, and algae, quartz-arenite outcrops are mostly barren. Surficial streams, flowing through the peat swamps, are rich in dissolved organic matter, derived from the decomposition of vegetation, which is responsible for the characteristic amber color of the waters.

The water flows on the plateaus, forming high waterfalls along the external cliffs, or sinking in fractures and cave systems to later resurge from springs scattered around the border of the tepuis (Mecchia & Piccini, 1999).

3.2.3 Previous studies on gypsum in venezuelan quartz-sandstone caves

The first discovery of gypsum in a quartz-sandstone cave was reported by the Sociedad Venezolana de Espeleologia in 1975. During an expedition to the huge sinkhole caves of the Sarisariñama Plateau, gypsum was found as "crusts up to 2.5 cm thick with transparent to white fibres perpendicular to the cave walls" (Urbani, 1980). The presence of gypsum and pyrophyllite led Zawidzki *et al.* (1976) to propose that the huge galleries beneath the collapse dolines of the Sarisariñama plateau were the result of a low-grade metamorphic event with related rising hydrothermal fluids possibly enriched in H_2S.

In 1993 gypsum was found in the "Sima Aonda Superior 4", a 105 m deep cave in the Auyan Tepui (Gori *et al.*, 1993). In this case the mineral occurred as centimetre size fibrous crystals growing within a bedding plane partly opened by a collapse. Forti (1994) noted that gypsum, and sulphate in general, was absent in the quartz-arenite hosting the cave, suggesting that the sulphur and calcium originated from organic matter transported by water into the cavities. Furthermore, he observed that the formation of gypsum was probably exceptional and limited to specific sites due to its ease of dissolution by condensation processes and seasonal floods (Badino, 2010). This follows the commonly held view that gypsum can be preserved only in passages lacking running streams or in zones with local evaporative conditions (MacDonald, 1953).

Gypsum was also recently documented in the "Charles Brewer Cave" in the Chimantha massif (Aubrecht *et al.*, 2012).

3.2.4 Previous occurrences of sanjuanite

The first occurrence of sanjuanite in Argentina (De Abeledo *et al.*, 1968) shows the same mineralogical association with gypsum and alunite as that found by our research group in the Akopan tepui, developing however in remarkably different environments: Carboniferous-Ordovician limestone bedrock and arid climate in Argentina, and Precambrian quartz-sandstone in tropical wet conditions in Venezuela. Unfortunately the original site of discovery in the San Juan province can no longer be found (Colombo *et al.*, 2011) and therefore a detailed comparison is impossible. However, in the last two years, sanjuanite was discovered not only in the Akopan-Dal Cin System from where our samples come, but also in other two caves of the tepui mountains: the Muchimuk cave system (Aubrecht *et al.*, 2012) and, in large amounts, in the recently discovered Imawarì Yeuta Cave in the Auyan Tepui (Sauro *et al.*, 2013c). This widespread presence in the quartz-sandstone caves from different tepuis, suggests that the formation of gypsum is driven by the same process at all these sites.

De Abeledo *et al.* (1968) suggested a hydrothermal origin for sanjuanite with ascending acidic solutions. Colombo *et al.* (2011) suggested instead that the origin of sulfur in sanjuanite could be related to the weathering under arid conditions of syngenetic sulphides like pyrite in pelites or in Fe^{3+}

oxy-hydroxide veins. Aubrecht *et al.* (2012) disagreed with such hypotheses, suggesting instead a probable origin from guano or accumulation of dead animal bodies, at least for the sanjuanite found in quartz-sandstone caves.

However, a clear understanding regarding the formation of this mineral, as well as that of the newly described rossiantonite, is still lacking.

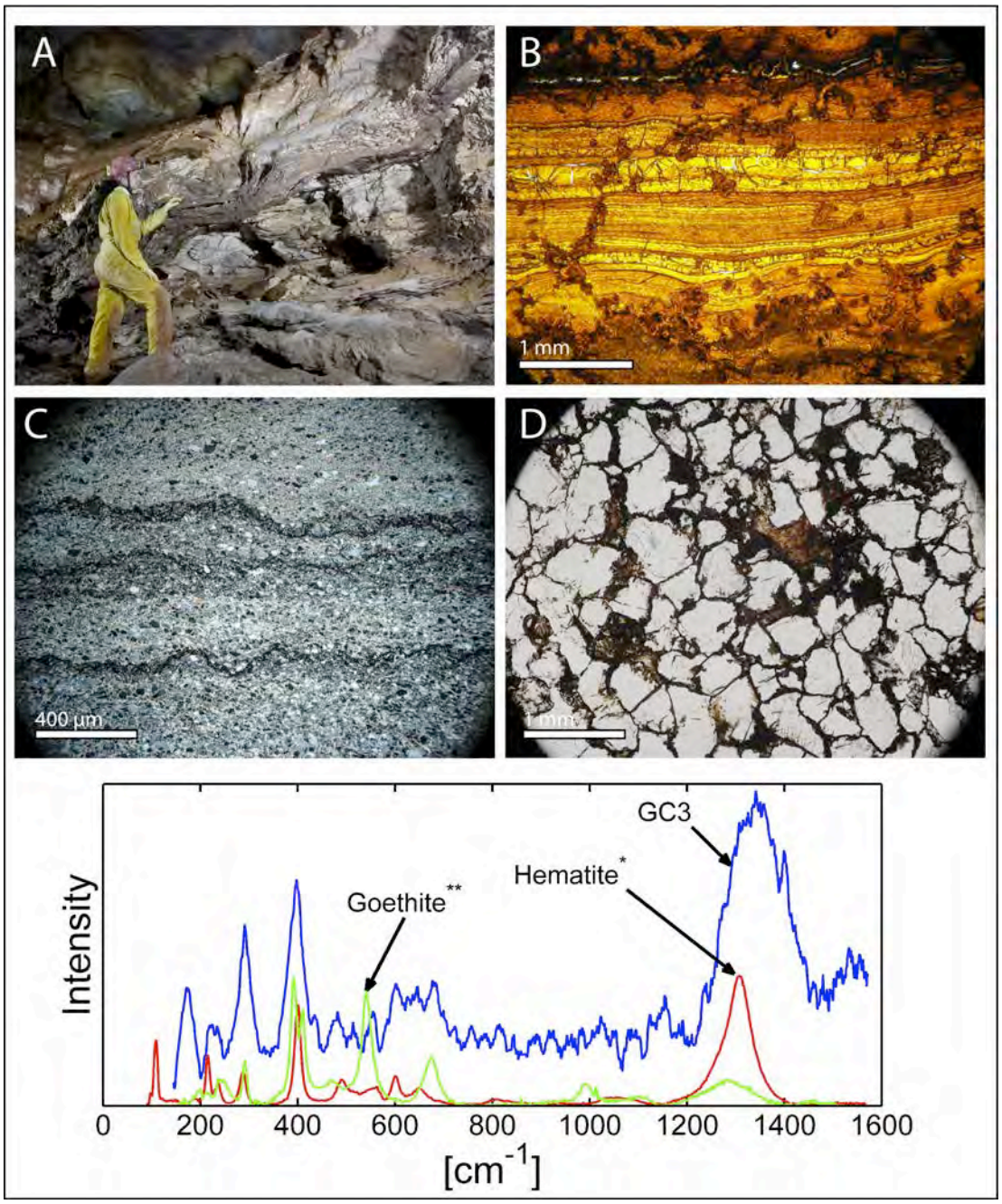

Fig. 2. Images of Banded Iron Formation and iron hydroxide layers from Guacamaya Cave and Akopan-Dal Cin System. A) Half-metre thick bed of BIF in the Tramo de Los Opales, Guacamaya Cave (photograph by Francesco Sauro); B) Thin section of the BIF sample GC3 from Guacamaya Cave; C) Quartz-sandstone with iron hydroxides as cement in between the quartz grains, Roraima Sur System; D) Thin layers of iron hydroxides in quartz-sandstone sample from Akopan-Dal Cin System. Panel below: Raman spectrum of sample GC3 (B). The mineral is identified as a mixture of goethite and hematite.

3.2.5 Cave morphologies and sampling sites

Our study focused on four different cave systems in the Auyan, Roraima and Chimantha tepuis (Fig. 1-1, 1-2, 1-3, 1-4). The Guacamaya Cave, in the Auyan Tepui is one of the longest caves in this massif (~1.1 km) and presents a typical horizontal development controlled by lithological changes. Its galleries follow the contact between the hard quartz-sandstone beds of the Mataui Formation and a metre-thick bed of iron hydroxides and amorphous silica (Fig. 2 A-B, Banded Iron Formation or BIF; Klein 2005). Along the walls close to the BIF, a variety of silica biospeleothems of different shape and size have formed (Sauro *et al.*, 2013b). The gypsum was collected in a dry passage called "Tramo de los Opales", characterized by strong air flow due to its location in between two entrances. Gypsum deposition preferentially occurs on the floor, in the form of crusts or acicular crystals around weathered blocks of quartz-sandstone fallen from the ceiling or as overgrowth on the surface of the amorphous silica biospeleothems.

The second sampling site was the Akopan-Dal Cin System in the Akopan Tepui, in the southern sector of the Chimantha massif. This is an active cave of more than 2.7 km length, draining the higher plateau of the mountain through a large, 105 m deep collapse doline (Mecchia *et al.*, 2009). At the bottom of the shaft the stream follows a horizontal conduit up to the lower entrance called "Resurgencia Dal Cin", where the stream exits from the cave and forms a 200 m high waterfall on the external Tepui cliff (Fig. 1-1). Just before the waterfall, a dry passage leads to another big entrance opening on the tepui cliff, the Akopan Cave. Gyspum, sanjuanite and rossiantonite were collected in this dry sector of the cave.

Also in the Akopan-Dal Cin System the development of the conduits is controlled by the lithology, following a quartz-arenitic centimetric bed characterised by millimetric bands of iron hydroxides (Fig. 2 C). Many silica biospeleothems are present, mostly in the dry passage between the Akopan Cave and the "Resurgence Dal Cin" and in the upper parts of the galleries, where the most interesting sample, Ak8, was collected from the floor. Sample Ak8 is made of pink-white crystalline sand composed of an association of amorphous silica, sulphates (gypsum, alunite; Fig. 3 A-B), and the rare phosphate-sulphates sanjuanite and rossiantonite (Fig. 3 C-D; Galli *et al.*, 2013). Gypsum was also collected from the surface and inside some silica biospeleothems within the same passage. Like for "Tramo de los Opales", this sampling site is characterized by intense airflow, being situated between the two main entrances of the system.

The third studied cave is the Roraima Sur Cave System, with about 15 km of length, located on the high plateau of the Roraima massif (Galán *et al.*, 2004). This cave is mainly horizontal but with a more complex pattern with respect to the two previously described caves: many sinking streams give access to a few main collector conduits surrounded by a maze of secondary passages. Also the speleogenesis of this cave is controlled by the lithology: Galán *et al.* (2004) noticed that the galleries follow a thin bed of siltstone, often of reddish-yellow colour. The colour is likely due to the presence

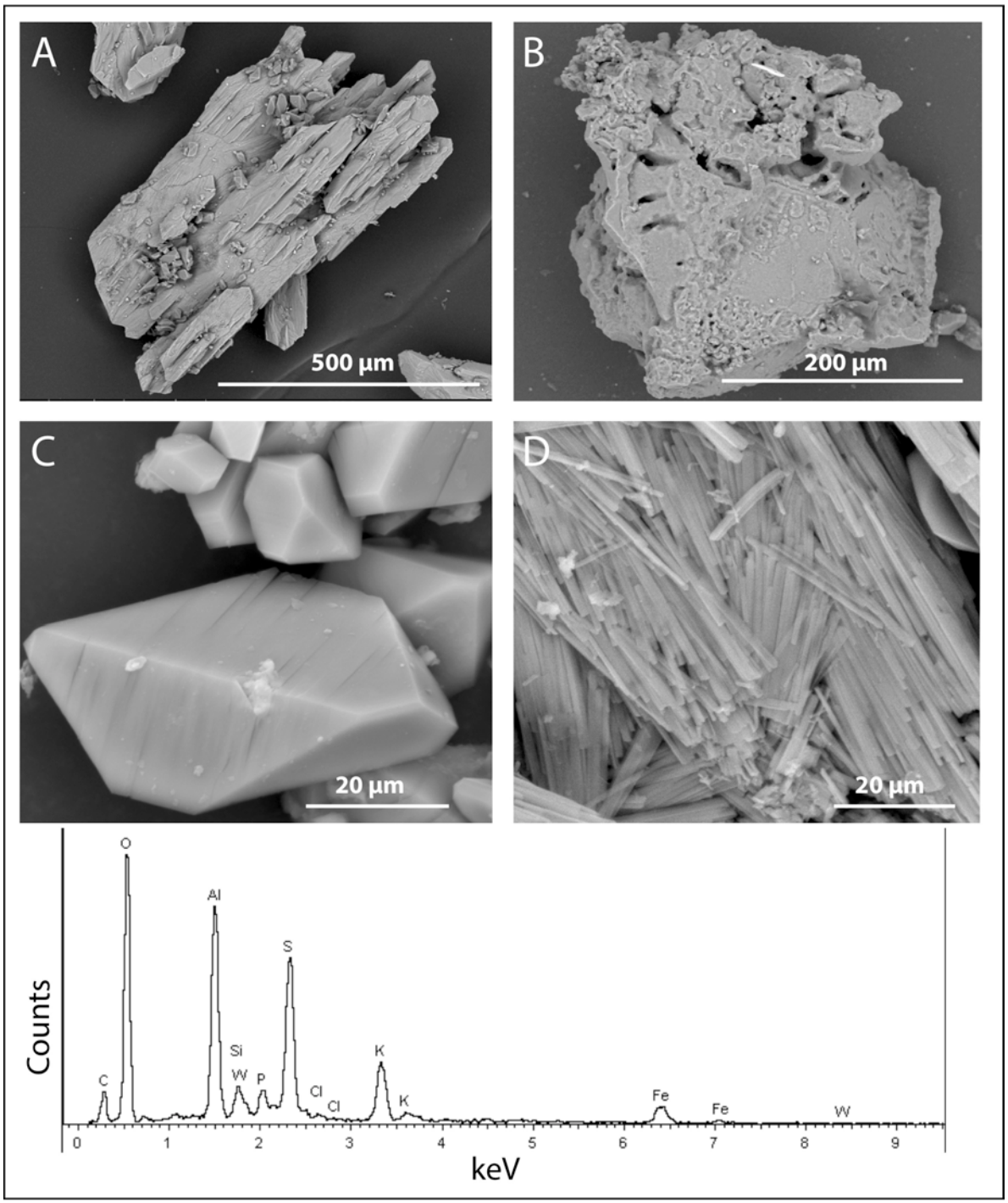

Fig. 3. SEM Secondary Electron images of gypsum (A), alunite (B), rossiantonite (C) and sanjuanite (D) from the sample Ak8. In the panel below the EDS qualitative chemical analysis for alunite is shown.

of iron hydroxides (Fig. 2 D), although they are less common here than in the Guacamaya Cave and the Akopan Dal Cin System. The gypsum sample collected in this cave was found on the floor of a dry passage, among quartz-sandstone boulders fallen from the cave ceiling. This cave is also characterised by fewer and smaller silica biospeleothems compared to the Akopan and Guacamaya caves (Carreño & Urbani, 2004).

An additional set of samples was collected recently in the Imawarì Yeuta cave (Sauro et al., 2013c), one of the longest quartzite caves of the world, with more than 15 km of length (this set was analysed after the publication of Sauro et al., 2014). This cave opens with various entrances on the north-eastern sector of the Auyan Tepui. It consists of three hydrologically independent collectors, two of which coming from the big sinkhole of Sima del Viento, while the other one derives from the catchment area of a large collapse doline to the north, about five hundred metres wide, and of a

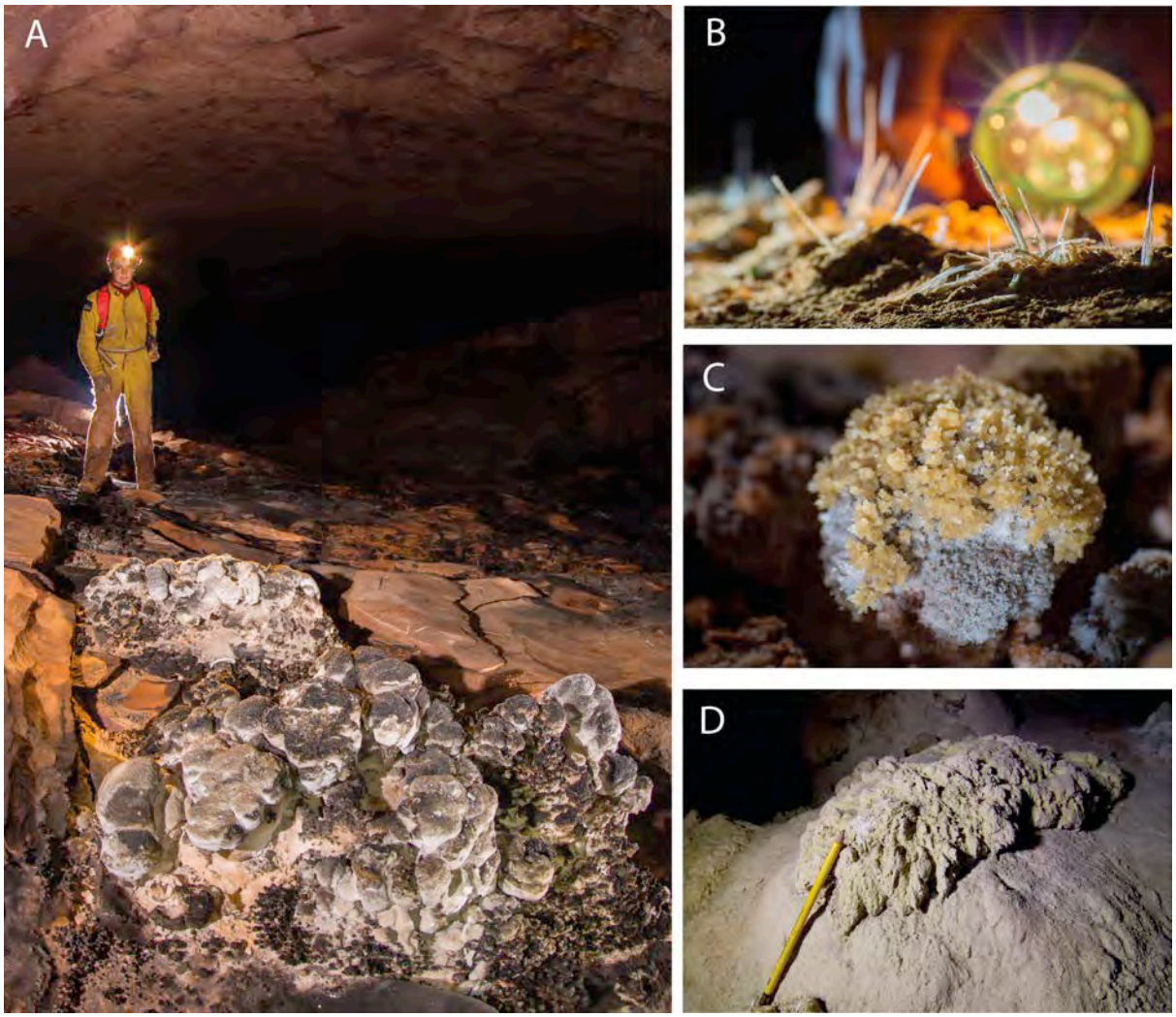

Fig. 4. Secondary minerals covering floors in Imawarì Yeuta. A) Gyspm deposits and crusts on the floor on a dry passage; B) Gypsum acicular crystals; C) Gypsum coralloid, resembling a desert rose; D) Sanjuanite speleothem on the floor.

nearby smaller sinkhole. Here a stream falls into the cave with a waterfall about 90 metres high. A labyrinth network of inactive galleries, developed along an evident bed, interconnects the different rivers. This "open" bed can reach impressive width (more than 300 metres in some sectors) creating huge environments where the ceiling is supported only by random pillars. One of the most impressive peculiarities of the cave is the presence of widespread crystallizations of gypsum, opal, and other secondary minerals (mainly aluminite and sanjuanite). Gypsum occurs in form of acicular crystals, flower-like forms, crusts and desert roses covering thousands of square metres of the cave floor (Fig. 4). Also deposits of iron hydroxides are present, in form of stalagmites up to 5 metres high, flowstones, rimstone dams, and coralloids. Anemolites, helictites and stalactites and other speleothems of opal and amorphous silica are present.

3.2.6 Material and methods

Mineral samples were collected using a steel spoon or a geological hammer (normally by scratching crusts or coatings). Nine samples of gypsum were collected, four of which were taken from crystals and aggregates on the floor, and the remaining five from the external surfaces of and within silica biospeleothems. Due to the extremely complex helicopter logistic necessary to reach the tepui caves, this is only a limited set of samples. Sample Ak8 was separated into three individual sulphate phases by picking single crystals under a stereoscopic microscope (gypsum, sanjuanite, and rossiantonite). Alunite was too fine-grained to be separated.

In addition, many samples of quartz-arenite host rock (5), iron hydroxide beds (5), and silica biospeleothems (3) were also collected.

3.2.6.1 Sample mineralogy (XRD and Raman)

For X-Ray Diffraction analyses (XRD) the samples were ground in an agate mortar, pressed in a plastic sample holder and analysed on a Philips PW 1050/25 and a PANalytical X'Pert PRO Diffractometer (experimental conditions 40Kv and 20 mA tube, CuKα Ni filtered radiation λ = 1.5418 Å) at the Department of Geology of Modena-Reggio Emilia University. In order to better identify iron hydroxides, a fresh cut surface of sample GC3 was analysed with a Horiba Jobin YVON – LABRAM HR Raman spectroscopy system, with spot size ~2 µm, hole 300 µm, slit 300 µm, 10x optical objective and 632.81 nm wavelength (i.e. red light) at the Department of Earth Science of ETH Zurich. For all the analyses and the chemical and crystallographic characterisation of rossiantonite see Galli *et al.* (2013).

3.2.6.2 Chemical analysis with WD-X Ray Fluorescence Spectrometer

Samples for wavelength dispersive X-ray fluorescence (WD-XRF) were ground to ultrafine powder and kept 24 hours at 110 °C. Ten grams of sample were mixed with 2.5 – 5 ml of Elvacite polymer

resin, dissolved in acetone. The mixture was stirred to allow acetone evaporation and Elvacite distribution. The resultant powder was placed in a penny shaped mould and compressed with a vertical pressure of 40 MPa for one minute.

The WD-XRF spectrometer Axios - PANalytical (Institute for Mineralogy and Petrology - IMP of ETH – Zurich) equipped with five diffraction crystals was used for this study. The SuperQ software package provided by PANalytical was employed for calibration and data reduction. Calibration is based on 30 certified international standards. The precision of analysed elemental abundances is better than ±0.2% for SiO_2, and ±0.1% for the other major elements with the exception of MnO and P_2O_5, which have concentration errors of ca. ±0.02%. For trace elements relative errors are better than 10% for concentrations of 10-100 ppm, better than 5% for higher concentrations and can reach as much as 50% at levels below 10 ppm. Therefore the detection limit is considered to be approximately 5-10 ppm.

For samples with SiO_2 concentration lower than the calibration limit we analysed a mixture of sample and ultrapure SiO_2. Finally, elemental concentrations of the samples were calculated according to the added SiO_2. In particular, sample GC3 was analysed mixing 2 grams of sample with 8 grams of SiO_2, while samples 16Eror was analysed mixing 5 grams of sample with 5 grams of SiO_2.

For many samples the sum of the element concentrations is less than 100%; this is related to the possible presence of water and organic matter within the samples. Conventionally, elements lighter than Na cannot be recognized with WD-XRF (Potts, 2005).

3.2.6.3 Scanning Electron Microscopy (SEM)

SEM analysis was carried out on a FEI Quanta 200F SEM at the Electron Microscopy Centre of ETH Zurich. Back Scattered Electron images (BSE) were taken under high vacuum (< 10^{-3} Pa) using an electron beam with 20 kV high-voltage, beam spot size of 5 units and aperture set at 40 µm. The working distance was maintained around 10 mm. An EDAX Pegasus detector was used for Energy Dispersive X-ray Spectroscopy mapping (EDS) of the selected elements distributions. The samples analysed were prepared in polished thin sections which were mounted on a stage and coated with a ~25 nm thick carbon layer.

3.2.6.4 Sulphur and oxygen stable isotope analyses

The samples for sulphur isotope analysis were wrapped in tin capsules with V_2O_5 and converted into SO_2 in a Thermo Fisher Flash-EA 1112 coupled with a Conflo IV, interfaced to a Thermo Fisher Delta V Isotope Ratio Mass Spectrometer (IRMS) at the Stable Isotopes Laboratory of ERDW ETH (Zurich). Isotope ratios are reported in the conventional δ-notation with respect to V-CDT (Vienna Cañon Diablo Troilite), where $\delta^{34}S_{sample\text{-}CDT} = [(^{34}S/^{32}S)_{sample}/[(^{34}S/^{32}S)_{CDT} -1]*1000$ in ‰ units. The method was calibrated with the reference materials NBS 127 ($\delta^{34}S$ = +21.1), SO5 ($\delta^{34}S$ = +0.49) and SO6 ($\delta^{34}S$ = -

34.05). Measurement reproducibility based on the repeated analysis of an internal standard was better than 0.3‰.

The oxygen isotope analyses were performed only on the samples from Akopan-Dal Cin, Guacamaya and Roraima Sur cave systems. Samples were dissolved in a 1M NaCl solution. After complete dissolution the solution was acidified to pH = 2 by adding HCl, and $BaSO_4$ was precipitated by adding a 1.5M $BaCl_2$ solution. The precipitated $BaSO_4$ was separated by centrifugation, washed three times with distilled water and dried at 60° C for two days. For isotopic analysis 0.2-0.3 mg of $BaSO_4$ were wrapped in silver capsules and converted to CO by pyrolysis at 1450°C in the presence of glassy carbon in a ThermoScientific TC/EA interfaced in continuous flow (CF) mode to a ThermoScientific Delta V mass spectrometer. All isotopic values are given in the conventional delta-notation vs. VSMOW. The method was calibrated with the reference materials NBS 127 ($\delta^{18}O$ = +8.59), IAEA-S05 ($\delta^{18}O$ = +12.13) and IAEA-S06 ($\delta^{34}O$ = -11.35). The average standard deviation between replicates was better than 0.5‰.

3.2.7 Results

3.2.7.1 Sulphur content of the host-rock

In the pure quartz-sandstone host rock WD-XRF analyses reveal that the concentration of sulphur is below the detection limit (<10 ppm), whereas phosphorus is present in significant concentrations, ranging between 0.01 and 0.1 %, probably related to the occurrence of apatite crystals (samples AK3A, AK4, AK5C, AKT, ROR17 in Table 1). In all the other analysed samples, including those collected from the BIF and the iron hydroxide layers, S concentrations were below the WD-XRF detection limit.

Despite a careful investigation by optical microscopy and SEM, no euhedral crystals of pyrite (common in many Precambrian BIFs, e.g. Klein, 2005; Bontognali *et al.*, 2013a) or pseudomorphs that could indicate replacement of ancient sulphides were observed in sample GC3.

Concentration of P in sample GC3 (2.11 %) is more than one order of magnitude higher than in the host rock.

In order to clarify BIF elemental distribution and further test if sulphur is present in significant concentrations, EDS elemental relative abundance maps were produced for sample GC3 (Fig. 5). Globular masses and whitish layers were identified in the sample where iron, oxygen and phosphorus are present in higher concentrations. Similar P-enrichments are often observed in BIF deposits, and attributed to the tendency of phosphorus to be absorbed onto iron oxides (Bjerrum & Canfield, 2002). On the contrary, sulphur counts were below background level and therefore no preferential distribution was observed.

Fluorescence analyses in hostrock and BIF samples.							
Sample		**SiO_2 (%)**	**Al_2O_3 (%)**	**Fe_2O_3 (%)**	**CaO (%)**	**P_2O_5 (%)**	**S (ppm)**
GC3	Iron hydroxide BIF-like strata	18,33	1,955	76,59	0	2.11	0
AK3A	Weathered quartz-arenite with cm dark bands	79.09	15.98	1.71	0	0.03	0
AK3B	Weathered quartz-arenite	82.94	11.13	0.34	0.006	0.02	0
AK4	Weathered quartz-arenite with mm dark bands	85.71	3.00	0.50	0.011	0.03	0
AK5A	Weathered quartz-arenite with mm dark bands	73.04	22.34	1.99	0	0.10	0
AK5B	Weathered quartz-arenite with cm dark bands	70.96	22.37	3.67	0	0.07	0
AK5C	Unweathered quartz-arenite	78.37	13.10	0.16	0	0.06	0
AKT	Unweathered quartz-arenite	89.12	3.04	0.10	0.016	0.01	0
ROR16	Weathered quartz-arenite	78.41	7.084	0.129	0.008	0.07	0
ROR17	Unweathered quartz-arenite	88.08	2.076	0.404	0.015	0.01	0

Table 1. Major elements and sulphur quantitative concentration from WD-XRF

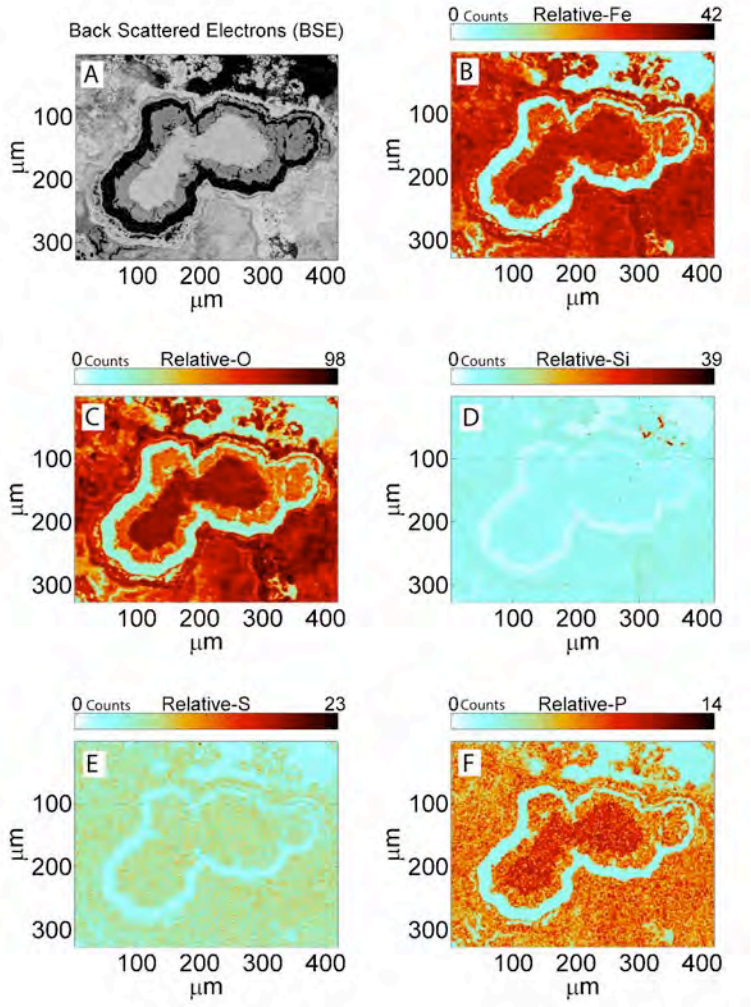

Fig. 5. SEM analysis of the BIF sample GC3 at low magnification. Panel A is a backscattered electron image (BSE) of sample GC3. Note the characteristic layered nodule, typical of hydrothermal precipitation. Energy dispersive X-ray spectroscopy abundance maps for different elements in the same thin section zone are shown in the top left image. The distribution of Fe, O and Si shows that the whole rock is made of iron hydroxides with minor amorphous silica. The sulphur map shows that this element is almost absent in the rock. Phosphate abundance map shows that the inner core of the nodule is richer in this element.

3.2.7.2 Sulphur and oxygen isotopes

The $\delta^{34}S$ and $\delta^{18}O$ of the sulphate-bearing minerals from the studied caves is given in Table 2 and Figure 6. The $\delta^{34}S$ shows a relatively constant composition between +18.6 ‰ and +19.4 ‰ for the Guacamaya and Roraima samples, whereas the Akopan-Dal Cin System and Imawarì Yeuta show slightly lower values respectively between +15.2 ‰ and +16.4 ‰. The samples from Imawarì Yeuta show a wider range from 12.2 ‰ to 22.5 ‰, with an average of 19.1 ‰. The $\delta^{18}O$ of the sulphate ion (Table 2) shows an average value of + 6.3 ‰ with only the gypsum sample from Akopan-Dal Cin System reaching +9 ‰.

Sample	*Description*	$\delta^{34}S$	$\delta^{18}O$
GC6A	Gypsum	19.0	5,6
GC6B	Gypsum	18.6	6,1
GC1E	Gypsum	18.6	6,5
GC1C	Gypsum	19.0	/
GC8	Gypsum	19,4	/
AK8gy	Gypsum	16.1	9
AK8sj	Sanjuanite	16.4	5,3
AK8rs	Rossiantonite	16.4	5,9
AK12	Gypsum	15.2	/
AK14	Gypsum	15.7	/
ROR1	Gypsum	18.3	5,7
V16sj	Sanjuanite	18.6	/
V16gy	Gypsum	20.5	/
V11	Sanjuanite	18.2	/
V1	Gypsum	20.8	/
V26	Gypsum	12.2	/
V2	Gypsum	20.9	/
V27	Gypsum	16.2	/
V4	Gypsum	18.4	/
V5gy	Gypsum	19.2	/
V5al	Aluminite	18.8	/
V6	Gypsum	22.5	/
V3	Gypsum	20.5	/
V21	Gypsum	19.6	/
V15	Gypsum	20.1	/
V20	Gypsum	20.4	/

Table 2. Sulphur and Oxygen stable isotopes (in ‰).

3.2.8 Discussion

3.2.8.1 Potential sources of sulphur

The chemical analyses of the quartz-sandstone host-rock indicate that the quartz-sandstone, BIF and iron hydroxide layers do not represent the major source of S for the secondary sulphate minerals found inside the caves. On the other hand, they could represent a significant source of phosphorus for the formation of minerals like rossiantonite and sanjuanite.

Congruently, even the sulphur isotope compositions exclude the hostrock or the BIF as possible sources of sulphur. Diffused hostrock sulphides produced by microbial sulphate reduction have a distinctly lower isotopic composition ($\delta^{34}S$ between -3 ‰ and -50 ‰; Brunner & Bernasconi, 2005; Seal, 2006), even for sulphides of Precambrian origin (Johnston, 2011).

Indeed, these sulphur isotope compositions are coincident or 2 to 6‰ lower than contemporary marine sulphate which remained around +21 to +22 ‰ even in the last thirty millions of years (Paytan *et al.*, 1998), the possible timespan of formation of these caves. Non-sea salt (nss) atmospheric sulphates produced by oxidation of Dimethyl Sulphide (DMS) at the air-seawater

interface can also account for these values of about 15 to 19 ‰ (Calhoun *et al.*, 1991).

The $\delta^{18}O$ data can also provide additional information on the origin of the sulphate ion. The mean $\delta^{18}O$ of dissolved sulphate in the ocean water is +9.5 ‰ (Longinelli & Craig, 1967), with only minor geographic variations and slight differences over the past few millions of years (from +8 ‰ to +13 ‰, Turchyn & Schrag, 2004). A similar value is expected for sulphate of seawater origin, although with a potentially wider range if we consider other secondary reduction/oxidation processes in the atmosphere and mixing with additional oxidized sulphur gases. Bao *et al.* (2004) found a $\delta^{18}O$ value of +9.3 ‰ for sea salt spray in Chile, whereas a wide range of values, from 5.6 ‰ to 16.8 ‰, with an average of +11.2 ‰, were found in dust traps in the South-western United States (Bao & Reheis, 2003). Therefore, the oxygen isotopic ratios found in quartz-sandstone cave sulphates could also fit the expected range of values for an atmospheric sulphate obtained by the mixing of seawater sulphate and the product of oxidation of reduced gas sources like terrestrial DMS or H_2S.

The tepui highlands, located relatively close to the Atlantic Ocean (about 450 km from Auyan and Chimantha tepui, 350 km from Roraima; Fig. 1), are characterized by extremely high rainfall (3400-3600 mm/year). The region is dominated by trade wind circulation, which brings in oceanic air masses from the equatorial and tropical Atlantic (Snow, 1976). In such climatic and geographic settings, rainwater, fog, and winds can represent a relevant means of sulphur transport over the continent from the air-seawater interface. While sea salt spray is known to have a limited transport capacity due to the relative big particle size (> 1 micrometer), nss marine sulphates (mostly produced by oxidation of DMS) can be easily transported inland from the coast. The tepui massifs represent the first orographic obstacle for air masses coming from the coast, crossing the river planes of French Guyana until reaching the high cliffs of these mountains, rising for more than 1500 metres from the surrounding lowlands (Fig. 7).

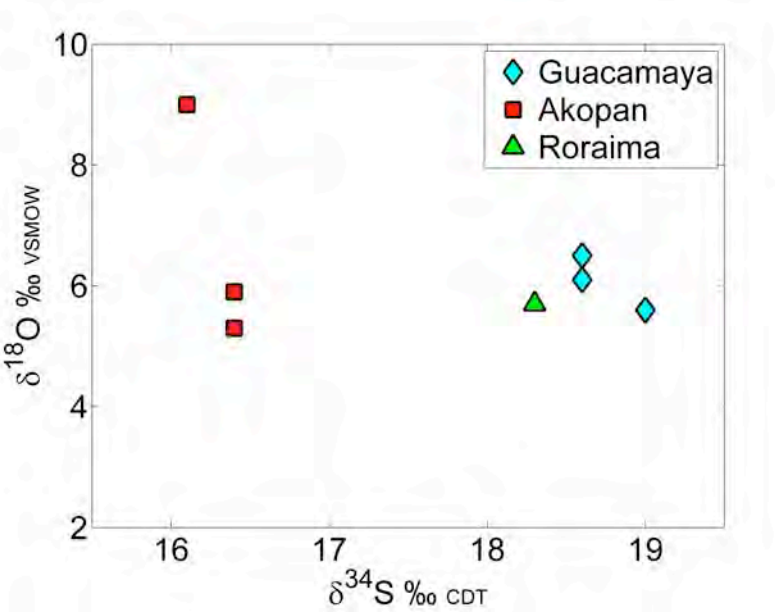

Fig. 6. Sulphur ($\delta^{34}S$) and oxygen ($\delta^{18}O$) isotope composition of sulphate minerals from quartz-sandstone caves.

The low pH of rainwater samples (average of 5.15, with the lowest value of 3.8) documented by our research group on Auyan, Chimantha and Roraima tepuis, suggests that rainfall probably contains a mixture of marine and terrestrial sulphate with also a reduced sulphur component (Mecchia & Piccini, 1999). Similar pH values were found by

Stallard & Edmond (1981) who showed that the precipitation contribution of sulphur in the Amazonian region results from mixing between seawater sulphate and biogenic terrestrial gases like DMS or H_2S produced by plants during photosynthesis (Winner *et al.*, 1981). The $\delta^{34}S$ of rainwater or aerosols depends on the relative contribution of each source with the tendency of lowering the value from +21 ‰ on the coasts (only seawater contribution, comprising sea-salt spray) to +11 ‰ in the inlands (predominantly terrestrial

biogenic gas contribution; Longinelli & Edmond, 1983). All the samples of sulphates collected in the quartz-sandstone caves are in this range and fit well with a nss marine sulphate source mixed with local biogenic gases like terrestrial DMS or H_2S.

However, it is possible to distinguish two different clusters with a slightly different mean value (Fig. 6): Auyan (Guacamaya) and Roraima caves have an average value of +19.20 ‰, whereas the association of sulphate and sulphate-phosphate from Chimantha (Akopan-Dal Cin System) shows a slightly lower average value of +15.96 ‰. Samples from Imawarì Yeuta show a higher variability with a group of samples around 16 ‰ while others over 20 ‰. These variability in the isotopic composition can be explained by taking into account additional sources of sulphur derived from the peat bogs found in many low topographical areas of Chimantha, in particular where diabases outcrop (Briceño *et al.*, 1990). The sediments in these anoxic peat bogs are expected to contain sulphide, which may be depleted in $d^{34}S$ due to microbial sulphate reduction. Once, during floods, the streams eroding these sediments sink into the caves, the sulphides can become oxidized and contribute a more negatively isotopic sulphate, hence explaining the lower $\delta^{34}S$ values like those documented in Akopan-Dal Cin System. Local oxidation of the sulphide transported by floods to the floor of the cave

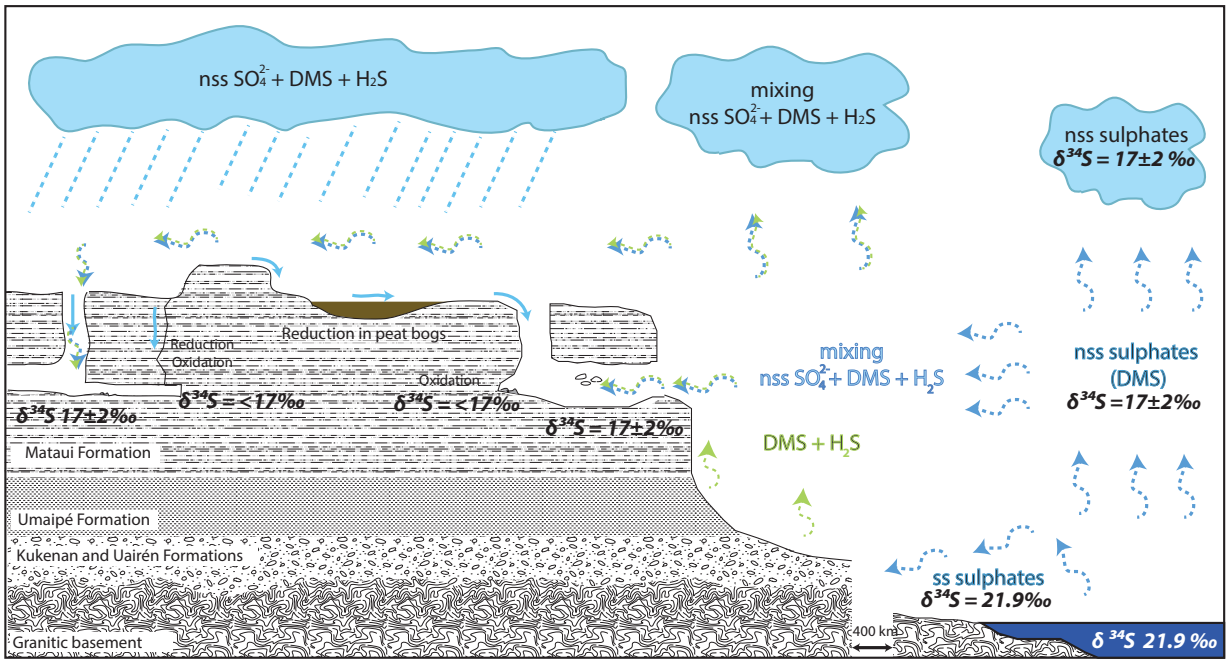

Fig. 7. Hypothetical schematic representation of the potential sulphur sources leading to the S isotopic composition of the sulphate-bearing minerals in the cave systems of the tepui area. Not to scale.

galleries is consistent with the highly acidic environment required for alunite formation (Khalaf, 1990). In fact authigenic alunite was found exclusively on the floor of the Akopan Cave associated with gypsum that has lower values of $\delta^{34}S$ with respect to Auyan and Roraima samples. In this case also the presence of major phosphorus allowing the formation of the exceptional phosphorus bearing sulphates sanjuanite and rossiantonite can be related to dissolved phosphate of organic origin carried into the caves by the stream and not only to the phosphorus in the BIF and the iron hydroxide layers.

Other potential factors lowering the isotopic signature could be related to the reduction-oxidation processes affecting water enriched in organic acids and sulphates slowly infiltrating from the surface directly through the fracture network below peat bogs and swamps. In fact Mecchia et al. (2014; chapter 2.2 in this thesis) found that waters from drippings and dripping fed ponds in the caves show the higher concentration of sulphates of the whole set of samples collected on the tepui area (around 0.6 mg L^{-1}). Because of the transparency and low conductivity of these waters, the reduction oxidation processes during the infiltration might explain also the consumption of the chromophoric organic elements that conversely characterises the stream waters.

In summary, even the isotopic signature suggests that the host rock of the caves does not represent the main source of sulphur, and an external source must be taken into account. This source could be represented by atmospheric nss sulphate from the Atlantic Ocean mixed with minor terrestrial sulphates derived by the oxidation of biogenic gaseous reduced sulphur (DMS or H_2S) with lower $\delta^{34}S$ values (Fig. 7).

3.2.8.2 Aerosol sulphate precipitation and potential biologic interactions

Sulphate and sulphate-phosphate minerals occur exclusively in specific sectors of the caves (Fig. 8). The presence predominantly on the walls and ceilings indicates that, differently from what observed in other active cave environments (Hill & Forti, 1997), their deposition cannot be simply attributed to the progressive evaporation of isolated water pools. Direct infiltration through the fracture network of waters slightly enriched in sulphates from peat bogs and swamps can account to significant amount of sulphates, as demonstrated in the chemical analyses of waters from drippings by Mecchia et al. (2014; chapter 2.2 in this thesis). However, in most cases, the sulphate minerals occur in close spatial association (i.e., on the surface or at millimetre distance) with silica speleothems that have been interpreted as biogenic stromatolites (Aubrecht *et al.*, 2008). XRD studies demonstrated that minor amounts of gypsum are present not only at the surface but also in the inner layers of the biospeleothems, suggesting that gypsum and amorphous silica may have formed almost simultaneously.

A peculiar characteristic of these caves is the presence of multiple entrances. Significant airflow caused by pressure and temperature gradients between different entrances located at different

altitudes or for chimney effects on the external cliffs of the tepui, was recognized at all the sites where opal biospeleothems and sulphate minerals were present. Aubrecht *et al.* (2008) suggested that such airflow carries aerosols, which can provide a relevant source of compounds of silica for the biospeleothems. Considering the long time needed for the growth of these silica formations (probably hundreds of thousands or even millions of years as suggested by U-Th dating, Lundberg *et al.*, 2010), the same aerosols can represent a significant source of sulphate.

Because of the heterogeneous morphology of the caves presenting several squeezes, curves and niches, airflow acceleration or deceleration produces adiabatic expansion or compression of the air that causes either evaporation or condensation in specific locations (Badino, 2010). These processes could result in a "wet deposition" mechanism as aerosols act as a nucleation mean for vapour condensation, producing mineral deposition on cave walls. Moreover, Dredge *et al.* (2013) observed that cave morphology controls the transportation and deposition of aerosol particulates through a cave network. Surface irregularities, and in particular prominent features, will result in air turbulence causing increasing particle collisions with the walls and therefore greater deposition at specific sites.

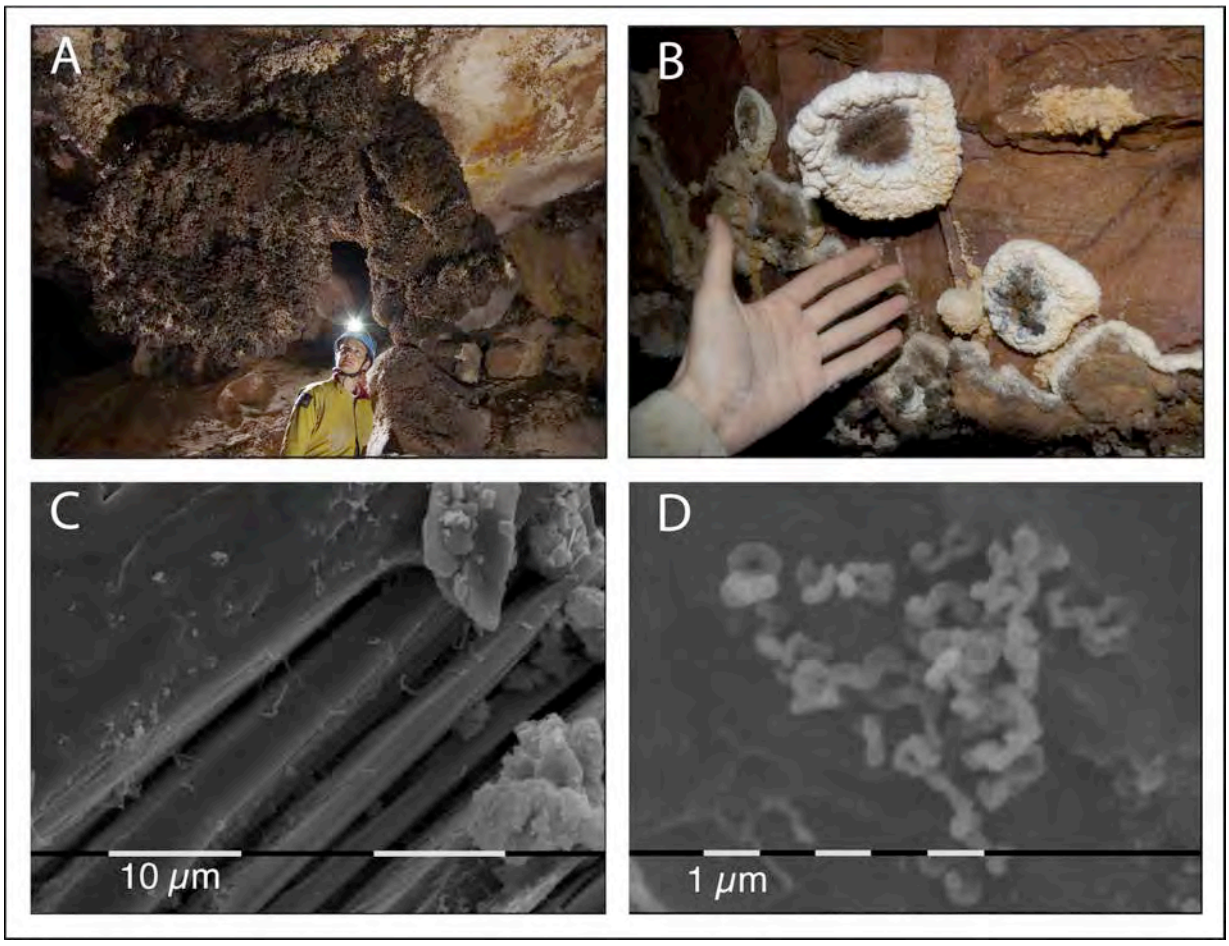

Fig. 8. A) Giant Chandelier of silica-biospeleothems just above the sampling site of Ak8 in the Akopan-Dal Cin System(photograph by Vittorio Crobu); B) Biospeleothems growing on sharp ledges on the wall and ceiling of Tramo de Los Opales in Guacamaya Cave (photograph by Francesco Sauro); C-D) SEM images of a gypsum crystal covered by biofilm and bacteria from Guacamaya Cave.

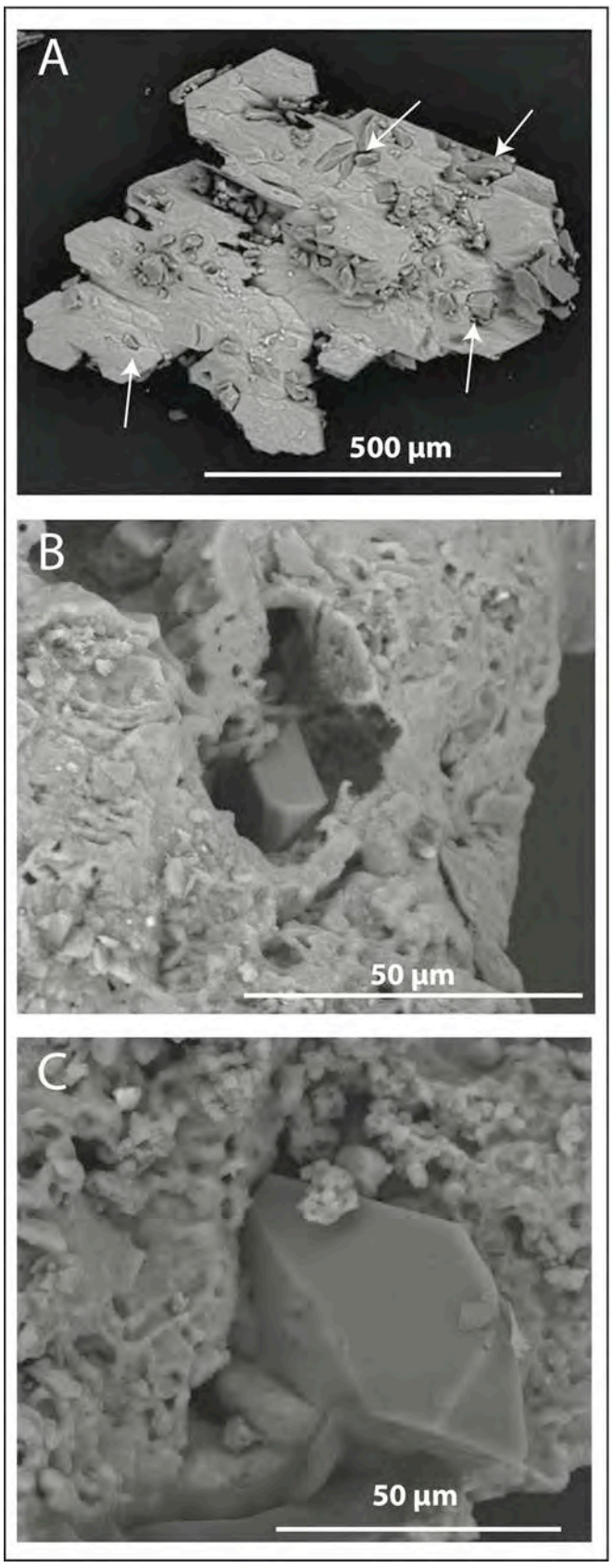

Fig. 9. A) Growing crystals of rossiantonite on gypsum (arrows indicating rossiantonite). B) A crystal of rossiantonite growing in a highly corroded alunite grain. C) Particular of rossiantonite crystal growing in a corrosion pit of an alunite grain.

This process can account for the accumulation of gypsum on sharp ledges and protuberances of the cave walls, and also for the formation of air-moulded biospeleothems (Sauro, 2013c; Fig. 8 B).

Although the exact role of microbes in the formation of the silica biospeleothems described by Aubrecht *et al.* (2008) remains elusive, the abundant presence of microfossils and cell moulds within amorphous silica demonstrates that microorganisms were present in that area of the cave at the time of their formation, influencing their morphology. Even if no readily discernible microfossils were identified encrusted within the studied sulphate minerals, SEM images show that microbial cells and filamentous features that are likely components of biofilms cover the surface of gypsum crystals (Fig. 8 C-D). It is possible that microbes were present at the sites of mineral formation exclusively because the same aerosols carrying Si and S were also providing them with nutrients essential for their metabolism, but they had no genetic relationship with the mineral product that may have formed through purely abiotic processes. Alternatively, it cannot be excluded that microbial biomass and extracellular polymeric substances (EPS) may have played a role in the formation of the sulphate minerals through a biomineralization process that is referred to as organomineralization (Dupraz *et al.*,

2009). Many studies have demonstrated that the functional groups occurring within microbial EPS selectively bind and concentrate cations mediating the nucleation of specific minerals (Douglas, 2005; Braissant *et al.*, 2007; Bontognali *et al.*, 2010), including gypsum (Cody & Cody, 1989; Ali-Bik *et al.*, 2011, Petrash *et al.*, 2012). Organomineralization of sulphate minerals is not characterized by any known distinctive isotopic signature, and EPS and microbial cells are not necessarily preserved in the final mineral product, making it difficult to prove the importance of organic molecules during the time of formation (Bontognali *et al.*, 2008, 2013b). Additional investigations are necessary to prove or reject the biogenicity of the sulphate, but such research is warranted by the close spatial association between sulphates and the biogenic silica speleothems, further supporting also our hypothesis of an aerosol source for the sulphate deposition. Secondary microbial feedback processes resulting in increased concentration of aerosol particulates on specific surfaces are considered a reliable mechanism also by Dredge *et al.* (2013), in their review on cave aerosols deposition.

Samples were found away from hydrologically active sectors, this fact was likely crucial to preserve the accumulation of secondary minerals from the erosive and dissolutive potential of running waters. In the peculiar case of the Akopan-Dal Cin System, sample Ak8 was collected on the floor of a dry passage that was the ancient paleo-thalweg of the underground river. In these settings the process of accumulation of the sulphate could be related either to the presence of a giant formation of silica speleothems on the ceiling above the collecting sites (Fig. 8B), or to the accumulation of organic matter carried into the cave by the ancient river. This last explanation fits well with the slightly different isotopic composition and also with the presence of great amounts of phosphorous and aluminium-rich clay minerals that caused the formation of sanjuanite and rossiantonite. SEM images show that rossiantonite grew inside gypsum crystals and in corrosion pits inside alunite (Fig. 9), suggesting that the minerogenesis of this phosphate-sulphate and also of sanjuanite could be related to a secondary hydration of the sulphates by phosphorous-rich waters.

3.2.9 Conclusions

Sulphates and the rare phosphate-sulphate minerals formed in the quartz-sandstone caves of the tepuis could be related to a very peculiar process of subsurface mineral accumulation never described previously. The quartz-sandstone host rock and also the iron hydroxide layers documented in the caves are depleted in sulphur suggesting that the minerogenesis is probably related to external sources. Even if the set of samples is limited, the range of S and O isotopic abundances indicates that an atmospheric aerosol source for the sulphate could be reasonably taken into account, most probably the result of oxidation of DMS of marine (nss sulphates) and terrestrial origin and minor microbially reduced sulphur from the forests or peatbogs within the watershed. This atmospheric sulphate may have been conveyed during millions of years into the caves through air currents accumulating sulphate minerals in dry branches or in the same locations where silica biospeleothems

have grown. The reason for the association of gypsum with these stromatolite-like formations is still unclear but there is evidence of potential microbial feedback in the accumulation of these minerals in specific sites. Further detailed microbiological-environmental studies could reveal important insights for understanding not only the geo-microbiological interaction in the sulphates genesis, but also the relationship between cave aereosols composition, bacterial activity and mineral deposition.

Local minor variations of the S isotopic signature may be related to additional minor sources of reduced sulphur from peat bogs and decomposed vegetation, directly entering into the systems carried by sinking streams, or slowly infiltrating through the fracture network. Dissolved phosphorus and/or decomposed organic matter, may account for a relevant source of phosphorus and acidity required for the formation of alunite, sanjuanite, and rossiantonite. Based on our data we suggest that in these settings there is no need to invoke hydrothermal events or oxidation of sulphides in the host rock for the formation of gypsum or of the rare sanjuanite and rossiantonite minerals as proposed by De Abeledo et al. (1968). Rossiantonite shows to be formed by substitution of gypsum and alunite, probably due to processes of re-hydration by phosphorous-rich waters.

Whereas the sources of sulphur in arid climate deserts are well studied (Chivas *et al.*, 1991; Eckardt & Spiro, 1999), in this tropical area of South America isotopic data are lacking because the preservation of sulphates is almost impossible in surface conditions. In these settings, quartz-sandstone caves represent a unique geochemical and biological environment, able to preserve and accumulate sulphates of probable external origin. Further isotopic studies on the different local atmospheric potential sources, the characterization of the cave aerosols and of the relationship with this peculiar sulphate accumulation will potentially provide fundamental information on the evolution of the sulphur cycle in tropical areas.

Acknowledgements

We want to thank the Venezuelan members of La Venta, Raul Arias Betancourt and Freddy Vergara Castro for the logistic support during the difficult missions on the tepui mountains. A great thanks also to Marco Mecchia, Leonardo Piccini and Laura Sanna for helping during the sampling. We also thank Lydia Zender and Enrico Dinelli for WDXRF analyses, Vangelis Moulas for Raman spectroscopy, and Dr. Karsten Kunze for SEM analyses, Stewart Bishop and Madalina Jaggi for assistance with isotope analyses, and Emily Rose Ciscato for helping us to edit the text.

References

Ali-Bik, M.W., Metwally, H.I.M., Kamel, M. G. and Wali, A.M.A. (2011) Gypsum and dolomite biomineralization in endoevaporitic microbial niche, EMISAL, Fayium, Egypt. Environmental Earth Sciences 62 (1), 151-159.

Aubrecht, R., Brewer-Carías, Ch., Šmída, B., Audy, M. and Kovácik, L. (2008) Anatomy of biologically mediated opal speleothems in the world's largest sandstone cave Cueva Charles Brewer, Chimanta Plateau, Venezuela. Sedimentary Geology 203, 181-195.

Aubrecht, R., Lánczos, T., Gregor, M., Schlögl, J., Smída, B., Brewer-Carías, Ch. and Vlcek, L. (2011) Sandstone caves on Venezuelan tepuis: Return to pseudokarst? Geomorphology 132, 351-365.

Aubrecht, R., Barrio-Amorós, C.L., Breure, A.S.H., Brewer-Carías, C., Derka, T., Fuentes-Ramos, O.A., Gregor, M., Kodada, J., Kováčik, Ľ., Lánczos, T., Lee, N.M., Liščák, P., Schlögl, J., Šmída, B. and Vlček L. (2012) Venezuelan tepuis: their caves and biota. Acta Geologica Slovaca Monograph, Comenius University, Bratislava, pp. 168.

Audra, P., Hobléa, F., Bigot, J.Y. and Nobécourt, J.C. (2007) The role of condensation-corrosion in thermal speleogenesis: study of a hypogenic sulfidic cave in Aix-les-Bains, France. Acta Carsologica 36(2), 185-194.

Badino, G. (2010) Underground Meteorology – "What's the weather underground?". Acta Carsologica 39(3), 427–448.

Bao, H. and Reheis, M.C. (2003) Multiple oxygen and sulfur isotopic analyses on water-soluble sulfate in bulk atmospheric deposition from the southwestern United States. Journal of Geophysical Research 108 (D14), 4430.

Bao, H., Jenkins, K.A., Khachaturyan, M. and Chong Díaz, G. (2004) Different sulfate sources and their post-depositional migration in Atacama soils. Earth and Planetary Science Letters 224, 577-587.

Bjerrum, C. J. and Canfield, D. E. (2002) Ocean productivity before about 1.9 Gyr ago limited by phosphorus adsorption onto iron oxides. Nature 417 (6885), 159-162.

Bontognali, T. R. R., Vasconcelos, C., Warthmann, R. J., Dupraz, C., Bernasconi, S. and McKenzie, J. A. (2008) Microbes produce nanobacteria-like structures, avoiding cell entombment. Geology 36 (8), 663-666.

Bontognali, T. R. R., Vasconcelos, C., Warthmann, R. J., Bernasconi, S. M., Dupraz, C., Strohmenger, C. J. and McKenzie, J. A. (2010) Dolomite formation within microbial mats in the coastal sabkha of Abu Dhabi (United Arab Emirates). Sedimentology 57 (3), 824-844.

Bontognali, T.R.R., Fischer, W.W. and Föllmi, K.B. (2013a) Siliciclastic associated banded iron formation from the 3.2 Ga Moodies Group, Barberton Greenstone Belt, South Africa. Precambrian Research 226, 116-124.

Bontognali, T.R.R., McKenzie, J.A., Warthmann, R.J. and Vasconcelos, C. (2013b). Microbially influenced formation of Mg-calcite and Ca-dolomite in the presence of exopolymeric substances produced by sulfate-reducing bacteria. Terra Nova 25 doi: 10.1111/ter.12072

Braissant, O., Decho, A. W., Dupraz, C., Glunk, C., Przekop, K. M. and Visscher, P. T. (2007) Exopolymeric substances of sulfate-reducing bacteria: Interactions with calcium at alkaline pH and implication for formation of carbonate minerals. Geobiology 5 (4), 401-411.

Brunner, B. and Bernasconi, S.M. (2005) A revised isotope fractionation model for dissimilatory sulfate reduction in sulfate reducing bacteria. Geochim. Cosmochim. Acta, 69, 4759-4771.

Brewer-Carías, C. and Audy, M. (2011) Entrañas del mundo perdido. Charles Brewer-Carías ediciones, Caracas.

Briceño, H.O. and Schubert, C. (1990) Geomorphology of the Gran Sabana, Guyana Shield, Southeastern Venezuela. Geomorphology 3, 125-141.

Briceño, H.O., Schubert, C. and Paolini, J. (1990) Table-mountain geology and surficial geochemistry: Chimantà massif, Venezuelan Guayana Shield. Journal of South America Earth Sciences 3 (4), 179-194.

Calhoun, J. A., Bates, T. S. and Charlson, R. J. (1991) Sulfur isotope measurements of submicrometer sulfate aerosol particles over the Pacific Ocean. Geophysical Research Letters, 18(10), 1877-1880.

Carreño, R. and Urbani, F. (2004) Observaciones sobre las espeleotemas del Sistema Roraima Sur. Boletin Sociedad Venezolana de Espeleologia 38, 28-33.

Chivas, A. R., Andrews, A. S., Lyons, W. B., Bird, M. I. and Donnelly, T. H. (1991) Isotopic constraints on the origin of salts in Australian playas. 1. Sulphur. Palaeogeography, Palaeoclimatology, Palaeoecology 84(1), 309-332.

Claypool, G.E., Holser, W.T., Kaplan, I.R., Sakai, H. and Zak I. (1980) The age curves of sulfur and oxygen isotopes in marine sulfate and their mutual interpretation. Chemical Geology 28, 199-260.

Clark, I.D. and Fritz P. 1997. Environmental Isotopes in Hydrogeology, Lewis.

Cody, A. M. and Cody, R. D. (1989) Evidence for Micro-Biological Induction of (101) Montmartre Twinning of Gypsum ($CaSO_4 \bullet 2H_2O$). Journal of Crystal Growth 98 (4), 721-730.

De Abeledo, M.E.J., Angelelli, V., De Benyacar, M.A.R. and Gordillo, C. (1968) Sanjuanite, a new hydrated basic sulfate-phosphate of aluminum. American Mineralogist 53, 1-8.

Doerr, S. H. (1999) Karst-like landforms and hydrology in quartzites of the Venezuelan Guyana shield: Pseudokarst or “real” karst? Zeitschrift fur Geomorphologie 43, 1-17.

Douglas, S. (2005) Mineralogical footprints of microbial life. American Journal of Science 305 (6-8), 503-525.

Dredge, J., Fairchild, I. J., Harrison, R. M., Fernandez-Cortes, A., Sanchez-Moral, S., Jurado, V. and Grassineau, N. (2013) Cave aerosols: Distribution and contribution to speleothem geochemistry. Quaternary Science Reviews, 63, 23-41.

Dupraz, C., Reid, R. P., Braissant, O., Decho, A. W., Norman, R. S. and Visscher, P. T. (2009) Processes of carbonate precipitation in modern microbial mats. Earth-Science Reviews 96 (3), 141-162.

Eckardt, F. D. and Spiro, B. (1999) The origin of sulphur in gypsum and dissolved sulphate in the Central Namib Desert, Namibia. Sedimentary Geology, 123(3), 255-273.

Forti, P. (1994) Los depósitos químicos de la Sima Aonda Superior y de otras cavidades del Auyán-tepui, Venezuela. Boletin Sociedad Venezolana de Espeleologia, 28, 1-4.

Forti, P. (2005) Genetic processes of cave minerals in volcanic environments: an overview. Journal of Cave and Karst Studies, 67, 3-13.

Galán, C. (1992) El clima. El macizo del Chimantá. In Un ensayo ecológico tepuyano (ed. O. Huber). Oscar Todtmann, Caracas, pp. 37-52.

Galán, C., Herrera, F.F. and Carreño R. (2004) Geomorfología e hidrología del Sistema Roraima Sur, Venezuela, la mayor cavidad del mundo en cuarcitas: 10,8 km. Boletin Sociedad Venezolana de Espeleologia, 38, 2-16.

Galdenzi, S. and Maruoka, T. (2003) Gypsum deposits in the Frasassi caves, Central Italy. Journal of Cave and Karst Studies, 65, 111-125.

Galli, E., Brigatti, M.F., Malferrari, D., Sauro, F. and De Waele, J. (2013) Rossiantonite, $Al_3(PO_4)(SO_4)_2(OH)_2(H_2O)_{10} . 4H_2O$, a new hydrated aluminium phosphate-sulfate mineral from Chimantha massif, Venezuela: description and crystal structure. American Mineralogist, 98, 1906-1913 .

Gibbs, A.K. and Barron, C.N. (1993) The Geology of the Guyana Shield. Clarendon Press, Oxford.

González de Juana, C., Picard, X. and Iturralde, J. M. (1980) Geología de Venezuela y de sus cuencas petrolífera. Edic. Foninvés, Caracas.

Gori, S., Inglese, M., Tognini, P., Trezzi, G. and Rigamonti, I. (1993) Auyan-tepui, speleologia tropicale nelle quarziti. Speleologia, 28, 23-33.

Hawkes, D.D. (1966) Differentiation of the Tumatumari-Kopinang Dolerite Intrusion, British Guiana. Geological Society of America Bulletin, 77(10), 1131-1158.

Hill, C.A. (1982) Mineralogy of Torgac Cave. Cave Research Foundation Annual Report, 17-18.

Hill, C.A. and Forti, P. (1997) Cave minerals of the world. National Speleological Society, Huntsville, USA.

Holt, B.D. and Kumar, R. (1991) Oxygen isotope fractionation for understanding the sulphur cycle. In Stable isotopes in the assessment of natural and anthropogenic sulphur in the environment (eds. H.R. Krouse, V.A. Grinenko). Wiley, pp. 27-41.

Hose, L.D., Palmer, A.N., Palmer, M.V., Northup, D.E., Boston, P.J. and Du Chene, H.R. (2000) Microbiology and geochemistry in a hydrogen-sulphide-rich karst environment. Chemical Geology, 169(3), 399-423.

Jagnow, D.H., Hill, C.A., Davis, D.G., DuChene, H.R., Cunningham, K.I., Northup, D.E. and Queen, J.M. (2000) History of sulfuric acid theory of speleogenesis in the Guadalupe Mountains, New Mexico. Journal of Cave and Karst Studies 62(2), 54-59.

Johnston, D.T. (2011) Multiple sulfur isotopes and the evolution of Earth's surface sulfur cycle. Earth-Science Reviews, 106, 161-183.

Khalaf, F.I. (1990) Diagenetic alunite in clastic sequences, Kuwait, Arabian Gulf. Sedimentology 37,155-164.

Klein, C. (2005) Some Precambrian banded iron formations (BIFs) from around the world: their age, geologic setting, mineralogy, metamorphism, geochemistry, and origin. American Mineralogist, 90, 1473-1499.

Klimchouk, A.B. (2009) Morphogenesis of hypogenic caves. Geomorphology, 106, 100-117.

Lazebnik, K.A., Zayakina, N.V. and Supletsov, V.M. (1998) The first find of the rare mineral Sanjuanite in Russia. Doklady Earth Sciences, 362(7), 922-924.

Longinelli, A. and Craig, H. (1967) Oxygen-18 variations in sulfate ions in sea-water and saline lakes. Science, 146, 56-59.

Longinelli, A. and Edmond, J.M. (1983) Isotope geochemistry of the Amazon basin: a reconnaissance. Journal of Geophysical Research, 88 (C6), 3703-3717.

Lundberg, J., Brewer-Carías, C. and McFarlane, D.A. (2010) Preliminary results from U–Th dating of glacial–interglacial deposition cycles in a silica speleothem from Venezuela. Quaternary Research, 74, 113-120.

MacDonald, G.J.F. (1953) Anhydrite-Gypsum equilibrium relations. American Journal of Science, 251, 884-898.

Martini, J.E.J., (2000) Dissolution of quartz and silicate minerals. In Speleogenesis Evolution of karst aquifers (eds. A.B. Klimchouk, D.C. Ford, A.N. Palmer and W. Dreybrodt). National Speleological Society, Huntsville, pp. 452-457.

Martini, J.E.J. (2004) Silicate Karst. In Encyclopedia of Caves and Karst Science (Ed. J. Gunn). Fitzroy Dearborn, London, pp. 1385-1393.

Mecchia, M., Sauro, F., Corongiu, C. and Crobu, V. (2009) Speleological explorations in the Chimantha massif quartzites (Gran Sabana, Venezuela). Supplement to Kur magazine 12, 1-16.

Mecchia, M. and Piccini, L. (1999) Hydrogeology and SiO_2 geochemistry of the Aonda Cave system (Auyantepui, Bolivar, Venezuela). Boletin Sociedad Venezolana de Espeleologia, 33, 1-11.

Onac, B.P. and Forti P. (2011) Minerogenetic mechanisms occurring in the cave environment: an overview. International Journal of Speleology, 40(2), 79-98.

Onac, B.P. and Veres, D.S. (2003) Deposition of secondary phosphates in a karst environment: evidence from Magurici Cave (Romania). European Journal of Mineralogy, 15(4), 741-745.

Onac, B.P., Wynn, J.G. and Sumrall, J.B. (2011) Tracing the sources of cave sulfates: a unique case from Cerna Valley, Romania. Chemical Geology, 288, 105-114.

Paytan, A., Kastner, M., Campbell, D. and Thiemens, M.H. (1998) Sulfur isotopic composition of Cenozoic seawater sulfate. Science 282 (5393), 1459-1462.

Palmer, A.N. and Palmer, M.V. (1995) Geochemistry of capillary seepage in Mammoth Cave. Proc. of the 4th Mammoth Cave Science Conf., Mammoth Cave , Kentucky (USA), pp. 119–133.

Petrash, D. A., Gingras, M. K., Lalonde, S. V., Orange, F., Pecoits, E., and Konhauser, K. O. (2012). Dynamic controls on accretion and lithification of modern gypsum-dominated thrombolites, Los Roques, Venezuela. Sedimentary Geology, 245, 29-47.

Piccini, L. and Mecchia M. (2009) Solution weathering rate and origin of karst landforms and caves in the quartzite of Auyan-tepui (Gran Sabana, Venezuela). Geomorphology, 106, 15-25.

Polyak, V.J. and Güven, N. (1996) Alunite, natroalunite and hydrated halloysite in Carlsbad Cavern and Lechuguilla Cave, New Mexico. Clays and Clay Minerals, 44, 843-850.

Polyak, V.J., McIntosh, W.C., Provencio P. and Güven, N. (1998) Age and origin of Carlsbad Caverns and related caves from $^{40}Ar/^{39}$ Ar of alunite. Science, 279, 1919-1922.

Potts, P. J. (2005) X-ray fluorescence and emission | X-Ray Fluorescence Theory. In Encyclopedia of Analytical Science (Second Edition) (Eds. P. Worsfold, A. Townshend and C. Poole C.). Elsevier, Oxford, pp. 408-418.

Reid, A.R. (1974) Stratigraphy of the type area of the Roraima Group, Venezuela. Bolletin de Geologia Venezuela, Pub. Especial 6, 343-353.

Rees, C.E., Jenkins, W.J. and Monster, J. (1978) The sulphur isotopic composition of ocean water sulphate. Geochimica et Cosmochimica Acta, 42(4), 377-381.

Santos, J.O.S., Potter, P.E., Reis, N.J., Hartmann, L.A., Fletcher, I.R. and McNaughton, N.J. (2003) Age, source, and regional stratigraphy of the Roraima Supergroup and Roraima-like outliers in northern South America based on U-Pb geochronology. Geological Society of America Bulletin, 115, 331-348.

Sauro, F., Piccini, L., Mecchia, M. and De Waele, J. (2013a) Comment on "Sandstone caves on Venezuelan tepuis: Return to pseudokarst?" by R. Aubrecht, T. Lánczos, M. Gregor, J. Schlögl, B. Smída, P. Liscák, Ch. Brewer-Carías, L. Vlcek, Geomorphology, 132, 351-365. Geomorphology, 197, 190-196.

Sauro, F., Lundberg, J., De Waele, J., Tisato N., Galli, E. (2013) Speleogenesis and speleothems of the Guacamaya Cave, Auyan Tepui, Venezuela. 16th International Congress of Speleology, Proceedings, 3, 298-304.

Sauro, F., Vergara, F., De Vivo, A. and De Waele, J. (2013c) Imawarì Yeuta: a new giant cave system in the quartz-sandstones of the Auyan Tepui, Bolivar State, Venezuela. 16th International Congress of Speleology, Proceedings, 2, 142-146.

Seal, R.R. (2006) Sulfur isotope geochemistry of sulfide minerals. In Reviews in Mineralogy and Geochemistry: sulfide mineralogy and geochemistry (Eds. D.J. Vaughan), Mineralogical Society of America, pp. 633-677.

Snow, J.W. (1976) Climate of northern South America. In Climates of Central and South America (Ed. W. Schwerdtfeger). Elsevier, New York, pp. 295-404.

Stallard, R.F. and Edmond, J.M. (1981) Geochemistry of the Amazon: 1. Precipitation chemistry and the marine contribution to the dissolved load at the time of peak discharge. Journal of Geophysical Research, 86, 9844-9855.

Teggin, D., Martinez, M. and Palacios, G. (1985) Un estudio preliminar de las diabasas del estado Bolivar, Venezuela. Memorias VI Congreso Geologico Venezolano. Caracas, pp. 2159-2206.

Tisato, N., Sauro, F., Bernasconi, S., Bruijn, R.H.C. and De Waele, J. (2012) Hypogenic contribution to speleogenesis in a predominant epigenic karst system: a case study from the Venetian Alps, Italy. Geomorphology, 151, 156-163.

Turchyn, A.V. and Schrag, D.P. (2004) Oxygen isotope constraints on the sulfur cycle over the past 10 million years. Science, 303 (5666), 2004-2007.

Twidale, C.R. and Vidal Romaní, J.R. (2005) Landforms and Geology of Granitic Terrains. A.A. Balkema Publishers, Leiden, Netherlands.

Urbani, F. (1977) Novedades sobre estudios realizados en las formas cársicas y pseudocársicas del Escudo de Guyana. Boletin Sociedad Venezolana de Espeleologia, 8(16):175-197.

Urbani, F. (1980) Lista de minerales secundarios encontrados en cuevas de Venezuela. El Guácharo 21, 44.

Urbani, F. (1981) Sveita, nuevo mineral de la cueva del Cerro Autana. El Guácharo 22, 30-31.

Urbani, F. (1996) Nota mineralógica preliminar sobre la plataforma de Aonda, Auyán-tepui, Bolívar. El Guácharo 38: 63.

Urbani, F., Talukdar, S., Szczerban, E. and Colveé, P. (1977) Metamorfismo de las rocas del Grupo Roraima. Edo. Bolívar y Territorio Federal Amazonas. Memorias V Congreso Geologico Venezolano, Caracas, pp. 623-638.

Winner, W.E., Smith, C.L., Koch, G.W., Mooney, H.A., Bewley, J. D. and Krouse, H.R. (1981) Rates of emission of H_2S from plants and patterns of stable sulphur isotope fractionation. Nature 289, 672-673.

Wray, R.A.L. 1997a. A global review of solutional weathering forms on quartz sandstones. Earth Science Reviews, 42, 137-160.

Wray, R.A.L. (1997b) Quartzite dissolution: karst or pseudokarst? Cave and Karst Science 24, 81-86.

Wray, R.A.L. (2000) The Gran Sabana: The World's Finest Quartzite Karst? In: Migon, P. (Ed.), Geomorphological Landscapes of the World. Springer, pp. 79-88.

Wray, R.A.L. (2011) Alunite formation within silica stalactites from the Sydney Region, South-eastern Australia. International Journal of Speleology, 40(2), 109-116.

Zawidzki, P., Urbani, F., and Koisar, B. (1976) Preliminary notes on the geology of the Sarisariñama plateau, Venezuela, and the origin of its caves. Boletin Sociedad Venezolana de Espeleologia, 7, 29-37.

CHAPTER 3.3

Part of this chapter is published in the Proceedings of the 16th International Congress of Speleology, Brno, Czech Republic, 21-28 July 2013, vol. 3, pp. 298-304.

MINERALS AND SILICA SPELEOTHEMS OF THE GUACAMAYA CAVE, AUYAN TEPUI, VENEZUELA

Francesco Sauro[1,2], Joyce Lundberg[3], Jo De Waele[1,2], Nicola Tisato[4], Ermanno Galli[5]

1) Department of Biological, Geological and Environmental Sciences, Bologna University, Via Zamboni 67, 40126 Bologna, Italy, cescosauro@gmail.com, jo.dewaele@unibo.it

2) Associazione di Esplorazioni Geografiche la Venta, Via Priamo Tron 35/F, 31030, Treviso

3) Department of Geography and Environmental Studies, Carleton University, Ottawa, Ontario, Canada, K1S 5B6

4) ETH Zurich, Geological Institute, Soneggstrasse 5, 8092 Zurich (Switzerland)

5) Department of Chemical and Geological, University of Modena and Reggio Emilia. Largo S. Eufemia 19, I-41121, Modena, Italy

Corresponding author: Francesco Sauro

Abstract

In March 2009 the Guacamaya Cave was discovered on the Auyan Tepui. It represents one of the longest caves explored on this table mountain, the only one known today with a complete horizontal development, comparable with those of the Brewer Cave System, in the Chimanta Tepui (the world largest sandstone cave). Guacamaya Cave presents peculiar morphologies, developed along an obvious bed of iron hydroxides and amorphous silica (Banded Iron Formation, BIF) interposed between hard and massive quartzite banks. In the walls around this layer, a variety of opal speleothems, of unusual dimensions and shapes, together with gypsum flowers and crusts have been documented.

Here we present a compositional and morphological characterization for the BIF layer and one tufa-like bio-speleothem. The speleogenetic control exerted by the BIF stratum is discussed, and in relation to collapse morphologies observed on the surface. An attempt to date the bio-speleothem with the U-Th system shows the difficulties of applying this method to these silica formations, because of post-depositional alteration in this porous material.

3.3.1. Introduction

In the last twenty years many new cave systems have been discovered in different “tepuis” (table mountains) of the Guyana Shield (Venezuela and Brazil), formed in the Precambrian quartzite sandstones of the Roraima Supergroup (Piccini and Mecchia 2007; Sauro 2009; Aubrecht et al. 2011). The formation of caves and karst features in quartzite rocks is considered exceptional given the low solubility and solution rates of quartz (Wray 1997a, 1997b). These recent explorations have shown that the largest karst systems in these poorly-soluble siliceous rocks are controlled predominantly by stratigraphic rather than by tectonic factors.

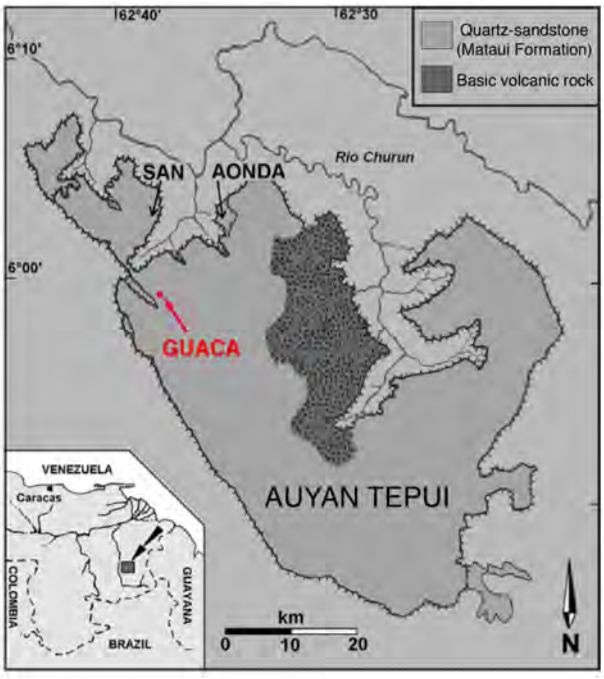

Fig. 1. The Auyan Tepuy with caves locations: Guacamaya Cave (Guaca), Sima Aonda (Aonda), Sistema Auyantepui Noroeste (SAN).

Many hypotheses were discussed by previous authors regarding the genesis of these caves, from the weathering process called “arenisation” (Martini 2000; Piccini and Mecchia 2009) to hypogenic processes related to hydrothermal activity (Zawidzki et al. 1976), or even diagenetic predisposition (Aubrecht et al. 2011), but these ideas are still in discussion and there is not yet a clear understanding of the main speleogenetic factors (Sauro et al. 2012b).

In this work we present a morphological description of the Guacamaya Cave, the longest horizontal cave explored in the Auyan Tepui (1.1 km). In addition to the impressive variety of silica bio-speleothems (Aubrecht et al. 2008a) and secondary minerals such as gypsum that were documented in a lateral fossil branch, this cave shows a peculiar characteristic not documented in other quartzite caves of the area: a bed of iron hydroxides (Banded Iron Formation) strictly controls its development.

We performed petrographic studies with thin section and SEM imaging, EDX and XRD chemical analysis on iron hydroxide layers, silica bio-speleothems and gypsum. In addition, following Lundberg et al. (2010), we attempted to date one of the bio-speleothem by the U-Th system.

3.3.2 Geographical and geological setting

The Gran Sabana is a wide geographical region located in northern South America, between Venezuela and Brazil, crossed by several tributaries of Rio Caroní, which in turn flows into the Orinoco River. The main massifs of the Gran Sabana, named "tepuis", have the shape of large table mountains. They are delimited by vertical to overhanging walls, often more than 1000 m high. The

massifs are separated from each other by the surrounding lowlands of the Wonkén planation surface (Briceño and Schubert 1990). More than 60 tepuis are present in the region and Guacamaya Cave opens in the northernmost one, the Auyan Tepui (700 km^2, Fig. 1), not far from the Angel Falls, considered the highest waterfall in the world (975 m).

Fig. 3. Lower valley entrance and the uroofed continuation of the cave.

From a geological point of view the Gran Sabana is part of the Guyana Shield. The igneous and ultra-metamorphic rocks in the northern portion of the shield (Imataca-Bolivar Province, after González de Juana et al. 1980) have an age of 3.5 Ga. The silico-clastic rocks (Roraima Group) belong to the continental-to-pericontinental environment of the Roraima-Canaima Province (Reid 1974). The age of this arenaceous group can be inferred only on the basis of the absolute dating of the granitic basement (2.3-1.8 Ga) and of the basaltic dykes and sills that cross the upper formation of the Roraima Group (1.4-1.8 Ga) (Briceño and Schubert 1990; Santos et al. 2003). The Roraima Group was also intruded by Mesozoic diabases (Hawkes 1966; Teggin et al. 1985). These form thin NE-trending dykes with ages around 200 Ma.

A slight metamorphism, with quartz-pyrophyllite paragenesis in the more pelitic beds, is the result of

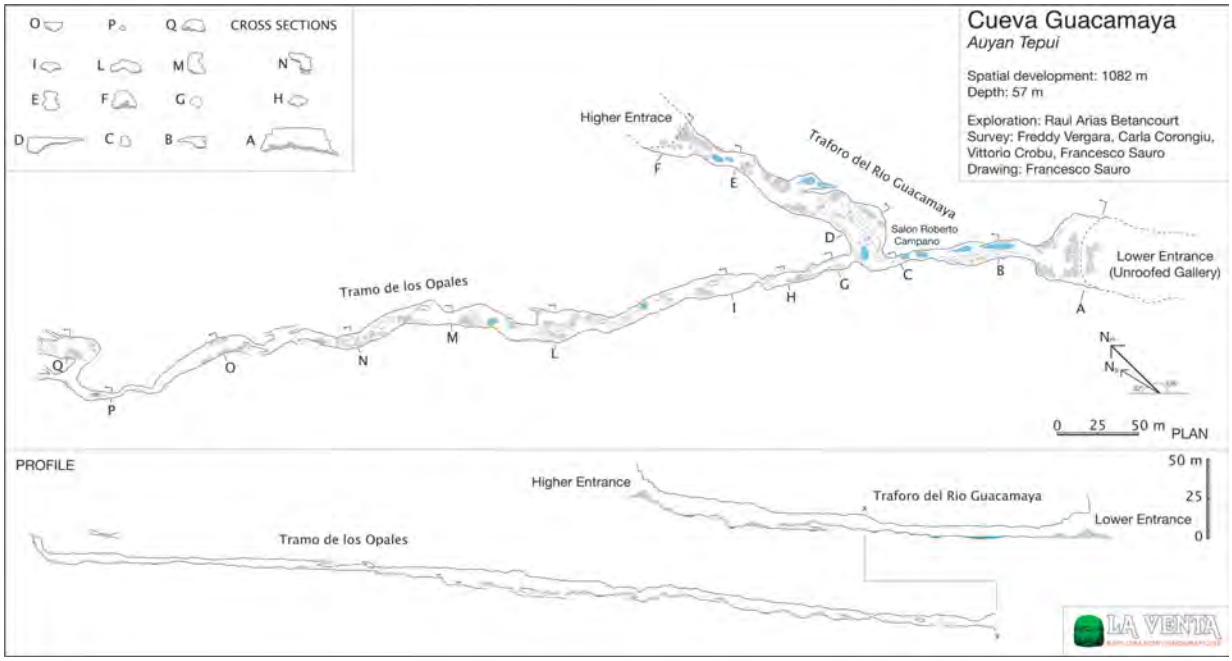

Fig. 2. Plan, profile and cross sections of Guacamaya Cave.

the lithostatic load of almost 3-km-thick sediments now eroded (Urbani et al. 1977).

Guacamaya Cave is developed in the Mataui Formation, the younger deposits of the Roraima Group, about one and a half billion years old (Santos et al. 2003). These are quartzitic sandstones of 600 to 900 metres thick, which form the highest part of the tepui. These sandstones are made up of quartz grains, representing well over 90% of the composition, held together by a cement, also mostly quartz, which gives them the term “quartz-arenite” (Martini 2000, 2004).

From a structural point of view folds are absent, except for some wide-curvature folds at a very large scale. The bedding in the proximity of the cave is slightly inclined toward the east. Some sets of mainly vertical fractures cut the plateaus, creating a regular network of quadrangular prisms. Important faults have not been observed, at any scale.

3.3.2.1. Morphological description

The main branch of Cueva Guacamaya is a hydrologic tunnel about 350 metres long. A permanent stream with a discharge of some litres per seconds crosses the cave from the highest entrance (Higher Entrance in Fig. 2) to the resurgence (Lower Entrance in Fig. 2). About one hundred meters from the lower entrance, a lateral fossil branch develops to the south for 700 metres ending in a boulder choke close to the surface (Tramo de los Opales). The passage is of significant size, more

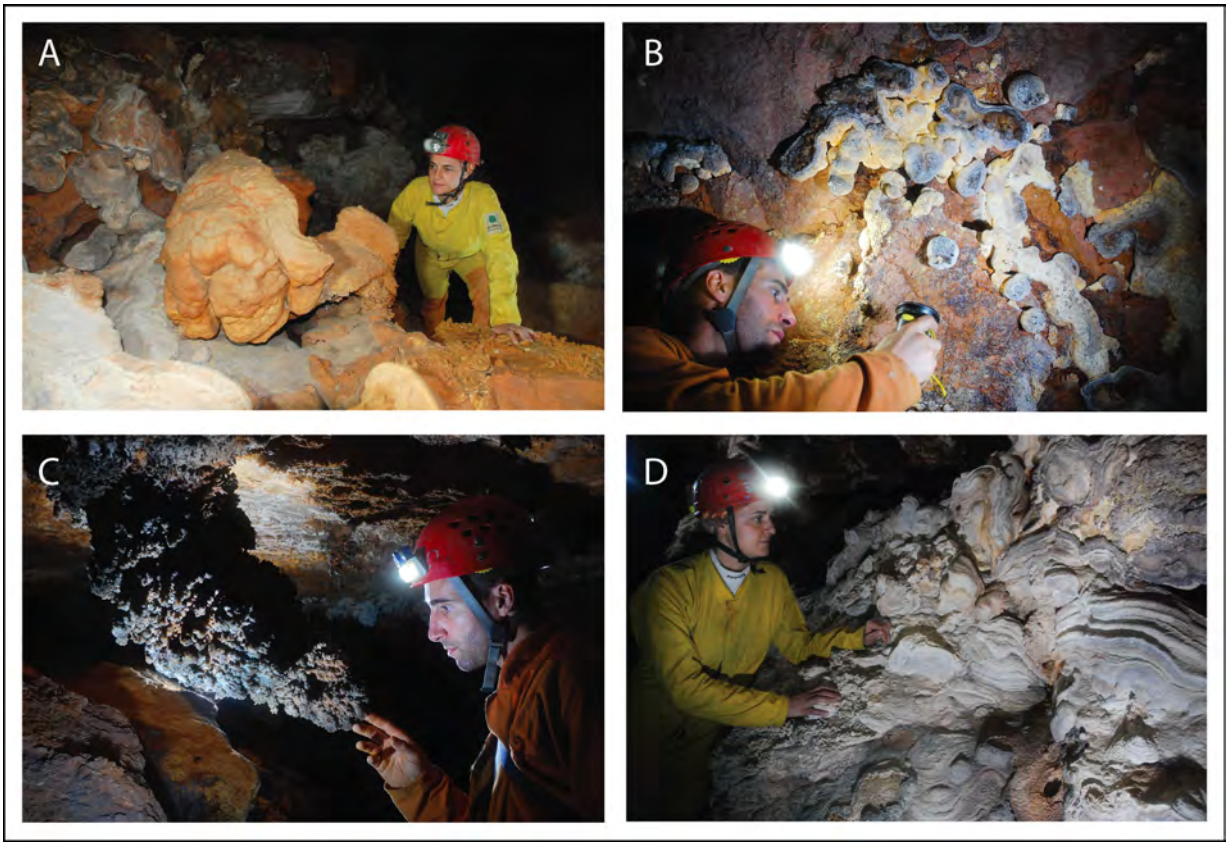

Fig. 4. Different morphotypes of biologically mediated silica speleothems. A) tufa-like speleothem; B) champinons agglomerate; C) Giant corralloid wind-guided stalactite; D) “clouds” formations on the wall; (Photos by F.Sauro).

than 30 metres wide and about 15 high in some sectors, with a great collapse room (Salon Roberto Campano) at the intersection of the two branches.

It is evident that the cave is part of a more extended system, now dissected and open to the surface: the valleys upstream and downstream of the cave represent the unroofed continuation of the main gallery, showing the same lithological control (Fig. 3). To the east a wide and complex area of tilted and fallen boulders is probably related to the collapse of the gallery in a more fractured sector of the plateau. In general the relict cave is situated at shallow depth from the surface, only 10-5 metres in some places.

Both the active and the fossil branches are developed along a layer of iron hydroxides with minor amorphous silica, similar to typical Banded Iron Formations, from some decimetre to a metre thick. This control is evident in the cross sections of the galleries showing an elliptical or keyhole profile. Original small phreatic conduits entrenched by vadose canyons are recognisable.

3.3.2.2. Silica speleothems and gypsum

The cave shows a wide variety of silica and opal speleothems, in particular in the "Tramo de los Opales" (Fig. 4). These formations are concentrated nearby the iron hydroxide layers, preferentially where the gallery cross sections are reduced, with increasing air flow. This branch of the cave is in fact characterised by a strong wind between the two main entrances and the highest final boulder choke open to the surface. Speleothems of different forms and dimensions were observed: coralloid speleothems like "dolls", tufa-like "champignons" (Fig. 4B), "kidneys" and all the morpho-types described by Aubrecht et al. (2008a). More complex composite formations completely cover the cave walls for several square metres (which we have called "clouds", Fig. 4D). A spectacular wind-guided coralloid stalactite 1 metre long was also documented (Fig. 4C).

In general, biologically mediated speleothems such as champignons grow mainly on sharp edges of quarzite blocks or emergent quartz veins (in relief due to differential weathering, resembling boxwork) and they show the tendency to growth toward the centre of the conduit.

Only few speleothems were sampled for this study, in particular a "champignon"-type bio-stromatolite, which we attempted to date.

Gypsum was commonly found in the dry gallery of "Tramo de los Opales". Two different preferential mineralization sites were observed: on the floor, in the form of acicular crystals around weathered blocks of quartzite fallen from the cave ceiling; or as overgrowth on the surface of the amorphous silica bio-speleothems.

3.3.3 Methods

For X-Ray Diffraction analyses (XRD) iron-hydroxide bed, silica biospeleothems and gypsum samples were ground to an ultrafine powder in an agate mortar and lightly pressed in a plastic sample holder.

XRD patterns were recorded with a Philips PW 1050/25 and a PANalytical X'Pert PRO Diffractometer (experimental conditions 40Kv and 20 mA tube, CuKα Ni filtered radiation λ = 1.5418 Å) at the Department of Geology of Modena-Reggio Emilia University. In order to better identify iron hydroxides we employed Raman spectroscopy on a fresh cut surface of sample GC3. The Raman spectrometer is an Horiba Jobin YVON – LABRAM HR, with spot size ~2 μm, hole 300 μm, slit 300 μm, 10x optical objective and 632.81 nm wavelength (i.e. red light).

For X ray fluorescence chemical analysis of the banded iron formation the sample was finely ground and analyzed in an Axios PANalitical spectrometer equipped with 5 diffraction crystals in the ETHZ Geologic Institute facilities (Zurich). Because of the uncommonly high iron content, samples had to be diluted with pure silica in order to compare them with standards. Thus, a variety of powder-pills with different percentages of sample and pure silica were analysed.

For Sem images we used a FEI Quanta 200F SEM equipped with an EDAX Pegasus detector for Energy Dispersive X-ray Spectroscopy mapping (ETH, Zurich).

For the dating attempt of the silica bio-speleothem the methods described by Lundberg et al. (2010) were applied. Small samples (~0.1 g) were taken from two different layers under binocular microscope avoiding the opalized laminations and the vuggy dark-colored material. Samples were ultrasonically-cleaned, spiked with ^{233}U–^{236}U–^{229}Th tracer, dissolved in a mixture of concentrated HNO_3 and HF over 48 h on a hot plate, dried, and then taken up in 7 N HNO_3. U and Th were isolated on anion exchange columns (Dowex AG1-X 200-400 mesh). Measurement of U and Th isotopic ratios was made by thermal ionization mass spectrometry (TIMS) using the Triton thermal ionization mass spectrometer at the Isotope Geochemistry and Geochronology Research Facility, Carleton University, Ottawa. Ontario. The analyses were accompanied by the processing of uraninite in secular equilibrium to ensure accurate spike calibration and fractionation correction. Activity ratios were calculated using half lives from Cheng et al. (2000).

3.3.4 Results and discussion

3.3.4.1 Banded Iron Formations, their geochemistry and their control on speleogenesis

X-Ray diffraction and Raman analyses show that the Banded Iron Formation is composed mainly of goethite and hematite, together with minor amorphous silica (Fig. 5C). In thin section and SEM images it presents a thin laminations, with nodules and goethite agglomerates. Also rare remnants of siderite and dolomite were identified by EDX punctual chemical analysis, both typical minerals of BIFs (Klein 2005).

WD-XRF Fluorescence analyses show that the BIF layer is composed of 76 % of iron with only 18 % silica, with minor phosphorus (2 %). Phosphorus is also typical of Banded Iron Formation because it tends to be absorbed into iron oxides (Bjerrum and Canfield 2002). Aluminium is below the 2 %, with potassium and calcium below the 0.01 %.

Of the minor elements, Zn and Cu are present, together with relatively high U and Th concentrations (respectively 96 and 24.5 ppm).

Aubrecht et al. (2011) described similar iron hydroxide deposits in the Churì Tepui as by-product of laterization (clay minerals turned to Fe-hydroxides by weathering).

In the case of Guacamaya Cave the strata consists in a continuous meter thick layer in between the quartz-sandstone beds. Its structure finely laminated (fig. 5C), its high content of iron (more than 70 %) and minor amorphous silica are in full agreement with the definition of James (1954) and Trendall and Morris (1983) for Precambrian banded iron formations. The depletion of Al and the lack of a typical latheritic profile suggest that this strata represents a true BIF formation deposited in a shallow marine environment and not a by-product of laterization. Alternatively, this layer could represent a only partially preserved paleo-soil (iron enriched part of the profile), related to weathering and temporary emersion just during the Precambrian (Gutzmer and Beukes 1998; Beukes et al. 2002).

In some place the iron hydroxide bed is folded and stretched, clearly because of shear related to the lithostatic load and the stronger rigidity of the overlying beds of quartz-sandstones. In places, where

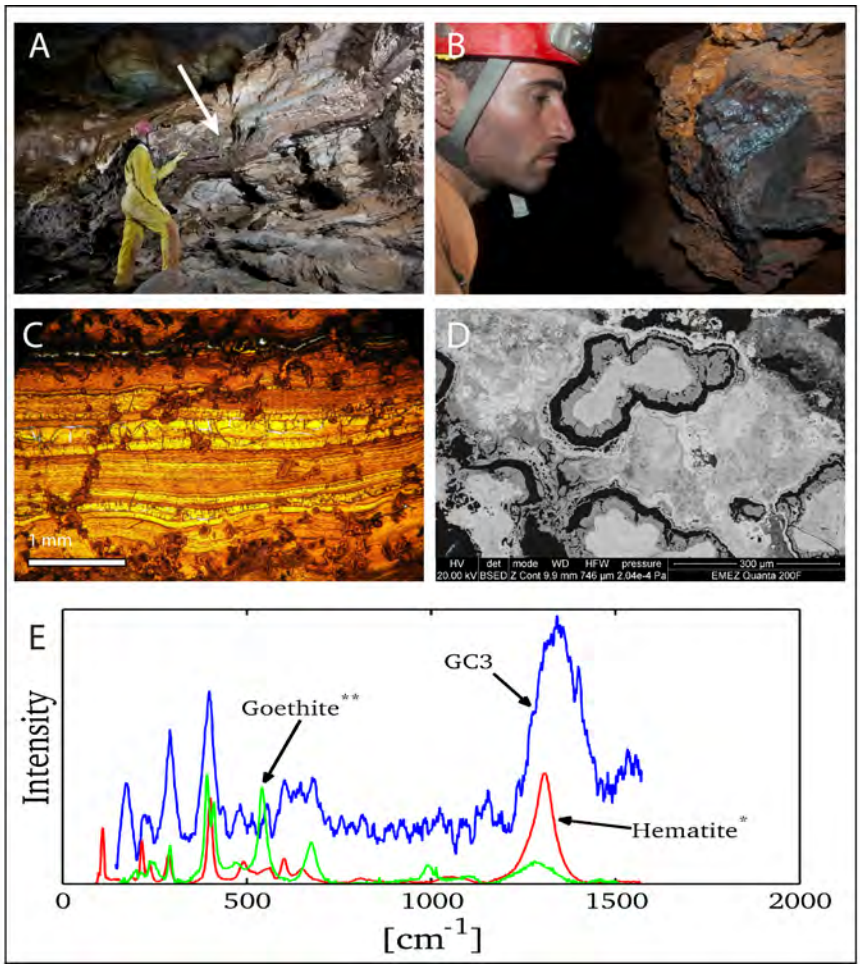

Fig. 5. The GC3 sample of the Banded Iron Formation bed: A-B) location of sampling in the Tramo de los Opales; C) thin layers of iron hydroxides in thin section; D) SEM image of iron hydroxides aggomerates in the not laminated part; E) Raman spectrum of GC3 compared with the spectrum of goethite and hematite.

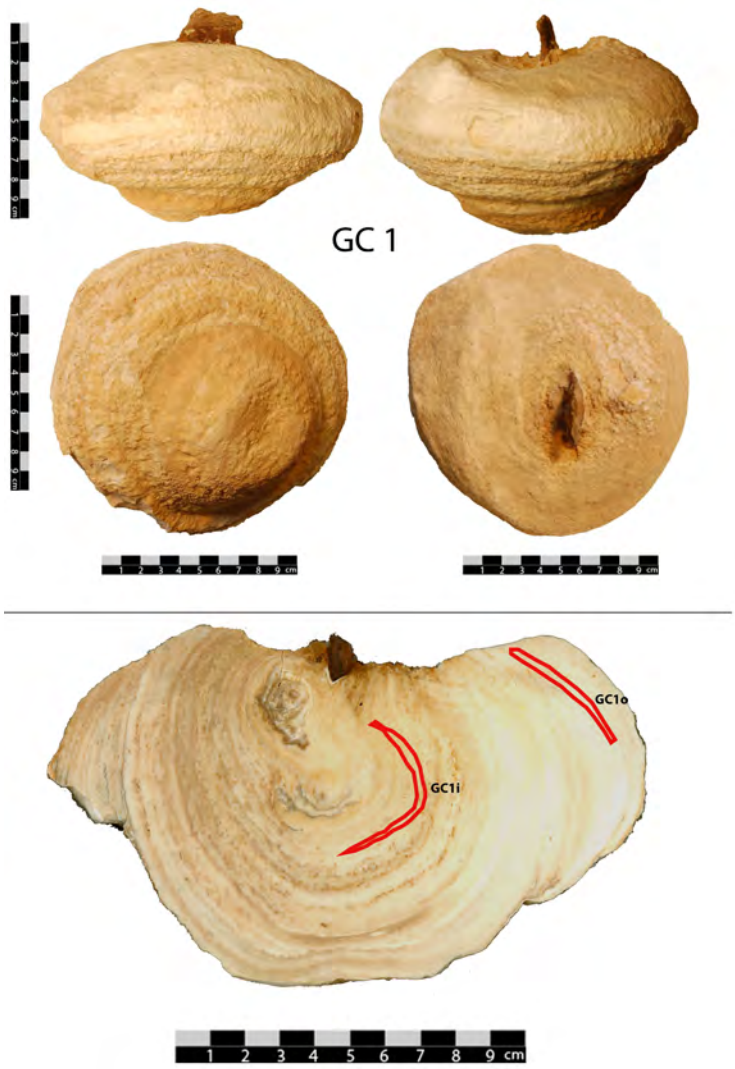

Fig. 6. The "champignons" bio-speleothem GC1.

the layer is stretched it is possible to observe the weathered iron hydroxides flowing out from the strata forming massive brownish flowstone, similar to other goethite speleothems described in other quartzite caves of the Sarisariñama and Chimanta tepuis (Zawidzki et al. 1976; Aubrecht et al. 2011).

Banded Iron Formations are well documented in other areas of South America (Dorr 1973) but were never described before in the Mataui Formation, probably because they are present only locally and because they are much easier weathered than the quartz-arenites.

The role of this bed in guiding the speleogenesis is particularly evident in the Guacamaya Cave, and also in the nearby higher platforms of the Auyan Tepui, where intensive collapses show a predominantly stratigraphical distribution (headwall retreat by basal erosion). It probably represents what is commonly defined as an "inception horizon" in classical karst (Lowe, 1992), due to peculiar chemical or rheological characteristics. Many of the hypotheses about speleogenesis in this region are consistent with the petrographic properties and behaviour of this bed. This could include regions of enhanced primary porosity, or even a seepage water alkalinisation effect on the contact with the quartz-sandstone beds, with increasing solubility of quartz and therefore arenization (Martini 2000). Micro-crystalline iron hydroxides in peculiar conditions are also more soluble than silica (Schwertmann, 1991) and this factor could enhance weathering. Further research is needed to better understand the main speleogenetic factors enhancing the opening of voids along this peculiar layer.

3.3.4.2. Silica biospeleothems

The tufa-like silica bio-speleothem (Fig. 6) is shown to consist of two main textures: tubular casts and peloids (Fig.7). Quartz grains, derived from weathering and arenization of the cave walls, are also

common. The inner layers are opalized, while the outer whitish layers are softer and preserve the original structure. The opalization is related to hydration processes, and therefore could be related to longer time of fluids seeping (and therefore with age) or with peculiar events The same opalization of the inner layers was observed also in the samples from Chimanta tepui described by Aubrecht et al (2008a) and Lundberg et al. (2010), suggesting that this process could be driven by regional climatic factors.

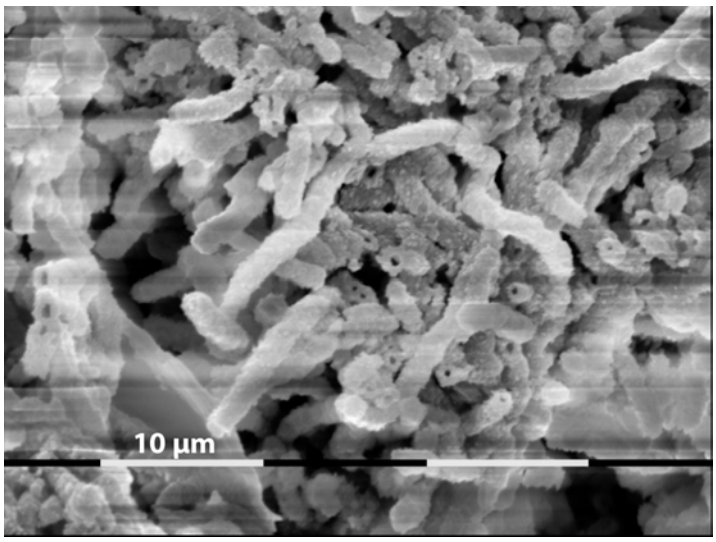

Fig. 7. Tubular cast structure of the outer layers in GC1.

The two layers sampled for U-Th dating (GCo and GCi in Fig. 6) show high but different contents of uranium: 4.33 ppm in the inner layer, 0.86 in the outer one. This disparity suggests a potential contamination of U rich particles of dust, probably related to the BIF layer that shows really high concentrations of this element. Particles of dust are impossible to observe in thin section or with an optical microscope, but are evident in SEM images. Therefore is not possible to exclude them during the sample preparation.

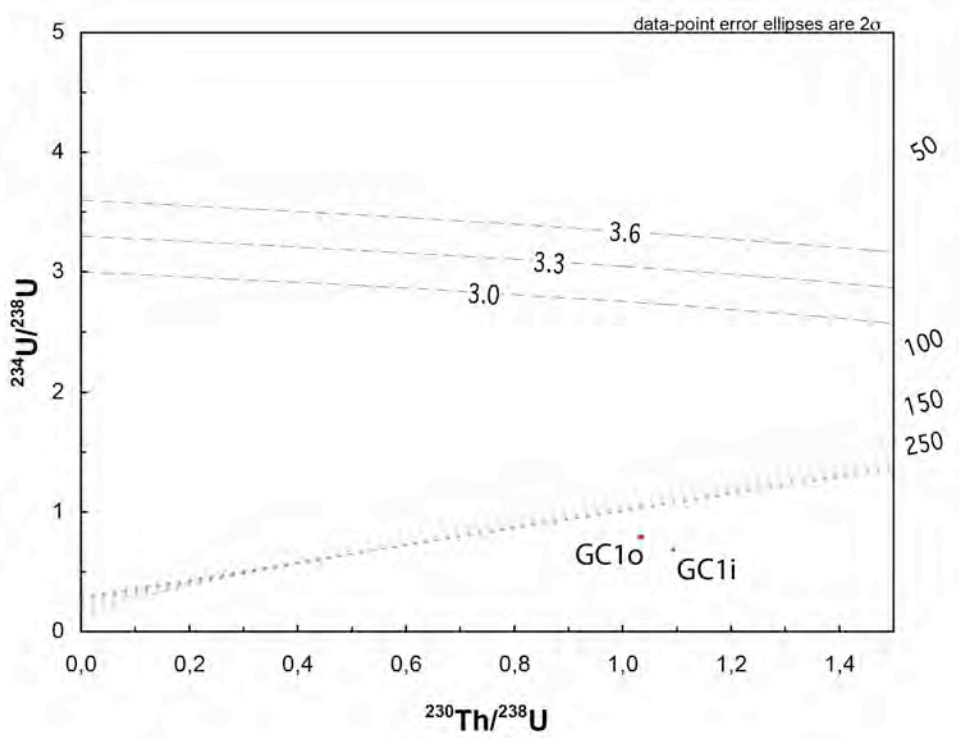

Fig. 8. Isotopic ratios from sample GC1 inner(i) and outer (o) layers. The lines labelled "3.6"," 3.3", and "3.0" are ingrowth curves for initial UU ratios, using ratios from Lundberg et al 2010 . Both samples lie outide of the dating envelope (graph was drawn using Ludwig 2000, Isoplot).

Sample	Age (ka)	U 238 conc microg/g	230 Th / 234U	2s Error	230 Th / 238U	2s Error	234U / 238U	2s Error
GC1 Inner layer	Not datable	4,33	1,6009	0,00354	1,0927	0,0022	0,6825	0,0007
GC1 Outer layer	Not datable	0,86	1,3124	0,0086	1,0339	0,0033	0,7878	0,0049

Table. 1. Concentrations of ^{238}U in the sample GC1 and isotopic ratios for different isotopes of U and Th

The isotopic ratios resulted from TIMS analysis are shown in table 1. The $^{230}Th/^{238}U$ versus $^{234}U/^{238}U$, plotted in Fig. 8. The ingrowth curves for initial $^{234}U/^{238}U$ ratios are those from dated speleothem of the Chimanta tepui published in Lundberg et al (2010). Figure 8 shows that both samples from GC1 lie outside of the dating envelope, and therefore cannot be dated by this method. This is due probably to depletion in ^{238}U in comparison with the original ratio, related to leaching, or contamination from other sources of uranium (dust particles). The porous nature of this material suggests that, in spite of the low solubility of silica, the system probably has been open for uranium migration.

With respect to the genesis of this silica bio-speleothem, some observation can be given (Fig. 9). All these speleothems grow on sharp edges, prominent veins of quartz and in proximity of the iron hydroxides layers. A control in their formation by air flow and condensation-evaporation processes is evident also in the anisotropy of the inner layers. These observations not only support the idea of Aubrecht et al. (2008b) that the major source of silica is related to a small-particle aerosol driven by air flows, but also

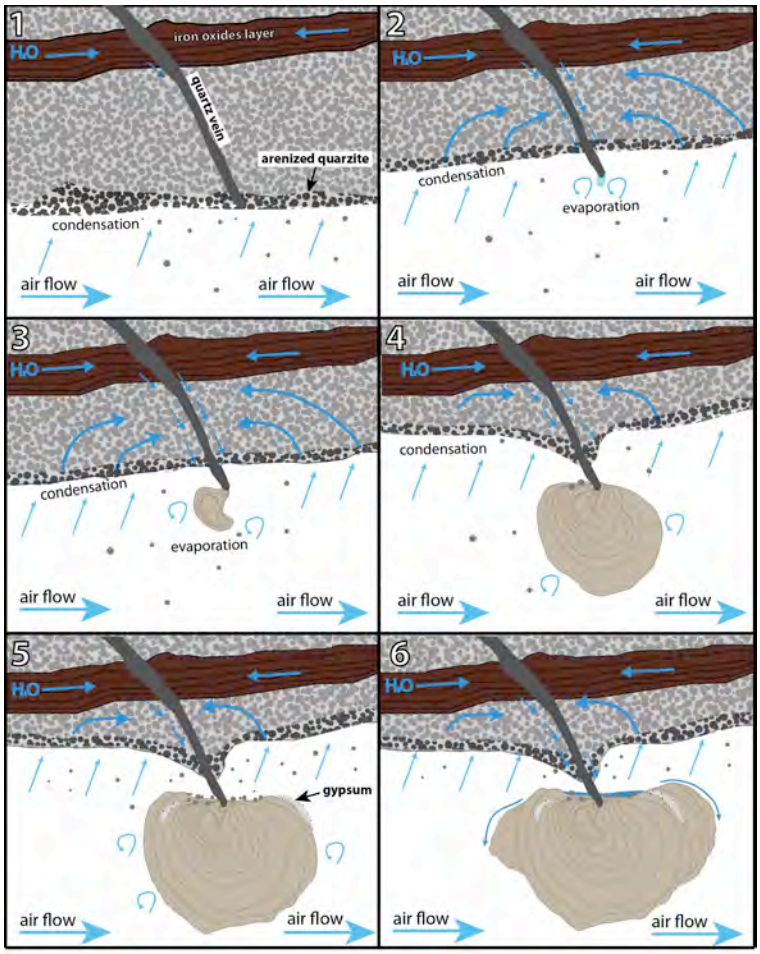

Fig. 9. Formation of a "champignons" speleothem on a quartz vein. 1) Initial condition. 2) The surrounding quartzite is weathered, the quartz vein remain in relief and became a preferential collector of seepage water enriched in silica. 3) Air flow controls the evaporation process and the shape of the biological mediated growing speleothems. 4) Grains of quartzite falling by the ceiling in consequence of weathering processes are incorporated in the growing layers. 4) Evaporation causes precipitation of gypsum on the speleothem surface. 5) The formation of a horizontal layer of water on the top of the "apple" leads to the formation of the protruding side of the speleothem.

suggest that silica dissolved by condensation waters could be an important source collected on quartz veins and prominent edges of the cave walls. The changing equilibriums between these two sources (growth driven more by aerosol or more by condensation water) in wetter and dryer periods could be the cause of the opalized layers and more porous external ones.

The presence of gypsum crystals on the speleothem surface and in trace in the inner layers suggests that evaporation processes were active during the formation of the speleothem and in its final growing stage.

3.3.5 Conclusions

Guacamaya Cave shows peculiar characters not described before in other quartz-sandstone caves of the Gran Sabana region. The presence of a BIF bed controlling the speleogenesis is evident, and the same layer is probably related to headwall retreat by basal erosion of the higher platform of Auyan Tepui. This layer show a composition typical of primary banded iron formation related to marine sedimentation or, alternatively, of a Precambrian paleo-soil.

The cave shows an exceptional variety of biologically mediated silica speleothems of different morphologies and sizes. Their formation is most likely related to aerosol sources of silica and condensation-evaporation processes. Post-depositional alteration, and the possible presence of contaminant dust, limits the ability to date these samples with the U/Th system.

References

Aubrecht R, Brewer-Carías Ch, Šmída B, Audy M, Kováčik L, 2008a. Anatomy of biologically mediated opal speleothems in the world's largest sandstone cave Cueva Charles Brewer, Chimanta Plateau, Venezuela. Sedimentary Geology 203, 181-195.

Aubrecht R, Lánczos T, Šmída B, Brewer-Carías Ch, Mayoral F, Schlögl J, Audy M, Vlček L, Kováčik L, Gregor M, 2008b. Venezuelan sandstone caves: a new view on their genesis, hydrogeology and speleothems. Geologica Croatica, 61, 345-362.

Aubrecht R, Lánczos T, Gregor M, Schlögl J, Šmída B, Brewer-Carías Ch, Vlcek L, 2011. Sandstone caves on Venezuelan tepuis: Return to pseudokarst? Geomorphology, 132, 351-365.

Gutzmer J, Beukes NJ, 1998. Earliest laterites and possible evidence for terrestrial vegetation in the Early Proterozoic. Geology, 26(3), 263-266.

Beukes NJ, Dorland H, Gutzmer J, Nedachi M, Ohmoto H, 2002. Tropical laterites, life on land, and the history of atmospheric oxygen in the Paleoproterozoic. Geology, 30(6), 491-494.

Bjerrum CJ, Canfield DE, 2002. Ocean productivity before about 1.9 Gyr ago limited by phosphorus adsorption onto iron oxides. Nature 417(6885), 159-162.

Briceño HO, Schubert C, 1990. Geomorphology of the Gran Sabana, Guyana Shield, Southeastern Venezuela. Geomorphology, 3, 125-141.

Cheng, H, Edwards RL, Hoff J, Gallup CD, Richards DA, Asmerom Y. 2000, The half-lives of uranium-234 and thorium-230. Chemical Geology, 169, 17-33.

Dorr JVN, 1973. Iron-formation in South America. Economic Geology, 68(7), 1005-1022.

González de Juana C, Picard X, Iturralde JM ,1980. Geología de Venezuela y de sus cuencas petrolífera. Edic. Foninvés, Caracas.

Isley AE, 1995. Hydrothermal plumes and the delivery of iron to banded iron formation. The Journal of Geology, 169-185.

Hawkes DD, 1966. Differentiation of the Tumatumari-Kopinang Dolerite Intrusion, British Guiana. Geological Society of America Bulletin, 77(10), 1131-1158.

Klein C, 2005. Some Precambrian banded iron-formations (BIFs) from around the world: Their age, geologic setting, mineralogy, metamorphism, geochemistry, and origin. American Mineralogist, 90, 1473–1499.

Lowe DJ, 1992. The origin of limestone caverns: An inception horizon hypothesis. Manchester Metropolitan University, Ph.D. thesis.

Ludwig KR, 2000. Isoplot: A geochronolgoical Toolkit for Microsoft Excel.Berkeley Geochronology Center, Special Publication No. 1a.

Lundberg J, Brewer-Carias C, McFarlane D.A, 2010 Preliminary results from U-Th dating of glacial-interglacial deposition cycles in a silica speleothem from Venezuela. Quaternary Research, 74, 113-120.

James HL, 1954. Sedimentary facies of iron-formation. Economic Geology, 49(3), 235-293.

Piccini L, Mecchia M, 2009. Solution weathering rate and origin of karst landforms and caves in the quartzite of Auyan-tepui (Gran Sabana, Venezuela). Geomorphology, 106, 15-25.

Martini JEJ, 2000. Dissolution of quartz and silicate minerals. In Speleogenesis-Evolution of karst aquifers. (Klimchouk et al. eds). National Speleological Society, Huntsville, 452-457.

Martini JEJ, 2004. Silicate Karst. In Encyclopedia of Caves and Karst Science (Gunn ed.). Fitzroy Dearborn, London, 1385-1393.

Reid AR, 1974. Stratigraphy of the type area of the Roraima Group, Venezuela. Bolletin de Geologia, Venezuela, Pub. Especial, 6, 343-353.

Santos JOS , Potter PE , Reis NJ , Hartmann LA , Fletcher IR, McNaughton NJ, 2003. Age, source, and regional stratigraphy of the Roraima Supergroup and Roraima-like outliers in northern South America based on U-Pb geochronology. Geological Society of America Bulletin, 115, 331-348.

Sauro F, 2009. Mondi Perduti, sugli altopiani quarzitici del Venezuela. Speleologia, 61, 38-47.

Sauro F, De Waele J, Forti P, Galli E, Vergara F, 2012a. Speleogenesi e speleotemi di opale della Cueva Guacamaya, Auyan Tepui, Gran Sabana, Venezuela. Atti del XXI Congresso Nazionale di Speleologia, Trieste, 291-298.

Sauro F, Piccini L, Mecchia M, De Waele J, 2012b. Comment on "Sandstone caves on Venezuelan tepuis: Return to pseudokarst?" by R. Aubrecht, T. Lánczos,M., Gregor, J. Schlögl, B. Smída, P. Smída, B., Brewer-Carías, Ch., Vlcek, L. Geomorphology, http://dx.doi.org/10.1016/j.geomorph.2012.11.015

Schwertmann U, 1991. Solubility and dissolution of iron oxides. Plant and Soil, 130 (1), 1-25.

Teggin D, Martinez M, Palacios G, 1985. Un estudio preliminar de las diabasas del estado Bolivar, Venezuela. Memorias VI Congreso Geologico Venezolano. Caracas, 2159-2206.

Trendall AF, Morris RC (Eds.),1983. Iron-Formation: Facts and Problems (Vol. 6). Elsevier Science.

Urbani F, Talukdar S, Szczerban E, Colveé P, 1977. Metamorfismo de las rocas del Grupo Roraima. Edo. Bolívar y Territorio Federal Amazonas. Memorias V Congreso Geologico Venezolano, Caracas, 623-638.

Wray RAL , 1997a. A global review of solutional weathering forms on quartz sandstones. Earth Science Reviews, 42, 137-160.

Wray RAL , 1997b. Quartzite dissolution: karst or pseudokarst? Cave and Karst Science, 24, 81-86.

Zawidzki P, Urbani F, Koisar B, 1976. Preliminary notes on the geology of the Sarisariñama plateau, Venezuela, and the origin of its caves. Boletin Sociedad Venezolana de Espeleologia, 7, 29-37.

4 – CONCLUSIONS AND FINAL REMARKS

The main conclusions of the presented thesis are:

Arenisation is the main process driving the speleogenesis in quartz-sandstones. The numerical model presented in chapter 2.1 clearly shows that, given enough time, arenisation is definitely a reliable process. The key factor in the formation of karst-like features and caves in this lithology is given mainly by the extremely slow dissolution kinetics of quartz, allowing the water to remain undersaturated, and therefore chemically aggressive, over long distances and times. Because of the long time needed to arenise the rock, this process is more prominent in geologically stable areas, like cratons and basins (of which the most representative examples are the Guyana Shield, the cratons of South Africa-Mozambique and Australia), generally with relatively high annual rainfall values. The geochemistry of surface and cave waters in the tepui mountains, described in chapter 2.2, confirms this hypothesis, showing that dripping and seepage waters are enriched in SiO_2 because the arenisation process is active along fractures and cave walls rather than along superficial and underground streams. However, in the more arkosic quartz-sandstone beds arenisation can develop not only because of quartz grain boundary dissolution, but also because of dissolution-recrystallization reaction transforming metastable pyrophyllite into kaolinite in the presence of water. Therefore arenisation must be considered in its wider significance, comprising all those weathering processes and chemical reactions able to weaken the rock and make it easily erodible by running waters. The “unlithified sands” theory proposed by previous researchers shows to be unreliable given the geologic history and the general morphologies and geographic distribution of the tepui caves, as discussed in chapter 2.3. Arenisation is a worldwide potentially efficient weathering mechanism (i.e. not related to local peculiar diagenetic conditions) explaining not only the caves of the tepui area but probably also those of many other karst-like quartz-sandstone landscapes of the world.

Crevices and tower fields at the surface, and pillars and maze networks in the cave systems are the expression of arenisation and consequent mechanical erosion creating anastomosing morphologies along fractures and bedding planes.

The variations in diffusion porosity between different beds (because of anisotropies and sedimentary features) together with different contents of clay minerals, are the main factors controlling the weathering rate and the development of arenisation features and caves along preferential layers. Iron hydroxide beds can also work either as aquicludes or aquitards focusing the flow of waters, boosting the arenisation in specific stratigraphic positions, as in the case of Guacamaya Cave described in chapter 3.3.

The degree of fracturing of the quartz-sandstone beds is another factor controlling the water infiltration and therefore the arenisation rate in specific layers.

The time of cave inception in quartz-sandstones is at least one order of magnitude longer than in classic carbonate caves. Thanks to the numeric model we are now able to assert that the cave inception phase, i.e. the time needed to predispose the rock to subsequent erosion and cave formation, is in the order of 600-1000 ka. However it is not easy to evaluate the time of the subsequent cave development phase, which is driven mainly by fluvial erosion, but if similar to carbonate karst, this phase could be at least one order of magnitude longer than the inception phase, i.e. around 6-10 My, or even more. It is interesting to note that, when the cave is formed, once abandoned by the water flow, it can remain almost unmodified for extremely long times, even hundred thousands of years. In this "senile" phase the arenisation can slowly continue but only through condensation-evaporation processes on the walls. The amount of silica removed though diffusion in this phase can precipitate on the cave walls because of evaporation processes or can be used by microorganisms to form different types of silica biospeleothems (see chapter 3.3).

The evolution of the tepui landscape, but probably also of other quartz-sandstone landscapes of the world, is modelled by weathering and erosional processes working mainly underground causing the opening of deep fractures (*grietas*) and the formation of extended horizontal conduit networks. The tepui top surface is lowering mostly through collapses related to these underground processes, while scarp retreat is controlled by the higher weathering rate of the more arkosic formations constituting the base of the massifs.
This landscape evolution model is confirmed by the water geochemistry and also by previous researches with cosmogenic isotopes on the erosion rate of the Gran Sabana area.

Speleogenesis in quartz-sandstone and quartzite rocks can develop not only in superficial epigenic conditions but also in deep hypogenic settings. Several authors in the past supposed the presence of caves and deep-seated voids carved in quartz-rich lithologies. With the study of Corona e' Sa Craba Cave in Sardinia we demonstrated that the hypogenic speleogenesis in quartzites really exists. In hydrothermal settings, because of the higher temperature, and peculiar geochemical conditions of the fluids (potentially reduced and with high amounts of dissolved cations) the solubility of quartz increases considerably with respect to surface conditions. High porosities and voids in fluid reservoirs hosted in quartz-rich rocks could be related to these hypogenic processes.

During the senile phase, quartz-sandstone caves are able to accumulate secondary minerals of external origin. This process is proportional to time and connectivity with the surface (dissection of

the system, opening of entrances, air flows, aerosols). These secondary deposits are composed mainly of sulphates and minor amounts of rare phosphate-sulphates, like sanjuanite and rossiantonite, the latter a new mineral for science discovered during this doctoral research. Thanks to isotopic studies and geochemical analyses of the potential host-rock sources, we found that these minerals are mainly of external atmospheric origin, transported inside the cave by air currents in form of aerosols. The reason for the association of gypsum with stromatolite-like formations is yet unclear but there are evidences of potential microbial feedback in the accumulation of these minerals in specific sites. This process of sulphate accumulation seems possible in quart-sandstone caves also because of the extremely long times of the senile phase, lasting probably for hundred thousands to even millions of years.

In general, thanks to these researches, we have now a more clear, and quantitative, view on the role and weight of the different weathering processes involved in the formation of caves and karst-like features in quartz-sandstone and quartzites.
However, the following aspects would need further researches in the future:

How much time could be necessary for the cave development phase? The problem of quantifying the mechanical erosion of the arenised rock by underground streams is still unresolved. This could be answered by means of erosion micrometer stations and long times of monitoring. In the frame of this thesis three of these station were set up in the Cave Imawarì Yeuta, however several years will be necessary to achieve the necessary data.

The sediments (chemical and physical ones) trapped in such old caves might contain palaeo-environmental and palaeoclimatic signals? This might span over the entire Quaternary or even more. Slack water deposits along stream beds, and especially airborne sediments (dusts) containing pollen. Also speleothems could be useful for paleoclimate researches, although the porosity of the silica speleothems could be a problem in dating (open system).

Which is the role of microbial interaction in the formation of these caves and their secondary deposits? The role of bacteria and fungi boosting the arenisation process and promoting the formation of silica speleothems could be crucial through bioweathering and biomineralisation processes as suggested previously by many authors. In this field, further studies will have to focus not exclusively on microbial communities and metabolisms but also on organic molecules that microbes excrete from the cell in the surrounding environments (called extracellular polymeric substances: EPS). Studies conducted in recent years have shown that some EPS have special

properties that promote the dissolution and re-precipitation of silicate minerals. Proving that quartz dissolution is locally catalysed by the presence of microbially produced organic molecules could provide new unexpected answers to the riddle.

Final acknowledgements

First of all, I am really grateful to my thesis supervisor Prof. Jo De Waele, for supporting this difficult project without any hesitation and encouraging me always (also with very good Belgian beer…).

This project wouldn't have been possible without the help and support of my expedition-mates Freddy, Carla and Vittorio: thank you for the time spent together, I wish hundred of these adventures!

Many, many thanks also to Tono De Vivo, Marco Mecchia, Leonardo Piccini, Tullio Bernabei and all the members of La Venta that supported the project with their great efforts. Thanks also to Raul Arias to always bring us back safe from the tepui. My gratitude goes also to Jesus Lira, who became a great friend in the difficult expedition of 2012.

Many thanks to Prof. Joyce Lundberg, for her useful suggestions and hospitality during my stay in Canada, and to Nicola Tisato, Marialuisa Tavagna, Giuditta Fellin, and Tomaso Bontognali for their help and hospitality during my visit to Zurich.

I want to thank also Prof. Paolo Forti and Prof. Ermanno Galli, for their contagious enthusiasm.

Thanks also to Prof. Enrico Dinelli, Prof. Giorgio Gasparotto, Prof. Vincenzo Picotti, Prof. Marco Antonellini, Prof. Dario Zampieri, Prof. Stefano Bernasconi, Dott. Fabio Gamberini, and Dott.ssa Irene Albino, for their suggestions and help in the laboratory analyses.

And most off all, many thanks to my parents Ugo and Laura, and to my loved girlfriend Daniela: thank you for trusting in me always!

Fundings

This project was supported mainly by La Venta Geographic Exploration Association and the Univerity of Bologna.

Every research and expedition was founded by different sponsors and institutions:

please see the specific acknowledgements at the end of each chapter.

This thesis was finished on February 17th 2014, Bologna, Italy